6-deoxy-6-amino chitosan: A plant defence priming biopolymer that enhances resistance against *Botrytis cinerea* in tomato and *Fusarium verticillioides* in maize

Naadirah Moola

Thesis presented for the degree of

Doctor of Philosophy in

Molecular and Cell Biology at the University of Cape Town

Bioengineering at the University of Gent

2024

Supervisors

Assoc. Prof. Mohamed Suhail Rafudeen

The Plants Stress Laboratory, Department of Molecular and Cell Biology, Faculty of Science, University of Cape Town

Assoc. Prof. Anwar Jardine

Department of Chemistry, Faculty of Science, University of Cape Town

Prof. dr. ir. Kris Audenaert

The Laboratory of Applied Mycology and Phenomics, Department of Applied Biosciences, Ghent University

Plagiarism Declaration

I, Naadirah Moola, hereby declare that the work on which this thesis is based is my original work (except where acknowledgements indicate otherwise) and that neither the whole work nor any part of it has been, is being, or is to be submitted for another degree in this or any other university. I and the supervisors authorize the Universities to consult and copy parts of this work for the purpose of research either the whole or any portion of the contents in any manner whatsoever. Every other use is subject to the copyright laws. Permission to reproduce any material contained in this work should be obtained from the authors.

Naadirah Moola

11/02/24

Publication Declaration

I confirm that I have been granted permission by the University of Cape Town's Doctoral Degrees Board to include the following publication in my thesis, and where co-authorships are involved, my co-authors have agreed that I may include the publication:

Moola, N., Jardine, A., Audenaert, K. and Rafudeen, M.S., 2023. 6-deoxy-6-amino chitosan: a preventative treatment in the tomato/*Botrytis cinerea* pathosystem. *Frontiers in Plant Science*, 14.

Signature:

Student Name: Naadirah Ismail Moola Student Number:

Acknowledgements

Alhamdullilah, without my Creator and His blessings, this journey would not have been possible!

I would like to take this opportunity to express my heartfelt gratitude to all those who have played a role in my PhD journey. Your support, guidance, and contributions have been invaluable. Unsurprisingly, it also takes a community to complete a PhD, so a gigantic thank you to:

The NRF, Harry Crossley, UCT, and MCB for the financial support over the years. You made my goal and dream a possibility!

My supervisor, Assoc. Prof. Suhail Rafudeen, you have been a beacon of support, strength, guidance, and empathic leadership. Your mentorship has been invaluable, and your belief in my abilities has propelled me forward, even in the face of challenges. Your positive and uplifting approach has made every PhD obstacle seem surmountable. Your dedication to my growth and success has been nothing short of inspiring and you've always 'made things happen' for me and my project. Shukran for believing in me and my abilities. I am fortunate to have had you as my supervisor. Your wisdom and encouragement will resonate with me long into the future.

My co-supervisor Assoc. Prof. Anwar Jardine, it is your parking lot conversation with Suhail that started this whole journey! Shukran for your enthusiasm, insights, collaboration, and financial contribution to the project. I am deeply appreciative of the opportunity to learn from your expertise so shukran for your pivotal role in shaping this research, your contributions have really enriched this journey.

My co-supervisor Prof. Kris Audenaert, thank you for taking a chance on me during my Masters, and for taking me on as a joint PhD student thereafter, for warmly welcoming me to the Lampions, for always including me in all of the Gent lab adventures, for the financial contributions to my project and for your valuable insights, ideas, and inspiration.

Dr Shane Murray, thank you for continuing to support and mentor me over the years, even though you were no longer my supervisor. Your kindness, care, and championing of me has always been remembered fondly. Thank you for ensuring that I had equipment and freezer space even after you left.

Prof. Jill Farrant, even though I was never officially your student, you supported and championed me since 2016!

Dr Shakeela Sayed, for what started off as a favour to chemistry, then became one of my biggest goals. Shukran for graciously accepting the role of my unofficial post-doc support and for entrusting me to contribute to your research. I am deeply appreciative of the countless hours you dedicated to synthesizing the polymer for me, your support, and guidance on chemistry-related matters. Your willingness to assist, even after your departure from UCT, speaks volumes about your commitment and generosity.

Dr Maarten Ameye and Boris Baekert, a sincere thank you for always being willing to help and for being friendly colleagues when I was all alone in a new country! Your help in setting up my large maize phytohormone experiment and in crushing/weighing the tissue was truly appreciated. Maarten, thank you for driving me to Merelbeke to conduct my metabolomics, for offering your R scripts to calculate the class data, for insight into my code, for reviewing my experiment protocols, help with the fluorescent microscope and the phenotyping platform.

Prof. Lynn Vanhaecke and Dr Lieven Van Meulenbroek, thank you for letting me use your UHPLC-MS facility. To Lieven, thank you kindly for setting up the machine reservations, for running the samples on the machine for me, and for doing the data processing, peak identifications, and peak integration.

Prof. Stefaan Werbrouck for allowing me to use your - 80 °C freezer, your autoclave and plant growth room.

Prof. Marthe de Boevre and her laboratory for your LC-MS mycotoxin analysis. Thank you for guiding me through the protocol and for allowing me lab space.

Dr Jiang Tan, thank you kindly for sharing your gfp transformation protocols, for allowing me to use from your plasmid stock, for guiding me through the protocol and for helping me troubleshoot!

Dr Noēmi de Zutter, thank you sharing your sand:SAP mix protocol, your white sand, for showing me how to measure the electrical conductivity, for allowing me to use your growth boxes and for any assistance offered with the phenotyping platform.

Dr Waldo Deroo, thank you letting me use your growth boxes and for helping me set up one of my maize experiments.

The Lampions, Michiel, Jonas, Trang, Dung Lee, and Jolien, thank you for your kindness and support during my research stay in Gent.

The Plant Stress Lab, Shandry, Llewelyn, Farah, Francois, Keren, thank you for always making me feel apart of the lab and for your support and cheer!

Dr Francois Du Toit, thank you for helping me with R and giving me a starting point with the exploratory data analysis.

Taybah Sayed, for the one month that you chose to help me set up some experiments, count spores, measure plates, and water plants, thank you! You came at a time of burnout when I desperately needed some support with my 300 plants and 120 plates!

Dr Mariam Awlia, Taybah Sayed, Robyn Craythorne, Sebastien Barnard, Matt Verbeek, thank you for helping me set up one of the largest time trial experiments I've had to do! Sebastien, Robyn, and Taybah, thank you for staying overnight in the lab to help me sample every 3hrs for 24 h!

Pei-Yin, Bronwyn, and Marilyn for help with all of the MCB equipment.

CPGR for conducting my proteomics, peptide and protein identification and data interrogation.

CAF for conducting the mass spectrometry analysis of the polymers.

OpenAI was utilized for checking spelling, grammar, synonyms, sentence structure and coherency where necessary.

Dr Shawn A. Christense from the United States Department of Agriculture, Agricultural Research Service, for conducting all of the GC-MS analysis on the phytoalexin work.

Jonathan Jayes for help with the cover artwork and Dall E.

The Shameless group: Matt, Jason, Tim, Lize, Frances, those tea breaks were day making!

Robyn, my dearest lab mate and friend, your belief in me, steady friendship, 28 min voice notes and perfectionist ways were a constant support and benefit to me, I will always be grateful.

To my loving and most patient friends, Fathima (Popz), Ashleigh (wife), Yo-neal, Ameera (AE), Lindsay, Astrid, Simone, Travis, Kevin, Molly, Adam, Safiyyah, Ania, Mariam, thank you for the countless pep talks, moments to rant and cry, love, and kindness, for being patient with my awol behaviour, and for the overall support through the years, I appreciate all of you!

Climbing saved me from going insane during my PhD so thank you to my climbing crew specifically Travis, you made the difficult days brighter with the climbing psych and tension board sessions. Thank you to the rest of the crew too, Zoe, Catie, Iva, Tiffany, Marijus, Nichola and Bloc11.

The trail running community and sport, specifically Becky and Tuesday Trails. You helped me build a pain cave and discipline that only ever benefitted me on the long days and nights of my PhD.

My loving family, Jim, Julia, Emma, and Eliza, thank you for being beacons of encouragement, support, and laughter. You have all wholly championed me and I feel most grateful to have had your support.

Aunty Moena, Uncle Sully, aunty Fia, uncle Achmat, Tietie, Rayghanna, Zaahidah, Shehaam, uncle Ebrahim, Veronique and the De Vries family, my other family and all of my aunts, uncles, and cousins who I have not

mentioned, I have felt the benefits of every dua, phone call, message, cheering and love for the last 6 years and I am deeply grateful to you.

Kashiefa (Bennie), my dearest sister, although you didn't get to see me reach this point, I thought about you every day, you were my anchor point through it all, my lighthouse and I know you're beaming at me even now.

Daadie, my beloved grandmother, whose belief in me and boundless love continue to inspire me. Your unwavering faith in my abilities, evident from the earliest days when you affectionately called me 'Dr', resonates deeply within me. Your duas were truly the most enriching for my life. This PhD journey, which I embarked upon with your blessings and encouragement, is dedicated to you.

Matt, my dearest husband, you probably met me at the more difficult part of the PhD, so I am deeply grateful to you for never losing patience, for being steadfast by my side even in my moments of madness and for championing me to the end. Best race finish together, ever! Thank you for helping me proofread my thesis!

And lastly, my most amazing parents, moms and pappieto, I made it! Your unwavering support and endless love have been my unshaken pillars of support. Even when the end seemed like a far-off dream, you never lost faith in my journey. Your patience, encouragement, and duas are what kept me going. Shukran for showing me what unconditional love truly means and for teaching me to never give up. This achievement belongs to all of us—it is a testament to your never-ending support and sacrifices. With heartfelt gratitude and boundless love, I owe you everything.

For Daadie and Bennie

Contents

List of Figures

List of Tables

Abstract

Aminochitosan, derived from chitosan, features enhanced water solubility, and improved antifungal efficacy attributed to an additional amine group at the C-6 position, hinting at its superior antifungal potential compared to native chitosan. This PhD thesis aimed to explore the optimal concentration of aminochitosan and its molecular weight fractions for enhanced antifungal and priming properties in the tomato/*Botrytis cinerea* and maize/ *Fusarium verticillioides* pathosystems.

In the *B. cinerea* pathosystem, various concentrations of aminochitosan were assessed for their antifungal effectiveness against *B. cinerea* growth and sporulation. Additionally, *in planta* studies were conducted to phenotype and quantify temporal stress responses using both qualitative and quantitative chlorophyll fluorescence imaging as well as DAB assays combined with microscopy. Despite batch-to-batch variations, aminochitosan consistently inhibited fungal growth and sporulation in a dose-dependent manner. *In planta*, aminochitosan pre-treatment induced robust defence responses in tomato leaves, resulting in a resistant phenotype that was mediated through a combination of enhanced photosynthetic efficiency as evidenced by enhanced F_v/F_m and chlorophyll content. The DAB assays suggested that these resistant phenotypes were also ROS-independent (H_2O_2 specifically) due to the strong positive impact of direct inhibition. The resistant phenotype and optimal efficacy of the aminochitosan MW fractions was observed at 3.5-15 kDa for antifungal efficacy and 15-20 kDa for *in planta* efficacy. Consequently, leaf senescence, hypersensitive responses and therefore necrosis were mitigated suggesting that aminochitosan primed defence responses in both mock and *B. cinerea* inoculated leaves.

A temporal, label-free quantitative proteomic analysis revealed the differential priming of key molecular mechanisms underpinning aminochitosan primed states both with and without *B. cinerea* infection at 6 and 9 hpi in the tomato/*B. cinerea* pathosystem. Aminochitosan treatment (1 mg/mL) differentially regulated proteins as early as 6 hpi with some of the induced responses being sustained up to 9 hpi. Additionally, several proteins were oppositely regulated between aminochitosan pre-treatment and *B. cinerea* infection, indicating differential regulation patterns between the “primed state” and the “triggered state”. The proteomic data therefore partially validated the ‘priming’ capacity of aminochitosan in 5-

week-old tomato leaves, specifically diamino 3 when used as a foliar spray at a concentration of 1 mg/mL.

The bimodal effects of aminochitosan in a maize/*Fusarium verticillioides* pathosystem were investigated by assessing the direct antifungal efficacy and elicitation of plant defence properties *in planta*. Aminochitosan displayed significant antifungal activity on both radial growth and sporulation at a minimum concentration of 1 mg/mL. Aminochitosan was also assessed *in planta* as preventative or curative treatments in maize seedlings infected with *F. verticillioides* at two time points. In the preventative treatment, salicylic acid accumulated during the early stages of infection (biotrophic phase) whereas in the curative treatment, jasmonic acid accumulated during the necrotrophic phase.

In summary, we demonstrated that water-soluble aminochitosan possesses key properties that enable plant priming in addition to its superior direct antifungal activity compared to native chitosan. We also identified the optimal molecular weights and concentrations necessary for achieving maximum and 50% inhibition activity.

Abbreviations

ACRE75	Avr9/Cf-9 rapidly elicited protein 75
mAriIdx	anthocyanin index
β	beta
C	carbon
C/N	carbon to nitrogen ratio
CHT	chitosan
ChlIdx	chlorophyll fluorescence index
Con	control
DAB	3’3’ diaminobenzidine
°C	degree(s) Celsius
D1	diamino 1
D2	diamino 2
D3	diamino 3
DA	degree of acetylation
DDA	degree of deacetylation
DP	degree of polymerization
dpi	days post inoculation
DS	degree of substitution
EA	elemental analysis
ESI	electrospray ionisation
ET	ethylene
F1	3.5-5 kDa
F2	15 kDa
F3	20 kDa
F4	20-99 kDa
F5	100 kDa
F_v/F_m	maximum efficiency of photosystem II
GlcN	glucosamine
GlcNAc	N-acetyl glucosamine
HMW	high molecular weight
h	hour(s)
hpi	hours post inoculation
H	hydrogen

H_2O_2	hydrogen peroxide
H_2O	water
JA	jasmonic acid
Inf	infected
kDa	kilodalton(s)
KH_2PO_4	potassium dihydrogen phosphate
LMW	low molecular weight
m/z	mass to charge ratio
µg	microgram(s)
µL	microlitre(s)
µM	micromolar
mg	milligram(s)
mL	millilitre(s)
min	minute(s)
mM	millimolar
MoA	mode(s) of action
M	molar
MW	molecular weight
N	nitrogen
NAc	N-acetyl
NaCl	sodium hydroxide
NH_4NO_2	ammonium nitrate
NO	nitric oxide
OH	hydroxyl/alcohol
PA	pattern of acetylation
PCD	programmed cell death
PDA	potato dextrose agar
PIRG	percentage inhibition of radial growth
Pol	polymer
PIS	percentage inhibition of sporulation
ROS	reactive oxygen species
SA	salicylic acid
V	volts
v/v	concentration of a solute in solution
w/v	mass concentration

%	percentage

This image was created with the assistance of DALL.E 2.

Chapter 1: Problem Statement and Thesis Outline

1.1 The global perspective shift towards “bio-friendly” plant protectants

“No one knows exactly how much food is lost on farms due to diseases and pests, whether measured in thousands of tons, or billions of dollars” (Pinstrup-Andersen, 2000; Flood, 2010).

The world’s ever-increasing population poses a large burden on agriculture and allied sectors to meet the demands for food security and safety (United Nations, 2022). This, coupled with anthropogenic activities, has had persistent negative effects on the environment. To meet the global demands for food production, agricultural productivity necessitates that it occurs either through an increase in crop yield, or by a reduction in crop loss due to biotic or abiotic stresses (Kumar, Ramlal, et al., 2021). The use of chemical pesticides (also referred to as fungicides, herbicides, or insecticides based on their intended use), while beneficial and intended to mitigate the costs of biotic stresses, have been proven to pose significant long-term risks to the environment and humans (Daraban, Hlihor & Suteu, 2023). According to Oerke et al., (2006), approximately one sixth of the global agricultural production is diminished annually by pathogens and pests pre-harvest, with additional loses in post-harvest storage (**Figure 1.1**) (Oerke, 2006; Flood, 2010; Bebber, Holmes & Gurr, 2014). Therefore, several alternative approaches to managing crop loss and reduced use of chemical pesticides have been explored extensively. One such attractive alternative are biopolymers as the current goal is to maximize output from depleting natural resources while safeguarding crops against post-harvest losses, all while minimizing adverse impacts on the environment (Kaur et al., 2012; Korbecka-Glinka, Piekarska & Wiśniewska-Wrona, 2022).

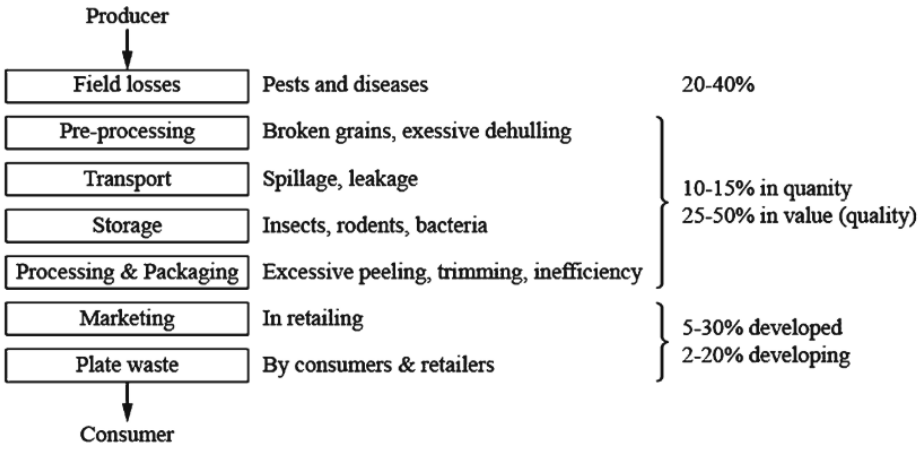

Figure 1.1: Pre- and post-harvest losses occurring throughout the food chain with an average of 35% of potential crop yield being lost to pests, pathogens, and disease. The additional losses after harvest account for an additional 35% loss. Figure adapted from Popp, Pető & Nagy, (2013).

Biopolymers or polysaccharides such as cellulose, carrageenan, laminarin and chitosan have been shown to be non-toxic, have multiple mechanisms of action (MoA), and exhibit broad-spectrum antimicrobial activity (Kaur et al., 2012; Korbecka-Glinka, Piekarska & Wiśniewska-Wrona, 2022). Chitosan and its derivatives possess the aforementioned favourable properties and is derived from the second-most abundant polymer in the world, chitin, thus making it an advantageous polymer of choice. To synthesize chitosan and its derivatives, chitin is processed by alkaline deacetylation to produce a polymer composed of N-acetyl glucosamine and glucosamine monomers/units (Verlee, Mincke & Stevens, 2017). The results are polymers of varying sequences, molecular weight (MW), solubility, degrees of deacetylation (DDA) and degrees of polymerization (DP) (see Section 2.2.1) (Verlee, Mincke & Stevens, 2017). The physiochemical properties of chitosan are such that it is insoluble in neutral aqueous solutions and requires a weak acid as a solvent, thus limiting its commercial use (Romanazzi, Feliziani & Sivakumar, 2018).

Various factors differentiating the solubility and biological activity of chitosan derivatives, notably the presence of reactive amine group(s) and the ratio of amine to N-acetyl groups (Liaqat & Eltem, 2018; Poznanski, Hameed & Orczyk, 2023). The reactive amine group(s) create a net positive charge and are proposed as integral to the MoA. This net positive charge allows chitosan to interact with anionic surfaces via strong electrostatic interactions (Kong et al., 2010). Thus, a derivative of chitosan namely, 6-deoxy-6-amino chitosan (herein referred to as aminochitosan), was synthesized to improve its water solubility and antimicrobial activity (Satoh et al., 2006). Aminochitosan is therefore water-soluble at neutral pH and is suspected to have improved biological activity compared to native chitosan (Sayed, Millard & Jardine, 2018). Despite there being a plethora of studies on chitosan and its derivatives, only a handful of studies are currently available for aminochitosan. Additionally, solubilizing aminochitosan in water according to the methods stated in these earlier studies have not been wholly successful (Satoh et al., 2006; Yang et al., 2012, 2015; Luan et al., 2018). However, aminochitosan synthesized by Sayed, Millard & Jardine et al. (2018) is proposed to have improved biological activity and solubility in water at a neutral pH.

Chitosan exerts its biological effects through a threefold mechanism involving antimicrobial activities, film-forming properties, and the activation of plant defence systems, specifically priming of plant defence (Xing et al., 2015; Romanazzi, Feliziani & Sivakumar, 2018). The mode

of action and resulting responses vary based on factors such as the pathosystem, microbial characteristics, environmental conditions, timing of application, and intrinsic and extrinsic physiochemical properties of chitosan (El Hadrami et al., 2010; Kong et al., 2010; Poznanski, Hameed & Orczyk, 2023). This is compounded by the significant differences in physiochemical properties between derivatives and batches of the biopolymer, especially since these have repercussions on efficacy.

Generally, the distribution of pathogens and the diversity within South Africa are dependent on socioeconomic and biophysical factors (Bebber, Holmes & Gurr, 2014). As such, two of the major pathosystems affected by fungal pathogens are tomato/*Botrytis cinerea* and maize/*Fusarium verticillioides*. As aminochitosan has not yet been investigated *in planta*, there is a knowledge gap to be filled. Furthermore, the profile of biopolymer-based plant protectants is lacking, and this poses a major obstacle to promoting them as viable alternatives to chemical pesticides, specifically around policy. Therefore, a more robust understanding of the MoA and the effects of biopolymer-based plant protectants could contribute to elevating their recognition among the public and policymakers (Kumar & Singh, 2015). This increased awareness may facilitate a better understanding of their role in promoting sustainability. The current objective is to maximize output from renewable natural resources while safeguarding crops against post-harvest losses, all while minimizing adverse impacts on the environment.

1.2 Thesis outline

As aminochitosan has not yet been investigated *in planta*, this is the first study to analyze its role as a protective priming agent in the tomato/*B. cinerea* and maize/*F. verticillioides* pathosystems. Additionally, as aminochitosan possesses an additional amino group, and a greater overall positive charge, we hypothesize that aminochitosan will demonstrate **superior biological activity compared to native chitosan, combining enhanced priming of plant defence responses with direct antifungal effects**. Moreover, as this is the first investigation into the effects of aminochitosan and its batch-batch variability in synthesis, **we hypothesize that there will be minor variations in the efficacy of the batches.** As molecular weight is a major definitive property of bioactivity of chitosan, **we hypothesize that the molecular weight variants of aminochitosan will display major variations in antifungal efficacy and *in***

planta **immunostimulatory**. Based on the literature on chitosan, **we hypothesize that the lower molecular weight variants will perform better in all applications**.

To examine these hypotheses, this PhD thesis has addressed the following research questions:

1. Are there batch-to-batch differences? If so, what are the contributing factors and the effects thereof?
2. Does aminochitosan offer dual protection against *B. cinerea* and *F. verticillioides* at the same concentrations?
3. What is the lowest concentration that achieves maximum biological activity, and does this differ for the antifungal efficacy compared to the *in planta* immunostimulatory efficacy?
4. Is aminochitosan effective both as a direct and systemic inducer of resistance?
5. Does priming occur in tomato and maize?
6. If priming occurs, what defence systems are induced after treatment with/without infection?

The research questions posed in this PhD thesis were systematically addressed, with each chapter delving into specific aspect(s):

Chapter 2 is an introductory chapter into chitosan and the defining physiochemical properties, the main MoA of chitosan according to these physiochemical properties and how this relates to plant-pathogen interactions, of which an overview will be given.

Chapter 3 examines aminochitosan in the dicotyledonous tomato/*B. cinerea* pathosystem with a focus on the batch-to-batch and molecular weight variants. Various concentrations were assessed for optimal antifungal efficacy, phenotypic variations *in planta*, effects of photosynthetic parameters *in planta*, and the accumulation of reactive oxygen species *in planta*. Finally, a chemical analysis of the elemental and molecular weight variants was assessed.

Chapter 4 aims to validate the results of Chapter 3 by label-free proteomic analysis of a batch-to-batch variant in the tomato/ *B. cinerea* pathosystem. Furthermore, Chapter 4 aims to

elucidate the temporal differences in the molecular mechanisms of priming, and protection of aminochitosan after treatment and with/without infection.

Chapter 5 further characterizes aminochitosan as a treatment in the monocotyledonous maize/*F. verticillioides* pathosystem and is achieved similarly to Chapter 3. However, the interaction between maize and *F. verticillioides* is first investigated by analyzing the tissue most affected by infection in seedlings (roots), the accumulation of mycotoxins and the induction of phytoalexins. Thereafter aminochitosan is assessed by analyzing its antifungal efficacy, *in planta* efficacy and priming through two different methods of application and a targeted metabolomic analysis of phytohormones.

Chapter 6 summarizes the main conclusions and situates them within the broader context of chitosan literature and plant protection. Finally, limitations, challenges, and research questions for coming research and challenges are discussed here.

This image was created with the assistance of DALL.E 2.

Chapter 2: General Introduction

2.1 Biopolymer-based protectants in agriculture

Phytopathogenic fungi pose a significant threat to food security and safety with ongoing economic losses today (Oerke, 2006; Raj et al., 2011). Although commonly controlled with synthetic fungicides (currently 230 available compounds/fungicides), the substantial growth in international concerns over the indiscriminate use of synthetic fungicides and their negative effects (**Figure 2.1**) on terrestrial and aquatic ecosystems, non-target organisms, and human health effects have warranted the development and use of alternative protectants that are cost-effective and contribute towards sustainable agricultural practices (De Waard, 1993; Sharma et al., 2020; Korbecka-Glinka, Piekarska & Wiśniewska-Wrona, 2022).

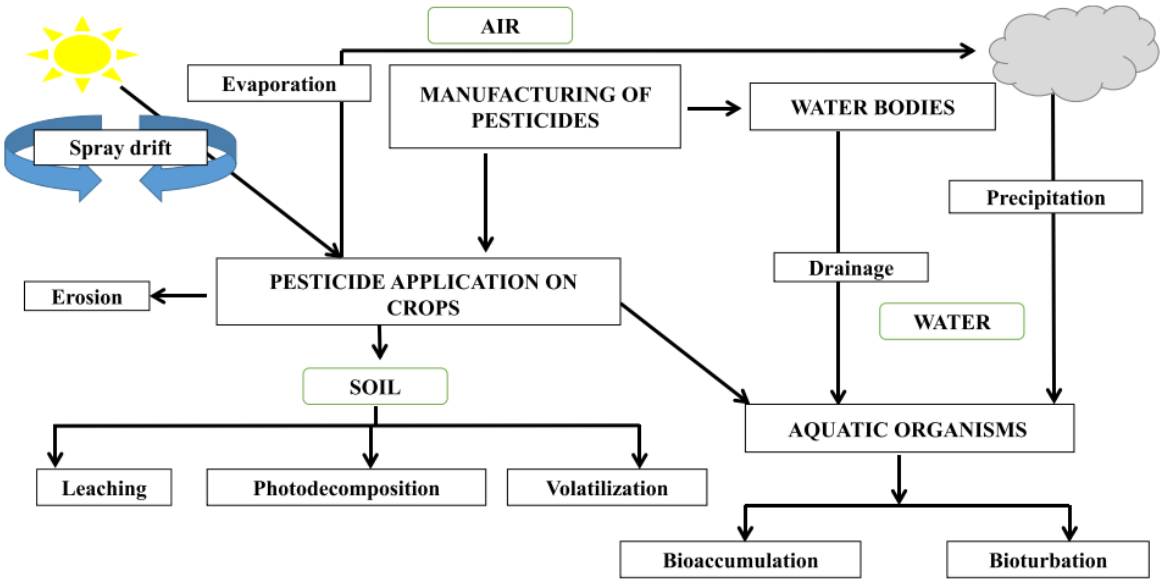

Figure 2.1: A flow chart depicting the exposure to chemical pesticides/fungicides. Adapted from Sharma et al. (2020).

Biopolymers are defined as naturally occurring polymers/macromolecules synthesized by living organisms (plants, animals, microorganisms) or "chemically synthesized from a biological starting material" and include proteins, nucleic acids (DNA/RNA), and the polysaccharides starch, pectin, cellulose, hemicellulose, chitin and chitosan to name a few (Raj et al., 2011; Kaur et al., 2012; Smith, Moxon & Morris, 2016). As such, they are utilized in a variety of industries including biotechnology, biofertilizers, biocontrol agents, waste treatment, medical technology, genetic engineering and agriculture (Kaur et al., 2012). The terms biopesticides, biopolymers, and biocontrol agents are often used interchangeably while slight nuances exist between these concepts.

Biopesticides are defined as being derived from “natural materials [such] as animals, plants, bacteria, and certain minerals” and are categorized as biocontrol agents (organisms such as bacteria, fungi, and viruses, the active mechanisms of protection), plant-incorporated protectants (e.g. transgenes in plants that produce protective compounds) and biochemical pesticide (substances that occur naturally and protect against pests and pathogens in a non-toxic manner) (Kumar, Ramlal, et al., 2021; Liu et al., 2021). Biocontrol agents are distinct from biopolymers in that biopolymers refer to large molecules synthesized by living organisms while biocontrol agents are the living organisms intentionally used to control pathogens, pests, diseases, or weeds (Kaur et al., 2012; Liu et al., 2021). Therefore, biocontrol agents are a type of biopesticide while biopolymers can be used for the development and formulation of biopesticides in combination with biocontrol agents, as seen in **Figure 2.2**. However, the common defining feature between these three concepts is that they are all alternative management methods to chemical pesticides (in agriculture).

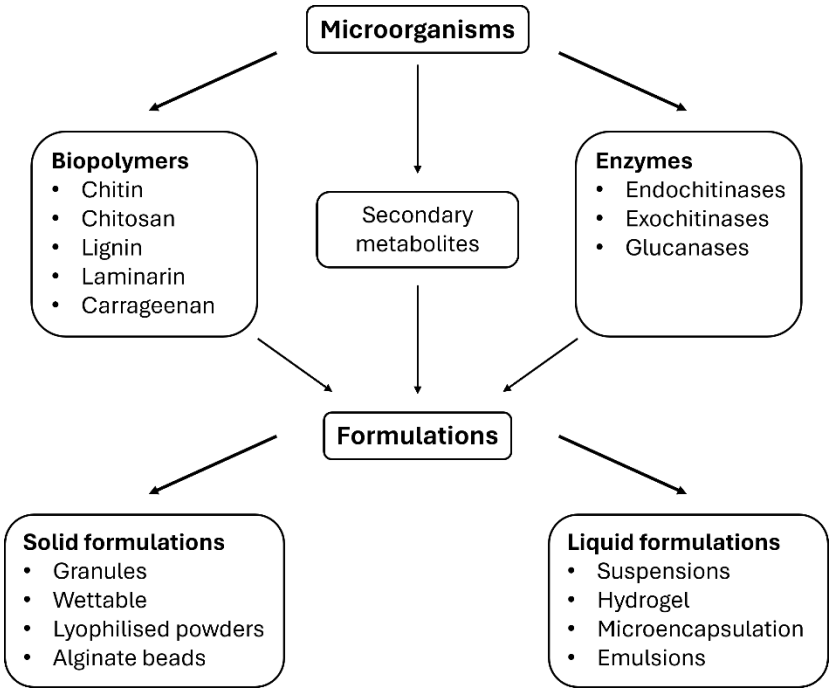

Figure 2.2: Different biocontrol strategies formulated against pathogens, adapted from Kaur et al. (2012).

Furthermore, the use of biopolymer-based fungicides or pesticides in managing plant-pathogen/pest interactions is beneficial over synthetic chemical compounds for the following reasons as highlighted by Kaur et al. (2012) and Kumar, Ramlal et al. (2021): can be used directly against phytopathogens, are non-toxic, cost efficient and cheaper compared to chemical pesticides, environmentally friendly (biodegradable, no bioaccumulation or contamination of water sources), can be combined with different biocontrol agents or

chemical fungicides, elicitor of plant defence system, the formulation can be readily manipulated and regulated at an industrial level, are comparatively stable, easy to store and transport and are much less restrictive as compared to live or whole organism for commercialization (Kaur et al., 2012; Kumar, Ramlal, et al., 2021). However, despite the aforementioned advantages, the use of biopolymers has been limited.

The challenges associated with biopolymers, as outlined by Malerba & Cerana (2019) and Gericke et al. (2024), underscore the complexity in their adoption. These challenges include formulation hurdles in achieving optimal ratios of active and inert ingredients, variability in preparation methods and testing standards, as well as inconsistencies in biophysical properties leading to unpredictable efficacy and shelf life (Malerba & Cerana, 2019; Gericke et al., 2024). Moreover, issues such as limited field trials, high production costs, registration requirements, and competition with synthetic pesticides further impede their widespread acceptance, especially among small-scale growers and policymakers. In light of these obstacles, De Waard et al.'s (1993) proposition regarding fungicide operation provides context for understanding the persistent reliance on conventional chemical controls despite the potential benefits of biofungicides. They suggest that by mitigating lesion development on host plants, alternative disease control compounds could serve as viable substitutes for fungicides, potentially improving the environmental sustainability of disease management practices. Their conclusion implied the activation of plant defence mechanisms alongside direct antifungal action. One such biofungicide that fulfills all the aforementioned criteria is that of chitosan.

2.2 Chitosan and its derivatives

2.2.1 Chitosan in the global market

Chitin and chitosan (CHT) have long been acknowledged for their beneficial properties, undergoing an exploration phase from 1930 to 1970 (Crini, 2019). Their industrial production and application commenced in 1971 and has continued to evolve and expand to the present day as seen by the growing number of publications in the fields of pharmaceuticals, biomedical, cosmetics, food, textiles, paper, enzymes, and more specifically, in the field of agriculture (**Figure 2.3**) (Crini, 2019; Li et al., 2020). These commercial applications are evidenced by the market of chitosan products which is valued at USD 4700 million with a

growth of ~5% each year and an expected compound annual growth rate of 17.3% between 2022 and 2030, to reach a market value of USD 15.1 million (Vieira et al., 2023).

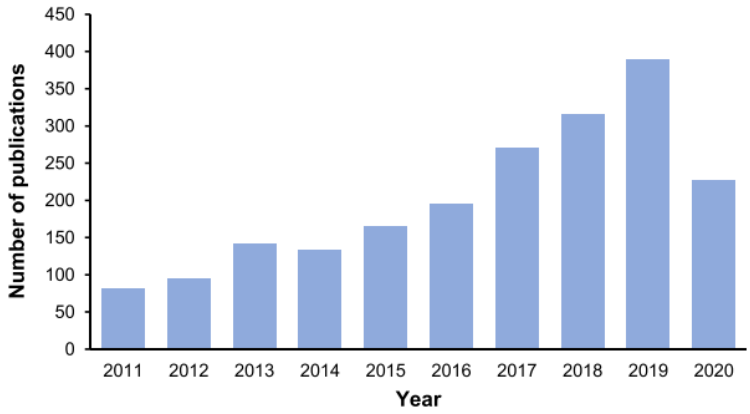

Figure 2.3: The number of publications on "chitin in agriculture" and "chitosan in agriculture" between the years of 2011 to September 2020 highlights the tremendous growth in the exploration of chitin and chitosan as a crop management strategy. Adapted from Li et al. (2020).

The substantial market value attributed to chitin stems from its status as the second most abundant polysaccharide, with arthropods (such as insects, crustaceans, and arachnids), mollusks (including squid pen beaks and cuttlefish bones), fungi (such as *Aspergillus niger, Penicillium notatum/chrysogenum*, and *Saccharomyces gutulata),* and algae (including diatoms and blue/brown algae) contributing to its production in volumes ranging from 10^{10} to 10^{11} tons (Hamed, Özogul & Regenstein, 2016; Yadav et al., 2019). The commercial and industrial utilization of CHT and its derivatives primarily relies on the approximately 10,000 tons of exoskeleton waste generated by the seafood processing industry (Yadav et al., 2019; Poznanski, Hameed & Orczyk, 2023). Nevertheless, the broader application of CHT has been hindered by challenges related to solubility in polar and water solvents. To address this limitation, researchers have delved into chemical and enzymatic modifications aimed at altering the physiochemical properties of CHT (Harish Prashanth & Tharanathan, 2007).

2.2.1 The chemistry of chitosan: molecular weight, degree, and pattern of deacetylation dictate its charge and bioactivity

The biological activity (bioactivity) of CHT is highly dependent on its physicochemical properties, primarily determined by its structure. CHT is derived from chitin through alkaline deacetylation resulting in a cationic polymer composed of D-glucosamine (GlcN) and N-acetyl-D-glucosamine (GlcNAc) monomers arranged in a random sequence. As depicted in **Figure 2.3A**, both chitin and CHT possess three reactive functional groups: primary and secondary

hydroxyl groups (at C-2, C-3, and C-6) and an acetamide group (in chitin) or an amino group (at C-2 for the deacetylated units of CHT only), which allow for modifications (Brasselet et al., 2019). The potential to modify these reactive functional groups enables a wide range of applications as these groups contribute to significant differences in physiochemical properties, particularly solubility.

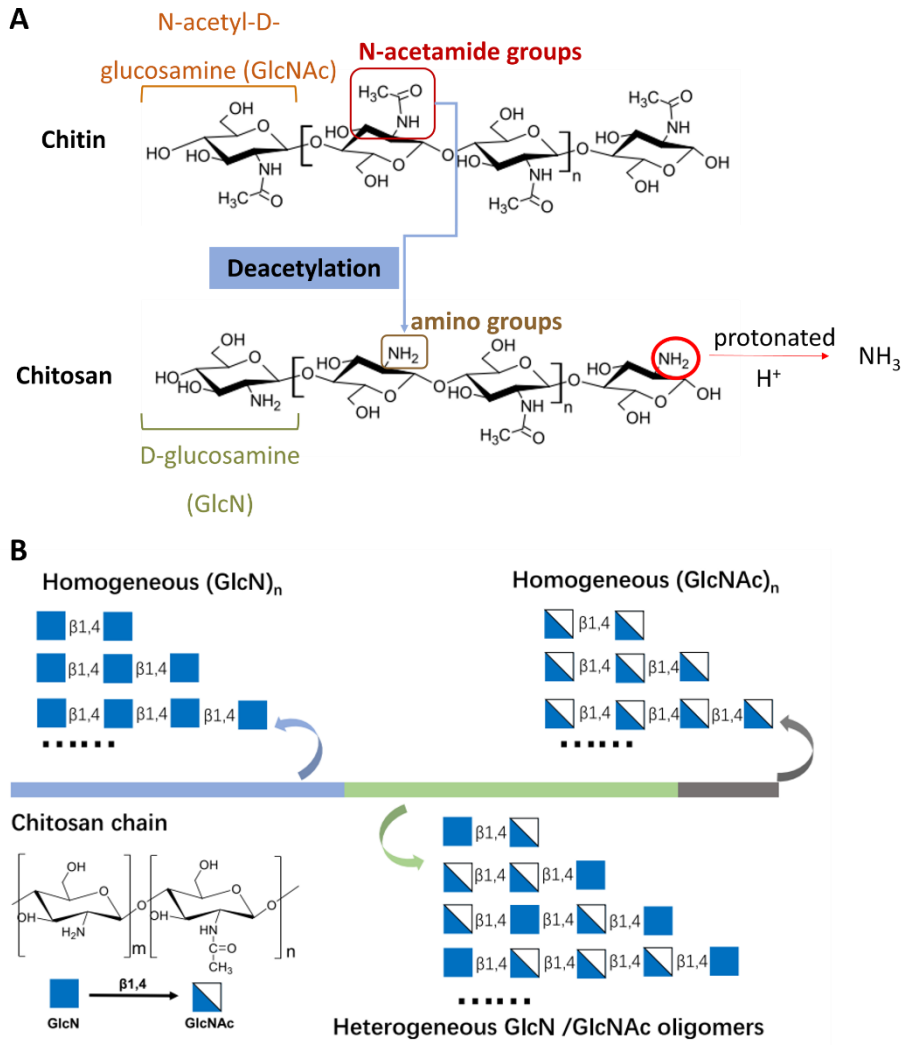

Figure 2.4: A) Primary structure of chitin and CHT. The chemical structures are adapted from Brasselet et al. (2019). **B)** Possible CHT monomers in a CHT chain after deacetylation. Blue represents GlcN and white represents GlcNAc. Figure 2.3B was adapted from Li et al. (2020).

The difference in the number of acetylated units between chitin and CHT significantly influences their functionality. Chitin, with more than >70% acetylated units, exhibits low aqueous solubility in most solvents as well as limited bioactivity due to this limited solubility (Sayed, Millard & Jardine, 2018). As a consequence, CHT and derivatives have dominated in various applications across a range of fields as opposed to chitin. As highlighted, CHT's solubility, bioactivity, and biodegradability are characterized and dependent on its structural characterization. One such crucial structural factor is the number of protonated amino groups,

or the ratio of deacetylated to acetylated units (GlcN:GlcNAc), otherwise known as the degree of deacetylation (DDA). CHT, with its higher ratio of acetylated units, displays insolubility in aqueous solutions but solubility in weak acidic solutions (1%/0.1 M) due to complete protonation of amino groups at pKa < 6.2 (Lodhi et al., 2014).

Another key structural feature, as illustrated in **Figure 2.3B**, is the heterogeneity of the polymer chain resulting from the random deacetylation process whereby some monomers are still acetylated (Li et al., 2020). This result is known as the pattern of acetylation (PA) and may present as homogenously GlcN or heterogenous with a random sequence of GlcN and/or GlcNAc (**Figure 2.3B**). Thus, it is important to note that "chitosan" does not denote a uniquely defined compound; rather, it encompasses polysaccharides with varying compositions of GlcNAc and GlcN units (Badawy & Rabea, 2011).

These structural factors significantly impact the molecular weight (MW) of CHT, which, in turn, influences solubility and ultimately bioactivity, as demonstrated in **Figure 2.5**. Badawy and Rabea, (2011) noted that the mean MW and polydispersity of CHT can vary considerably among preparations. Polydispersity refers to the distribution or spread of MW sizes within a CHT polymer. Typically, the MW of CHT is a combination of larger and smaller MW chains, indicating higher polydispersity, while more uniformity in chain lengths suggests lower polydispersity (Brasselet et al., 2019). However, a common challenge noted in the literature is the lack of consensus regarding the definitions of chitooligosaccharides/oligomers/low (often used interchangeably) and medium or high MW CHT (Verlee, Mincke & Stevens, 2017). This ambiguity complicates discussions surrounding CHT's MW and its implications for various applications. For example, Poznanski, Hameed, and Orczyk (2023) categorized CHT batches as four groups: very low, low, medium, and high MW. Here, the very low MW batches were defined as oligomers, while low MW batches were defined as having an average MW below 100 kDa. Medium MW batches were defined as ranging from 100 to 1000 kDa, and high MW batches as comprising sizes that exceeded 1000 kDa. In contrast, Poznanski, Hameed, and Orczyk (2023) and Verlee, Mincke & Stevens, (2017) presented a different categorization/definitions of the various MW ranges. They instead defined CHT as oligo-chitosan when the MW was ≤ 16 kDa, corresponding to approximately 100 monomeric units of 100% deacetylated CHT. Furthermore, they classified low MW CHT as ranging from > 16-190 kDa, medium MW from > 190 - 300 kDa, and anything > 300 kDa as high MW. These

varying definitions of MW categories and definitions demonstrate the challenge in standardizing terminology to allow for comparisons to be drawn across studies in the CHT literature.

In addition to DDA and MW, CHT polymers are also typically assessed based on their degree of polymerization (DP). This property signifies the count of monomeric units within a CHT chain, dictating its length, with the transition from CHT oligomers to polymers typically assumed around a DP of 20 (Lodhi et al., 2014; Lemke, Jünemann & Moerschbacher, 2022). Although it is difficult to deduce a single definition of a CHT oligomer, one working definition is that of Liaqat & Eltem, (2018) who defined CHT oligomers as having a DP of below 20 and an average MW greater than 3.9 kDa. Additionally, it has been demonstrated that the bioactivity of low MW CHT (a MW of <10 kDa) exhibits greater antimicrobial activity than native CHT (Badawy & Rabea, 2011; Liaqat & Eltem, 2018). However, in addition to the lower MW, a DP of at least seven is also required as lower MW fractions with DP < 7 were shown to have little or no activity (Badawy & Rabea, 2011; Liaqat & Eltem, 2018). Thus, the characteristic properties of CHT are interconnected and impart an additional layer of complexity on the bioactivity of CHT (**Figure 2.4**) and are in part addressed in the addendum of Chapter 3. Figure 2.4 depicts the factors that contribute to the variations in CHTs efficacy and bioactivity and the interconnected of these parameters.

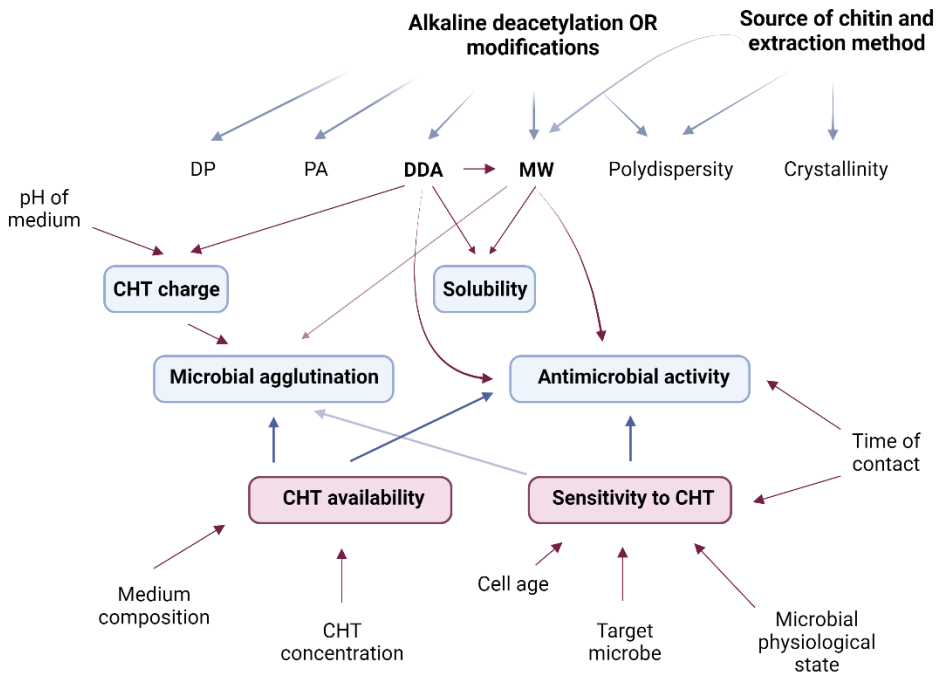

Figure 2.5: The parameters affecting the physiochemical properties of CHT and in turn, the bioactivity. This figure depicts this multiplicity /interconnectedness. Arrows indicate a relationship. DP = degrees of polymerization, PA = pattern of acetylation, DDA = degree of deacetylation, MW= molecular weight. This figure was adapted from Kong et al. (2010) and Brasselet et al. (2019) and created in BioRender.com.

An effective approach to improve both the solubility and bioactivity of CHT involves modifying the reactive groups towards adjusting the GlcN:GlcNAc ratio (DDA) and the MW (Verlee, Mincke & Stevens, 2017). Therefore, the physicochemical properties driving the observed bioactivity of CHT warrant further investigation, particularly considering their intrinsic link to the source of chitin and the methods of extraction utilized (Brasselet et al., 2019). Furthermore, due to these variations in sources between batches and the random nature of alkaline deacetylation, differences in CHT properties are inevitable across batches, despite stringent processing regulations and protocols. In this thesis, Chapter 3 addresses the effects of batch-to batch variations.

2.2.3 6-deoxy-6-amino chitosan (aminochitosan)

Numerous modifications and derivatives of CHT have been synthesized with the aim of achieving a commercially-available water-soluble derivative through chemical derivatization. Since the DDA of CHT is directly correlated with the number of positive charges and solubility, a logical expectation would be that an increase in the DDA would yield a polymer with the most favorable properties (Moran et al., 2018). Therefore, the addition of an amine-group at the C-6 position of CHT has led to the synthesis of a water-soluble (neutral pH) CHT derivative, 6-deoxy-6-amino chitosan, herein referred to as aminochitosan (**Figure 2.6**) (Satoh et al., 2006; Yang et al., 2012; Sayed, 2018). Aminochitosan therefore possesses a higher DDA and positive charge density (the degree of protonation of amino groups), due to a higher degree of substitution (DS) where DS denotes the number of -OH (or other) groups substituted with amine groups per glucosamine unit (Kong et al., 2010). Sayed, Millard & Jardine, (2018) developed a protocol for synthesizing aminochitosan using a greener, shorter, and more scalable pathway. This method avoids hazardous chemicals and generates less waste compared to previous synthesis protocols. Thus, aminochitosan's aqueous solubility is highly advantageous and facilitates a broader range of applications, particularly in agriculture (Sayed, Millard & Jardine, 2018).

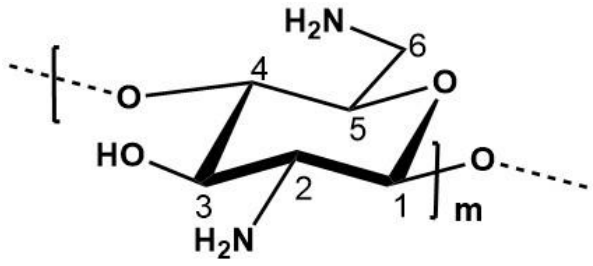

Figure 2.6: Molecular structure of aminochitosan. This image was sourced from Sayed (2018).

2.3 Plant-pathogen interactions and plant immunity

To ensure survival, plants need to be able to both perceive and enact a timely and rapid evasion or counteractive response to a range of pathogen attacks. Consequently, plants have evolved sophisticated signaling and defence systems that provide both basal and adaptive immunity to a broad and specialized range of pathogens (Huot et al., 2014). However, the induction of defence is not without its energetic and resource costs which have been associated with reduced growth as a result of a decrease in photosynthesis and a general diversion of resources from growth to defence (Huot et al., 2014). Therefore, a balance between growth and defence is necessary to ensure optimized plant fitness (Huot et al., 2014).

To respond to various stresses or triggers, whether they be extracellular or intracellular, plants modulate their innate immune system based on the mechanisms of attack and lifestyle of the pathogen (Nishad et al., 2020). These plant pathogens are typically classified into two lifestyles: necrotrophic pathogens, which destroy host cells using phytotoxins and cell-wall-degrading enzymes before consuming the contents, and biotrophic pathogens, which acquire nutrients from living host tissues through specialized feeding structures (Glazebrook, 2005). Some pathogens may also exhibit both lifestyles at different stages of their life cycle and are termed hemi-biotrophs (Glazebrook, 2005; Pieterse et al., 2012).

2.3.1 Plant immunity models

The recognition and response to these pathogens is described by several models with the most well known being the ‘zig-zag model’ proposed by Jones and Dangl (2006), which describes a constant coevolution between plants and pathogens. In this model, recognition of conserved structural molecular patterns of pathogens or microbes (PAMPs or MAMPs) are recognized by host pattern recognition receptors (PRR) on the cell surface, leading to PAMP/MAMP triggered immunity (PTI or MTI). However, if the pathogen is successful in its

invasion, it utilizes effector proteins to obstruct PTI, thus inducing effector triggered susceptibility. The recognition of these effectors by plant resistance genes (R genes) subsequently lead to effector triggered immunity (ETI) (Jones & Dangl, 2006). However, since the proposition of this model, many adjustments have been made towards a more inclusive one. This is due to the model's difficulty in application to necrotrophs and its failure to integrate previous pathogen attack events (Cook, Mesarich & Thomma, 2015).

One such inclusion is that of damage associated molecular patterns (DAMPs), patterns of the host itself that are due to damage caused by pathogens (van der Burgh & Joosten, 2019). Further accommodations were made to blur the divisions between the strict use of the terms and models and to include all possible patterns and invasion patterns (IPs) in the 'invasion model' suggested by Cook et al. (2015). In this model, recognition of IPs through IP receptors (IPRs) results in an IP triggered response (IPTR). This response either leads to continued symbiosis (successful defence) by failure to suppress or the exploitation of IPTR (e.g. necrotrophic). Alternatively, it may result in the cessation of symbiosis by IPTR suppression (e.g. biotrophic). This model also attempts to account for multiple recognition events and invader strategies (Cook, Mesarich & Thomma, 2015). However, the latest model suggested by van der Burgh & Joosten, (2019) is that of the 'danger model'.

Here, the distinction between different types of plant immune responses is abolished and instead, the attack is framed by the location of where the 'danger signal' is recognized. As such, recognition of extracellular immunogenic patterns (ExIP) lead to extracellular triggered immunity (ExTI) or intracellular triggered immunity (InTi) by the recognition of intracellular immunogenic patterns (InIP) (van der Burgh & Joosten, 2019).

2.3.2 Plant defence mechanisms against pathogens

This section will not be exhaustive and will instead aim to summarize key contributing mechanisms to plants defence. As mentioned above, the pathogens lifestyle affects the mechanisms of plant defence, evasion or endurance when affecting host plants within a pathogens host range. However, pathogen evasion may also occur through non-host resistance, which allows plants to resist pathogens that fall outside of their typical range and has been described as "more durable" due to the presence of various elicitors/effectors and the involvement of multiple resistance traits (Hadwiger & Tanaka, 2017). This contrasts to the

Jones and Dangle model where the plant receptor proteins must have a broad gene bank to match the diverse effectors they encounter (Isaac et al., 2009; Hadwiger & Tanaka, 2017).

The plant innate immunity comprises both local and systemic responses and is composed of several defence mechanisms which are categorized as being either pre-existing, basal, part of non-host resistance, or induced (Doughari, 2015; Reimer-Michalski & Conrath, 2016). The pre-existing structural defence mechanisms are often basal structures that present physical or structural barriers to pathogen entry in addition to providing strength and rigidity. These include but are not limited to, the epidermis, waxy layer, cuticle, cell wall, and guard cells, stomata, and lenticels (Doughari, 2015). These pre-existing biochemical defence mechanisms are either constitutively expressed in plants (important for physiology) or are formed in response to biotic stress. Examples of these biochemical compounds include antimicrobial compounds such as secondary metabolites, terpenoids, polyamines, alkaloids, flavonoids, and cyanogenic glycosides; toxic inhibitors such as phenolics, saponins, glucanases, chitinases, reactive oxygen species (ROS), nitric oxide (NO); phytoanticipins like quinones, steroids, glycoalkaloids, and glucosinolates; and phytohormones such as auxins, cytokinins, salicylates, jasmonates. These biochemical compounds may act as signaling molecules after the recognition of an attack and are key in the activation of downstream signaling cascades and defence responses (Caarls, Pieterse & Van Wees, 2015). Moreover, plants rely on individual cells to trigger innate immunity, serving as both sources of systemic signals and possessing the capacity to retain memory of prior infections (Reimer-Michalski & Conrath, 2016). These pathways can be directly activated by signal recognition in tissue initially affected/stimulated, otherwise known a localized acquired resistance, or in systemic tissue (tissue situated distal from the site of the initial attack) through induced resistance, resulting in a broad range of protection in the entire plant (Conrath, 2009; Pieterse et al., 2014).

Generally involved in the modulation of growth and development, plant hormones (phytohormones) are also induced following the activation of plant defence mechanisms, or other early molecular recognition events where they play crucial roles in initiating the plant immune signaling network both locally and systemically (Pieterse et al., 2012). Typically, jasmonic acid (JA) and ethylene (ET) activate resistance against necrotrophic pathogens while salicylic acid (SA) signaling induces resistance against biotrophic and hemi-biotrophic pathogens, the two groups often showing antagonistic relationships (Robert-Seilaniantz,

Grant & Jones, 2011). Furthermore, hormones such as JA, ET, abscisic acid (ABA), gibberellins (GAs), auxins, cytokinins (CKs), brassinosteroids, and nitric oxide (NO) are also recognized as modulators of the plant immune signaling network (Pieterse et al., 2012). These hormonal interactions, known as hormone cross-talk, finely regulate immune responses in a cost effective-manner, determining tissue susceptibility or resistance to invading organisms and demonstrating the plant's adaptive capacity (Pieterse, Ton & Loon, 2001; Pieterse et al., 2012).

Another key signaling mechanism in plant responses to biotic and abiotic stresses involves the rapid and transient production of reactive oxygen species (ROS) through an oxidative burst (Tripathy & Oelmüller, 2012). ROS play essential roles as signaling molecules, regulating growth, development, and responses to environmental stimuli, particularly in defence against pathogens (Das & Roychoudhury, 2014). Generated primarily in cellular compartments such as chloroplasts, mitochondria, and peroxisomes, ROS includes free radicals like O^{-2}, OH, and non-radicals such as H_2O_2 and $^1O_2$, with the apoplast serving as an additional site of ROS generation. In favorable conditions, plants produce ROS at basal levels, efficiently scavenged by antioxidant mechanisms such as superoxide dismutase (SOD), catalase (CAT), and non-enzymatic compounds such as ascorbic acid and glutathione (Tripathy & Oelmüller, 2012; Das & Roychoudhury, 2014). However, the delicate balance between ROS generation and scavenging can be disrupted by various stress factors, resulting in oxidative stress and damage, characterized by elevated levels of ROS that can damage cells and eventually lead to cell death (Tripathy & Oelmüller, 2012; Das & Roychoudhury, 2014). As such, ROS play a dual role: they serve as inevitable by-products of aerobic metabolism while also acting as markers during stressful conditions, triggering stress-signaling components to prevent further damage (Tripathy & Oelmüller, 2012; Das & Roychoudhury, 2014).

Similarly, Rojas et al. (2014) highlights the intricate interplay between primary metabolic pathways and defence responses in plants, including the upregulation of defence-related pathways that are often accompanied by the downregulation of genes associated with photosynthesis and chlorophyll biosynthesis (Bilgin et al., 2010; Rojas et al., 2014). This metabolic shift from source to sink likely facilitates the allocation of energy towards defense-related processes, enhancing the expression of defense-related genes and the production of secondary metabolites (Rojas et al., 2014). It also potentially reallocates nitrogen resources towards defense responses, necessitating a rebalancing of protein levels and a redirection of

energy towards defense mechanisms (Bilgin et al., 2010). Additionally, the upregulation of specific metabolic pathways, such as glycolysis and the tricarboxylic acid cycle, highlights the pivotal role of primary metabolism in supporting induced plant defence responses (Rojas et al., 2014).

2.3.3 Priming and plant protection

Induced resistance (IR) is a plant's enhanced defensive state, activated by specific environmental cues such as chemical or biological inducers which confer protection to "nonexposed parts against future attack by pathogenic microbes", thus decreasing the plants susceptibility to future pathogen attacks (Pieterse et al., 2014; Vieira et al., 2023). Systemic acquired resistance (SAR) and induced systemic resistance (ISR) are two distinct forms of this enhanced defence mechanism. They involve pre-conditioning plant defences through prior infection or treatment, resulting in increased resistance against a broad range of pathogens (Vieira et al., 2023). This heightened state of resistance is a physiological response to specific stimuli, effectively countering subsequent biotic challenges. However, SAR and ISR differ based on the nature of the elicitor, the regulatory pathways involved and the organism (Choudhary, Prakash & Johri, 2007; Hönig et al., 2023).

SAR is generally associated with pathogen attack and the accumulation of SA (though not solely dependent) and the upregulation of SAR genes producing the pathogenesis-related (PR) proteins (Hönig et al., 2023). Conversely, ISR is associated with root colonization by beneficial microbes and the accumulation of the phytohormone JA and ET (Conrath, 2009; Hönig et al., 2023). However, the mobile signals associated with the activation of SAR remain speculative (Fu & Dong, 2013). The compounds known to elicit ISR include lipopolysaccharides, cellulases, flagella, siderophores, as well as proteins and peptides with defence activating functions (Pieterse et al., 2014). Unlike ISR, SAR involves defence PR genes while ISR is generally not dependent on pathogen attack and the expression of defence genes, as this would result in high fitness costs. Therefore, a common feature for the resistance responses in both ISR and SAR is through 'priming' as SAR responses can be primed by chemical compounds for stronger SA-dependent defence responses (Conrath et al., 2006, 2015; Hönig et al., 2023). IR can be a result of both direct and primed defence responses and does not exclude systemic effects at a local site of infection (Vieira et al., 2023).

Priming, on the other hand, is the induction of physiological, epigenetic and metabolic changes upon an initial priming stimulus, otherwise known as the 'primed state', and is followed by a faster and/or stronger defence response in subsequent exposures to a triggering stimulus, therefore increasing the capacity for defence and resistance in local or systemic tissue (Conrath et al., 2015; Mauch-Mani et al., 2017; Hönig et al., 2023). Thus, the trade-off between resistance and defence costs are overcome by priming. As mentioned earlier, chemical compounds whether endogenous or exogenous and of both artificial (synthetic or non-organismal) and natural origin, can be termed priming stimuli. Additionally, the stress itself, an indicator of an impending stress or a beneficial organism are equally considered priming stimuli. The resulting 'primed state' and the effects thereof may be transient, sustained in a single life cycle or transgenerational, indicating an epigenetic component (**Figure 2.7**). Therefore, "the information of the priming stimulus is stored, eventually until exposure to a triggering stimulus" thus creating a "memory" (Martinez-Medina et al., 2016). Priming is considered adaptive and generally low cost to fitness. During the primed stare, defence responses are marginally and transiently induced by the priming stimuli which instead promote a permanently heightened state of defence awareness. Moreover, the absence of a subsequent triggering stimulus in primed plants only results in marginally activated defence responses (Martinez-Medina et al., 2016).

Priming has been show to regulate the biosynthesis of phytoalexins, phytohormones (SA, JA and ET), defence proteins, ROS, lignin and callose deposition, the activation of MAP-kinases; hypersensitive response, elevated levels of PRRs, dormant cellular signalling enzymes and proteins, changes to chromatin, and histone modifications in defence gene promoters (Rabea et al., 2003; Raafat et al., 2008; Goy, Britto & Assis, 2009; Iriti et al., 2009; Hadwiger, 2013; Conrath et al., 2015; Hönig et al., 2023). Distinguishing between naïve (unprimed plants) and primed plants is challenging as improved plant performance under attack does not necessarily reflect a primed state as there are several mechanisms by which plants regulate their defence (**Figure 2.7**). Therefore, as stated by Martinez-Medina et al., (2016), priming, allocation and ecological costs as well as the supporting phenotypic analysis of the defensive state need to be determined in naïve-primed, naïve-triggered, and primed and triggered plants, specifically near the end of the memory-retaining period. The aforementioned is addressed in Chapters 3 (phenotypic analysis) and 4 (temporal priming). Allocation costs are "fitness losses caused by

allocation of metabolic resources toward defence that would otherwise have been allocated to growth and reproduction" and "ecological costs occur when fitness-relevant interactions of an organism with its natural environment are impaired" (Martinez-Medina et al., 2016). Van Hulten et al. (2006) determined that low doses of b-aminobutyric acid (BABA) induced a primed state with minor growth reduction in contrast to direct induction of defence by high doses of BABA which strongly affected these fitness parameters (van Hulten et al., 2006).

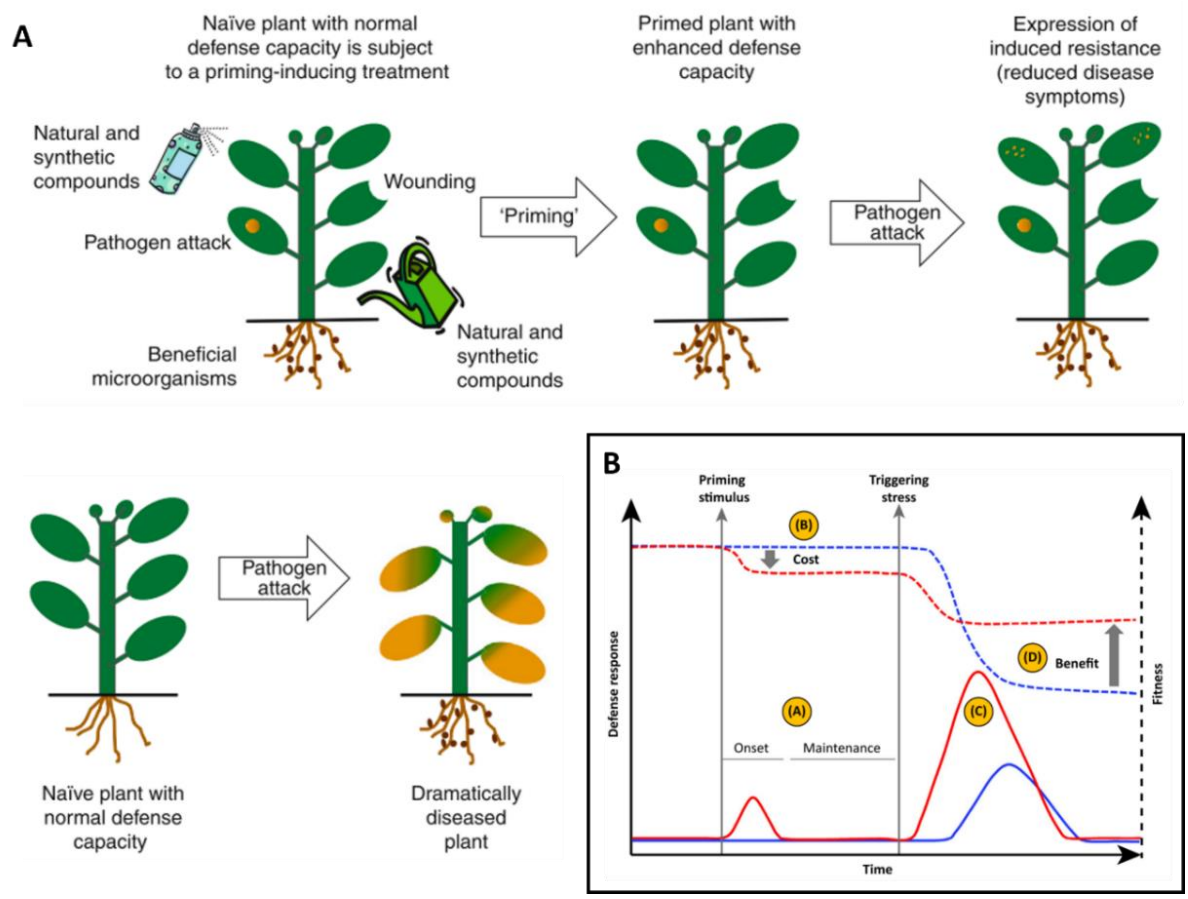

Figure 2.7: A) Different priming stimuli cause a primed state in which primed conditions respond with more robust, and/or rapid induction of defence responses upon a triggering stimuli like pathogen attack. This enhanced fitness, resistance and reduction of disease symptoms are absent in naïve/non-primed pants. Adapted from Conrath (2009). **B)** Graph representing the defence responses (solid lines) and plants resources (dashed lines) in primed (red line) and non-primed plants (blue line). (A-B) Depicts the low resource cost of priming after a priming stimulus, as defence is induced at a low level, transiently. (C) After a triggering stimulus, primed plants exhibit a more intense defence response than non-primed plants as primed plants mobilize cellular defence in a faster, earlier, stronger, and/or more sustained manner than do unprimed plants. (D) Better performance: primed plants are expected to defend better against a given stressor than unprimed plants. Therefore, priming enhances plant fitness in hostile environments. Adapted from Martinez-Medina et al. (2016).

Priming stands out as a promising strategy for effective plant protection in agriculture, capitalizing on plants' inherent broad-spectrum defence capabilities (Ameye, 2017). This

approach, unlike direct defence activation, minimizes developmental costs while enhancing resilience against a range of stressors. However, careful consideration of optimal stimulation levels is crucial to avoid potential drawbacks such as unintended direct resistance induction, which could impact overall fitness (Mauch-Mani et al., 2017).

2.4 Chitosan in crop protection

CHT's biological activities are actioned through a triple-acting system of direct antimicrobial activities, film-forming properties and the activation or enhancement of plant defence systems and have been reviewed extensively against several economically important crops and pathogens (Rinaudo, 2006; Hernández-Lauzardo et al., 2008; Goy, Britto & Assis, 2009; El Hadrami et al., 2010; Kong et al., 2010; Badawy & Rabea, 2011; Xing et al., 2015; Romanazzi, Feliziani & Sivakumar, 2018). The following section briefly highlights some of the proposed MoA for both CHT's antifungal activity and *in planta* immunostimulatory activity.

2.4.1 Chitosan's mechanism of action against microorganisms

As highlighted in **Figures 2.5**, the MoA and responses thereto are dependent on the intrinsic physiochemical properties of CHT which include MW, DDA, DP, and positive charge density (number of positive charges distributed along the length of the polymer due to protonation, determined by MW, pH and ionic strength)(Kong et al., 2010; Badawy & Rabea, 2011). Other properties not relating to the intrinsic properties affecting the bioactivity, termed extrinsic physiochemical properties, include microbial factors (life cycle stage, cell age, cell wall/membrane composition etc.), environmental factors (pH of the solvent, time spent and temperature in storage), the plant/pathogen pathosystem, physical state/formulation of chitosan (nanoparticles, hydrogels, microspheres), concentration and the starting material and chemical/enzymatic processing to obtain CHT (El Hadrami et al., 2010; Kong et al., 2010; Poznanski, Hameed & Orczyk, 2023). However, conflicting reported results have created ambiguity regarding the influence of physiochemical properties on the antimicrobial activity of CHT with many varying hypotheses (some confirmed and others not) on the MoA (Badawy & Rabea, 2011). In general, these studies regard CHT as either bactericidal (killing live bacteria or a portion of them) or bacteriostatic (inhibiting bacterial growth without necessarily killing them), often without distinguishing between the two effects (Goy, Britto & Assis, 2009).

Recent literature tends to classify CHT more as bacteriostatic rather than bactericidal (Goy, Britto & Assis, 2009).

The molecular mechanisms underlying the antimicrobial activity of CHT and its oligomers are extensive and sometimes contradictory, yet they concur that one of the main proposed and accepted MoA is the interaction between positively-charged pronated amino groups of CHT and the negatively-charged molecules, phospholipids, or metals found on cell walls or membranes of microorganisms through electrostatic interactions (presumably competing with other polycations like Ca^{2+}) (Palma-Guerrero et al., 2010; Verlee, Mincke & Stevens, 2017 and the references therein). Here, the interaction causes permeabilization of the cell membrane, leading to internal osmotic imbalances due to potential leakage of internal materials and consequently, the inhibition of microorganism growth (Goy, Britto & Assis, 2009; Verlee, Mincke & Stevens, 2017). Another proposed MoA is the entry of CHT into the cell nuclei where it is presumed that CHT enters the cell after aforementioned cell membrane permeabilzation. Following entry into the nuclei, CHT is proposed to interact with chromatin, DNA, and RNA (Hadwiger, Beckman & Adams, 1981; Kashige et al., 1994; Ma et al., 2009; Hadwiger, 2015; Hadwiger & Tanaka, 2017). Although various studies have demonstrated this putative MoA, it is considered to have a low probability of occurrence. The prevailing MoA is thus thought to be electrostatic interactions leading to membrane destabilization (Raafat et al., 2008; Goy, Britto & Assis, 2009).

As mentioned earlier, the type of microorganism also plays a large role in the effectivity of CHT as mircroorganisms may be roughly divided into four groups based on their membrane compositions: chitosan-sensitive fungi, chitosan-resistant fungi, gram positive bacteria, gram negative bacteria (Palma-Guerrero et al., 2010; Verlee, Mincke & Stevens, 2017). Here, the MoA depends on the nature of the cell membrane (Figures 2.8). CHT is ineffective against CHT-resistant fungi due to differences in membrane fluidity, which is determined by phospholipid fatty acid composition. This highlights the role of fungal properties in susceptibility. (Palma-Guerrero et al., 2010; Verlee, Mincke & Stevens, 2017).

Other MoA involve direct interference with the pathogen, such as morphological changes at all developmental stages including mycelial growth, sporulation and germination (Rabea et al., 2003; Goy, Britto & Assis, 2009; Kong et al., 2010; Ana Niurka Hernández-Lauzardo, 2011;

Hadwiger, 2013; Xing et al., 2015; Verlee, Mincke & Stevens, 2017; Luan et al., 2018; Romanazzi, Feliziani & Sivakumar, 2018). Another MoA is metal chelation, where amino groups bind to metal cations, thereby suppressing spore elements and sequestering essential nutrients needed for microbial growth. This MoA predominates at higher pHs, where more amino groups remain unprotonated and available for metal chelation (Goy, Britto & Assis, 2009 and the references therein). CHT and derivatives are also capable of forming a viscous solution in various organic acids and have been used to make functional films. This has been tested directly against a range of fungi as highlighted in the review by Verlee et al. (2017) and the references therein with varying antimicrobial efficacies (dependent on the microorganism) (Ziani et al., 2009). However, this characteristic of CHT suggests its potential for more effective utilization in directly coating foods as a preservative or as an edible coating instead. Lastly, as CHT is generally a heterogenous copolymer, it is polydisperse (has a wide range of MW). As such, Poznanski, Hameed & Orczyk (2023) proposed that low MW and high MW CHT have different MoA. In **Figure 2.8**, low MW CHT is hypothesized to penetrate the cell wall, altering RNA, DNA, and chromatin activity, while high MW CHT is proposed to interact with the cell surface, causing permeabilization or forming an impermeable layer that blocks solute transport (Kong et al., 2010). However, there is no agreed upon distinction or hypothesis for the obsereved differences seen between low and high MW CHT.

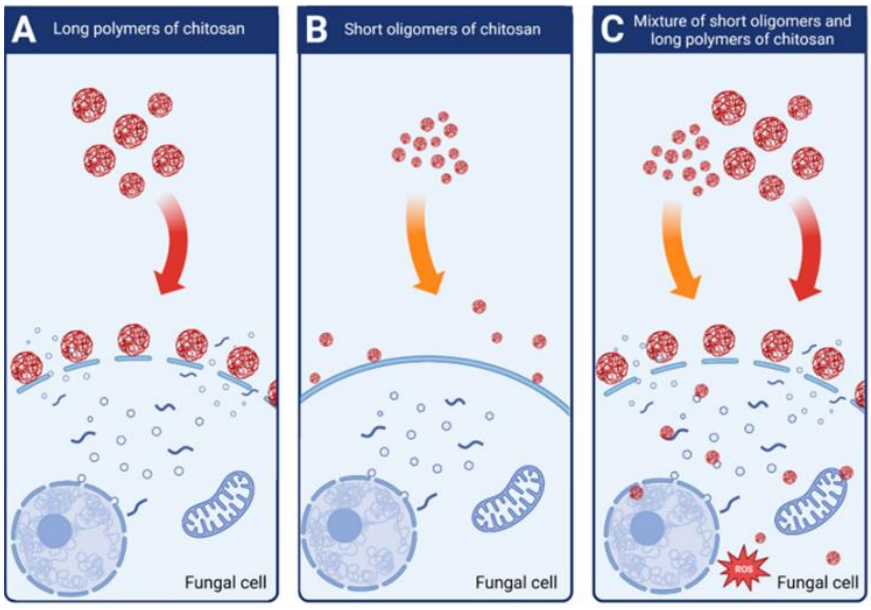

Figure 2.8: The effects of polydispersity and MW on the antifungal activity of different MW fractions of CHT. "(A) High MW CHT destabilizes fungal cell membranes leading to the leakage of intracellular components. (B) Low MW CHT fractions do not destabilize fungal membranes and show very weak antifungal effect. (C) Chitosan mixture of high and low MW fractions shows strong antifungal activity. High MW fractions destabilize the membranes allowing the low molecular fractions to penetrate fungal cell and to disturb cell processes." Adapted from (Poznanski, Hameed & Orczyk, 2023).

With respect to aminochitosan, an increase in the number of amino groups is theorized to result in enhanced interactions and direct antimicrobial activity as the surface of the cell is predominantly negatively-charged, making the number of amino groups on the CHT backbone vital for strong electrostatic interactions. Therefore, modifications to CHT, like with aminochitosan, mainly consisting of GlcN and not GlcNAc, eliminate interfering N-acetyl groups, enhancing positive-negative interactions with the cell surface. However, regions with excessive positive charges may rupture the cell membrane due to the strong electrostatic interactions, potentially leading to cell death. As a result, N-acetyl groups may serve as a means of reducing the ionic interactions, thus minimizing the possible toxicity of the polymer (Moran et al., 2018). Ultimately, the MoA for antifungal activity is an intricate process of "untargeted molecular events taking place simultaneously and successively, rather than being confined to a certain target molecule" (Kong et al., 2010).

2.4.2 Chitosan's mechanism of action *in planta*

In brief, CHT has emerged as a pivotal natural molecule influencing various physiological responses in plants. Its application *in planta* is often for its strong elicitor properties rather than its direct antimicrobial properties and these elicitor properties have been demonstrated across a broad range of economically important cops including tomato and maize (Bhaskara Reddy et al., 2000; Liu et al., 2007; Guan et al., 2009; El Hadrami et al., 2010; Mandal et al., 2013; Choudhary et al., 2017; Zachetti et al., 2019; El Amerany et al., 2020; Suarez-Fernandez et al., 2020; Czékus et al., 2021).

CHT applications in plants exhibit diverse physiological responses and antimicrobial activities across various crops. Some of its plant defence elicitation properties may be related to various PR proteins, defence-related compounds, and secondary metabolites as seen in **Figure 2.9** (Xing et al., 2015). Most notably it induces downstream signal pathways involving Ca^{2+}, ROS, NO, phytoalexins, pectinases, chitinases, PR proteins (PR-1, PR-5), glucanases, phytohormones (SA, JA, ABA) and antioxidants (Kaur et al., 2012; Xing et al., 2015; Li et al., 2020; Yu et al., 2023). These result in biochemical and molecular alterations despite the specific receptors for CHT remaining unclear. More specifically, CHT has been shown to function as a general elicitor of non-host resistance, SAR, callose deposition, and the inhibition of plasma membrane H^+-ATPase activity (Kaur et al., 2012; Singh et al., 2018). However, the

effects of CHT as an elicitor of plant defence is highly variable in the literature due to it being contingent upon factors such as its concentration, plant species, and developmental stage, specific microorganisms, DDA, MW, derivatives, and method of application (seed, root, foliar or soil), which are not standardized across experiments (El Hadrami et al., 2010; Liaqat & Eltem, 2018).

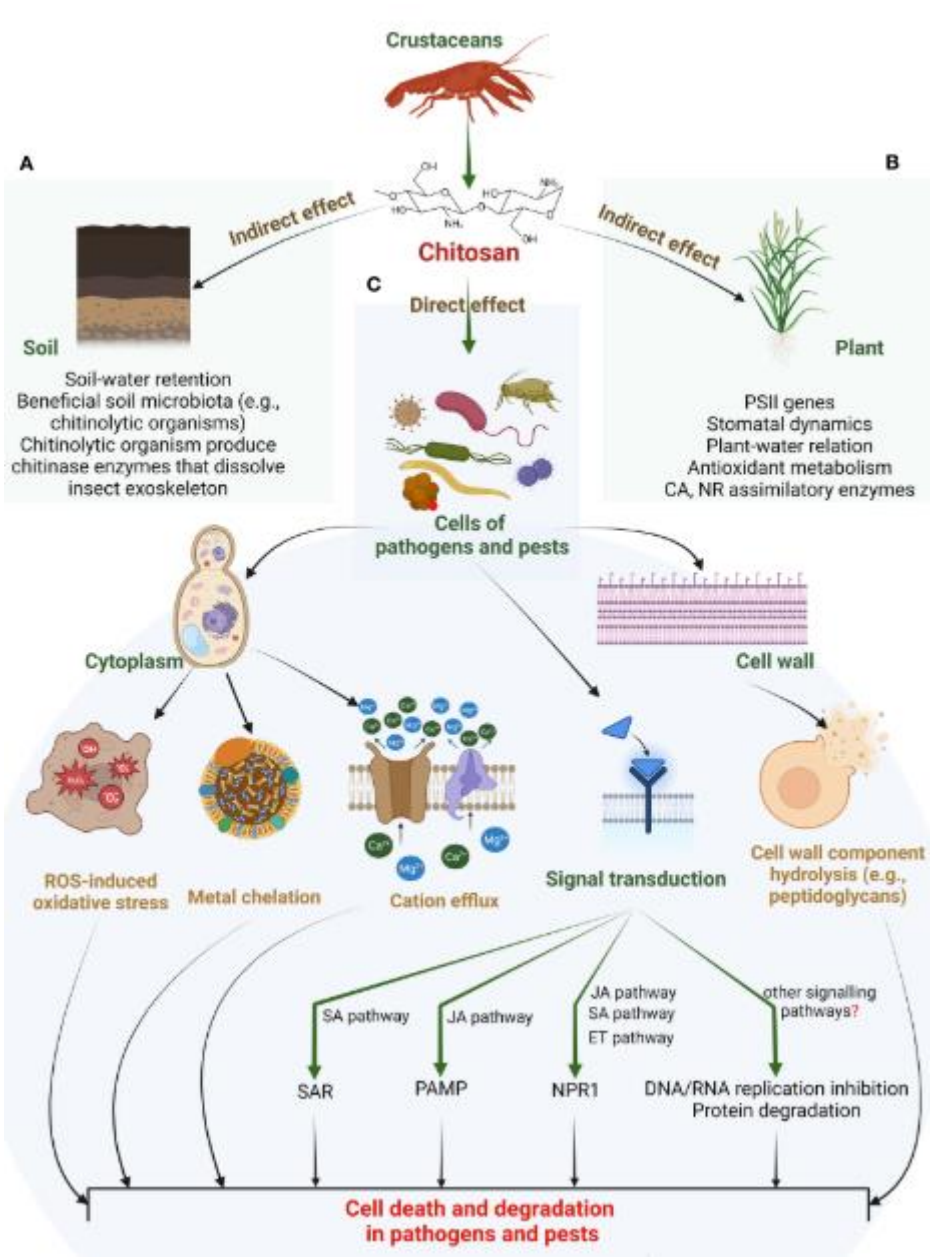

Figure 2.9: CHT MoA for stress tolerance against biotic stresses in higher plants. "Chitosan can cause hydrolysis of the cell wall components. This, along with metal chelation and cation efflux from the cytoplasm, disrupts ROS-antioxidant metabolism in pathogen/pest cells. This could result in cell degradation or death of plant invaders. It is suggested that these direct actions can rely on chitosan's intricate crosstalk with certain phytohormones such as JA, SA, ET, ABA, and GA and the activation of defensive genes and TFs (see panel C). Apart from this, other signalling pathways could be facilitating chitosan-induced biotic tolerance in plants" (Mukarram et al., 2023). PSII, photosystem II; CA, carbonic anhydrase; NR, nitrate reductase; ROS, reactive oxygen species; SAR, systemic induced resistance; PAMP, pathogen-associated molecular pattern; NPR1, natriuretic peptide receptor A/guanylate cyclase A; SA, salicylic acid; JA, jasmonic acid; ET, ethylene; GA, gibberellic acid; ABA, abscisic acid; TFs, transcription factors (Mukarram et al., 2023). This figure was adapted from Mukarram et al. (2022).

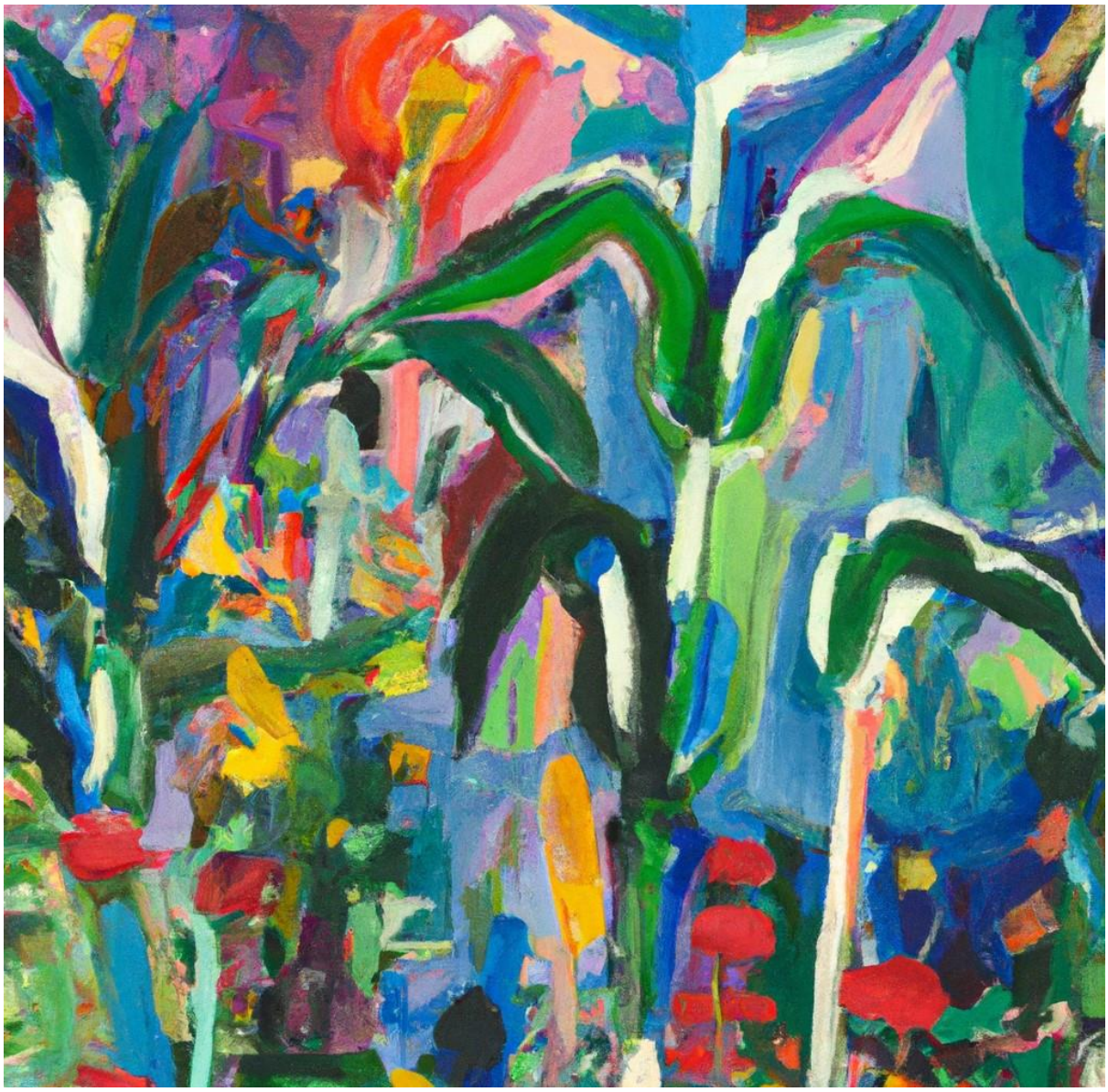

This image was created with the assistance of DALL.E 2.

Chapter 3: 6-deoxy-6-amino chitosan: A preventative treatment in the tomato/*Botrytis cinerea* pathosystem

The majority of this chapter (excluding the addendum) have been published in Moola, N., Jardine, A., Audenaert, K. and Rafudeen, M.S., 2023. 6-deoxy-6-amino chitosan: a preventative treatment in the tomato/*Botrytis cinerea* pathosystem. *Frontiers in Plant Science*, 14. The above publication has been reformatted to fit the coherency and consistency as required of a PhD thesis. As such, changes to the numbering of the figures, the layout and appearance of figures have been done to fit the style of the chapter. Furthermore, the supplementary figures and tables have also been reformatted to fit the aforementioned thesis requirements.

3.1 Abstract

6-deoxy-6-amino chitosan (aminochitosan) is a water-soluble chitosan derivative with an additional amine group at the C-6 position. This modification has improved aqueous solubility, antifungal activity and is hypothesized to have enhanced *in planta* antifungal activity compared to native chitosan. Gray mold in tomatoes is caused by the fungus, *Botrytis cinerea*, and poses a severe threat both pre- and post-harvest. To investigate the optimal concentration of aminochitosan and its lower molecular weight fractions for antifungal and priming properties in the tomato/*B. cinerea* pathosystem, different concentrations of aminochitosan were tested on *B. cinerea* growth and sporulation and *in planta* as a foliar pre-treatment in tomato leaves. The leaves were monitored for photosynthetic changes using multispectral imaging and hydrogen peroxide accumulation using DAB. Despite batch-to-batch variations in aminochitosan, it displayed significantly greater antifungal activity against *B. cinerea* than native chitosan at a minimum concentration of 1 mg/mL. A concentration-dependent increase in the antifungal activities was observed for radial growth, sporulation, and germination with the maximum inhibition for all biopolymer batches and lower MW fractions at 2.5 and 5 mg/mL, respectively. However, the inhibition threshold for aminochitosan was identified as 1 mg/mL for spores germinating *in planta*, compared to the 2.5 mg/mL threshold. The pre-treatment of leaves displayed efficacy in priming direct and systemic resistance to *B. cinerea* infection at 4-, 6- and 30-days post-inoculation by maintaining elevated F_v/F_m activity and chlorophyll content due to a stronger and more rapid elicitation of the defence systems at earlier time points. Moreover, these defence systems appear to be ROS-independent at higher concentrations (1 and 2.5 mg/mL). In addition, aminochitosan accumulates in the cell membrane and therefore acts to increase the membrane permeability of cells after foliar spray. These observations corroborate the notion that aminochitosan biopolymers can exert their effects through both direct mechanisms of action and indirect immunostimulatory mechanisms. The contrast between antifungal efficacy and *in planta* efficacy highlights the bimodal mechanisms of action of aminochitosan and the advantageous role of primed plant defence systems.

3.2 Introduction

Tomato (*Solanum lycopersicum* L.) is an important crop that alone accounted for almost 25% of the total global vegetable crop production increase between 2000 and 2021 (FAOSTAT, 2022). Gray mold disease is caused by the polyphagic, necrotrophic fungal pathogen, *Botrytis cinerea*, and affects over 1400 known hosts in 586 plant genera, including tomato (Fillinger & Elad, 2016). The life cycle of *B. cinerea* is complex, resulting in varying symptoms across different plant tissues and organs (Fillinger & Elad, 2016; Poveda, Barquero & González-Andrés, 2020). It can infect all plant parts both pre- and post-harvest (including endophytic activity), and lie dormant or remain active during harvest or storage (Fillinger & Elad, 2016). Thus, economic impacts include direct losses (unmarketable crops or yield loss) and indirect losses (quality, harvest timing and control strategies) that amount to billions in annual economic losses (Fillinger & Elad, 2016; Poveda, Barquero & González-Andrés, 2020). To date, the predominant gray mold management strategy has been the use of fungicides, despite the challenges and concerns associated with their negative effects on the environment (Fenner et al., 2013) and human health (Verger & Boobis, 2013), lasting residues in food (Popp, Pető & Nagy, 2013), and acquired fungicide resistance, resulting in an ever-increasing effective dosing requirement for crops (Pengfei Leng, 2011; Fillinger & Elad, 2016). These disadvantages have resulted in stricter regulations governing the application of fungicides and the permitted residue levels, resulting in a shift towards implementing eco-friendly alternatives (De Waard, 1993; Williamson et al., 2007). Biopolymers are thus viable alternatives to fungicides owing to their non-toxicity, multiple MoA and broad-spectrum antimicrobial activity (Kaur et al., 2012).

Chitosan is a biopolymer of interest due to the above characteristics, with the addition of its biocompatibility, chemical versatility, and biodegradability properties (Kong et al., 2010; Verlee, Mincke & Stevens, 2017). Moreover, *B. cinerea* has been shown to be chitosan-sensitive due to the structural composition of the cell membranes (Palma-Guerrero et al., 2010). Produced via alkaline deacetylation of chitin; chitosan and its derivatives are biopolymers composed of *N*-acetyl glucosamine and glucosamine monomer units respectively (Verlee, Mincke & Stevens, 2017). The commercial sources of chitin used for chitosan synthesis are largely obtained from derived from the waste of the seafood industry

or are otherwise sourced from mushroom waste and the exoskeletons of insects (Hadwiger, 2013; Liaqat & Eltem, 2018; Terkula Iber et al., 2022). However, chitosan's insolubility in neutral aqueous solutions as well as moderate antimicrobial activity relative to chemical biocides have limited its commercial development in the agricultural sector (Hu et al., 2016; Romanazzi, Feliziani & Sivakumar, 2018).

Various modifications of chitosan by means of *O*- or *N*-conjugation have been shown to improve physiochemical properties such as solubility and antimicrobial activity (Verlee, Mincke & Stevens, 2017; Brasselet et al., 2019). Some of the key factors differentiating the biological activity and solubility of chitosan derivatives are the presence of reactive amine group(s) and the ratio of amine to *N*-acetyl groups (Liaqat & Eltem, 2018; Poznanski, Hameed & Orczyk, 2023). The reactive amine group(s) create a net positive charge and are proposed as integral to the mechanism of action. This net positive charge allows chitosan to interact with anionic surfaces via strong electrostatic interactions (Kong et al., 2010). Therefore, chitosan with an additional amine group termed 6-deoxy-6-amino chitosan (herein referred to as aminochitosan) was synthesized to improve its biological activity and water-solubility (Satoh et al., 2006).

Studies have reported that aminochitosan has improved antibacterial activity (Yang et al., 2012) and antioxidant activity (Yang et al., 2015; Luan et al., 2018) when compared to native chitosan. However, due to the difficulties in dissolving aminochitosan in neutral pH water as prepared following the earlier methods stated, an improved synthesis of aminochitosan was deduced. Aminochitosan, soluble in water at pH 7, was synthesized in a shorter, greener, and more scalable synthetic protocol by Sayed, Millard & Jardine et al., (2018). Compared to the abovementioned reported studies, this water-soluble aminochitosan is proposed to have improved biological activity and is soluble in water at a neutral pH (Sayed, Millard & Jardine, 2018). However, other deterministic factors affecting the physiochemical properties and biological activity of chitosan include the degree of deacetylation (DDA), polymerization (DP), and substitution (DS), as well as the molecular weight (MW) (Bellich et al., 2016).

Chitosan's biological activities are actioned through a triple-acting system of antimicrobial activities, film-forming properties, and the elicitation of plant defence systems (Xing et al., 2015; Romanazzi, Feliziani & Sivakumar, 2018). The MoA and responses thereto vary

depending on the pathosystem, microbial factors, physical state of chitosan (e.g. nanoparticles), environmental factors, time of application, and intrinsic and extrinsic physiochemical properties of chitosan (El Hadrami et al., 2010; Kong et al., 2010; Poznanski, Hameed & Orczyk, 2023). The MoA for the antimicrobial activity are proposed to be through a combination of direct physiochemical interference with the pathogen, which includes the formation of a film layer, induction of pathogen-related morphological changes at all developmental stages, and direct interaction with DNA/chromatin (Rabea et al., 2003; Goy, Britto & Assis, 2009; Kong et al., 2010; Ana Niurka Hernández-Lauzardo, 2011; Hadwiger, 2013; Xing et al., 2015; Verlee, Mincke & Stevens, 2017; Luan et al., 2018; Romanazzi, Feliziani & Sivakumar, 2018). In addition, the indirect MoA arises from the elicitation and exploitation of the plant's innate immunity, resulting in induced resistance (IR) through various systemic mechanical, biochemical, and molecular changes within the plant (El Hadrami et al., 2010; Hadwiger, 2013; Aranega-Bou et al., 2014). IR can be elicited systemically through direct signal recognition in locally infected tissue or by priming, which may be activated by treatment with natural or synthetic chemicals like chitosan or through infection (Aranega-Bou et al., 2014; Mauch-Mani et al., 2017). Priming is defined as induced physiological, epigenetic, and metabolic changes upon the initial stimulus, which is followed by a robust defence response that is faster and/or stronger upon subsequent exposures to stimuli with a generally low cost to plant fitness (Aranega-Bou et al., 2014; de Vega, Newton & Sadanandom, 2018). Therefore, priming increases the capacity and efficiency of defence and resistance through amplified defence signals, rather than direct activation of defence responses (Aranega-Bou et al., 2014; Mauch-Mani et al., 2017).

As aminochitosan has not yet been investigated *in planta*, this is the first study to analyze its role as a protective priming agent in the tomato/*B. cinerea* pathosystem. Moreover, this is the first study to investigate the effects of aminochitosan and its batch-to-batch variability in synthesis as well as the bioactivity of lower MW fractions.

3.3 Materials and methods

3.3.1 Plant material

Tomato (*Solanum lycopersicum* L.*)* cv. Moneymaker seeds were collectively germinated before being transplanted into individual pots containing potting soil. Seedlings were grown at 23 °C with an 16 h light/8 h dark cycle (Audenaert, De Meyer & Höfte, 2002). After 5 weeks, when the plants consisted of tertiary leaves with five leaflets, 80-120 plants were randomized and used for each experiment.

3.3.2 Botrytis cinerea

The *B. cinerea* isolate R16 (Faretra and Pollastro, 1991) was grown on potato dextrose agar (PDA) for 2 weeks at room temperature under 12-h dark/12-h UV light conditions. Control (mock) and spore suspensions were made, each containing 0.01 M glucose and 6.7 mM KH_2PO_4, with either 1 x 10^6 spores/mL of *B. cinerea* (*B. cinerea* spore suspension) or distilled water (mock solution) added (Audenaert, De Meyer & Höfte, 2002).

3.3.3 Biopolymers

Chitosan (CHT, crab origin, DDA > 90%) was purchased from AK Scientific Inc.. The 6-deoxy-6-amino chitosan biopolymer (aminochitosan, shrimp shell origin, > 96% DDA, Sayed et al., 2018) with batch-to-batch variants termed diamino 1 (D1), diamino 2 (D2), and diamino 3 (D3), were synthesized by the Department of Chemistry at the University of Cape Town, South Africa. The batch-to-batch variants were approximately 15 kDa, as inferred from the 15 kDa dialysis MW cutoff used during purification. Additional fractionation was performed on the parent biopolymer (the biopolymer in which the fractions were derived from, **Figure S3.1**), D3, with the following MW cut-offs: 3-5 kDa (Fraction 1, F1), 15 kDa (Fraction 2, F2), 20 kDa (Fraction 3, F3), 20-99 kDa (Fraction 4, F4) and 100 kDa (Fraction 5, F5). The biopolymers are henceforth termed either D1, D2, or D3 for the batch-to-batch variants and F1, F2, F3, F4 or F5 for the respective MW fractions. Biopolymer solutions were freshly prepared 1 day before the start of all experiments at the following concentrations: 0.5 mg/mL (0.05%), 1 mg/mL (0.1%), 2.5 mg/mL (0.25%), and 5 mg/mL (0.5%). Solutions for the aminochitosan biopolymers were prepared in distilled water, and chitosan was prepared in 1% (v/v) acetic acid. Working

concentrations of chitosan had an acetic acid concentration of 0.1%. Biopolymer solutions were stirred overnight and sonicated for 2 h before use.

3.3.4 Biopolymer application as foliar spray: direct and systemic

The biopolymers were assessed for two different MoA *in planta*: the direct effects of biopolymer application, termed "direct treatment," and the indirect, systemic effects of biopolymer application, termed "systemic treatment". For both types of treatment, the tertiary leaves of 5-week-old tomato plants were pre-treated by foliar spray until run-off (approximately 1.4 mL per leaf) with the different concentrations of the biopolymers, 24 h before *B. cinerea* inoculation (see Section 3.3.3). For the direct treatment, all five leaflets were sprayed (**Figure S3.2A**). To assess the systemic effect, the first primary leaflet of each leaf was covered with foil before the remaining four leaflets were sprayed (**Figure S3.2A**).

3.3.5 Biopolymer Elemental Analysis (EA)

Elemental analyses of elemental composition ratios (carbon and nitrogen, C/N) and the degree of substitution for chitosan and the aminochitosan fractions (see Section 3.3.3) were conducted on a Thermo Flash 1112 Series CHN Analyzer and the EA Euro 3000 by the Department of Chemistry at the University of Cape Town. The ratio C:N was used to determine the degree of substitution (DS) using the following equation (Sayed, 2018):

$$\mathrm{DS} = \left[\frac{\left(\frac{\mathrm{C}}{\mathrm{N}}\,\mathrm{derivative}\right)}{\left(\frac{\mathrm{C}}{\mathrm{N}}\,\mathrm{chitosan}\right)}\right] \times \mathrm{DDA}(96\%)$$

3.3.6 Antifungal assays

3.3.6.1 Effects on mycelial radial inhibition

The direct effects of the biopolymers were assessed as in El-Ghaouth et al. (1992) using a mycelial radial growth assay. Fungal discs (10 mm) taken from actively growing 2-week-old *B. cinerea* plates were placed centrally on PDA media amended with a biopolymer (CHT, D1, D2, D3, F1, F2, F3, or F5). The final concentrations of the amended media were 0.5, 1 or 2.5 mg/mL. Unamended PDA, water (PDA dilution control, data not shown), and 0.1% (v/v) acetic acid were used as controls. Plates were grown under 12-h dark/ 12-h UV (combined UVA and

UVC) conditions for 11 days. Radial growth measurements (expressed as an average mycelial area in mm^2) and macro-photos were taken at 1-5, 8-, and 11-days post-initiation. The percentage inhibition of radial growth (PIRG%) was calculated as in Al-Hetar et al. (2011). Experiments were performed with five biological replicates per treatment, per experiment, and repeated twice. The percentage inhibition of radial growth (PIRG%) was calculated as in Al-Hetar et al., 2010.

$$PIRG\% = \frac{(Control - Treatment)}{Control} \times 100\%$$

3.3.6.2 Effects on sporulation

B. cinerea spores were harvested from the 11-day-old plates in 5 mL of water and filtered through sterile Miracloth (Pabón-Baquero et al., 2015). The concentrations of spores were determined using a hemocytometer and expressed as the number of spores (spores/mL). The experiment was repeated twice with 5 biological replicates for each biopolymer and concentration. The percentage inhibition of sporulation (PIS%) was calculated as in Al-Hetar et al. (2011).

$$PIS\% = \frac{(Control - Treatment)}{Control} \times 100\%$$

3.3.7 *In planta*: direct and systemic effects in detached whole leaves and leaf discs

3.3.7.1 Experiment set up: inoculation and lesion frequency

Twenty-four hours after spraying, whole leaves were excised at the base of the petiole before being wrapped in paper towels and placed on a tray. The leaves were then suspended above wet paper towels, with the stems immersed in distilled water. Individual leaflets were inoculated with two 10 µL droplets of either *B. cinerea* spore suspension or mock solution on either side of the midrib. The trays were then sealed with transparent lids to ensure a high-humidity environment and grown under a 16-h light/ 8-h dark cycle (**Figure S3.2A**). Disease progression was assessed by counting the number of spreading necrotic lesions compared to resistant lesions (**Figure S3.2B**). Plants with lesions displaying resistance to the development of spreading lesions were termed resistant lesions. Here, resistant lesions are defined as lesions that do not follow the same trajectory as spreading lesions but instead remain

confined to the bounds of the initial droplet area with no detrimental effects to the leaf. Plants with lesions displaying resistance to the development of spreading lesions were termed resistant lesions.

3.3.7.2 Image analysis for phenotyping disease progression: F_v/F_m, ChlIdx, and mAriIdx

Leaflets were imaged using the CropReporter PathoViewer platform at 4- and 6-days post-inoculation (dpi). The non-sprayed first primary leaflet of each leaf was imaged to assess the systemic treatment effect in systemically sprayed leaves, while all five leaflets were imaged to assess the direct treatment. The PathoViewer (Department of Crops and Plants, Ghent University, Belgium), a non-invasive multispectral imaging platform, was used for the analysis of photosynthetic changes in real time, as in De Zutter et al. (2021). The platform used an automated, high-resolution, multispectral camera system mounted to a Cartesian-coordinate grid table contained in a light (Sun LED modules) chamber with controlled temperature and humidity (CropReporter, PhenoVation). The monochrome camera system captured absorption, reflection, and fluorescence patterns at a high temporal and spatial resolution of 6 µm and fitted with optical filters. The following parameters were calculated in a pixel-by-pixel manner from the obtained images: the average maximum efficiency of photosystem II (F_v/F_m) (Baker, 2008), RGB values, and the stress indices, namely the average chlorophyll fluorescence index (ChlIdx, a measure "leaf yellowing and chlorophyll content") (De Zutter et al., 2021) and the average modified anthocyanin index (mAriIdx) (Gitelson, Chivkunova & Merzlyak, 2009). The PhenoVation imaging software and algorithms (PhenoVation, Wageningen, the Netherlands) were used to calculate the average F_v/F_m, ChlIdx, and mAriIdx along with the standard deviations for each leaflet from these images (De Zutter et al., 2021). As such, the effects of the biopolymers on the overall leaf health and disease progression were assessed based on the phenotypic changes observed over the course of the experiment (Baker, 2008; De Zutter et al., 2021).

3.3.7.3 Time-course analysis of hydrogen peroxide accumulation (DAB assay)

The protocols of Asselbergh et al. (2007) and Thordal-Christensen et al., (1997) were used with the following amendments: after spraying (see Section 3.3.4) and 1 h of drying, whole leaves were excised from multiple plants and randomized for each treatment. Leaf discs were

taken with a 1 cm cork borer and floated (abaxial side down) in 24-well plates containing 1.5 mL of water per well. Twenty-four hours after the leaves were sprayed, leaf discs were inoculated with two 5 µL droplets of mock or spore suspension on either side of the midrib (Audenaert, De Meyer & Höfte, 2002; Asselbergh et al., 2007). The samples were allocated into different time groups, where the infection was allowed to establish for either 4, 8, 12, 24, 48, or 72 h before staining. Prior to staining, the 24-well plates were imaged with the PathoViewer platform (see Section 3.3.7.2) for macroscopic images. The protocol of Thordal-Christensen et al., (1997) was used for the 3',3'-diaminobenzidine (DAB) staining and amended as follows: at each time point post-inoculation, the water was replaced with 1.5 mL of 1 mg/mL DAB. Leaf discs were floated for 4 h before being de-stained (boiled) in a lactophenol mixture (phenol: glycerol: lactic acid: water: ethanol (1:1:1:1:2) for 30 min. Following H_2O_2 staining, fungal structures were stained with 0.02% (w/v) Trypan Blue in distilled water (for 30 s). After staining, the leaf discs were mounted on glass slides in 50% (v/v) glycerol. Brightfield microscopy was performed with an Olympus BX-51 microscope and a Nikon Ti inverted Eclipse microscope using the NIS-Elements AR imaging software.

3.3.7.4 Time course analysis: spore germination

Leaf discs used in the DAB assay (see Section 3.3.7.3) were used to analyze the effects of diamino 1 compared to water on spore germination at two time points, 16 h post inoculation (hpi) and 20 hpi.

3.3.7.5 Time-course analysis: gene expression of *SlACRE75*

This analysis was set up as the phenotyping experiment (see Section 3.3.7.1) with the following amendments: Individual leaflets were harvested and considered biological replicates. Therefore, five biological replicates (five leaflets) were harvested from one tertiary leaf for the direct treatment and one biological replicate (one leaflet) for the systemic treatment. Leaflets were harvested and flash frozen at 6 and 9 hpi for the direct treatment and at 96 hpi for the systemic treatment (**Figure S3.2A**). The harvested tissue was analyzed for gene expression of *ACRE75*. Primers for *ACRE75* were synthesized using sequences from De Vega et al. (2021). The reference genes, *SICBL1* and *LSM7,* were selected from Rezzonico, Nicot & Fahrentrapp (2018) and primers synthesized accordingly (Rezzonico, Nicot &

Fahrentrapp, 2018). RNA was extracted using the PureLink® Plant RNA Reagent (Thermo Fisher Scientific, Waltham, USA) as recommended. The cDNA was synthesized from 1 µg of RNA using the Maxima First Strand cDNA Synthesis Kit with dsDNase (Thermo Fisher Scientific, Waltham, USA). RT-qPCR was conducted using KAPA SYBR® FAST qPCR Master Mix (2X) Universal (KAPA Biosystems, Salt River, Cape Town) on a Rotor-Gene™ 6000 real-time rotary analyzer (Corbett Life Science, Sydney, Australia). The data was analyzed in qbase (Biogazelle, Zwijnaarde, Belgium) and normalized to the two reference genes using the geNorm normalization algorithm of the software where the reference genes target stability levels were defined by the stability and variability of the reference genes by calculating the geNorm stability M-value and the coefficient of variation of the normalized reference gene expression levels. The threshold value was set at 1 for the geNorm expression stability value and 0.3 for the coefficient of variation. The maximum replicate variability was set to 0.1, and any replicate with a difference > 0.1 was excluded under quality control.

3.3.8 Statistical Analysis

Plots were generated using the R software version 3.6.0 (R Core Team, 2020) and the packages ggplot2 (Wickham, 2016). The non-parametric Kruskal-Wallis test was used for multiple comparisons, followed by a *post hoc* analysis using Dunn's test for pairwise comparisons. An FDR-corrected significance value of 0.05 was used for all analyses.

3.4 Results

3.4.1 Antifungal activity of aminochitosan against *B. cinerea*

Two batches of aminochitosan were synthesized to assess the batch-to-batch variability and are referred to as diamino 1 (D1) and diamino 2 (D2). The biopolymers were assessed for their efficacy against *B. cinerea* compared to chitosan (CHT).

The biopolymer treatments displayed radial growth in concentric rings and excessively branched mycelia with a prevalence for "upward growth" (**Figure 3.1B**). In addition, the CHT treatments displayed haloes around the mycelial growth (**Figure S3.6**). The direct antifungal activities of CHT, D1, and D2 showed a significant increase in inhibitory activity with increasing concentrations of the biopolymers compared to the PDA control (**Figures 3.1A**, **1B**, and **Table**

3.1). Notably, variations in the efficacy of the concentrations were observed across the biopolymers, as D1 exhibited significant radial growth inhibition (PIRG%) compared to CHT and D2 at 2.5 mg/mL (**Table 3.1**). To account for the inhibitory effects of acetic acid on fungal growth (data not shown), a 0.1% (v/v) acetic acid control was included as a control for CHT since CHT is only soluble in weak acids. The 0.1% acetic acid control was shown to be statistically different to the PDA control and generally no different to 0.5 and 1 mg/mL but significantly different to 2.5 and 5 mg/mL (**Table 3.1**). Maximum PIRG% for each of the biopolymers was observed between 2.5 and 5 mg/mL despite the large variance in the standard deviations (**Figure 3.1B** and **Table 3.1**).

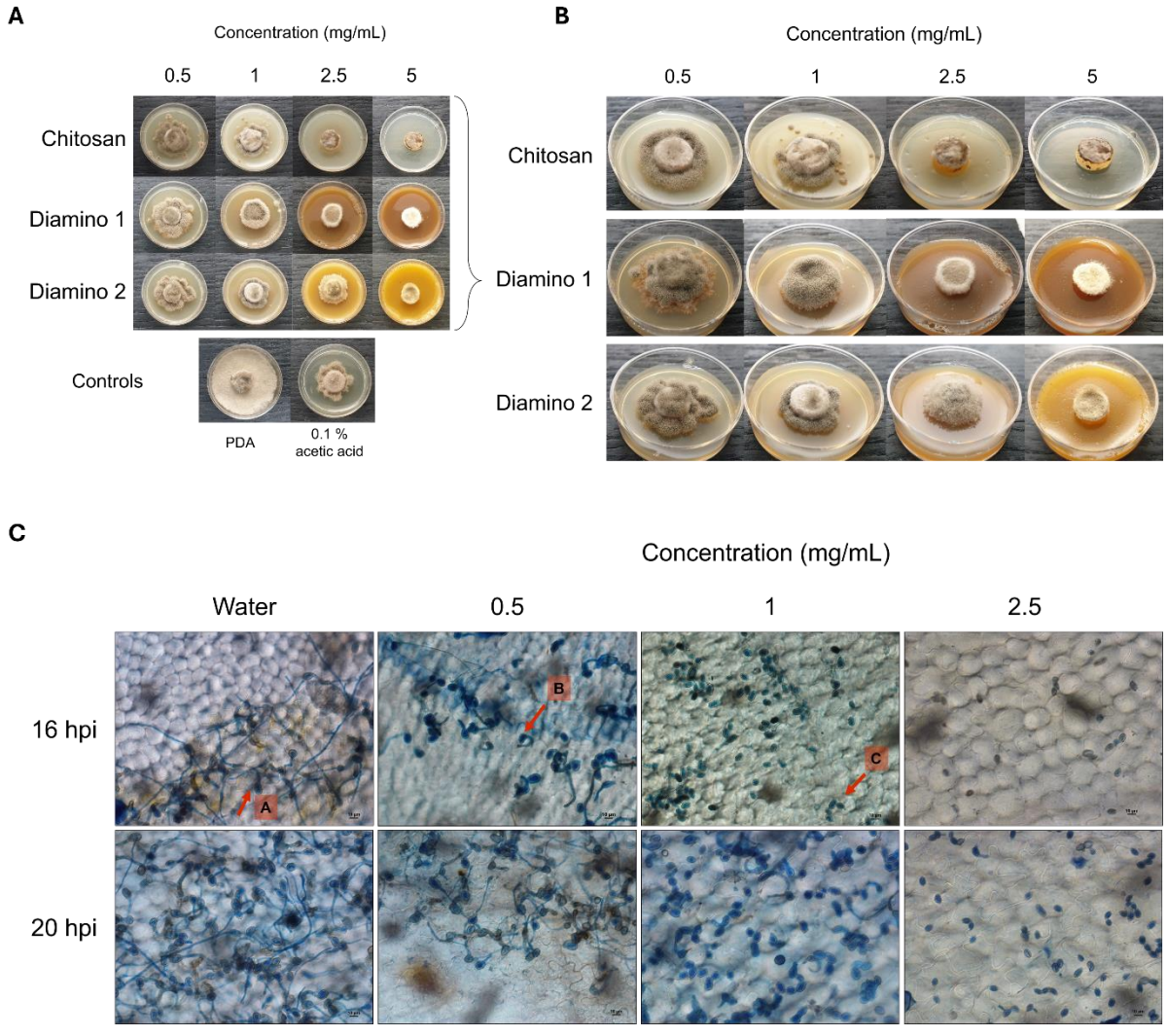

Figure 3.1: The direct antifungal effects of chitosan and aminochitosan batches on *B. cinerea* growth, 11 days after incubation. **(A)** An overview of the phenotypic effects relative to the controls (PDA and 0.1% (v/v) acetic acid). **(B)** A detailed view of the macroscopic and morphological changes. The images represent one of five biological replicates. The experiment was repeated twice. **(C)** The phenotypic effects of water and D1 at 0.5, 1 and 2.5 mg/mL concentrations on the germination, germ tube formation, and elongation of *B. cinerea* spores

visualized at 40X magnification (scale bar = 10 µm.). The images display germination at 16 and 20 h post inoculation. Arrows (A-C) indicate the average phenotype for each concentration. Spores were inoculated onto leaf discs and stained with Trypan Blue for visualization. The images represent an average of 4 biological replicates. The experiment was repeated once.

Intriguingly, the inhibitory effects of the biopolymers on the sporulation of *B. cinerea* displayed an increase in the number of spores/mL for CHT, D2, and D1 at 0.5 mg/mL compared to the PDA control which increased in that respective order (**Table 3.1**). This correlated with the phenotypic changes seen in the mycelial growth for the biopolymer treatments at 0.5 mg/mL. These were marked by the appearance of ashen, gray-colored masses in concentric rings compared to the PDA control, which displayed a uniformly light-colored growth (**Figures 3.1A** and **3.1B**). Similarly, the 0.1% acetic acid control exhibited a comparable phenotypic effect on sporulation as 0.5 mg/mL of CHT (**Figure 3.1**). Overall, the biopolymers showed an initial increase in the average spores/mL at the lowest concentration assessed, followed by a decrease in the average spores/mL with increasing biopolymer concentrations (**Figures 3.1A**, **3.1B**, and **Table 3.1**).

Table 3.1: The effects of different concentrations of chitosan (CHT) and aminochitosan variants on the average mycelial radial inhibition and sporulation of *B. cinerea*, 11 days after incubation.

		Radial Inhibition		**Sporulation**	
Treatment	Concentration (mg/mL)	Growth area (mm^2) ± SD	PIRG (%) ± SD	Spores/mL ± SD	PIS (%) ± SD
PDA	0	491 ± 0	0 ± 0^{a}	21 133 ± 17 365	0 ± 0^{a}
0.1% acetic acid	0	133 ± 39	73 ± 15^{bc}	31 260 ± 17 442	7 ± 24^{a}
Chitosan	0.5	298 ± 195	39 ± 32^{b}	44 633 ± 33 383	-27 ± 56^{a}
	1	70 ± 58	86 ± 10^{cd}	35 967 ± 30 505	3 ± 57^{a}
	2.5	56 ± 84	89 ± 14^{de}	5 600 ± 5 808	84 ± 13^{b}
	5	0 ± 0	100 ± 0^{e}	100 ± 141	99 ± 1^{b}
PDA	0	491 ± 0	0 ± 0^{a}	21 133 ± 17 365	0 ± 0^{a}
Diamino 1	0.5	279 ± 109	43 ± 16^{b}	103 850 ± 120 703	-164 ± 217^{b}
	1	118 ± 151	76 ± 22^{bc}	16 200 ± 5 940	59 ± 15^{ab}
	2.5	0 ± 0	100 ± 0^{c}	0 ± 0	100 ± 0^{c}
	5	0 ± 0	100 ± 0^{c}	0 ± 0	100 ± 0^{c}
PDA	0	491 ± 0	0 ± 0^{a}	21 133 ± 17 365	0 ± 0^{a}
Diamino 2	0.5	314 ± 148	36 ± 14^{b}	65 400 ± 104 790	-70 ± 215^{a}
	1	65 ± 27	87 ± 5^{c}	33 600 ± 54 487	14 ± 138^{a}
	2.5	34 ± 12	93 ± 2^{cd}	1333 ± 14 045	97 ± 4^{b}
	5	7 ± 11	98 ± 2^{d}	450 ± 636	98 ± 3^{b}

PIRG% = percentage inhibition of radial growth (PIRG), and PIS% = percentage inhibition of sporulation (PIS). A negative PIS% indicates growth greater than the control. Statistical significance was calculated between concentrations for each polymer. Means ± SD (standard deviation) followed by the same superscript letter are not significantly different from each other. Different letters indicate significant differences between concentrations. The presence of two letters indicates either similarity or difference across multiple concentrations for that polymer (Kruskal-Wallis test followed by Dunn's *post hoc* test, $p < 0.05$). The values shown are the average of three experiments.

As D1 exhibited greater radial growth inhibition compared to D2, it was selected to analyze the effects of aminochitosan on the germination of *B. cinerea in planta.* The germination of spores on tomato leaflets sprayed with D1 showed increasing inhibition of germination and germ tube length with increasing concentrations of D1 (**Figure 3.1C**). Complete inhibition of germination can be observed at 2.5 mg/mL of D1 (**Figure 3.1C**). At concentrations of 0.5 and 1 mg/mL of D1, the germ tube lengths were shorter than the water treatment. Notably, 1 mg/mL of D1 demonstrated the greatest variability in both the number of spores germinating and the germ tube length (data not shown).

3.4.2 Multispectral analysis of the *in planta* direct and systemic effects of aminochitosan using F_v/F_m, chlorophyll index and anthocyanin index

To determine if aminochitosan exhibits comparable efficacy *in planta* as the antifungal efficacy results, detached whole tomato leaves were pre-treated with aminochitosan 24 h before *B. cinerea* inoculation (**Figure S3.2A**). Leaves were treated with one of the following variable combinations: the mode of application (direct/systemic), the treatment (biopolymer/water), and the inoculation solution (*B. cinerea*/mock). The disease progression of an artificial *B. cinerea* inoculation on tomato leaves (Benito et al., 1998) is displayed in **Figure S3.2B** while the induced resistance eliciting properties of aminochitosan are displayed in RGB images in **Figures S3.2A** and **S3.2B**.

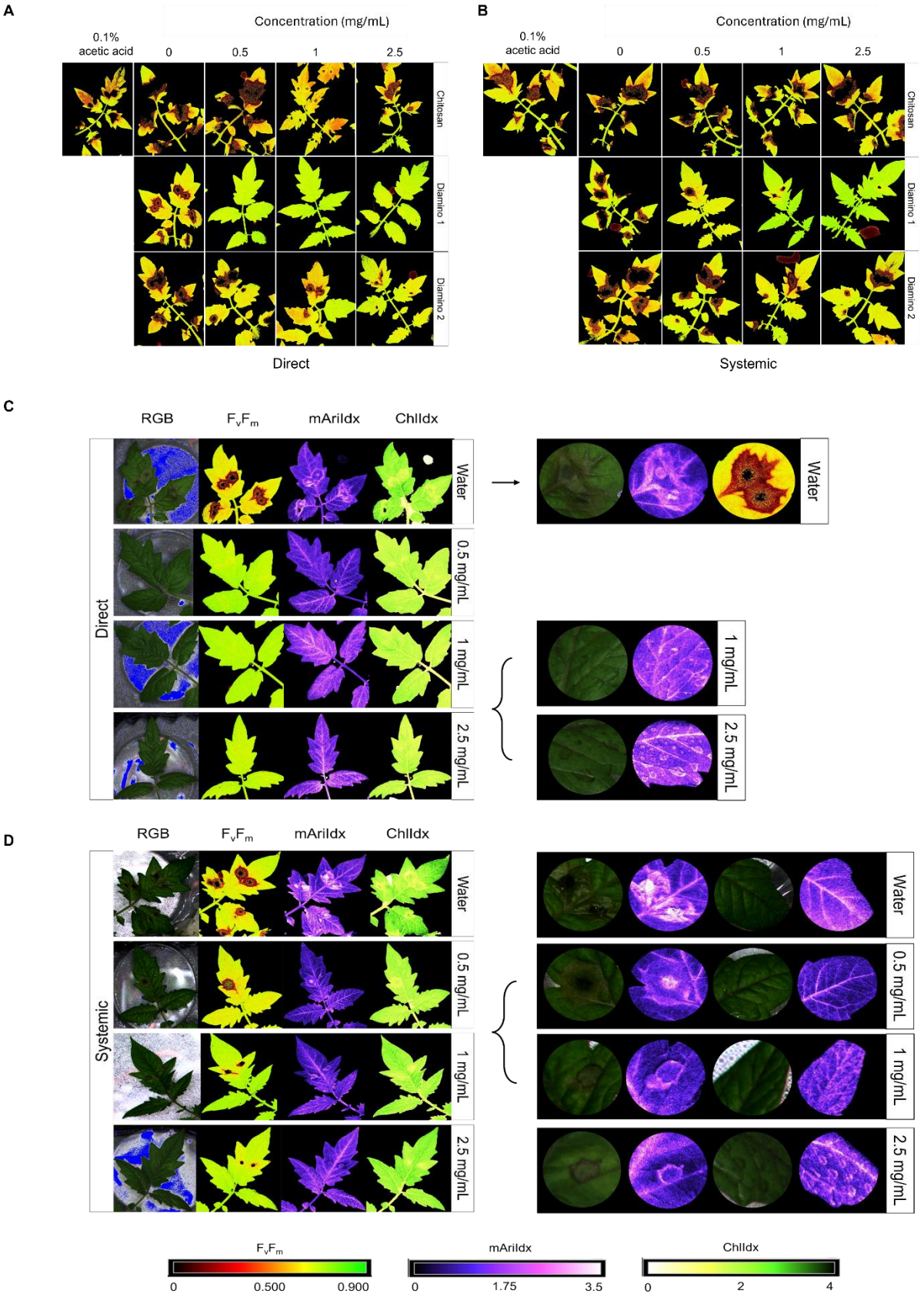

Figure 3.2: The phenotypic effects of chitosan (CHT), diamino 1 (D1), and diamino 2 (D2) treatment on the disease progression of *B. cinerea*, 4 days post-inoculation (dpi). The treatments were evaluated by direct or systemic application and imaged thereafter. Lesion development and progression were noted by the spreading

of dark red/black (F_v/F_m, 0-0.5) or yellow/white (ChlIdx, 0-1.8) spots as measured by the false color scales. Healthy leaf tissue was noted as yellow/green (F_v/F_m,0.7-0.9) or green (ChlIdx, 1.9-2.5) by the false color scales. **(A)** Images displaying the direct effects of treatment on F_v/F_m at 4 dpi. (**B)** Images displaying the systemic effects of treatment on F_v/F_m at 4 dpi. **(C)** RGB, F_v/F_m, mAriIdx, and ChlIdx images of direct D1 treatment at 4 dpi and a detailed view of the effects with 1 and 2.5 mg/mL. (**D**) RGB, F_v/F_m, mAriIdx, and ChlIdx images of systemic D1 treatment at 4 dpi and a detailed view of all concentrations. Leaves were inoculated 24 h after polymer spraying with two 10 µL droplets of a *B. cinerea* spore suspension (1 x 10^6 spores/mL containing 0.01 M glucose and 6.7 mM KH_2PO_4). The images represent the average phenotype of two experiments.

A significant and completely resistant phenotype with 100% resistant lesions (i.e., no visible disease symptoms) was observed at 4 dpi for all concentrations of D1 applied as a direct treatment and was maintained at 6 dpi, with more than 95% resistant lesions for all concentrations assessed (**Figure 3.2C** and **Table 3.2**). These observations were compared to the water treatment + *B. cinerea* inoculation, of which 91 and 94% of lesions were necrotic at 4 and 6 dpi, respectively (**Table 3.2**).

Table 3.2: The effects of chitosan (CHT), diamino 1 (D1), and diamino 2 (D2) on disease progression measured as the percentage of resistant lesions at 4- and 6-days post-inoculation (dpi).

		% Resistant lesions			
		Direct		Systemic	
Polymer	Concentration (mg/mL)	4 dpi	6 dpi	4 dpi	6 dpi
Water	0	8^a	7^a	17^a	0^a
0.1 % acetic acid	0.1	21^{ab}	13^a	0^a	0^a
Chitosan	0.5	5^a	2^a	0^a	0^a
	1	68^c	54^b	0^a	0^a
	2.5	31^b	10^a	0^a	0^a
Water	0	9^a	6^a	0^a	0^a
Diamino 1	0.5	100^b	96^b	25^{ab}	0^a
	1	100^b	95^b	50^{bc}	50^b
	2.5	100^b	98^b	92^c	58^b
Water	0	44^a	12^a	28^a	11^a
Diamino 2	0.5	76^b	23^a	29^a	14^a
	1	58^c	43^b	42^a	8^a
	2.5	73^b	55^b	46^a	19^a

The data shows an average of two experiments, with 30-45 leaflets per experiment. The significance between concentrations for each polymer is denoted with letters. The same letters are not statistically different from each other (Kruskal-Wallis test followed by Dunn's *post hoc* test, $p < 0.05$).

Direct treatment with D2 + *B. cinerea* inoculation also displayed significant resistance at 4 dpi and 6 dpi for all concentrations assessed but was less protective than D1 (**Figure 3.2C** and **Table 3.2**). CHT direct treatment + *B. cinerea* inoculated leaves had a lower efficacy at 4 and 6 dpi when compared to D1 and D2 treatment (**Table 3.2** and **Figure 3.2C**). At 4 dpi, the 1 and 2.5 mg/mL concentrations of CHT treatment were significantly resistant. However, it is worth noting that the 0.1% acetic acid control + *B. cinerea* inoculated leaves displayed a small but

nonsignificant increase in the percentage of resistant lesions (22%), compared to the water treatment (8%) and were not statistically different from the highest CHT concentration (**Figure S3.2C** and **Table 3.2**).

The systemic protective effects of D1 treatment + *B. cinerea* inoculation at 4 dpi displayed significant resistant lesions at 50 and 90% for 1 and 2.5 mg/mL, respectively and were maintained at 6 dpi for 1 mg/mL (50%), with a decrease at 2.5 mg/mL (58%) (**Figure S3.2D** and **Table 3.2**). However, there were overlapping protective effects between the concentrations given the large standard deviations. In contrast to D1, D2's protective effects at 4 and 6 dpi were nonsignificant when compared to the water treatment at 4 dpi but still maintained resistant lesions at 1 and 2.5 mg/mL with 42 and 46%, respectively (**Table 3.2**). CHT displayed the lowest efficacy of the biopolymers at both 4 and 6 dpi, with no resistant lesions at all concentrations evaluated for the systemic treatment.

Images quantifying the changes in the photosynthetic performance of leaves treated and/or inoculated were used to assess the health of the leaf and/or disease progression of *B. cinerea* inoculation at 4 dpi. The photosynthetic performance was measured by quantifying the efficiency of photosystem II (F_v/F_m) and the stress indices, namely the chlorophyll index (ChlIdx) and the modified anthocyanin index (mAriIdx). **Figure 3.2A**, **3.2B** and **Figure S3.2** display images that visualize the effects of the direct and systemic biopolymer treatment on lesion development. **Figures 3.3** and **S3.4** show the distributions and mean values for F_v/F_m (**Figures 3.3A** and **S3.4**), ChlIdx (**Figure 3.3B**), and mAriIdx (**Figure 3.3C**). All observations were compared to the water treatment + *B. cinerea* inoculated images (**Figure 3.2)** and the distributions (**Figures 3.3** and **S3.4**) at 4 dpi.

3.4.2.1 Direct biopolymer or water treatment and *B. cinerea* inoculation

The direct application of D1 treatment + *B. cinerea* inoculation resulted in significant F_v/F_m values that were consistently higher than the F_v/F_m values for D2 and CHT at all concentrations (**Figures 3.3A and S3.4A**). This was visualized by the absence of red lesions in the F_v/F_m images and correlated with the F_v/F_m distributions (**Figures 3.2A** and **3.3A**).

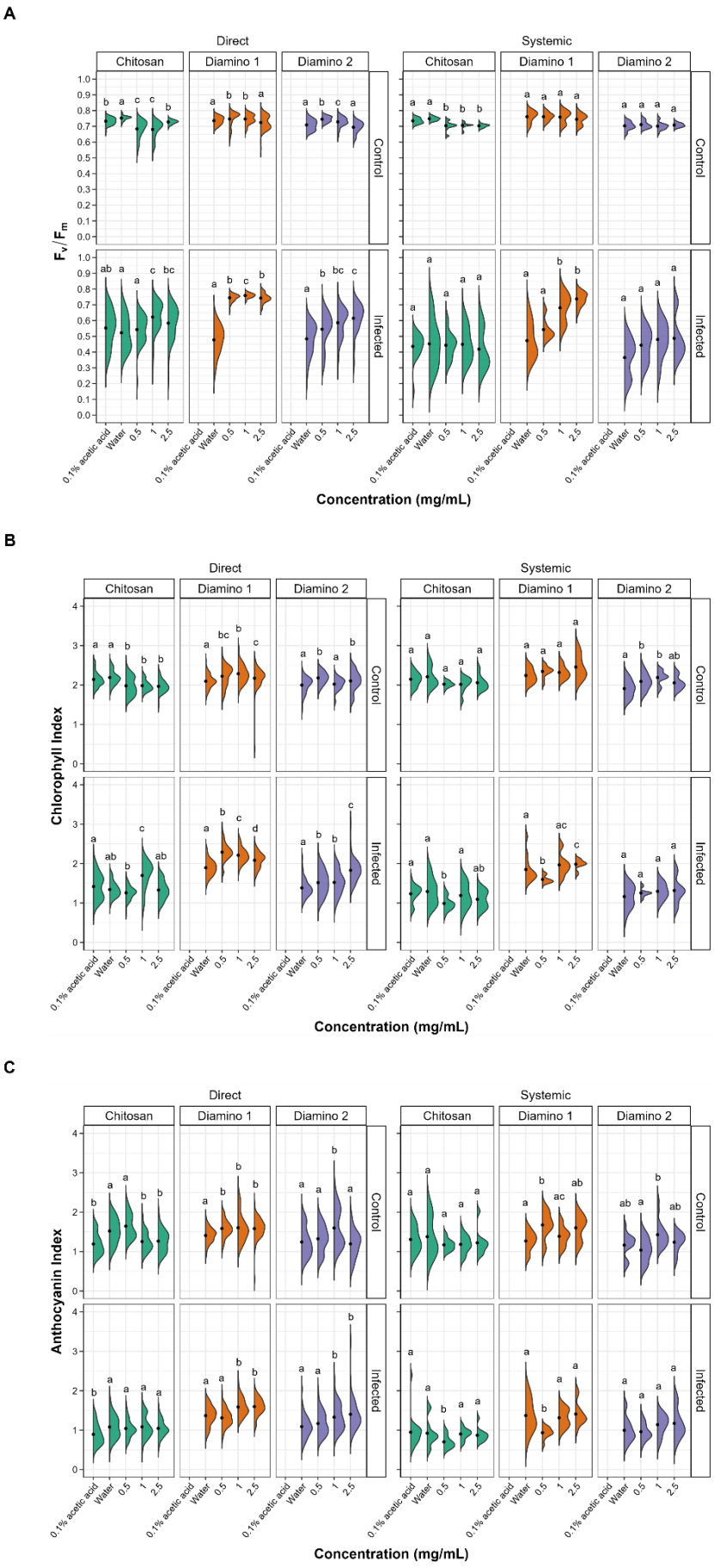

Figure 3.3: The effects of direct and systemic chitosan (CHT), diamino 1 (D1), diamino 2 (D2), and controls (water and 0.1% (v/v) acetic acid) treatment on the overall health of *B. cinerea* or mock inoculated leaves at 4 days post-inoculation. Overall health was assessed using **(A)** F_v/F_m, **(B)** chlorophyll index (ChlIdx) and **(C)** the modified anthocyanin index (mAriIdx). n = 45 leaflets per treatment. The black dots represent the mean of each half violin. Concentrations with different letters are statistically significant (Kruskal-Wallis test followed by Dunn's *post hoc* test, $p < 0.05$).

The direct treatment with D2 + *B. cinerea* inoculation also resulted in significant average F_v/F_m values at all concentrations, but with a concentration-dependent increase (**Figure 3.3A)**. The direct treatment with CHT + *B. cinerea* inoculation significantly increased the average F_v/F_m values for 1 and 2.5 mg/mL concentrations, with 0.1% acetic acid having the same significance as the 2.5 mg/mL concentration (**Figures 3.3A** and **S3.4A**). The significant protective antifungal effects (**Table 3.1**) and increased protective *in planta* effects (**Table 3.2**) for 0.1% acetic acid were also noted phenotypically by the reduced red lesion sizes (**Figure 3.2A**) and in the increase in the distribution and average F_v/F_m values when compared to the water treatment (**Figures 3.3A** and **S3.4A**). Correspondingly, direct 0.1% acetic acid treatment + *B. cinerea* inoculation resulted in a similar nonsignificant increase in the average ChlIdx values (**Figure 3.3B**). Direct D1 and D2 treatment + *B. cinerea* inoculation showed a significant increase in the distribution of ChlIdx values at all concentrations assessed, with notable differences between the concentrations of D1 treatment (**Figure 3.3B**).

The mAriIdx values for direct treatment with CHT + *B. cinerea* inoculation were the same as for the water treatment (**Figure 3.3C**). However, the 0.1% acetic acid control was statistically lower than the water treatment and all concentrations of CHT (**Figure 3.3C**). In contrast, both D1 and D2 direct treatment + *B. cinerea inoculation* had statistical increases in the average mAriIdx at 1 and 2.5 mg/mL concentrations (**Figure 3.3C**). This was noted phenotypically in **Figure 3.2C**, where higher levels of mAriIdx are visible at the sites corresponding to 1 and 2.5 mg/mL of D1 treatment. Visually, this appeared concentration-dependent, as the accumulation was more visible at 2.5 mg/mL compared to 1 mg/mL and was not observed at 0.5 mg/mL.

3.4.2.2 Systemic biopolymer or water treatment and *B. cinerea* inoculation

The F_v/F_m values for the systemic D1 treated + *B. cinerea* inoculated leaflets corroborated the phenotyping data (**Figure 3.2B**) and were also significantly higher than the water treatment (**Figure 3.3A** and **S3.4B**) with a concentration-dependent increase in the average F_v/F_m (**Figure 3.3A**). D1 also displayed marked differences in the proportion of healthy F_v/F_m levels, 4 and 5, at all concentrations assessed compared to D2 and CHT (**Figure S3.4B**). Although the F_v/F_m distributions of D2 did not exhibit a significant difference from the water treatment, the data points tended to cluster at higher values compared to the water treatment. This suggests that

some protective effects may have been elicited (**Figure 3.3A**). Like the phenotyping data in **Figure 3.2B** and Section 3**.3.2**, the average F_v/F_m values for CHT, and 0.1% acetic acid treated + *B. cinerea* inoculated leaflets were nonsignificant when compared to the water treatment (**Figures 3.2B, 3.3A**, and **S3.4B**). The distribution of ChlIdx values for the D1, D2 and CHT systemically treated + *B. cinerea* inoculated leaflets was nonsignificant at all concentrations assessed except for 0.5 mg/mL of the D1 and CHT treatments, which were lower than the water treatment (**Figure 3.3B**).

Correspondingly, a significant decrease in the average mAriIdx at 0.5 mg/mL compared to the water treatment for D1 and CHT systemically treated + *B. cinerea* inoculated leaflets was also seen (**Figure 3.3C**). However, in contrast to the ChlIdx, a nonsignificant increase in mAriIdx distribution was observed at 1 and 2.5 mg/mL for D1 and D2 systemically treated + *B. cinerea* inoculated leaflets (**Figure 3.3C**). This was noted phenotypically in **Figure 3.2D,** where higher levels of anthocyanin were visible at the sites corresponding to 1 and 2.5 mg/mL of D1 treatment on systemically treated leaves.

3.4.3.3 Direct biopolymer or water treatment and mock inoculation

D1 and D2 directly treated and mock inoculated leaflets displayed significant increases in the average F_v/F_m values for 0.5 and 1 mg/mL, with a nonsignificant decrease in the average for the 2.5 mg/mL concentration (**Figure S3.4A**). A similar increase was observed for the average ChlIdx values for D1 and D2 directly treated and mock inoculated leaflets (**Figure 3.3B**). D1 treatment showed significant increases at all concentrations, whereas D2 treatment was only significant at 0.5 and 2.5 mg/mL (**Figure 3.3B**). D1 and D2 treatment displayed a significant increase in the average mAriIdx values for all concentrations, while D2 was only significant at 1 mg/mL (**Figure 3.3C**). This increase was visible in the D1 phenotyping images in **Figure S3.3C**, where areas with residual dry droplets correspond to higher mAriIdx values (according to the false color scale).

Contrastingly, for leaflets directly treated with CHT and mock inoculated, a significant decrease in the average F_v/F_m, ChlIdx, and mAriIdx values was observed at all concentrations assessed (except 0.5 mg/mL mAriIdx) (**Figure 3.3A**, **3.3B**, and **3.3C**, respectively). This significant decrease in F_v/F_m and mAriIdx was also observed for the 0.1% acetic acid treatment

+ *B. cinerea* inoculated leaves when compared to the water treatment + *B. cinerea* inoculated leaves (**Figures 3.3A**, **3.3B**, and **3.3C**).

3.4.3.4 Systemic biopolymer or water treatment and mock inoculation

For the systemic application of D1 and D2 treatments and mock inoculation, no differences were seen in the distribution or average F_v/F_m values for all concentrations assessed compared to the water treatment (**Figure 3.3A**). However, when looking at the distribution of the F_v/F_m levels in **Figure S3.4B**, D1 displayed a higher proportion of levels 4 and 5 compared to D2 (**Figure S3.4B**). D1 systemically treated and mock inoculated leaflets displayed a nonsignificant increase in ChlIdx values at all concentrations, whereas D2 treated and mock inoculated leaflets were significantly greater at 0.5 and 1 mg/mL concentrations (**Figure 3.3B**). The average mAriIdx values for D1 and D2 treatments were not significant as the distributions were large, often with two clusters of data points indicating protective effects in a fraction of the leaflets assessed (**Figure 3.3C**). This increase was visible in the D1 phenotyping images in **Figure S3.3D**. Additionally, as in the systemic *B. cinerea* inoculated leaflets, little to no anthocyanin accumulated at the site of infection when treated with 1 and 2.5 mg/mL of D1 but appeared phenotypically similar at 0.5 mg/mL (**Figure 3.2C**). Treatment with CHT and mock inoculation was significantly lower at all concentrations for the average F_v/F_m (**Figure 3.3A** and **S3.3B**). There were no changes observed in the ChlIdx and mAriIdx values at all concentrations of CHT treatment and mock inoculation assessed (**Figures 3.3B** and **3.3C**).

3.4.4. Characterizing an early defence response in tomato leaflets: aminochitosan and H_2O_2 production

The production of reactive oxygen species (ROS) is frequently observed as a dominant and early defence response (Thordal-Christensen et al., 1997). Hence the impact of D1 on hydrogen peroxide (H_2O_2) production was evaluated in a time course series using DAB staining to compare H_2O_2 accumulation at the site of inoculation. This method yields brown precipitates that indicate the presence of H_2O_2 accumulation allowing both macroscopic and microscopic assessment.

3.4.4.1 Macroscopic observations

The macroscopic progression of disease symptoms were visualized over time using RGB and dark-adapted chlorophyll fluorescence (F_v/F_m) images (**Figure 3.4A** and **Figure 3.4B** respectively) as the use of chlorophyll fluorescence allowed for earlier detection of disease symptoms (Pavicic et al., 2021).

In the RGB images, disease symptoms were only observable from 48 hpi for both CHT and D1 (**Figure 3.4A**). For the chlorophyll fluorescence images, dark spots on the leaflets that signify the lack of chlorophyll fluorescence served as an indicator for necrotic lesions. Mock inoculated leaflets displayed no dark spots (data not shown). The initial development of necrotic lesions was first observed at 16 hpi for the water treatment, at 20 hpi for 0.5 mg/mL of CHT treatment and at 24 hpi for 0.5 mg/mL of D1 treatment (**Figure 3.4B**). D1 treatment significantly protected against necrotic lesion development for 1 and 2.5 mg/mL up to and including 72 hpi (**Figure 3.4A** and **Table S3.1**). Lesion development for 0.1% acetic acid was protective up to 20 hpi compared to the water treatment at 16 hpi (**Figure 3.4A** and **Table S3.1**).

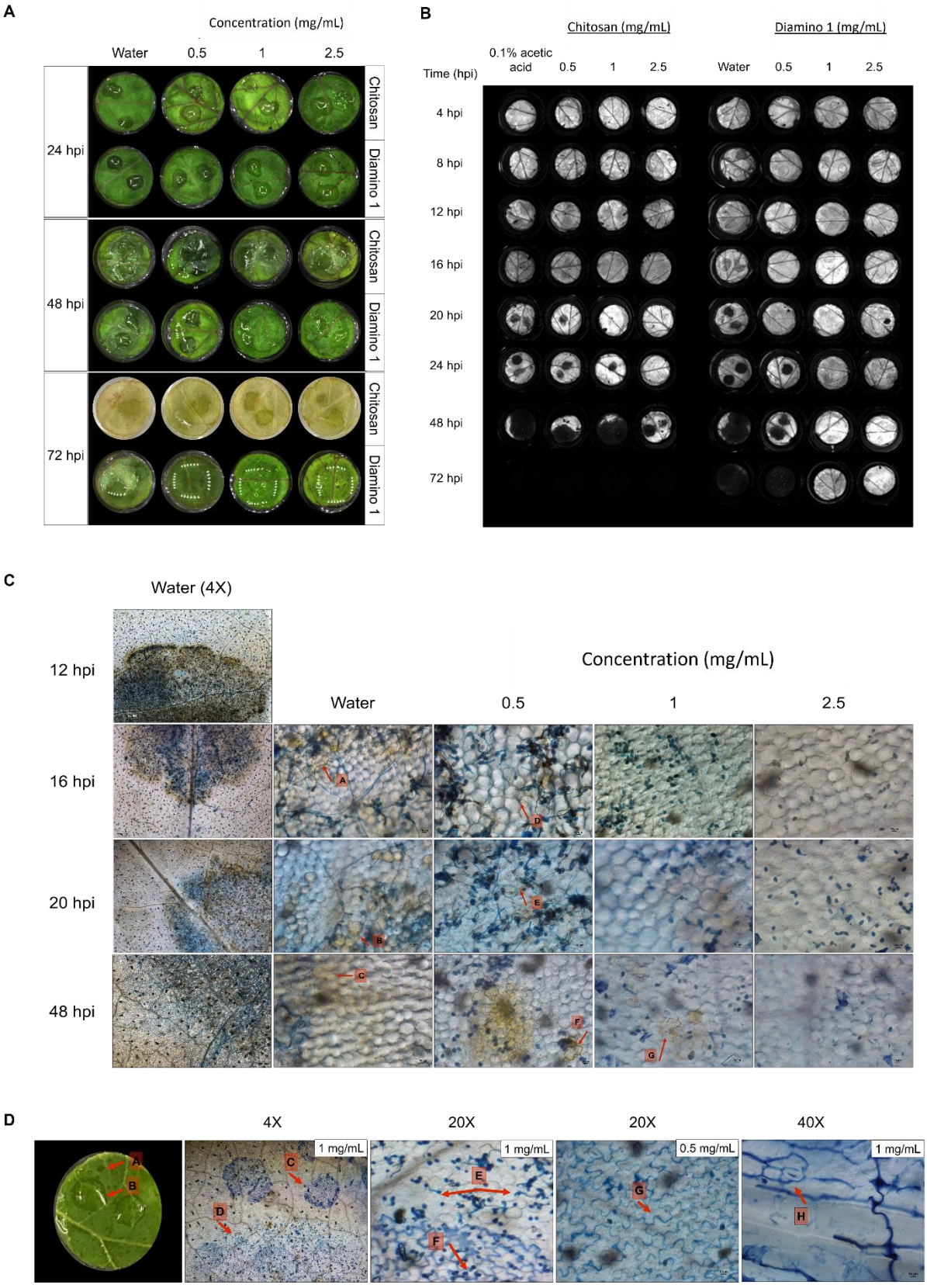

Figure 3.4: The temporal progression of *B. cinerea* disease symptoms on leaf discs treated with chitosan (CHT) and diamino 1 (D1). **(A)** The macroscopic development of spreading lesions over 24, 48 and 72 hpi. Lesions are denoted by their signature "wet" and "brown" phenotype at 48 hpi, followed by the growth of white mycelia at 72 hpi. (**B**) A chlorophyll fluorescence image showing the temporal development of lesions highlighted by the

absence of chlorophyll (dark lesions) at the inoculation sites for the different time points. One of five representative biological replicates are shown. **(C)** DAB staining visualizing the accumulation or absence of H_2O_2 at 4X (water only) and 20X (water and D1 treatment). The experiment was repeated twice. (**D)** The co-staining of D1 with Trypan Blue. The accumulation of D1 in the walls of cells as indicated by arrows G and H. The diamino droplets sprayed onto the leaflets are labeled with arrows, A-C. Differences in the germination of spores covered by visible droplets compared to free spores are indicated by arrows C-F. The images represent an average of five biological replicates. The experiment was repeated once. Scale bar 4X magnification = 200 µm, 20X magnification = 100 µm and 40X magnification = 10 µm.

3.4.4.2 Microscopic observations

No H_2O_2 accumulation was observed in the water/biopolymer treated and mock inoculated leaflets (data not shown). In the water-treated + *B. cinerea* inoculated leaflets, H_2O_2 accumulation was visible at 4X magnification around the entire lesion perimeter and within the infection droplet from 12 hpi (**Figure 3.4C**). A decrease in the intensity of DAB staining was observed for the water-treated leaflets between 20 and 48 hpi (**Figures 3.4C**).

Intriguingly, leaflets treated with D1 displayed a decrease in H_2O_2 accumulation with an increase in concentration as well as an increase in the intensity of DAB staining over time (**Figure 3.4C**). Therefore, the time taken to accumulate H_2O_2 levels comparable to the water-treated leaflets was only achieved at later time points. Leaflets treated with 0.5 mg/mL of D1 displayed lesions with sparse areas of minimally visible H_2O_2 accumulation at 16 and 20 hpi (**Figure 3.4C**, **arrows D** and **E**) with a minimal increase in the intensity of DAB staining at 24 hpi (**Figure 3.4C**, **arrow F)**. For leaflets treated with 1 and 2.5 mg/mL of D1, no H_2O_2 accumulation was visible up to 16 hpi and 20 hpi (for 2.5 mg/mL) (**Figures 3.4C**). Between 20 and 48 hpi, D1 at 1 mg/mL displayed a low intensity of DAB staining in few cells (**Figure 3.4C, arrow G**) with D1 at 2.5 mg/mL only displaying H_2O_2 accumulation observed at 48 hpi (**Figure 3.4C)**.

The microscopic observations revealed an interaction between D1 and Trypan Blue (**Figure 3.4D, arrows C**). The area occupied by the droplets corresponded with the D1 droplet residues that were separate to the *B. cinerea* droplet residue (**Figure 3.4D**, **arrow A** and **B,** respectively). At higher magnification, the droplet areas also displayed an accumulation of Trypan Blue within the anticlinal walls of cells within the epidermis of the leaf tissue and exhibits the same lobed shape as the cells (**Figure 3.4D**, **arrow G** and **H**). Most notably, the spores beneath the D1 droplet area have little to no germinated spores when compared to

the spores within the inoculation droplet that do not intersect with the D1 droplet (**Figure 3.4D**, **arrows E** and **F**).

3.4.5 The antifungal and *in planta* efficacy of molecular weight variants of aminochitosan

Due to the observable differences in the antifungal and *in planta* efficacies of D1 and D2, a third biopolymer batch was synthesized and further fractionated to allow for chemical and biological characterization of the different MW fractions. The third biopolymer batch will herein be referred to as diamino 3 (D3), and the D3 MW fractions will be referred to as fractions 1-5 (F1-F5).

3.4.5.1 Elemental analysis of D3 and D3 lower MW fractions

Elemental analysis (EA) was used to determine whether varying efficacies of the aminochitosan batches were due to differences in their nitrogen composition. EA was conducted by identifying the percentage of carbon (C), nitrogen (N) and hydrogen (H) in D1, D2, D3, and the D3 MW fractions, F1 (3.5–5 kDa), F2 (15 kDa), F3 (20 kDa), F4 (20–99 kDa), and F5 (100 kDa). Data including the percentage of hydrogen are not shown. The EA data displayed a clear increase in the percentage of nitrogen content for D1, D2, D3, F1, F2, F3, and F5 compared to native CHT (**Table 3.3**). F4 displayed the lowest percentage of nitrogen compared to the MW fractions and was also lower than the nitrogen content for CHT. In addition to determining the elemental composition, the ratio of carbon to nitrogen (calculated as C/N) was used to determine the degree of substitution (DS), the number of hydroxyl groups substituted with amino groups; a key factor when evaluating the formation of aminochitosan (Sayed, 2018). The DS values for D1 and D2 were within 0.08 of each other and were therefore within close range. The lowest DS was obtained for D3 (0.63), while the highest DS was obtained for F4 (0.81) (**Table 3.3**). D1 (0.76) F2 (0.77), F3 (0.78) and F5 (0.78) displayed the most similar DS (**Table 3.3**).

Table 3.3: Elemental analysis of carbon (C) and nitrogen (N) for chitosan (CHT), diamino 1 (D1), diamino 2 (D2), diamino 3 (D3), and diamino 3 MW fractions (F1-F5).

Polymers	Mass fractions of elements		C/N	DS[1]
	*C (%)	*N (%)		
Chitosan	44.04 ± 0.10	6.62 ± 0.15	6.62	-
Diamino 1	44.24 ± 0.23	9.40 ± 1.00	4.70	0.76
Diamino 2	38.14 ± 0.30	7.94 ± 1.02	4.80	0.70
Diamino 3	44.15 ± 0.54	10.10 ± 1.05	4.37	0.63
3.5 - 5 kDa (F1)	35.43 ± 0.30	6.83 ± 1.67	5.19	0.75
15 kDa (F2)	37.03 ± 0.23	6.98 ± 0.12	5.31	0.77
20 kDa (F3)	40.88 ± 0.81	7.64 ± 0.02	5.35	0.78
20 - 99 kDa (F4)	31.49 ± 0.46	5.67 ± 0.11	5.55	0.81
100 kDa (F5)	39.86 ± 0.14	7.45 ± 0.01	5.35	0.78

* = as determined by elemental analysis. C/N = the ratio of carbon to nitrogen used to calculate the DS. DS = degree of substitution which denotes the number of -OH groups that were substituted with amine groups.[1]The formula used to calculate DS can e found in Section 3.3.5. The data represents the average of two experiments.

3.4.5.2 The antifungal effects of different aminochitosan MW fractions on *B. cinerea* growth and sporulation

The antifungal activity of D3 and the D3 MW fractions was investigated, with the quantitative and phenotypic effects shown in **Table 3.4** and **Figure 3.5**, respectively. A statistical increase in the PIRG% was observed for D3 treatment at 1 mg/mL and 2.5 mg/mL when compared to the PDA control (**Table 3.4**). Furthermore, a statistical increase in the PIS% was observed for all concentrations of D3 when compared to the PDA control (**Table 3.4**).

When comparing the phenotype and radial inhibition of the lower MW fractions, F1 and F2 appear to perform better than D3, while F1 and F3 appear to perform similarly to D3, at 1 and 0.5 mg/mL respectively (**Figure 3.5** and **Table 3.4**). No significant differences in the efficacy between F1, F2, and D3 on the phenotype and radial inhibition were observed at 1 mg/mL, while F3 was significantly different. In addition, F1, F2, and D3 were similar at 2.5 mg/mL whereas the efficacy of F3 at 2.5 mg/mL was significantly lower at the same concentration (**Table 3.4** and **Figure 3.5**).

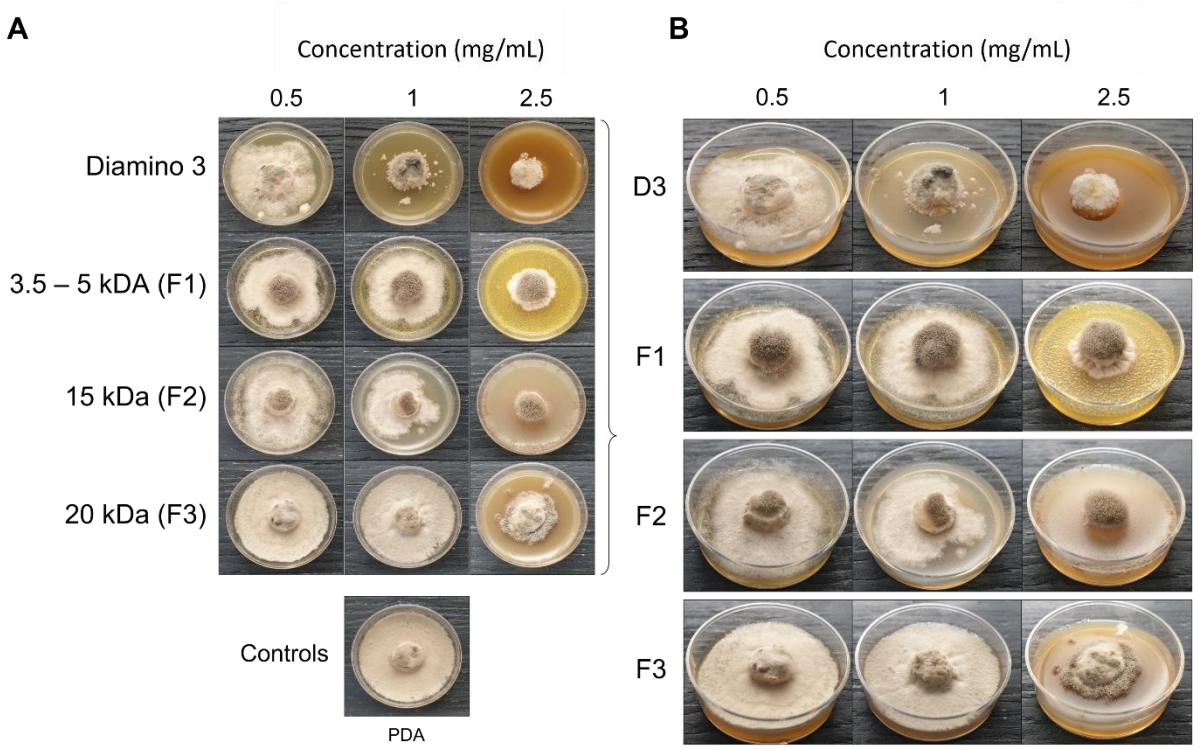

Figure 3.5: The phenotypic effects of diamino 3 (D3) and the D3 lower MW fractions (F1-F3) on the radial growth *of B. cinerea*, 11 days after incubation. **(A)** An overview of the effects relative to the PDA control. **(B)** A detailed view of the macroscopic and morphological changes. The images represent one of five biological replicates. The experiments were repeated twice.

When compared to the PDA control, F1 and F2 showed significant inhibitory effects on sporulation at 1 and 2.5 mg/mL, and at 1 mg/mL for F3 (**Table 3.4**). Large standard deviations for the sporulation data are to be noted as limiting factors. F5 displayed no effects on radial inhibition and sporulation at all concentrations assessed when compared to the PDA control (data not shown).

Table 3.4: The effects of various concentrations of diamino 3 (D3) and the D3 MW fractions (F1-F3) on the average mycelial radial growth and sporulation of *B. cinerea*, 11 days after incubation.

Treatment	Concentration (mg/mL)	**Radial Inhibition**		**Sporulation**	
		Growth area (mm^2) ± SD	PIRG (%) ± SD	Spores/mL ± SD	PIS (%) ± SD
PDA	0	491 ± 0	0 ± 0^{a}	21 133 ± 17 365	0 ± 0^{a}
Diamino 3	0.5	457 ± 48	7 ± 7^{a}	5 500 ± 1 980	77 ± 18^{b}
	1	237 ± 259	52 ± 37^{b}	4 750 ± 4 455	86 ± 8^{b}
	2.5	49 ± 58	90 ± 8^{c}	5 850 ± 8 132	85 ± 21^{b}
	5	20 ± 33	96 ± 0^{c}	300 ± 0	100 ± 0^{b}
PDA	0	491 ± 0	0.00^{a}	11 900 ± 14 100	0^{a}
F1 (3.5-5 kDa)	0.5	358 ± 87	28.36^{ab}	8 300 ± 4 600	30.25^{a}
	1	235 ± 93	52.23^{bc}	3 700 ± 4 200	68.91^{ab}
	2.5	47 ± 38	90.49^{c}	500 ± 0	95.80^{b}
PDA	0	491 ± 0	0.00^{a}	11 900 ± 14 100	0^{a}
F2 (15 kDa)	0.5	373 ± 162	23.97^{ab}	23 500 ± 32 200	-97.48^{a}
	1	270 ± 133	45.01^{bc}	2000 ± 3 600	83.19^{b}
	2.5	0 ± 0	100.00^{c}	100 ± 200	99.16^{b}
PDA	0	491 ± 0	0.00^{a}	11 900 ± 14 100	0^{ab}
F3 (20 kDa)	0.5	455 ± 80	7.33^{a}	5 500 ± 5 500	53.78^{ac}
	1	491 ± 0	0.03^{a}	1 500 ± 900	87.39^{c}
	2.5	121 ± 75	75.42^{b}	19 100 ± 9 100	-60.50^{b}

PIRG% = percentage inhibition of radial growth (PIRG), and PIS% = percentage inhibition of sporulation (PIS). A negative PIS% indicates growth greater than the control. Statistical significance was calculated between concentrations for each polymer. Means ± SD (standard deviation) followed by the same superscript letter are not significantly different from each other. Different letters indicate significant differences between concentrations. The presence of two letters indicates either similarity or difference across multiple concentrations for that polymer (Kruskal-Wallis test followed by Dunn's *post hoc* test, $p < 0.05$). The values shown are the average of three experiments.

3.4.5.3 The *in planta* effects of aminochitosan 3 (D3) and the D3 MW fractions, on eliciting resistance in the tomato/*B. cinerea* pathosystem

The direct and systemic effects of D3 and the D3 lower MW fractions were analyzed for their efficacy in eliciting a resistant phenotype at 4, 6, and 30 dpi (**Figure S3.5** and **Table 3.5**) and H_2O_2 production at 4, 8, 12,16, and 20 hpi (**Figure 3.6**). When compared to the water treatment, direct treatment with D3, F2, and F3 significantly increased the percentage of resistant lesions at 4 and 6 dpi (**Table 3.5** and **Figure S3.5**). Notably, at 4 and 6 dpi, F2 and F3 displayed a decrease in the percentage of resistant lesions at 2.5 mg/mL when compared to 1 mg/mL of the respective biopolymer (**Table 3.5**). Direct treatment with F1 statistically

increased the resistant phenotype at 1 and 2.5 mg/mL at both 4 and 6 dpi compared to the water treatment but was less effective than D3 (except at 6 dpi for 2.5 mg/mL), F2 and F3 (**Table 3.5**).

The systemic treatment yielded variable results at the different concentrations applied due to large standard deviations with overlapping ranges (**Table 3.5**). Systemic treatment with D3, F2, and F3 was significantly protective at 1 and 2.5 mg/mL when compared to the water treatment at 4 and 6 dpi (**Table 3.5**). Systemic F1 treatment, when compared to the water treatment, was significantly protective at 0.5 and 2.5 mg/mL at 4 and 6 dpi (**Table 3.5**). Furthermore, the systemic protection provided by F2 was greater than D3 (**Table 3.5**). Notably, similar to the results from direct treatment, a decrease in the percentage of resistant lesions was observed for 2.5 mg/mL of D3, F2, and F3 treatments at 4 and 6 dpi but was not observed for F1 treatment (**Table 3.5**). At 30 dpi, F2 remained significantly protective for both direct and systemic treatments at all concentrations compared to the water treatment (**Figure S3.5D**). At 30 dpi, F2 was protective at all concentrations (**Figure S3.5D**), while F1 and D3 were not (data not shown).

Table 3.5: The effects of various concentrations of diamino 3 (D3) and the D3 MW fractions (F1-F3) on disease progression measured as the percentage of resistant lesions at 4- and 6-days post-inoculation (dpi).

		% Resistant lesions			
		Direct		Systemic	
Biopolymer	Concentration (mg/mL)	4 dpi	6 dpi	4 dpi	6 dpi
Water	0	36^{a}	21^{a}	37^{a}	17^{a}
Diamino 3	0.5	63^{b}	42^{b}	57^{ab}	27^{ab}
	1	80^{c}	63^{c}	56^{ab}	47^{bc}
	2.5	83^{c}	56^{c}	75^{b}	64^{c}
Water	0	34^{a}	28^{a}	38^{a}	29^{a}
F1 (3.5-5 kDa)	0.5	47^{ab}	43^{ab}	67^{b}	58^{bc}
	1	59^{b}	47^{b}	33^{ab}	17^{ab}
	2.5	79^{c}	69^{c}	83^{b}	67^{c}
Water	0	34^{a}	29^{a}	38^{a}	29^{a}
F2 (15 kDa)	0.5	100^{b}	99^{b}	67^{b}	50^{a}
	1	99^{b}	97^{b}	83^{b}	75^{c}
	2.5	79^{c}	79^{c}	75^{b}	67^{b}
Water	0	34^{a}	28^{a}	38^{a}	29^{a}
F3 (20 kDa)	0.5	98^{b}	88^{b}	50^{ab}	50^{ab}
	1	96^{b}	96^{b}	100^{b}	100^{b}
	2.5	86^{b}	81^{b}	67^{b}	50^{ab}

The data shows the average of two experiments, with 30-90 leaflets per experiment. The significance between concentrations for each polymer is denoted with superscript letters. The same letters are not statistically different from each other (Kruskal-Wallis test followed by Dunn's *post hoc* test, $p < 0.05$).

To analyze the temporal regulation of H_2O_2 production, D3 and the lower MW fractions were evaluated using a time course series (**Figure 3.6**). Unlike the water and D1 treated and mock inoculated leaflets, treatment with 0.5 mg/mL of F1 and F3 and 1 mg/mL of F2 + mock inoculation resulted in H_2O_2 accumulation that was indiscriminate across the leaflets at 20 hpi (**Figure 3.6B**). In contrast to D1 and D2 treatment, H_2O_2 accumulation was macroscopically visible from 16 hpi onwards in D3 treated + *B. cinerea* inoculated leaflets (**Figure 3.6C**). No discernible differences in the patterns of H_2O_2 accumulation for *B. cinerea* inoculated leaflets were observed for all concentrations of F1, F2, and F3 assessed (**Figure 3.6C**). However, these MW fractions exhibited H_2O_2 accumulation as early as 4 hpi compared to 16 hpi for D3 treated + *B. cinerea* inoculated leaflets (**Figure 3.6C**). Furthermore, an increase in concentration resulted in a marginal decrease in the intensity of DAB staining for D3, F1, F2, and F3 as

evident from the differences in the quantity and color intensity of brown lesion spots (**Figures 3.6A** and **3.6C**).

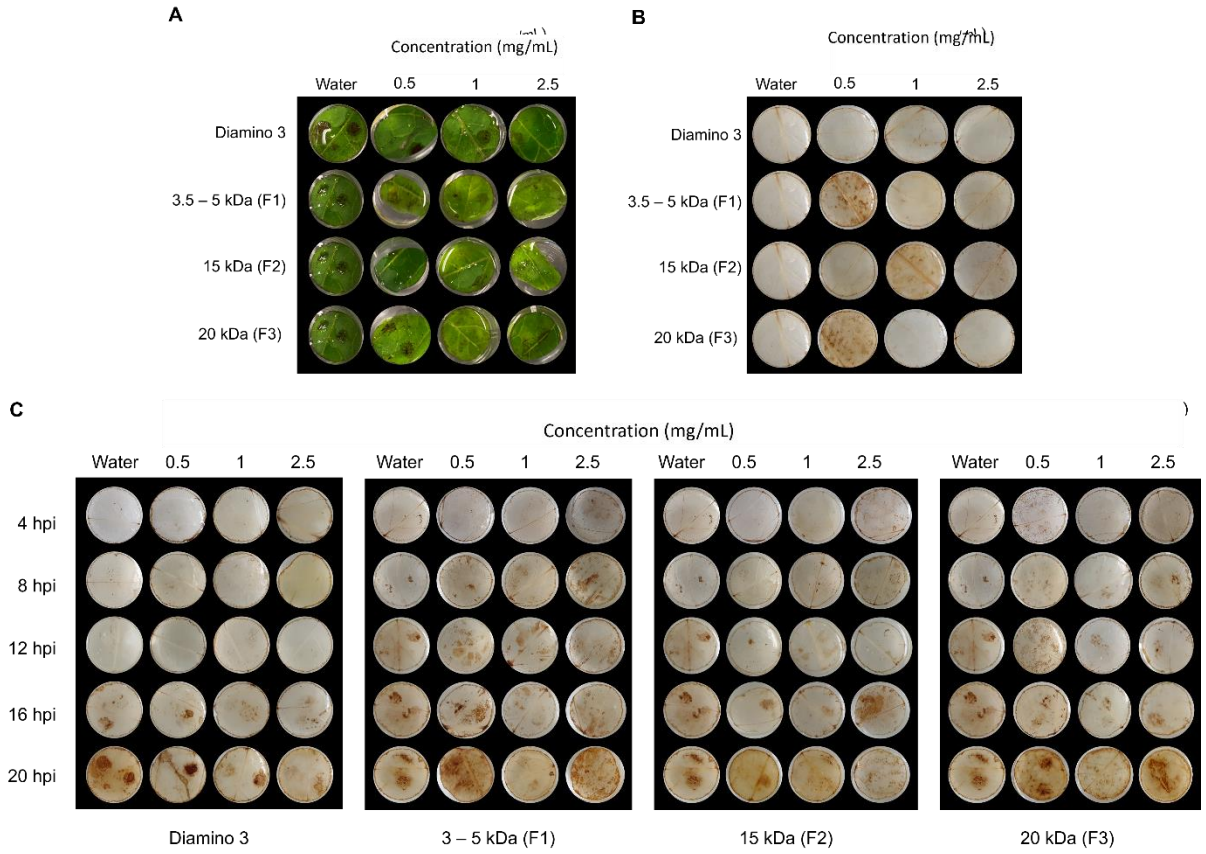

Figure 3.6: The temporal accumulation of H_2O_2 in leaf discs treated with diamino 3 (D3) and D3 lower MW fractions (F1-F3) and visualized with DAB staining at 4, 8-, 12-, 16- and 20-h post-inoculation (hpi) with *B. cinerea*. (A) Macroscopic images of DAB staining at 20 hpi displaying the progression of disease symptoms as noted by the appearance of brown spots in the RGB image. (B) Macroscopic image of DAB staining in de-stained leaf discs sprayed with different polymer concentrations and inoculated with a mock solution at 20 hpi. (C) The macroscopic, temporal H_2O_2 accumulation at 4, 8, 12, 16, and 20 hpi. This image correlates with the RGB image in (A). Leaf discs were inoculated with two 10 µL droplets of a *B. cinerea* spore solution (1 x 10^6 spores/mL containing 0.01 M glucose and 6.7 mM KH_2PO_4) 24 h after spraying. The image here represents one of four biological replicates.

3.4.6 The role of aminochitosan in priming *ACRE75*

De Vega et al. (2021) investigated and reported induced resistance and the temporal priming of the tomato Avr9/Cf-9 rapidly elicited protein 75 (*ACRE75*) by a commercially available water-soluble chitosan in tomato leaf discs infected with *B. cinerea* (De Vega et al., 2021). In the present study, the relative expression levels of *ACRE75* were measured in response to

mock/*B. cinerea* inoculation and different concentrations of direct D3 treatment at 6 and 9 hpi and systemic D3 treatment at 96 hpi.

D3 treated + mock inoculated leaflets displayed a significant increase in *ACRE75* normalized expression levels for 1 and 2.5 mg/mL concentrations at 6 hpi when compared to the water treatment (**Figure 3.7**). However, D3 treated + *B. cinerea* inoculated leaflets at 6 hpi had lower *ACRE75* relative expression levels compared to mock inoculated leaflets (**Figure 3.7**). Treatment with 2.5 mg/mL of D3 was significantly different from the water treatment at 6 hpi in *B. cinerea* inoculated leaflets. The 2.5 mg/mL concentration also showed the highest average relative expression levels for *ACRE75* at 6 hpi in D3 treated + mock/*B. cinerea* inoculated leaflets (**Figure 3.7**). Thus, at 6 h post-inoculation, both the mock and *B. cinerea* inoculated leaflets exhibited a concentration-dependent increase in normalized relative gene expression **(Figure 3.7**).

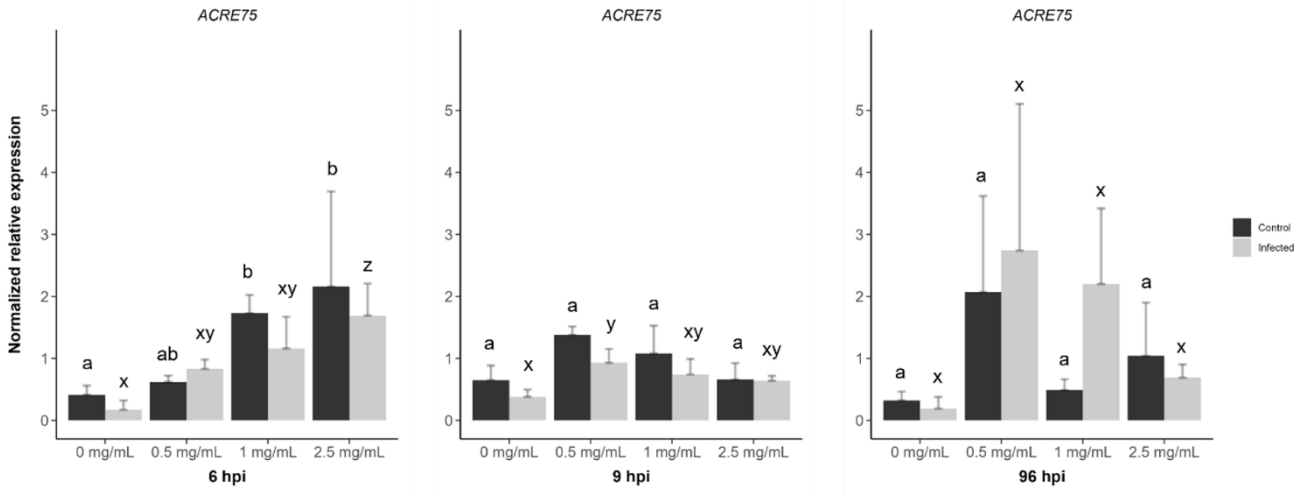

Figure 3.7: The effects of diamino 3 (D3) treatment compared to water treatment in *B. cinerea* and mock inoculated leaflets on the priming of *ACRE75* at 6, 9 and 96 h post inoculation (hpi). Different letters indicate statistically significant differences. a/b indicates differences between controls and x/y/z indicate differences between infected samples. (Kruskal Wallis test followed by Dunn's *post hoc* test, $p < 0.05$). n = 3 per concentration.

However, at 9 hpi, the relative gene expression decreased with increasing concentration for both genes, with 0.5 mg/mL of D3 treatment showing the highest nonsignificant averages for both mock and *B. cinerea* inoculated leaflets (**Figure 3.7**). A similar trend was observed with systemic D3 treatment and + mock/*B. cinerea* inoculation at 96 hpi (**Figure 3.7**). Overall, *ACRE75* had higher average expression levels in the D3 treated and mock inoculated leaflets compared to the water treatment at both 6 and 9 hpi (**Figure 3.7**). However, the standard

deviation for D3 treatments was greater, specifically in the treated and *B. cinerea* inoculated leaflets compared to the mock inoculated leaflets (**Figure 3**).

3.5 Discussion

Considering that amino groups are a defining factor in the physiochemical and biological properties of CHT derivatives; aminochitosan possesses improved functionality compared to native CHT (Satoh et al., 2006; Yang et al., 2012, 2015; Luan et al., 2018). To date, this is the first study to characterize aminochitosan dissolved exclusively in water (pH = 7) for its antifungal and *in planta* immunostimulatory properties, with a focus on the tomato*/B. cinerea* pathosystem. However, batch-to-batch variations posed a challenge in obtaining consistent data in characterization of physiochemical properties and biological activity. One such variation noted was in the solubility of D2 which was not observed for D1, D3, or the lower MW fractions of D3. However, when comparing the elemental composition of the batches, minor variation was seen between D1 and D2 with a bigger difference being seen in D3 (with no effect on the solubility). Thus, these differences are potentially due to the variability in the source materials utilized to synthesize aminochitosan batches (Croisier & Jérôme, 2013; Sayed, 2018). Other known contributors to the solubility of CHT and derivatives are DDA, DS and MW (Luan et al., 2018). The DDA and DS determine the number of amine groups available for protonation, while the MW affects the number of charged amino groups available for intermolecular interactions with the solvent (water) (Croisier & Jérôme, 2013; Bellich et al., 2016). Aminochitosan with a high DDA and DS and a low MW is more soluble than aminochitosan with a low DDA, DS and a high MW (Bellich et al., 2016). Therefore, potential differences in MW resulted in small but measurable variations in the efficacy of the batches both for its antifungal and *in planta* immunostimulatory properties, as observed between D1 and D2.

3.5.1 Antifungal effects of aminochitosan against *B. cinerea*

Aminochitosan, specifically D1, displayed significantly greater inhibition of *B. cinerea* than CHT at a minimum concentration of 1 mg/mL. Similar results were reported by De Vega et al. (2021), who reported significant inhibition of *B. cinerea* with water-soluble CHT at a concentration of 0.1% (1 mg/mL) and higher (De Vega et al., 2021). Another study on

aminochitosan (DS of 0.81, C/N 2.834) and CHT (DDA of 95% and MW of 700 kDa) by Luan et al., (2018) was investigated against various species in the *Fusarium* genus. The study demonstrated that aminochitosan at a concentration of 0.5 mg/mL exhibited more than a 20% increase in antifungal activity. However, both CHT and their aminochitosan were dissolved in 0.35% acetic acid (Luan et al., 2018). In the present study, the antifungal activity of CHT was confounded using acetic acid as a solvent for CHT on account of acetic acid displaying significant radial growth inhibition at a concentration of 0.1%. Furthermore, these results were no different from the effects of the 0.5 and 1 mg/mL concentrations of CHT, indicating a protective effect of 0.1% acetic acid. Acetic acid, amongst others, has been shown to display antimicrobial activity *in planta* and *in vitro* as the undissociated form of acetic acid is lipophilic, allowing penetration of the cell membrane (Narendranath, Thomas & Ingledew, 2001). Once inside the cell, a decrease in the pH of the cytoplasm disrupts the cell membrane and inhibits metabolic processes necessary for fungal growth (Kang, Park & Go, 2003; Hassan, Sand & El-Kadi, 2012; In et al., 2013). A study by Narendranath, Thomas & Ingledew (2001) reported a reduction in growth rates and glucose consumption of *S. cerevisiae* as the concentration of acetic acid in the media increased (Narendranath, Thomas & Ingledew, 2001).

In the present study, a concentration-dependent increase in the antifungal activities of CHT, D1, and D2 was observed for radial growth and sporulation compared to the PDA control. Maximum inhibition for all the biopolymers was seen between the 2.5 and 5 mg/mL concentrations. Large standard deviations between the biopolymers for these concentrations were potentially due to the abovementioned batch-to-batch variations and inhibitory effects of acetic acid. At 0.5 mg/mL, an increase in sporulation and the number of spores/mL was observed for CHT, D2, and D1 in that respective biopolymer order. This could be attributed to the differences in the DDA between CHT and aminochitosan (as well as its DS at C-6 of the polymer) At low concentrations, CHT is the least inhibitory as it has a lower DDA than aminochitosan, whereas D1 and D2 have greater DDA and DS. However, no general trend can be deduced from the increase or decrease in DDA (Younes et al., 2014).

In addition, the haloes observed around the mycelial growth for CHT are indicative of the ability of *B. cinerea* to degrade the polymer, using the resulting monomers as a nutrient

source with the outcome of media clearing. A study by Palma-Guerrero et al., (2007) reported a similar result for *Verticillium dahlia,* where its growth on PDA increased at 0.5 and 1 mg/mL and only decreased at 2 mg/mL. They suggested that *V. dahlia* was capable of using CHT as a nutrient source at lower concentrations and also reported the degradation activity of CHT, as noted by the appearance of halos around the mycelial growth at 0.5 and 1 mg/mL concentrations (Palma-Guerrero et al., 2007). Therefore, at low concentrations, *B. cinerea* may utilize aminochitosan as a nutrient source, with an apparent preference for an increased number of amine groups. This was noted in the differences between D1 and D2 inhibition, where D1 displayed the greatest increase in sporulation, which additionally correlated with its higher nitrogen percentage due to extra amine group(s) on aminochitosan. Harper et al., (1981) showed that omitting NH_4NO_2 from the growth medium resulted in a significant decrease in the growth of *B. cinerea* and in the percentage of spreading lesions *in planta*. They concluded that nitrogen sources such as nitrate or ammonium support and enhance growth (Harper, Strange & Langcake, 1981).

The germination data for D1 suggests the presence of a concentration threshold beyond which impaired germination or complete inhibition of germination occurs for aminochitosan and is maintained over time. The data in this study suggests that this threshold for aminochitosan is 1 mg/mL for spores germinating *in planta,* compared to the 2.5 mg/mL threshold for direct antifungal efficacy. Similarly, a study by Palma-Guerrero et al., (2007) reported that the spores of two plant pathogenic and two myco-parasitic fungi were more sensitive to CHT treatment than hyphae as growth was irreversibly inhibited at a concentration of 0.01 mg/mL (Palma-Guerrero et al., 2007). Hence, the *B. cinerea* spore suspension used *in planta* was more sensitive than the *B. cinerea* fungal discs used in the antifungal assays, which contained a mixture of hyphae and spores. The contrast between these efficacies highlights the bimodal MoA of aminochitosan and the advantageous role of primed plant defence systems.

3.5.2 Effect of aminochitosan in plants

Image-based quantification of photosynthetic parameters is non-destructive, non-invasive, sensitive, rapid, and allows for high-throughput screening (Meng et al., 2020; Pavicic et al., 2021). Chlorophyll fluorescence imaging is generally used to assess and quantify the

photosynthetic performance and efficiency of leaves including plant-pathogen interactions (Rolfe & Scholes, 2010; Pérez-Bueno, Pineda & Barón, 2019). Furthermore, it accounts for the spatiotemporal heterogeneity of photosynthesis across the total leaf area (Bayçu et al., 2018). Plant-pathogen interactions regularly result in altered energy expenditure as a defence strategy and a decrease in photosynthesis and related chloroplastic metabolisms after the onset of chlorosis and necrosis at local infection sites (Berger et al., 2007; Fagard et al., 2014; Rojas et al., 2014). In order to analyze maximum photosynthetic efficiency of Photosystem II (PSII, also a measure of F_v/F_m), it is necessary to distinguish between the rates of photosynthesis, fluorescence emission, and heat dissipation as these factors are in competition with each other (Murchie & Lawson, 2013; Pérez-Bueno, Pineda & Barón, 2019). When challenged, plants adapt by increasing their capacity for heat dissipation, while F_v/F_m remains unchanged. However, if the stressor exceeds this adaptive capacity, a decrease in F_v/F_m is observed, with the potential for extreme inhibition of PSII activity (Pérez-Bueno, Pineda & Barón, 2019).

Image-based analysis corroborated the RGB findings (aminochitosan as a protective treatment up to 4 and 6 dpi) by analyzing photosynthetic parameters (F_v/F_m, ChlIdx, and mAriIdx). F_v/F_m was shown to be inversely associated with lesion development as noted by the absence of “red lesions” with an increase in F_v/F_m or by an increase in lesion size and disease progression with decreasing F_v/F_m (Rolfe & Scholes, 2010; Meng et al., 2020). F_v/F_m is therefore a useful indicator for the early signs of priming, infection, locally enhanced photosynthesis and a potentially enhanced defence response as a means of constraining pathogen growth to the site of infection (Berger et al., 2004; Rolfe & Scholes, 2010; Meng et al., 2020).

The data in the present study show enhanced photosynthesis in both the inoculation droplet site and in the surrounding areas. However, this observation is not restricted to the intercostal areas containing infection sites, as observed in Berger et al. (2004); rather, it is ubiquitous across the lamina. Therefore, maintaining heterogenous photosynthesis for as long as possible is a key aspect of the plant's defence strategy (Berger et al., 2004). The sustained elevated photosynthetic activity may be due to priming of a stronger and more rapid elicitation of the defence systems at earlier time points, resulting in an unsuccessful infection.

This is in contrast to the various chlorophyll fluorescence imaging studies on a few pathosystems, including the tomato/*B. cinerea* pathosystem, that have shown the downregulation of photosynthesis, chlorophyll fluorescence, and induction of sink metabolism after compatible pathogen interactions locally at the site of interaction and in surrounding tissues (Berger et al., 2004, 2007; Scharte, Schon & Weis, 2005; Bonfig et al., 2006; Muniz et al., 2014; Smith et al., 2014; Meng et al., 2020). As stated in Kanwar & Jha (2019), the data from Chou et al. (2000) and Berger et al. (2004) suggest that necrotrophic interactions generally result in rapid changes to photosynthesis that are visible before any apparent disease phenotype (Kanwar & Jha, 2019). The D1 data agree with this observation, where changes in photosynthesis are sustained and quantified, extending up to 4 and 6 dpi without an apparent disease phenotype. However, the D2 data is similar to that of Chou et al. (2000) and Berger et al. (2004), where infected leaves generally displayed inhibition of photosynthesis at the site of infection with an area of maintained photosynthetic parameters (healthy areas) in the immediate surrounding uninfected leaf areas, noted as “green islands”, is a representation of the spatiotemporal heterogeneity of infection (Chou et al., 2000; Berger et al., 2004; Pérez-Bueno, Pineda & Barón, 2019).

The term “green island” has been a descriptor for biotrophic interactions where areas of senescence are halted and photosynthetic activity is maintained, although at a lower level. Therefore, the occurrence of green islands is generally seen at later stages of disease progression, where the site of infection remains green while the surrounding tissue senesces (Walters, McRoberts & Fitt, 2007). Polyamines (PA) are a group of compounds that retard senescence and accumulate in green islands (Walters, McRoberts & Fitt, 2007). Naturally occurring PA, such as spermine and spermidine, are synthesized in plants and are defined as low molecular weight polycations containing amino groups (Janse van Rensburg, Limami & Van den Ende, 2021). PAs are both water-soluble and insoluble, which is similar to aminochitosan (and in contrast to CHT). This property coupled with its positive charge allows for differential distribution and localization as well as electrostatic interactions with nucleic acids, acidic proteins, and phospholipids (Janse van Rensburg, Limami & Van den Ende, 2021). Aminochitosan therefore bears similarity to PAs; its biological activity may be mediated through similar mechanisms and pathways that prevent senescence, resulting in a resistant phenotype of varying degrees.

Comparably, exogenous PA application was shown to prime resistance and increase stress tolerance to *B. cinerea* infection in *Arabidopsis* (Janse van Rensburg, Limami & Van den Ende, 2021), maintain the integrity of the thylakoid membrane during leaf senescence (Besford et al., 1993), prevent the loss of or elevate chlorophyll content (Galston & Sawhney, 1990; ElSayed et al., 2022), maintain normal or elevated PSII activity (Legocka & Zajchert, 1999; ElSayed et al., 2022), and impede the initial stages of crown rust infection by affecting germ tube growth and appressorium formation (Montilla-Bascón et al., 2016). Furthermore, high total chlorophyll was correlated with basal leaf resistance (Meng, Höfte & Van Labeke, 2019). In this study, foliar application of aminochitosan displayed efficacy in priming direct resistance to *B. cinerea* infection by maintaining elevated ChlIdx and PSII activity as well as directly inhibiting germination *in planta*.

Interestingly, a decrease in F_v/F_m, and therefore photosynthesis, was observed at 2.5 mg/mL of aminochitosan application. This may be indicative of a decrease in the efficiency of PSII due to the destabilization of chloroplasts and thus PSII (Meng et al., 2020). Hence, at 2.5 mg/mL, aminochitosan may be moderately cytotoxic when sprayed directly onto leaves. The decrease in F_v/F_m visually and quantitatively overlapped with the decrease in ChlIdx at 2.5 mg/mL as areas with residual dry droplets matched areas of decreased ChlIdx. This observation was also noted for the mock inoculated leaves treated with 2.5 mg/mL of D1 and therefore indicates that the observed effects are not due to the establishment of an infection but rather to the concentration of the treatment. Moreover, this appears to be concentration-dependent, as the same observation is absent at 0.5 mg/mL but can be seen for several leaves at 1 mg/mL. Similarly, various studies have reported negative effects on the establishment of necrotic lesions and their severity with high concentrations of exogenous PA application or endogenous accumulation (Yoda, Yamaguchi & Sano, 2003; Marina et al., 2008; Nambeesan et al., 2012).

In addition to its priming and resistance inducing properties in plants, PA are also crucial for the normal growth and development of fungi. A study by Rajam, Weinstein & Galston, (1985) demonstrated that D,L-alpha-difluoromethylornithine (DFMO), a specific inhibitor of the enzyme critical for fungi's PA synthesis, was significantly inhibited the growth of various phytopathogenic fungi, an effect reversed by putrescine or spermidine, underscoring the

essential role of PA in fungal hyphal growth. As seen in this study, low concentrations of aminochitosan stimulated *B. cinerea* growth. Moreover, DFMO demonstrates plant protective efficacy against bean rust fungus in Pinto bean plants, retarding lesion appearance between 2-6 days in infected leaves and unsprayed leaves suggesting the translocation of the protective effect from treated areas (systemic effects)(Rajam, Weinstein & Galston, 1985). Therefore, higher concentrations of aminochitosan may potentially inhibit the PA synthesis of *B. cinerea* given the similar outcomes to that of DFMO.

In this study, in addition to F_v/F_m and ChlIdx, mAriIdx was used as a measure of anthocyanin accumulation in leaves (Meng et al., 2020). Anthocyanins are reported to have putative functions in halting leaf senescence as well as being regulators of ROS signaling pathways (Hatier & Gould, 2008). The accumulation of anthocyanin was visible at the *B. cinerea* inoculation sites in water-treated leaflets but was variable in aminochitosan-treated leaflets. Similar results were observed by Meng et al. (2020), where mAriIdx was seen accumulating at the site of infection with *B. cinerea* in untreated leaves (Meng et al., 2020). In the present study, the accumulation of anthocyanins appeared to visually decrease with an increase in the concentration of aminochitosan at the site of *B. cinerea* inoculation. This suggests that anthocyanin accumulation is an indicator of leaf susceptibility to successful infections when treated with aminochitosan. Leaves treated with 0.5 mg/mL of aminochitosan had greater anthocyanin accumulation and disease resistance than the water treatment. However, they were more susceptible than those treated with 1 and 2.5 mg/mL where little to no anthocyanins were visible at the sites of inoculation thus indicating a resistant interaction. This suggests priming mechanisms that are independent of anthocyanin accumulation and ROS accumulation at later time points when treated with higher concentrations of aminochitosan in *B. cinerea* inoculated leaves. A likely explanation is that the direct antifungal activity of aminochitosan at higher concentrations is severe, resulting in lower ROS production, less oxidative stress (HR-like response), and lower anthocyanin concentrations than at lower concentrations of aminochitosan.

In the mock inoculated leaves treated with aminochitosan at 1 and 2.5 mg/mL, anthocyanin accumulation overlapped with the dried aminochitosan droplets. In contrast to infected leaves, this suggests that foliar anthocyanins are primed in uninfected leaves in response to

higher concentrations of aminochitosan. Additionally, the enhanced F_v/F_m values and thereby enhanced photosynthetic activity observed in these leaves may indicate an increase in starch and sugar production. As sugar accumulation is positively correlated with anthocyanin concentration, accumulation in older leaves may act as a mechanism for regulating sugar content in an attempt to circumvent early senescence elicited by high sugar levels in source tissues (Pourtau et al., 2006; Landi, Tattini & Gould, 2015). Thus, anthocyanins are potentially alternative sinks that avoid excess carbon and sugar accumulation to mitigate possible "sugar-induced leaf senescence" induced by enhanced photosynthetic activity after application of a high concentration of aminochitosan (Landi, Tattini & Gould, 2015).

In addition to the local resistance induced by direct CHT application, systemic resistance has also been reported for various pathosystems (Benhamou & Thériault, 1992; Vasyukova et al., 2001; Faoro et al., 2008; Siddaiah et al., 2018). The significantly elevated F_v/F_m induced by direct aminochitosan application was also seen with the systemic pre-treatment of D1 at 4 and 6 dpi. This corresponded to a reduction in lesion sizes and the number of spreading lesions. The effects were concentration-dependent, with 1 and 2.5 mg/mL performing significantly better than 0.5 mg/mL but still being protective at 0.5 mg/mL. Notably, at both 0.5 mg/mL and 1 mg/mL, the occurrence of spreading and resistant lesions on individual leaflets varied, as regulation of the defence systems is expectedly heterogeneous within each individual leaflet (Pérez-Bueno, Pineda & Barón, 2019). The successful priming of a resistant response systemically highlights the benefits of a more efficient and effective induction of the innate immune system globally (Pastor et al., 2013).

Priming results in a combination of physical and chemical responses that include ROS and have been reported for a variety of pathosystems using CHT and derivatives at various concentrations and stages of development (Rabea et al., 2003; Raafat et al., 2008; Goy, Britto & Assis, 2009; Hadwiger, 2013; Betsuyaku et al., 2018). H_2O_2 accumulation is a crucial, early-phase defence response that functions as a signaling molecule, a cell wall modifier, and a mediator of hypersensitive responses (Lin et al., 2005; Asselbergh et al., 2007). In this study, lesions were absent at 1 and 2.5 mg/mL of D1 application, as in the whole leaf analysis, and was coupled with generally little to no H_2O_2 accumulation at these concentrations (a decrease in accumulation with an increase in D1 concentration). Additionally, the time taken to

accumulate H_2O_2 comparable to the water treatment increased with an increase in concentration. These results corroborate the aforementioned anthocyanin and direct antifungal/inhibitory efficacy data that suggest that aminochitosan functions in a ROS-independent manner, especially at higher concentrations where direct inhibition takes precedence.

Despite H_2O_2 generally being a marker for an upregulated defence response, it is also known to contribute to successful infections by necrotrophs such as *B. cinerea* (Stamelou et al., 2021). Meng et al. (2019) reported that in strawberry leaves infected with *B. cinerea*, "H_2O_2 levels were positively correlated with disease severity" and that lower levels were a better indicator for resistance (Meng, Höfte & Van Labeke, 2019). Other studies have reported similar effects of high H_2O_2 levels and hypersensitive responses having a positive correlation with necrosis (Govrin & Levine, 2000; Khanam et al., 2005). The effects on PSII functionality reported by Adamakis et al. (2020) and Stamelou et al. (2021), showed that lower ROS levels were favorable for the activation of defence responses, whereas high ROS levels were detrimental to the functionality of PSII, indicating toxicity (Adamakis et al., 2020; Stamelou et al., 2021). Hence, lower concentrations of aminochitosan may be favoured due to its low and slow increase in H_2O_2 levels, resulting in maintained PSII functionality compared to the decrease seen at 2.5 mg/mL. Adamakis et al. (2020) and Stamelou et al. (2021) suggested that with short-term exposure, PSII functionality increased rapidly but that with longer exposure, inhibition indicated a "time-dependent hormetic response". Hormesis typically denotes a biphasic response that is depicted by a U/J shape to a stress or elicitor that elicits advantageous effects at low concentrations (eustress) and a toxic effect at high concentrations (Vargas-Hernandez et al., 2017). Therefore, at time points earlier than 4 dpi, 2.5 mg/mL of aminochitosan is beneficial to the leaves, but at later time points, the benefits decrease. A functional use of this dose response in plants is for elucidating optimal biostimulant concentrations that achieve the best adaptive response to disease resistance (Vargas-Hernandez et al., 2017).

The microscopic observations also revealed an interaction between D1 and Trypan Blue, which can be seen by the appearance of blue circles correlating with the droplet residues that remained on the leaf tissue after treatment with D1. As Trypan Blue is a negatively-charged

diazo dye, it is capable of interacting with a cationic compound such as aminochitosan (Vargas-Hernandez et al., 2017), or in this instance, D1. Therefore, Trypan Blue permeates through the cell walls of living cells that have altered membrane permeability due to the interaction with aminochitosan (Tran et al., 2011). As stated in Tran et al. (2011), the blue coloration of cells should be assessed with caution as it may not signify cell lysis but rather an increase in membrane permeability due to pore formation (Vargas-Hernandez et al., 2017). Therefore, this suggests that aminochitosan acts to increase the membrane permeability of cells after foliar spray thereby allowing the permeation of aminochitosan into the cell membranes and cells. Most notably, when compared to the spores outside of the D1 droplet area, the spores beneath the D1 droplet area had minimal or no germination efficacy. In addition to destabilizing the cell membrane, the film-forming properties of CHT may function as a physical barrier to the efflux of nutrients from the plant, thereby reducing nutrient availability for fungal growth. This hypothesis has been supported by studies that show nutrient deprivation and a lack of fungal growth as a result of these film-forming properties (El-Ghaouth, Smilanick & Wilson, 2000; Ait Barka et al., 2004). These observations corroborate the notion that aminochitosan biopolymers like D1 can exert their effects through both direct MoA and indirect immunostimulatory mechanisms.

3.5.3 The importance of molecular weight on the biological activity of aminochitosan

The D3 MW fractions were analyzed to assist in determining the optimal MW range for future applications of aminochitosan in the tomato/*B. cinerea* pathosystem and others. The elemental analysis (EA) results verified the higher DDA in aminochitosan, as evidenced by the elevated percentages of nitrogen compared to CHT. As per the literature, the C/N ratios of aminochitosan and fractions in this study were closer to that of completely deacetylated chitosan (5.145) compared to CHT which was closer to chitin (6.861), the completely *N*-acetylated biopolymer (Galed et al., 2008). The proportion of nitrogen between the biopolymers differed slightly, with the amino biopolymers exceeding the value for CHT. These values are in agreement with the DS values reported in studies on aminochitosan and range between 0.70-0.98 (Satoh et al., 2006; Yang et al., 2012; Luan et al., 2018; Sayed, 2018). Therefore, it may be assumed that the differences in efficacy between the biopolymers are not due to their elemental composition and proportions and are potentially due to MW

differences. However, it is worth noting that EA has certain limitations that may lead to an overestimation of the DS (Sayed, 2018).

Additionally, despite the relatively high DS values and elevated nitrogen percentages for the D3 MW fractions, the antifungal activity of the biopolymers was variable relative to the EA data. In summary, the results demonstrated that a minimum concentration of 1 mg/mL is required for significant direct antifungal activity of D3 and D3 MW fractions. Furthermore, an increase in the efficacy of the concentrations with a decrease in the MW was observed, indicating a trend between the MW and biological activity. From this study, the MW range of 3.5-15 kDa (F1) appeared to be the most effective against *B. cinerea* at concentrations of 0.5, 1, and 2.5 mg/mL. However, it is worth noting that the differences in MW efficacy may be influenced by the potential agglomerative nature of CHT in the culture medium. This implies that the formation of aggregates between CHT and the media decreases the theoretical amount of chitosan dissolved in solution and impedes antifungal activity (Lee, Koo & Park, 2016). Nonetheless, the findings of this study agree with the results of Hernández-Lauzardo et al. (2008) and Badawy & Rabea (2009). They showed that low MW CHT had stronger antifungal effects against *Rhizopus stolonifera* and *B. cinerea* compared to high MW CHT at a concentration between 0.5 mg/mL and 4 mg/mL (Hernández-Lauzardo et al., 2008; Badawy & Rabea, 2009). In these studies, a wide range of MW values were defined, with Hernández-Lauzardo et al. (2008) defining low to high MW as 17.4-30.7 kDa and Badawy & Rabea (2009) defining their low to high MW range from 5-57 kDa, with an ultra-high MW of 290 kDa. The proposed variations in the mode of action of CHT and aminochitosan are consistent with both low and high MW. Low MW CHT disrupts the fungal cell wall more efficiently due to its smaller size (as with F1), while high MW CHT creates a protective barrier or film that reduces microbial growth by binding to the cell surface (as evident from the reduced antifungal efficacy of the F4 (20-99 kDa) and F5 (100 kDa) (Bellich et al., 2016).

In the present study, the MW range for optimal antifungal activity, 3.5-15 kDa, is in contrast with the optimal *in planta* MW range of 15-20 kDa. F1 was significantly protective, but only at the higher concentrations and was less protective than F2 (15 kDa) and F3 (20 kDa). These results are in opposition to findings reported by Vasyukova et al., (2001), who showed that maximal disease resistance to *Phytophthora infectans* infection in potatoes was displayed by

low MW CHT (5 kDa) treatment compared to the intermediate effects of 24 kDa CHT and the ineffective 200 kDa CHT (Vasyukova et al., 2001). However, the variable definitions for MW ranges result in inconsistencies within the literature. The direct and systemic treatment with D3 and the lower MW fractions, F2 and F3, resulted in significant resistance at 4 and 6 dpi with F2 and F3 providing greater protection than D3. Notably, F2 and F3 displayed a decrease in resistance at 2.5 mg/mL, at 4 and 6 dpi when compared to 1 mg/mL of the respective biopolymers for direct and systemic treatment. These results correspond with the D1 *in planta* results at 2.5 mg/mL, where a concentration-dependent threshold and response were observed. The disease resistance for direct and systemic treatment by F2 and F3 was also retained up to 30 dpi compared to D3, F1, and water treatment, which were not protective. This suggests that fractionating the biopolymer to a select MW results in stronger biological activity *in planta* compared to a wider MW range found within a copolymer not strictly synthesized to a MW.

Consequently, it is noteworthy that the lower MW fractions showed no true discernible differences in the patterns of H_2O_2 accumulation for all concentrations of F1, F2, and F3 assessed. As hypothesized, F2 accumulation appeared closest to that of D3 as F2 and D3 are both approximately 15 kDa. Similar to D1 and D3 treated + *B. cinerea* inoculated leaflets, an increase in concentration resulted in a decrease in the intensity of DAB staining for F1, F2, and F3. Lin et al. (2005) demonstrated that CHT-induced H_2O_2 accumulation in rice cell culture; however, its capacity was dependent on the MW range of CHT. Like these findings, aminochitosan-induced H_2O_2 accumulation in tomato leaflets inoculated with *B. cinerea* appeared to have variable time responses to the different MW fractions. This further highlights the importance of characterizing the optimal ranges of MW for maximum biological activity.

The impact of variations in MW on the antifungal activity of CHT and its derivatives is a widely studied topic with conflicting and inconclusive findings in the literature (Kong et al., 2010; Liaqat & Eltem, 2018; Poznanski, Hameed & Orczyk, 2023). The absence of uniform definitions for “high” and “low” MW CHT in the literature adds to the inconsistencies since the ranges considered "high" and "low" overlap across studies and could therefore be defined oppositely in others. Therefore, it is challenging to ascertain the ideal MW of aminochitosan to achieve

maximum antifungal efficacy based on current data, and it should instead be chosen based on the intended application (Poznanski, Hameed & Orczyk, 2023).

3.5.4 Aminochitosan primes *ACRE75*

ACRE genes have been reported as being involved in R gene-mediated defences and various defence signaling pathways (Durrant et al., 2000). Furthermore, the induction of most ACRE genes may occur via ROS-independent pathways as they do not require ROS for upregulation. This may support the notion that aminochitosan primes a defence response in a ROS-independent manner or through late H_2O_2 accumulation (Durrant et al., 2000). Therefore, *ACRE75* was analyzed for temporal regulation in response to different concentrations of D3 treatment when applied as a direct treatment in mock or *B. cinerea* inoculated leaflets at 6, 9, or 96 hpi or as a systemic treatment in mock or *B. cinerea* inoculated leaflets at 96 hpi.

D3 treatment + mock inoculation resulted in greater average relative expression of *ACRE75* compared to the water treatment at both 6 and 9 hpi for 1 and 2.5 mg/mL. This observation suggests that aminochitosan may act as an elicitor of *ACRE75* priming both mock and *B. cinerea* inoculated leaflets for a stronger expression with and without infection. Moreover, the relative expression of *ACRE75* was positively regulated, with an increase in concentration at 6 hpi for both mock and *B. cinerea* infected leaflets, indicating a concentration-dependent response at the earlier time points. However, at 9 hpi, the greatest increase in relative expression was for 0.5 mg/mL, with a subsequent decrease in expression for 1 and 2.5 mg/mL for both mock + *B. cinerea* inoculated leaflets. A study by Iriti and Faoro, (2009) noted concentration and the physiochemical properties of CHT as key factors modulating priming and direct defences, as at certain concentrations, beneficial programmed cell death may switch to non-beneficial necrotic lesions due to cytotoxicity (Betsuyaku et al., 2018). Therefore, elucidating the optimal concentration for non-toxic priming is key to utilizing aminochitosan to its full potential. At 96 hpi, systemic treatment with 0.5 mg/mL displayed the greatest priming in both mock and *B. cinerea* inoculated leaflets. This suggests that lower concentrations of aminochitosan are sufficient for priming systemic a defence response that results in the accumulation of *ACRE75,* and that the protection may be sustained up to and including 96 hpi.

3.6 Conclusions

Here we have demonstrated aminochitosan as a preventative treatment to *B. cinerea* infection when applied as a foliar spray in 5-week-old tomato leaves. Aminochitosan displayed significantly improved biological activity *in planta* when applied directly and as a systemic treatment that was sustained for up to 30 days post-inoculation. The resistant phenotype is mediated through a combination of enhanced F_v/F_m and ChlIdx. The mechanism of action appears to be ROS-independent at higher concentrations due to the severity of direct antifungal activity. Consequently, leaf senescence, hypersensitive responses and therefore necrosis are mitigated which suggests that aminochitosan primes defence responses in both mock and *B. cinerea* inoculated leaves. However, the concentrations for appear to differ for optimal antifungal and *in planta* efficacy. Additionally, the lower MW fractions suggest a narrow range in which optimal/maximal efficacy is effected for direct antifungal activity compared to *in planta* activity, which additionally is pathosystem dependent. This study provides a base for further research into the effects of aminochitosan in other pathosystems and larger field trials with a focus on “omics” for further elucidation on the MoA.

3.7 Addendum: Supplementary figures

Table S3.1: The effects of the chitosan and aminochitosan variants on disease progression in *B. cinerea* inoculated leaf discs measured as the percentage of resistant lesions at 4, 8, 12, 16, 20, 24, 48 and 72 hpi.

Treatment	Concentration (mg/mL)	% Resistant lesions Time (hpi) 4	8	12	16	20	24	48	72
Water	0[a]	100[a]	100[a]	100[a]	13[a]	0[a]	0[a]	0[a]	0[a]
0.1% acetic acid	0.1[ab]	100[a]	100[a]	100[a]	100[b]	0[a]	0[a]	0[a]	0[a]
Chitosan	0.5[ab]	100[a]	100[a]	100[a]	100[b]	38[ab]	13[a]	13[a]	0[a]
	1[ab]	100[a]	100[a]	100[a]	100[b]	50[b]	25[a]	0[a]	0[a]
	2.5[b]	100[a]	100[a]	100[a]	100[b]	88[b]	88[b]	25[a]	13[a]
Water	0[a]	100[a]	100[a]	100[a]	13[a]	0[a]	0[a]	0[a]	0[a]
Diamino 1	0.5[b]	100[a]	100[a]	100[a]	100[b]	100[b]	63[b]	50[b]	25[a]
	1[b]	100[a]	100[a]	100[a]	100[b]	100[b]	100[b]	75[b]	100[b]
	2.5[c]	100[a]	100[a]	100[a]	100[b]	100[b]	100[b]	100[b]	100[b]

The data shows the average of two experiments with 5 leaflets per time point. The significance between concentrations for each polymer is denoted with letters; the same letters are not statistically different from each other (Kruskal Wallis test followed by Dunn's *post hoc* test, $p < 0.05$).

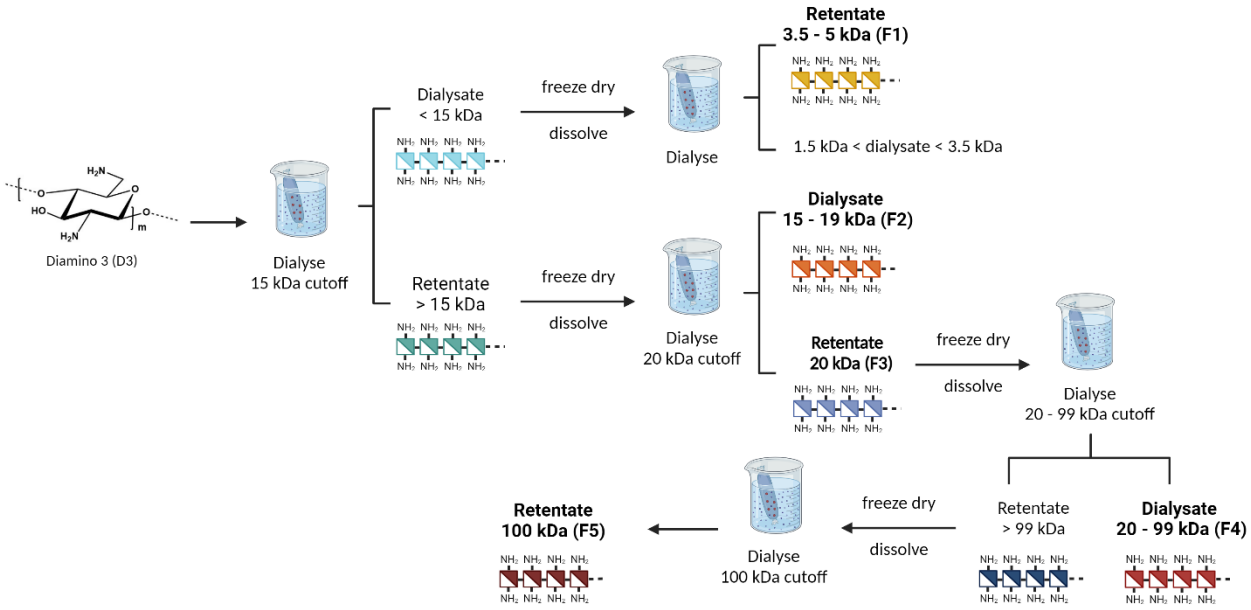

Figure S3.1: The fractionation process applied to obtain the diamino 3 (D3) MW fractions. The representative monomer structures are not drawn to true MW sizes. Retentate refers to that which is retained after being dialysed. Created with BioRender.com.

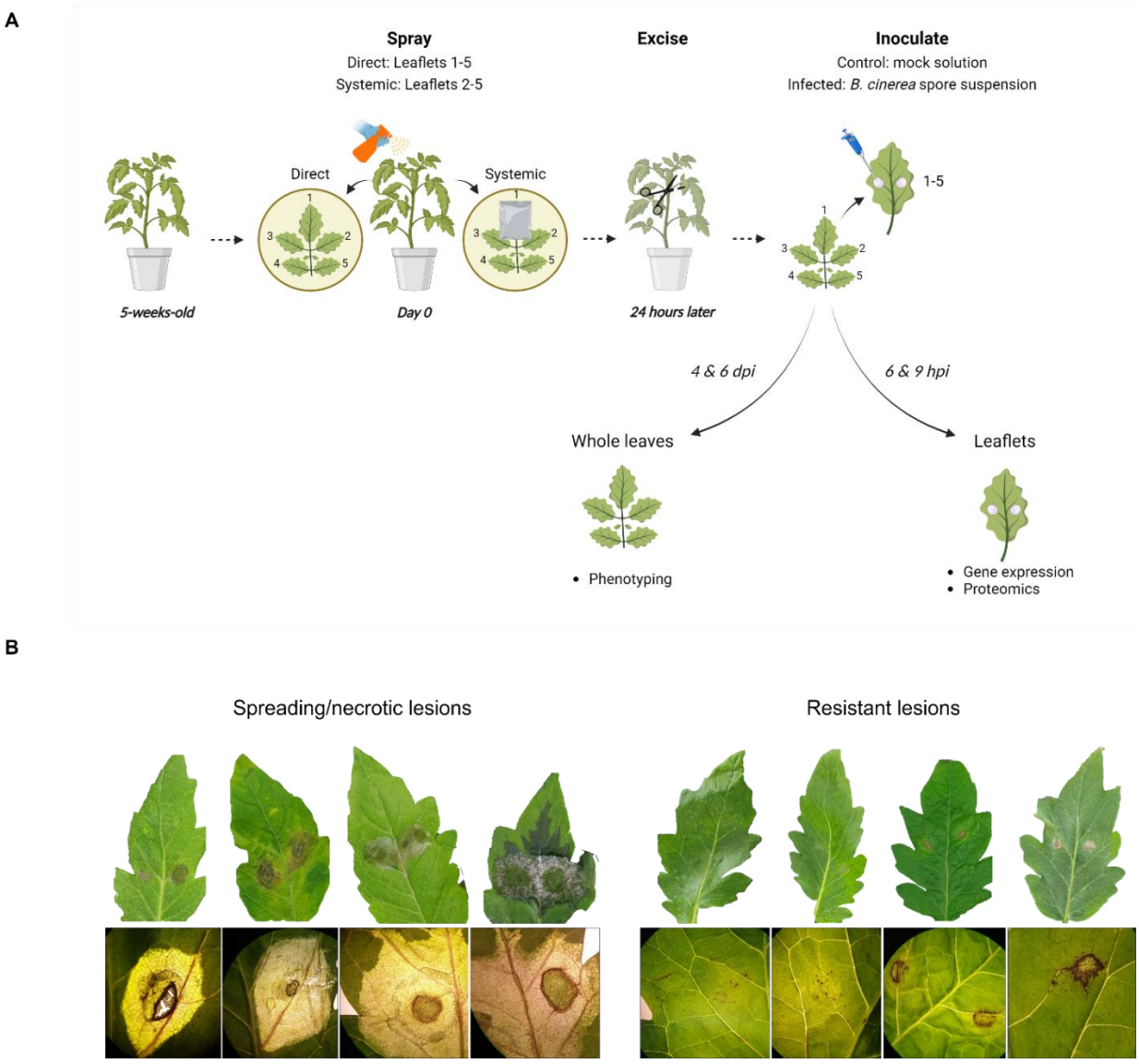

Figure S3.2: (A) Schematic of the experimental set-up used for the *in planta* experiments. 5-week-old tomato plants were treated with a foliar spray of chitosan or aminochitosan at a concentration of 0.5, 1 or 2.5 mg/mL or control (water or 0.1% (v/v) acetic acid). After 24h, leaves were excised and inoculated with either a solution of *B. cinerea* spore suspension (1 x 10^6 spores/mL containing 0.01 M glucose and 6.7 mM KH_2PO_4) or mock solution (water containing 0.01 M glucose and 6.7 mM KH_2PO_4). Leaves or leaflets were harvested at varying time points for phenotyping, gene expression or proteomics analysis. Disease progression is measured by the presence or absence of necrotic/resistant lesions. This figure was created with BioRender.com. **(B)** The range of phenotypical differences between spreading (susceptible) and resistant lesions. Spreading and necrotic lesions appear as a mixture of "wet," light brown and with/without grey mycelia typically characterized by the initial appearance of primary dark brown necrotic spots around the edge of the lesion between 24 and 48 hpi. At 72 hpi the lesions vary in size with the defining trait of a "wet" or "water-soaked" lesion. Resistant lesions are lesions that do not progress to a "water-soaked" lesion and instead remain as dark brown spots in a small, contained area. Resistant lesions may appear macroscopically as scatterings of brown or as white, dry, hardened, circular lesions.

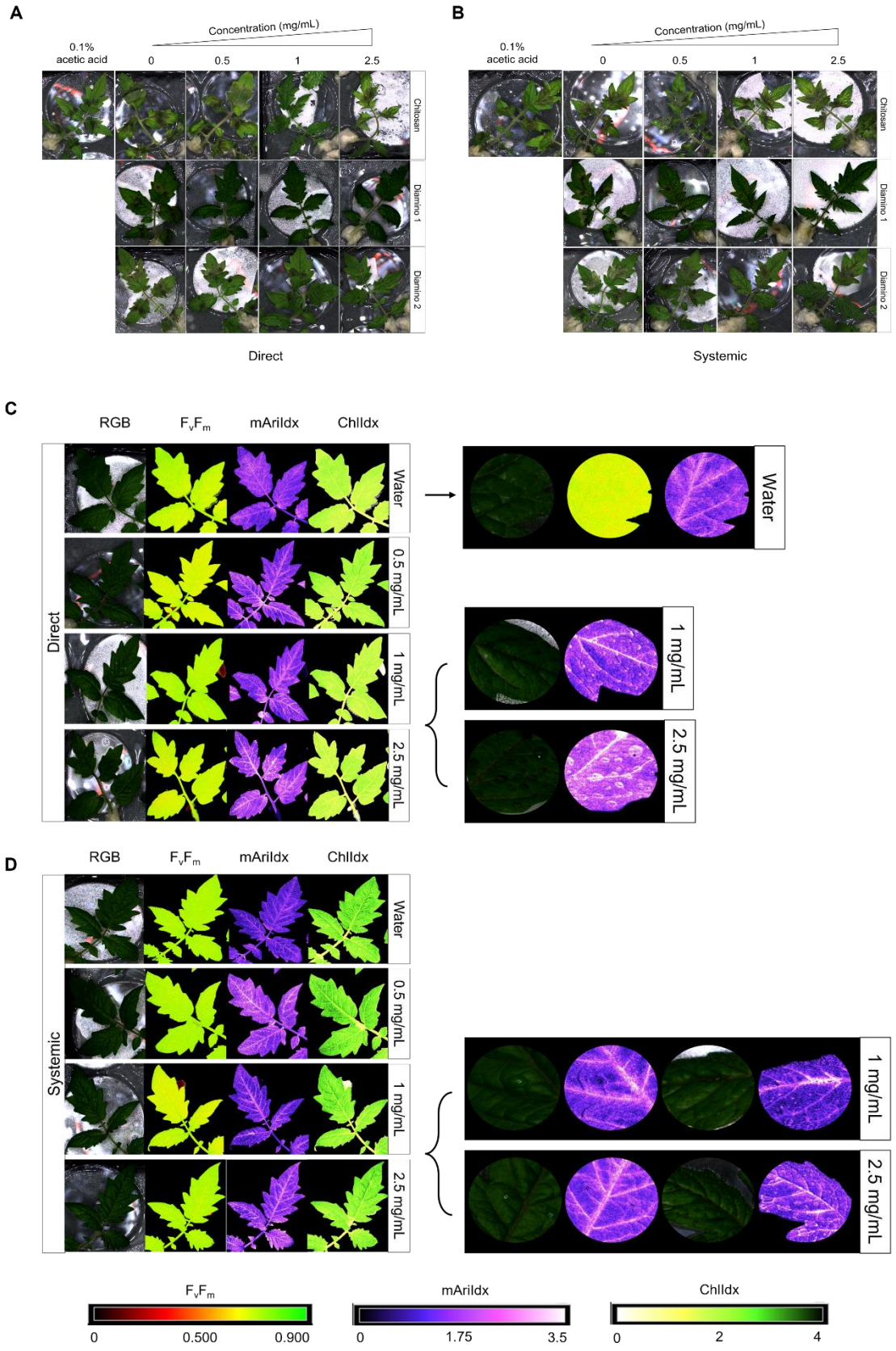

Figure S3.3: The effects of direct or systemic chitosan (CHT), diamino 1 (D1) and diamino 2 (D2) treatment on leaf health including photosynthetic parameters after mock inoculation at 4 days post inoculation (dpi). Any lesion development and progression may be noted by the spreading of dark red/black (F_v/F_m, 0-0.5) or yellow/white (ChlIdx, 0-1.8) spots as measured by the false color scales. Healthy leaf tissue is noted as

yellow/green (F_v/F_m,0.7-0.9) or green (ChlIdx, 1.9-2.5) by the false color scales. (A) RGB images of leaves treated directly at 4 dpi. (B) RGB images of leaves treated systemically at 4 dpi. The images represent the average phenotype of 2 experiments. (C) RGB, Fv/Fm, mAriIdx and ChlIdx images of direct D1 treatment in mock-inoculated leaflets at 4 dpi with a detailed view of the effects of direct treatment with 1 and 2.5 mg/mL. (D) RGB, F_v/F_m, mAriIdx and ChlIdx images of systemic D1 treatment in mock-inoculated leaflets at 4 dpi with a detailed view of the effects of direct treatment with 1 and 2.5 mg/mL. Leaves were inoculated 24 h after polymer spraying with two 10 µL droplets of a water solution containing 0.01 M glucose and 6.7 mM KH_2PO_4. The images represent the average phenotype of 2 experiments.

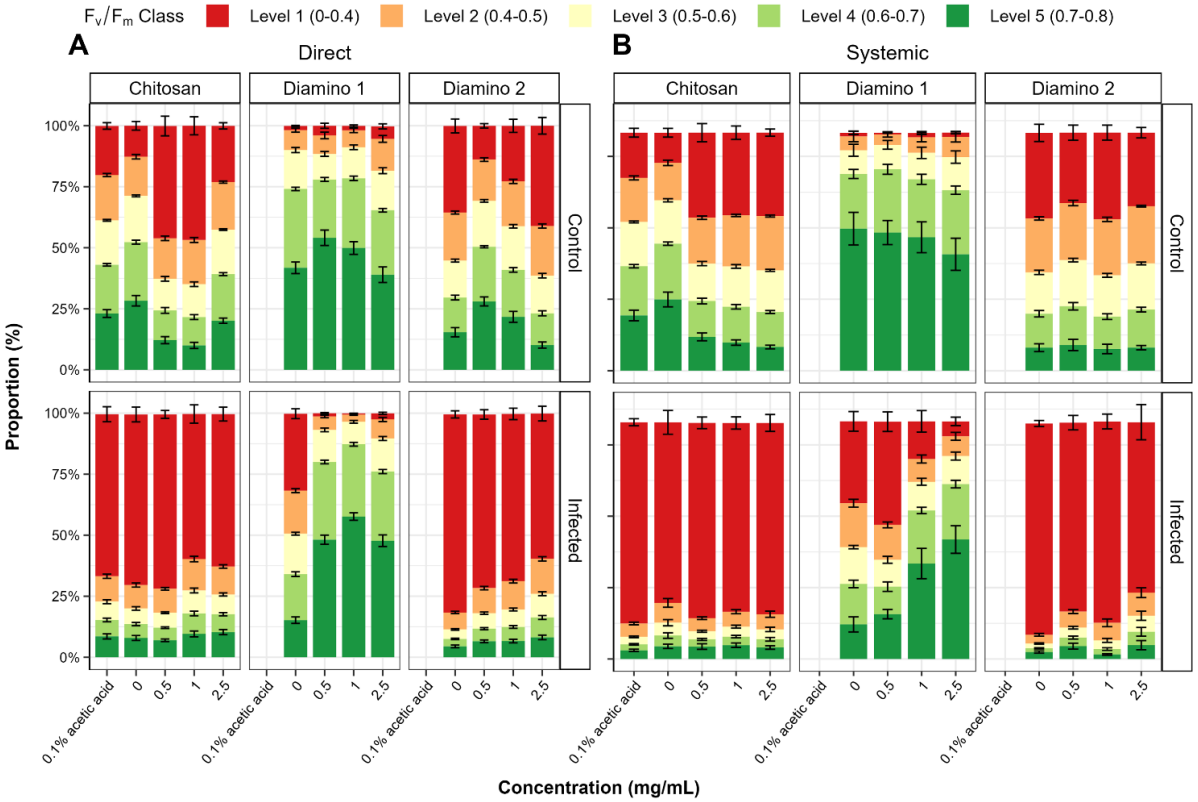

Figure S3.4: The effects of chitosan (CHT), diamino 1 (D1) and diamino 2 (D2) on the F_v/F_m of mock and *B. cinerea* inoculated leaves, 4 days post-inoculation. Healthy leaf conditions are represented by levels 3, 4 and 5. Infected leaf conditions are represented by levels 1-2 with the highest severity of infection = level 1. n = 9 leaves, 45 leaflets per treatment.

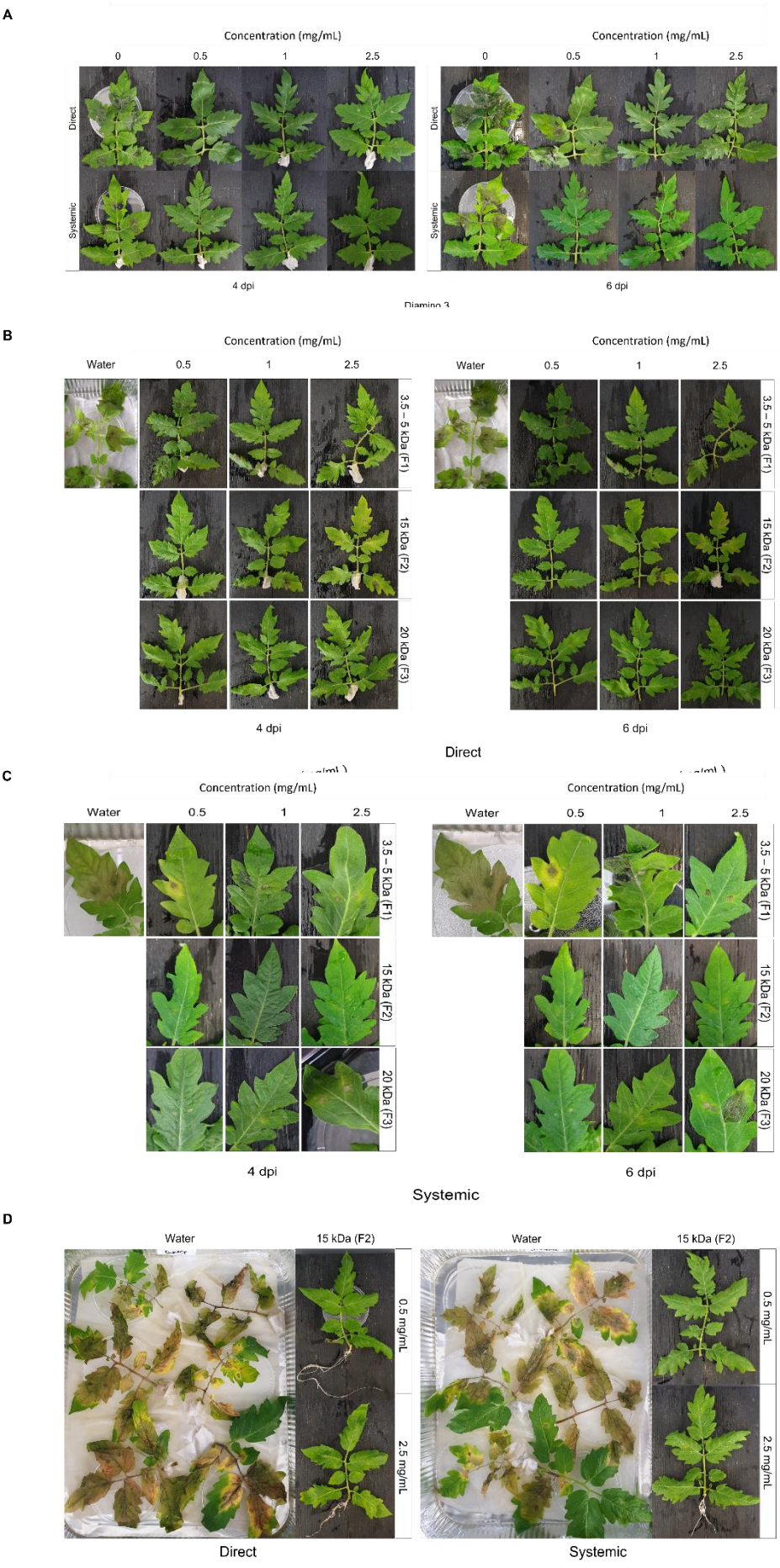

Figure S3.5: The phenotype of *B. cinerea* infected 5-week-old detached tomato leaves treated with various concentrations of diamino 3 (D3) and D3 MW fractions, at 4- and 6-days post inoculation (dpi). **(A)** Direct and systemic application of D3. (**B)** Direct effects of the MW fractions (F1-F3) **(C)** Systemic effects of the MW fractions (F1-F3). **(D)** Direct and systemic treatment of 0.5 and 2.5 mg/mL of F2 in *B. cinerea* inoculated leaves at 30 dpi. Leaves were inoculated with two 10 µL droplets of a *B. cinerea* spore solution (1 x 10^6 spores/mL containing 0.01 M glucose and 6.7 mM KH_2PO_4). The images represent the average phenotype of 2 experimental repeats.

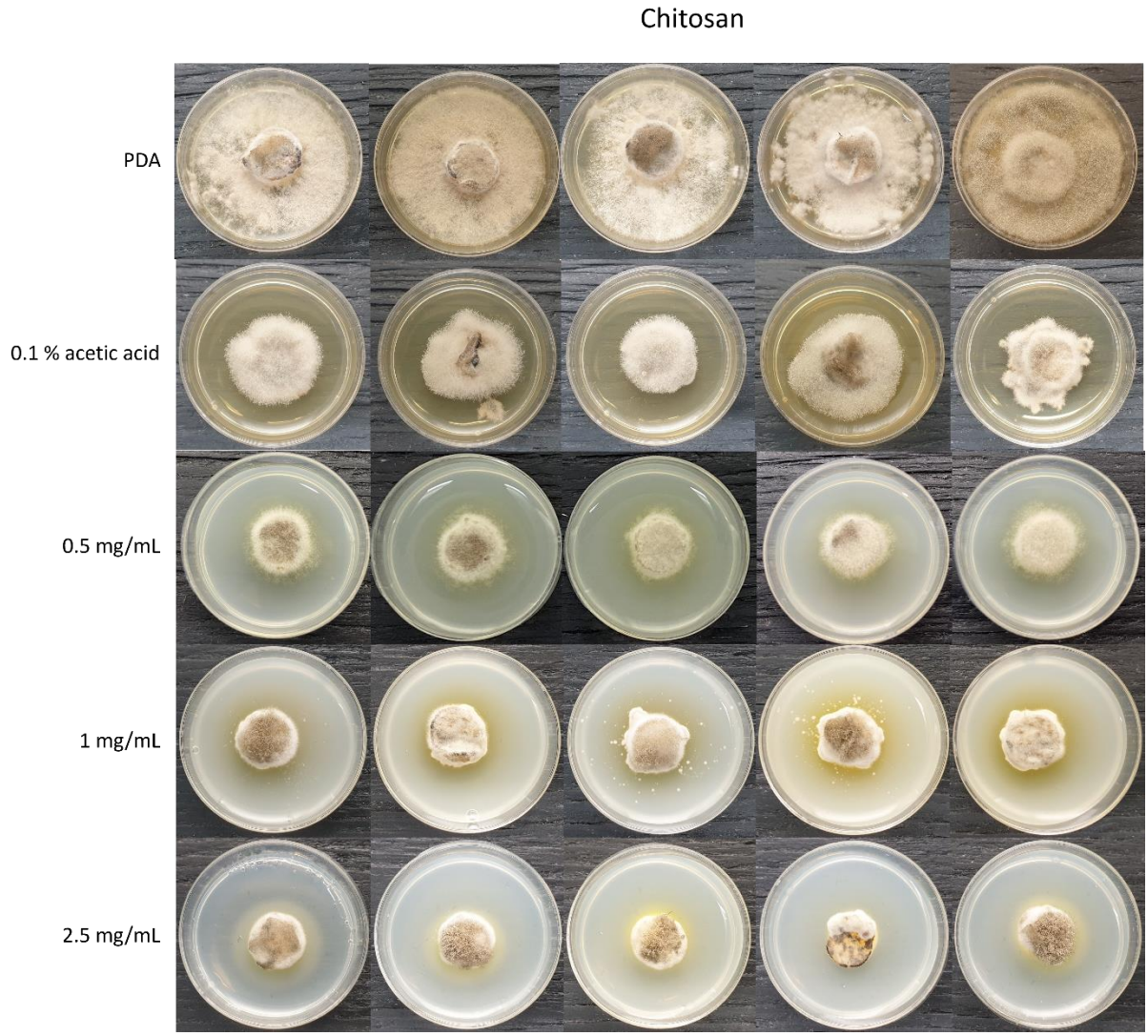

Figure S3.6: Images displaying the inhibition of *B. cinerea* growth at 11 dpi on PDA or PDA amended with 0.5, 1 or 2.5 mg/mL of chitosan or 0.1% acetic acid. The visibility of "haloes" can be seen for all concentrations with differing appearances with the growth patterns and inhibition appearing similarly.

3.8 Addendum: Mass spectrometry analysis of aminochitosan batches and the MW variants

In Chapter 3, noteworthy distinctions were observed between batches (D1, D2, and D3) of aminochitosan and its D3 MW derivatives (F1–F5) both on direct antifungal and *in planta* bioactivity (**Figure S3.1**). To pinpoint potential contributing differences, ESI TOF-MS analysis was conducted allowing for the characterization of the mass fragmentation spectra for each biopolymer.

3.8.1 Methods

3.8.1.1 Mass spectra analysis of aminochitosan: Electrospray Ionization Time-of-Flight Mass Spectrometry (ESI TOF-MS)

5 mg of the biopolymers were sent for analysis at the Central Analytical Facilities at Stellenbosch University. The biopolymers were dissolved in distilled water and directly injected for TOF-MS analyses, which was performed on a Waters SYNAPT G2 mass spectrometer. The analysis was performed in positive mode using an ESI source and a cone voltage of 15V.

3.8.2 Results

3.8.2.1 Mass spectra analysis of the aminochitosan batches and the D3 MW fractions

The ESI TOF-MS analysis included identifying the respective monomer(s)/oligomer(s) and the degree of polymerization (DP) within the upper MW limits of detection for the instrument. Thus, an accuracy bias for TOF-MS would be toward the lower molecular fractions, typically below the 100kDa cut off. Notably, the true molecular weight distributions of polysaccharides are often difficult to analyze directly by mass spectrometry because of their polydisperse nature (Deery, Stimson & Chappell, 2001). Size exclusion based separation is known to improve sensitivity of higher MW fragments by minimization of detector saturation due to the presence of more abundant lower MW fragments (Deery, Stimson & Chappell, 2001). This is observed in **Figure 3.8** as you inspect the abundance of the same highest MW ion in the batch-to-batch variants compared to the increasing MW ions of the fractions.

The biopolymers were detected in a range of 100–1200 *m/z*, with most of the peaks falling in the 140–650 *m/z* range (**Figure 3.8**). This is a relatively broad distribution of mass peaks indicating a broader polydispersity or range of polymer chain lengths/heterogenous lengths. The aminochitosan batches and MW fractions produced the following monomers (single repeating unit) at low *m/z* values: glucosamine (D = $GlcN_2$) dehydration peak at an *m/z* of 144.07, a $GlcN_2$ peak at 162.08, and an *N*-acetyl glucosamine (A = GlcNAc) peak at 204.09. These monomers indicate the dissociation of the β(1-4) glycosidic linkage and are due to polymer hydrolysis and/or ESI mediated dissociation, resulting in multimers of varying DPs**.** Monomers have a DP of 1 while oligomers have a DP > 1 and as such, the mass spectra and potential DPs for each biopolymer were noted and tabulated within each chart (**Figure 3.8**). From **Figure 3.8**, batch-to-batch variants, D1, D2 and D3, all have DPs of 1-4 whereas the D3 MW fractions have DPs of 1-4 (20 kDa), 1-5 (3.5-5 and 100 kDa) and 1-6 (15 a 20-99 kDa). However, some of the fractions may contain more than the abovementioned as there were a few unidentified *m/z* values at the higher end of the spectrum (> 800). The oligomers were detected at higher *m/z* values corresponding to the combined mass of multiple repeating units. The repeating units observed were of the possible forms of D and A; DP2: D_2A_0, D_1A_1, DP3: D_3A_0, D_2A_1, D_1A_2, D_0A_3, DP4: D_4A_0, D_3A_1, D_2A_2, D_1A_3, DP5: D_5A_0, D_4A_1, DP6: D_5A_1. The multimer combinations comprising the DP varied marginally for the batch-to-batch variants compared to the MW fraction as seen in **Figure 3.8**. Furthermore, the number of mass peaks detected increased with an increase in DP (**Figure 3.8**).

Diamino 1

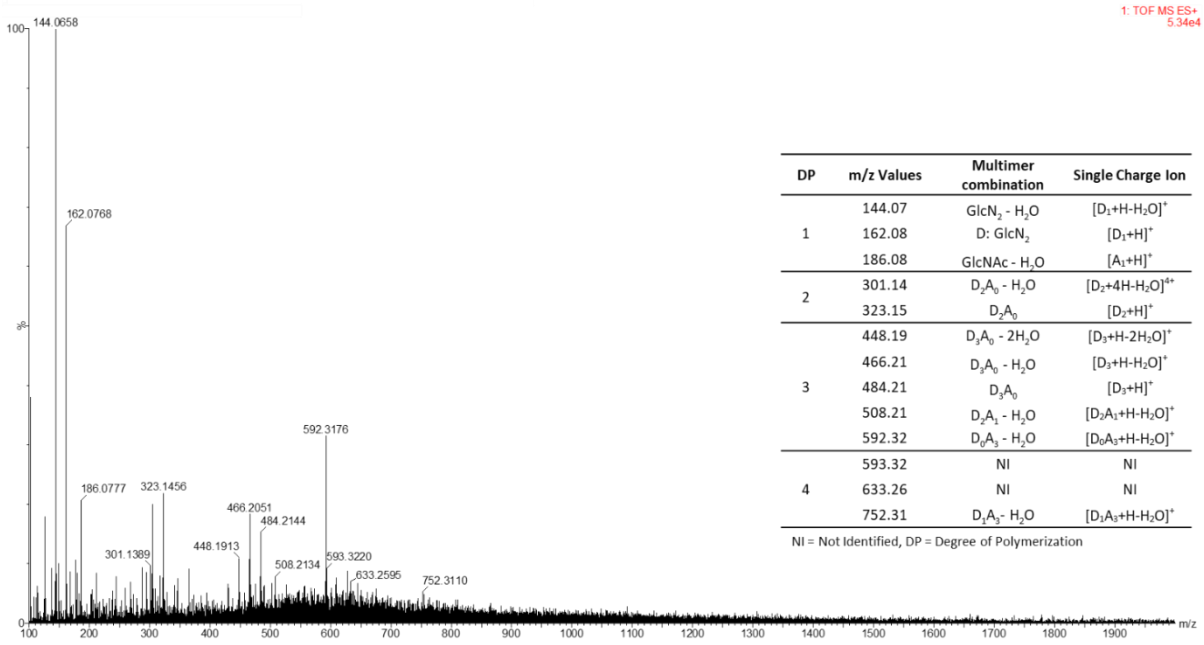

DP	m/z Values	Multimer combination	Single Charge Ion
1	144.07	$GlcN_2$ - H_2O	$[D_1+H-H_2O]^+$
	162.08	D: $GlcN_2$	$[D_1+H]^+$
	186.08	GlcNAc - H_2O	$[A_1+H]^+$
2	301.14	D_2A_0 - H_2O	$[D_2+4H-H_2O]^{4+}$
	323.15	D_2A_0	$[D_2+H]^+$
3	448.19	D_3A_0 - $2H_2O$	$[D_3+H-2H_2O]^+$
	466.21	D_3A_0 - H_2O	$[D_3+H-H_2O]^+$
	484.21	D_3A_0	$[D_3+H]^+$
	508.21	D_2A_1 - H_2O	$[D_2A_1+H-H_2O]^+$
	592.32	D_0A_3 - H_2O	$[D_0A_3+H-H_2O]^+$
4	593.32	NI	NI
	633.26	NI	NI
	752.31	D_1A_3- H_2O	$[D_1A_3+H-H_2O]^+$

NI = Not Identified, DP = Degree of Polymerization

Diamino 2

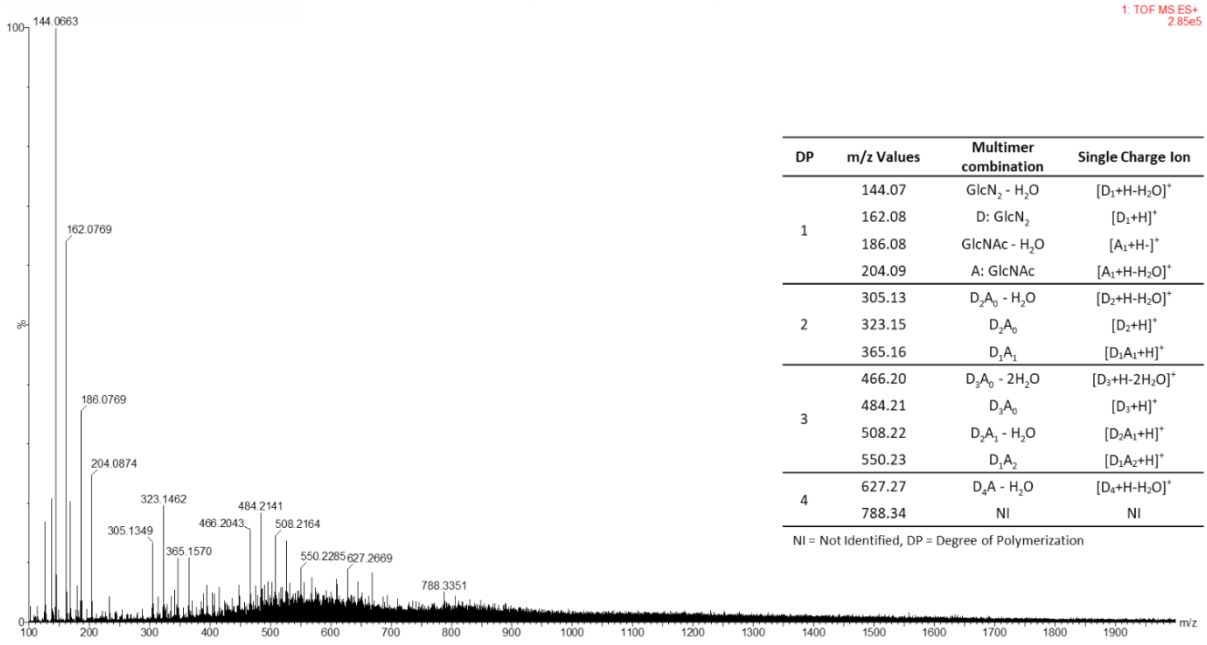

DP	m/z Values	Multimer combination	Single Charge Ion
1	144.07	$GlcN_2$ - H_2O	$[D_1+H-H_2O]^+$
	162.08	D: $GlcN_2$	$[D_1+H]^+$
	186.08	GlcNAc - H_2O	$[A_1+H-]^+$
	204.09	A: GlcNAc	$[A_1+H-H_2O]^+$
2	305.13	D_2A_0 - H_2O	$[D_2+H-H_2O]^+$
	323.15	D_2A_0	$[D_2+H]^+$
	365.16	D_1A_1	$[D_1A_1+H]^+$
3	466.20	D_3A_0 - $2H_2O$	$[D_3+H-2H_2O]^+$
	484.21	D_3A_0	$[D_3+H]^+$
	508.22	D_2A_1 - H_2O	$[D_2A_1+H]^+$
	550.23	D_1A_2	$[D_1A_2+H]^+$
4	627.27	D_4A - H_2O	$[D_4+H-H_2O]^+$
	788.34	NI	NI

NI = Not Identified, DP = Degree of Polymerization

Diamino 3

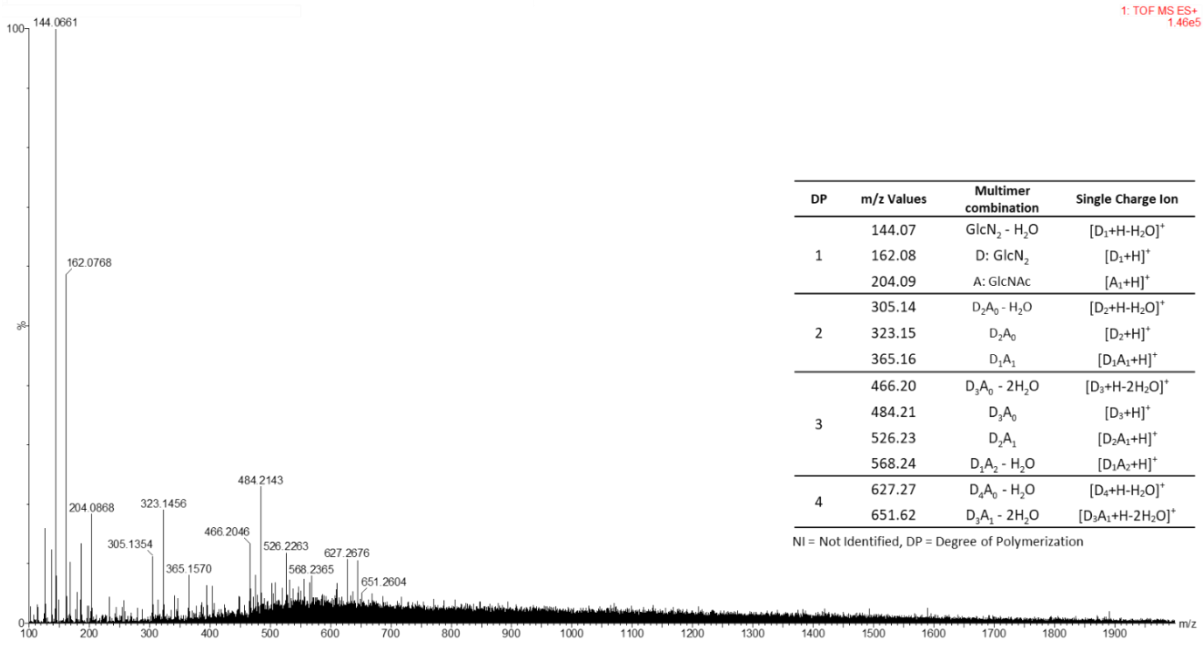

DP	m/z Values	Multimer combination	Single Charge Ion
1	144.07	$GlcN_2$ - H_2O	$[D_1+H-H_2O]^+$
	162.08	D: $GlcN_2$	$[D_1+H]^+$
	204.09	A: GlcNAc	$[A_1+H]^+$
2	305.14	D_2A_0 - H_2O	$[D_2+H-H_2O]^+$
	323.15	D_2A_0	$[D_2+H]^+$
	365.16	D_1A_1	$[D_1A_1+H]^+$
3	466.20	D_3A_0 - $2H_2O$	$[D_3+H-2H_2O]^+$
	484.21	D_3A_0	$[D_3+H]^+$
	526.23	D_2A_1	$[D_2A_1+H]^+$
	568.24	D_1A_2 - H_2O	$[D_1A_2+H]^+$
4	627.27	D_4A_0 - H_2O	$[D_4+H-H_2O]^+$
	651.62	D_3A_1 - $2H_2O$	$[D_3A_1+H-2H_2O]^+$

NI = Not Identified, DP = Degree of Polymerization

3.5-5 kDa

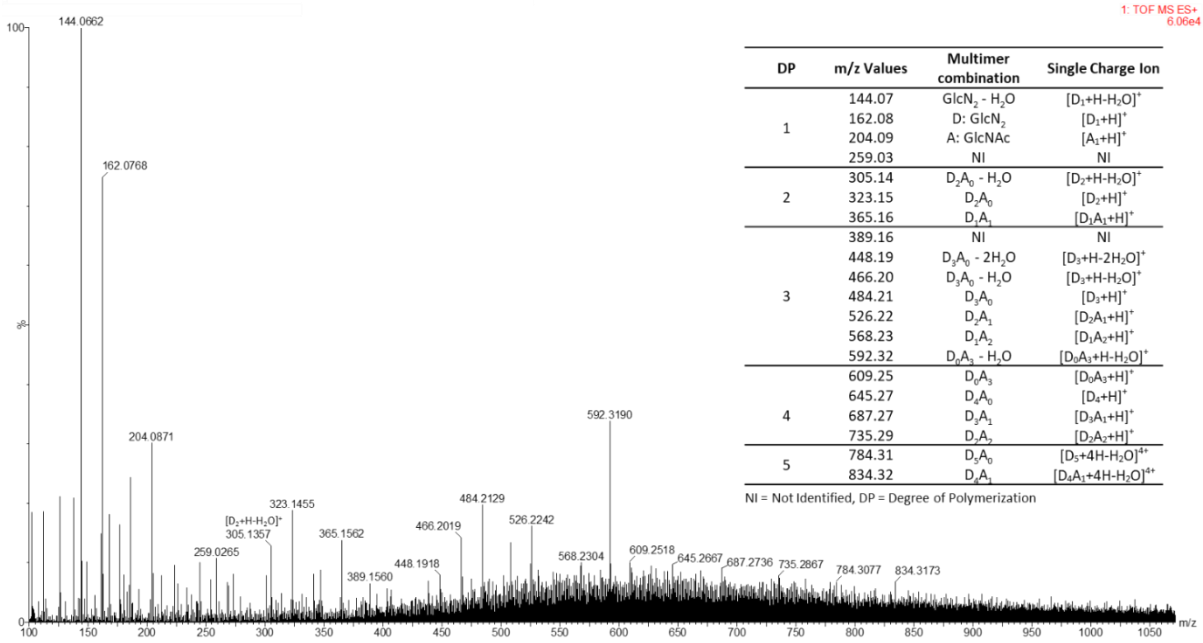

DP	m/z Values	Multimer combination	Single Charge Ion
1	144.07	$GlcN_2$ - H_2O	$[D_1+H-H_2O]^+$
	162.08	D: $GlcN_2$	$[D_1+H]^+$
	204.09	A: GlcNAc	$[A_1+H]^+$
	259.03	NI	NI
2	305.14	D_2A_0 - H_2O	$[D_2+H-H_2O]^+$
	323.15	D_2A_0	$[D_2+H]^+$
	365.16	D_1A_1	$[D_1A_1+H]^+$
3	389.16	NI	NI
	448.19	D_3A_0 - $2H_2O$	$[D_3+H-2H_2O]^+$
	466.20	D_3A_0 - H_2O	$[D_3+H-H_2O]^+$
	484.21	D_3A_0	$[D_3+H]^+$
	526.22	D_2A_1	$[D_2A_1+H]^+$
	568.23	D_1A_2	$[D_1A_2+H]^+$
	592.32	D_0A_3 - H_2O	$[D_0A_3+H-H_2O]^+$
4	609.25	D_0A_3	$[D_0A_3+H]^+$
	645.27	D_4A_0	$[D_4+H]^+$
	687.27	D_3A_1	$[D_3A_1+H]^+$
	735.29	D_2A_2	$[D_2A_2+H]^+$
5	784.31	D_5A_0	$[D_5+4H-H_2O]^{4+}$
	834.32	D_4A_1	$[D_4A_1+4H-H_2O]^{4+}$

NI = Not Identified, DP = Degree of Polymerization

15 kDa

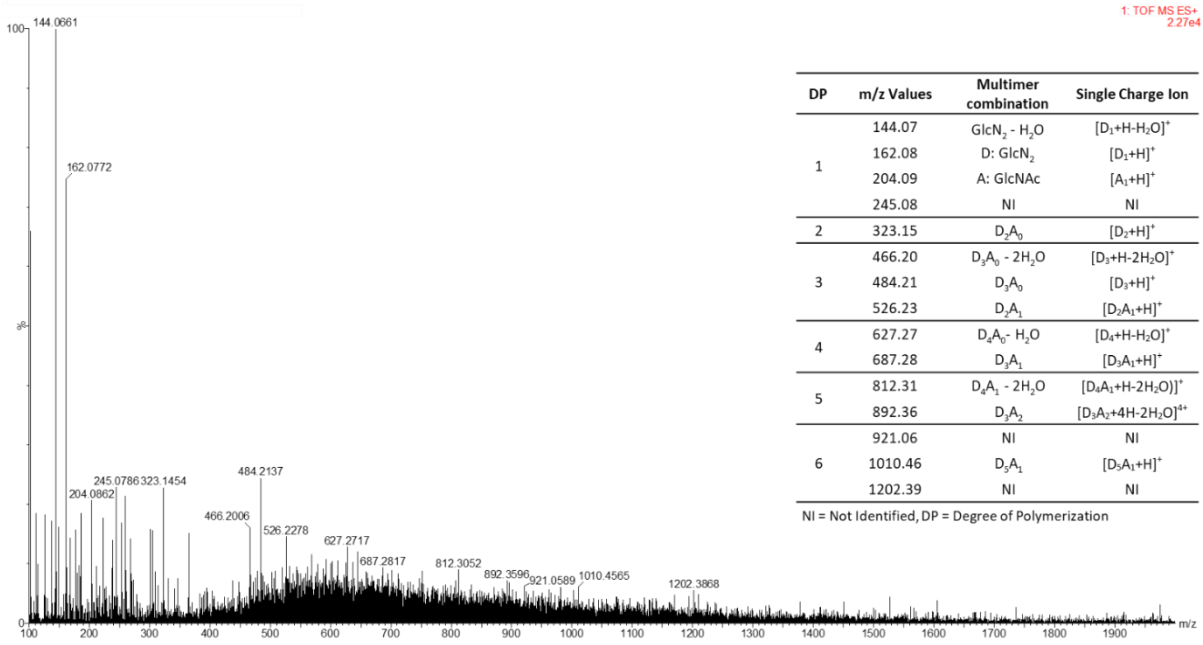

DP	m/z Values	Multimer combination	Single Charge Ion
1	144.07	$GlcN_2$ - H_2O	$[D_1+H-H_2O]^+$
	162.08	D: $GlcN_2$	$[D_1+H]^+$
	204.09	A: GlcNAc	$[A_1+H]^+$
	245.08	NI	NI
2	323.15	D_2A_0	$[D_2+H]^+$
3	466.20	D_3A_0 - $2H_2O$	$[D_3+H-2H_2O]^+$
	484.21	D_3A_0	$[D_3+H]^+$
	526.23	D_2A_1	$[D_2A_1+H]^+$
4	627.27	D_4A_0- H_2O	$[D_4+H-H_2O]^+$
	687.28	D_3A_1	$[D_3A_1+H]^+$
5	812.31	D_4A_1 - $2H_2O$	$[D_4A_1+H-2H_2O)]^+$
	892.36	D_3A_2	$[D_3A_2+4H-2H_2O]^{4+}$
6	921.06	NI	NI
	1010.46	D_5A_1	$[D_5A_1+H]^+$
	1202.39	NI	NI

NI = Not Identified, DP = Degree of Polymerization

20-99 kDa

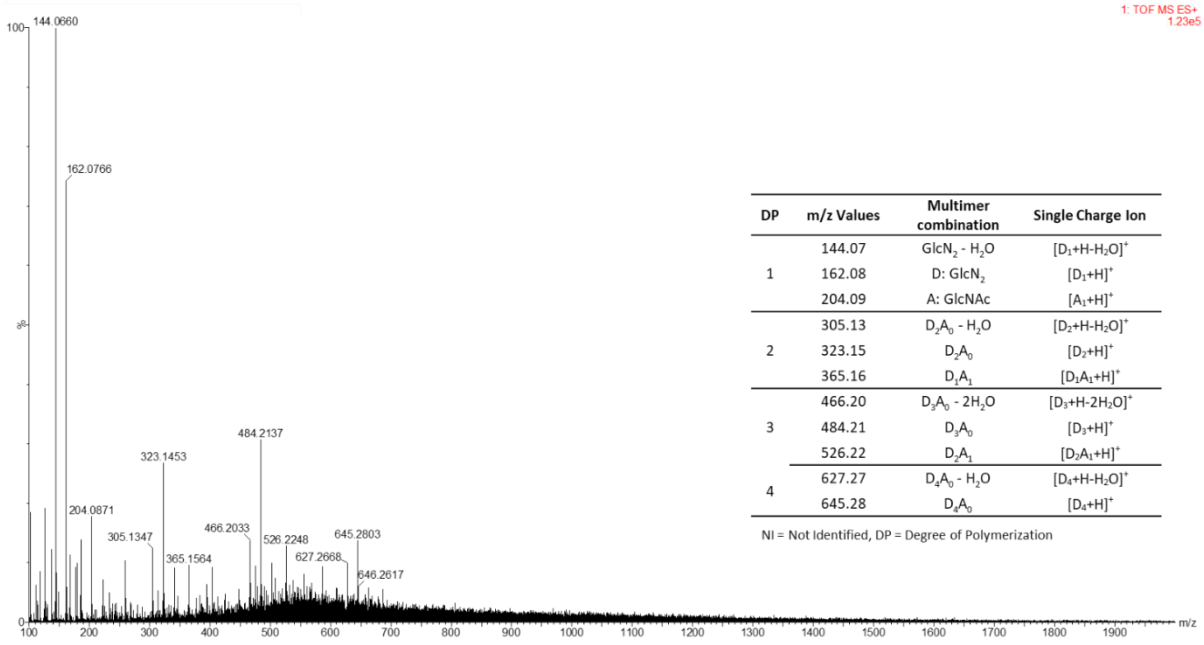

DP	m/z Values	Multimer combination	Single Charge Ion
1	144.07	$GlcN_2$ - H_2O	$[D_1+H-H_2O]^+$
	162.08	D: $GlcN_2$	$[D_1+H]^+$
	204.09	A: GlcNAc	$[A_1+H]^+$
2	305.13	D_2A_0 - H_2O	$[D_2+H-H_2O]^+$
	323.15	D_2A_0	$[D_2+H]^+$
	365.16	D_1A_1	$[D_1A_1+H]^+$
3	466.20	D_3A_0 - $2H_2O$	$[D_3+H-2H_2O]^+$
	484.21	D_3A_0	$[D_3+H]^+$
	526.22	D_2A_1	$[D_2A_1+H]^+$
4	627.27	D_4A_0 - H_2O	$[D_4+H-H_2O]^+$
	645.28	D_4A_0	$[D_4+H]^+$

NI = Not Identified, DP = Degree of Polymerization

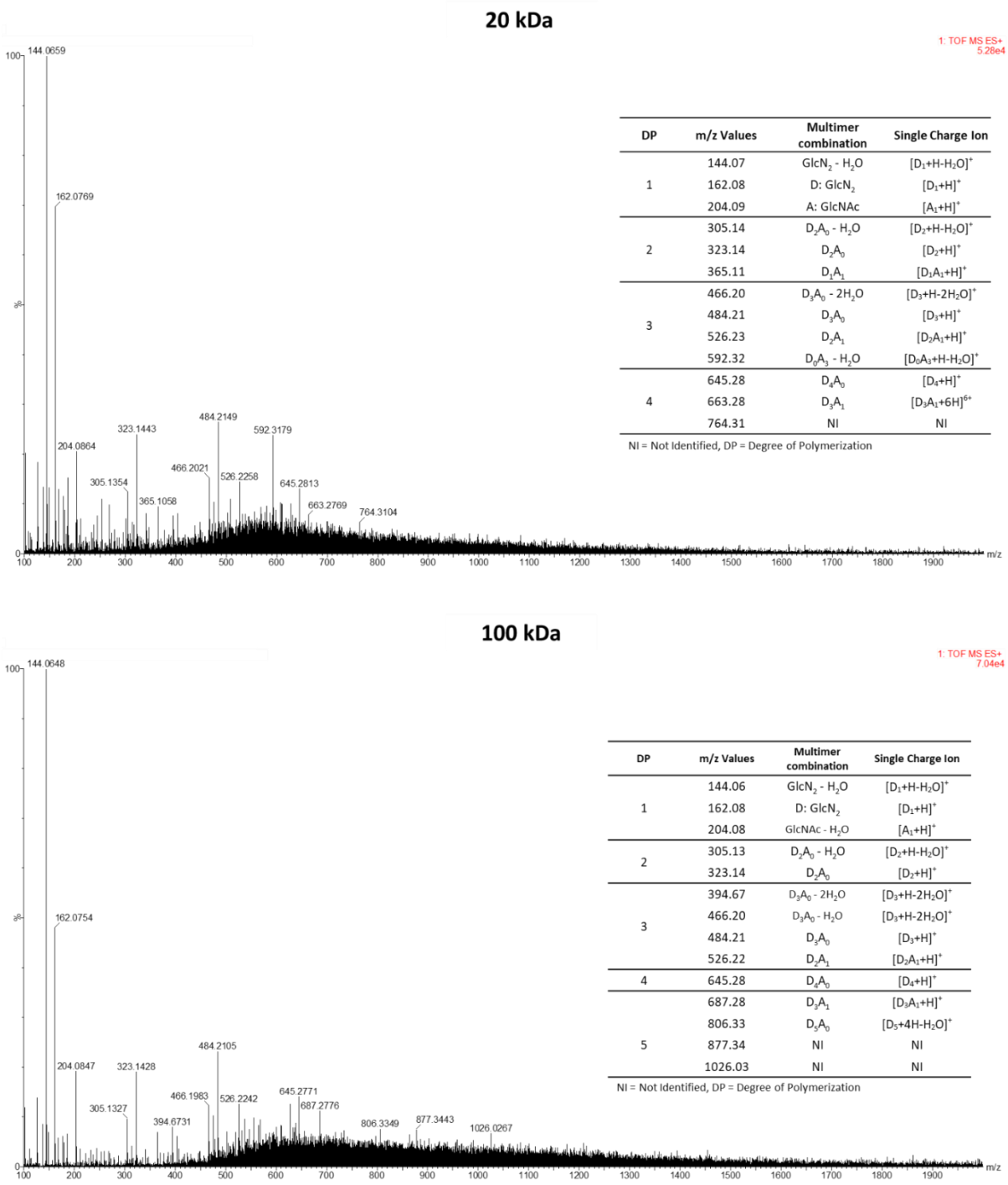

DP	m/z Values	Multimer combination	Single Charge Ion
1	144.07	$GlcN_2$ - H_2O	$[D_1+H-H_2O]^+$
	162.08	D: $GlcN_2$	$[D_1+H]^+$
	204.09	A: GlcNAc	$[A_1+H]^+$
2	305.14	D_2A_0 - H_2O	$[D_2+H-H_2O]^+$
	323.14	D_2A_0	$[D_2+H]^+$
	365.11	D_1A_1	$[D_1A_1+H]^+$
3	466.20	D_3A_0 - $2H_2O$	$[D_3+H-2H_2O]^+$
	484.21	D_3A_0	$[D_3+H]^+$
	526.23	D_2A_1	$[D_2A_1+H]^+$
	592.32	D_0A_3 - H_2O	$[D_0A_3+H-H_2O]^+$
4	645.28	D_4A_0	$[D_4+H]^+$
	663.28	D_3A_1	$[D_3A_1+6H]^{6+}$
	764.31	NI	NI

NI = Not Identified, DP = Degree of Polymerization

DP	m/z Values	Multimer combination	Single Charge Ion
1	144.06	$GlcN_2$ - H_2O	$[D_1+H-H_2O]^+$
	162.08	D: $GlcN_2$	$[D_1+H]^+$
	204.08	GlcNAc - H_2O	$[A_1+H]^+$
2	305.13	D_2A_0 - H_2O	$[D_2+H-H_2O]^+$
	323.14	D_2A_0	$[D_2+H]^+$
3	394.67	D_3A_0 - $2H_2O$	$[D_3+H-2H_2O]^+$
	466.20	D_3A_0 - H_2O	$[D_3+H-2H_2O]^+$
	484.21	D_3A_0	$[D_3+H]^+$
	526.22	D_2A_1	$[D_2A_1+H]^+$
4	645.28	D_4A_0	$[D_4+H]^+$
5	687.28	D_3A_1	$[D_3A_1+H]^+$
	806.33	D_5A_0	$[D_5+4H-H_2O]^+$
	877.34	NI	NI
	1026.03	NI	NI

NI = Not Identified, DP = Degree of Polymerization

Figure 3.8: ESI TOF mass spectral data for the aminochitosan batches (D1, D2 and D3) and MW fractions (F1, F2, F3, F4, F5). Each spectral chart also contains a table denoting the observed fragments with the potential degrees of polymerization (DP).

From the mass spectra in **Figure 3.8**, the primary characteristic *m/z* values were noted and analyzed for clustering based on the overlapping *m/z* values between the batches and MW derivatives. **Figure 3.9A** displays the *m/z* values for each biopolymer and the number of intersecting peaks between them. F1 and F5, the two most dissimilar MW fractions, displayed fewer intersecting mass peaks than the other fractions. Additionally, D1, the biopolymer that

exhibited the most significant direct antifungal and in planta bioactivity, displayed six unique peaks, compared to the three peaks observed in both D2 and D3 (**Figure 3.9A**).

The dendrogram in **Figure 3.9B** displays the relationship between the biopolymers based on the vertical height distances between the biopolymers and clusters, where the height differences define the similarity or dissimilarity of clusters and individual biopolymers. As seen in **Figure 3.9B**, the biopolymers were divided into three clusters, with F1 (3.5–5 kDa) and F5 (100 kDa) being the most dissimilar and appearing in two separate clusters while D1, D2, D3, F2 (15 kDa), F3 (20 kDa), and F4 (20–99 kDa) are clustered together in cluster three. However, D2 had greater dissimilarity to the other biopolymers in cluster three compared to D1 while D3 appeared to be more similar to the MW fractions F2, F3, and F4, indicating that they share a high percentage of intersecting *m/z* values (**Figure 3.9B**). The latter result is to be expected as the fractions are derived from D3.

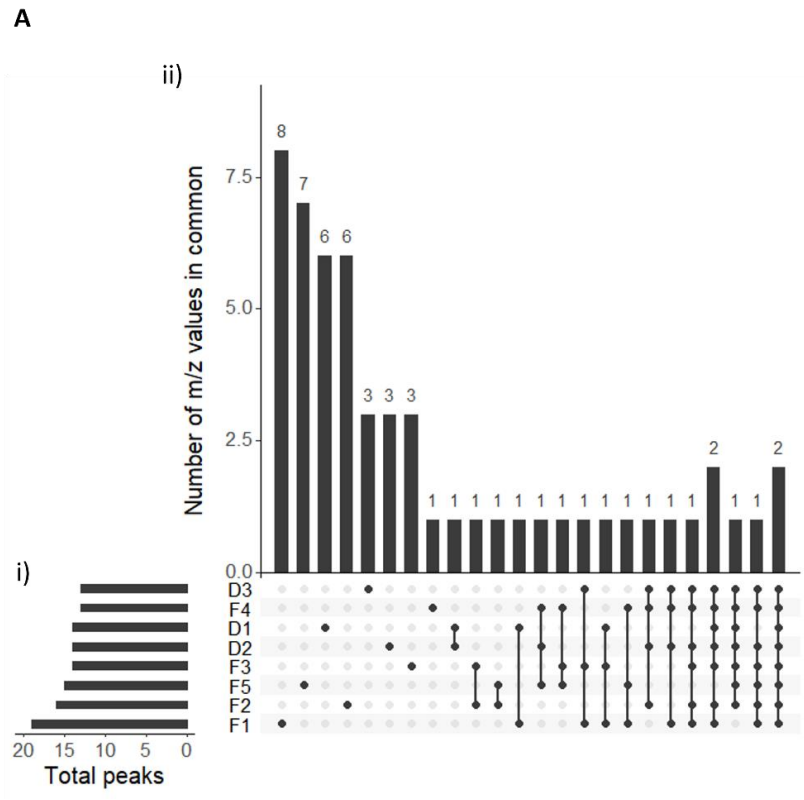

B

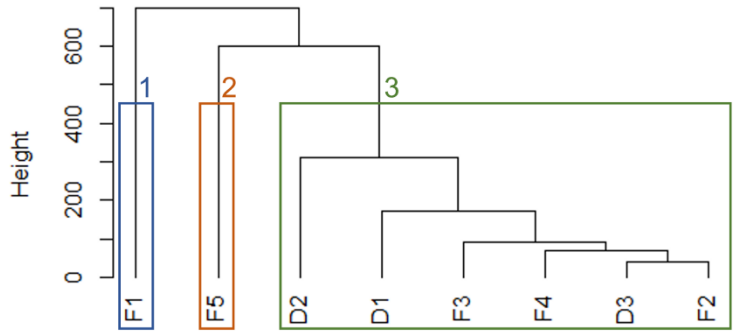

Figure 3.9: (A) UpSet plot of the identified *m/z* peaks for each biopolymer. **(i)** The total number of peaks identified for each polymer. **(ii)** The number of intersecting peaks between polymers. **(B)** Hierarchical clustering dendrogram of the biopolymers and their respective *m/z* values. The colour-coded boxes represent their respective clusters, and the height of the tree denotes the similarity between the biopolymers. D1 (Diamino 1), D2 (Diamino 2), D3 (Diamino 3), F1 (3.5–5 kDa), F2 (15 kDa), F3 (20 kDa), F4 (20–99 kDa), and F5 (100 kDa). Clustering was performed with Ward's linkage using Euclidean distance.

Biopolymers that had at least two overlapping mass peaks were selected and displayed in **Table 3.6**. From Table 3.6, *m/z* values 162.08 and 484.21 corresponding to $GlcN_2$ monomer and $(GlcN_2)$ oligomer were the only *m/z* value to be shared by all the biopolymers.

Table 3.6: Common characteristic *m/z* values between the polymers, occurring in at least two polymers.

Polymers	***m/z* Values**
D1, D2, D3, F1, F2, F3, F4, F5	162.08, 484.21
D1, D2, D3, F1, F2, F3, F4	144.07
D2, D3, F1, F2, F3, F4, F5	466.2
D1, D2, D3, F1, F2, F3, F4	323.15
D2, D3, F1, F2, F3, F4	204.09
D2, D3, F1, F4	365.16
D3, F1, F2, F3	526.23
D2, D3, F2, F4	627.27
F3, F4, F5	645.28
D1, F1, F3	592.32
D2, F4, F5	305.13
D3, F1, F3	305.14
F4, F5	526.22
D1, D2	186.08
D1, F1	448.19
F2, F5	687.28

3.8.3 Discussion and Conclusion

The efficacy and biological activity of CHT (by extension, aminochitosan) is intricately correlated with its chemical structure (Verlee, Mincke & Stevens, 2017). As such, Chapter 3 highlights the observed differences in the direct antifungal and *in planta* efficacy of the aminochitosan biopolymers. However, the conclusion was that these observed differences were not attributed to slight and nonsignificant differences in the EA data and therefore required additional characterization of the biopolymers to underpin these differences in efficacy. To assist in determining the physiochemical similarity or dissimilarity between the batches and MW derivatives, the aminochitosan batches and D3 MW fractions were analyzed by ESI-TOF MS.

The instability of the β-1,4-*O*-glycoside bonds that link the repeating monomers of aminochitosan allowed for further dissociation by ESI (Liaqat & Eltem, 2018). Since the batches of aminochitosan were synthesized independently, slight differences in the physiochemical properties were to be expected which is furthered by the process in which CHT is obtained. Chemical deacetylation of chitin in the synthesis of CHT is random and results in the irregular distribution of β-(1–4)-linked GlcN (D) and GlcNAc (A) units (Sayed, 2018; Li et al., 2020). Thus, CHT is not defined by a single molecular structure and may be heterogeneous or homologous with respect to the composition of D and A (varying DDA). Homologous CHT consists solely of either D or A, while heterologous CHT consists of multimers of varying D and A (Li et al., 2020). In addition, the homo- or heterogenous polymers also posses varying degrees of depolymerization (DP), polydispersity, pattern (PA) and fraction (DA) of *N*-acetylated groups. Consequently, the observed difference in the solubility of D2 may be attributed to the above as DP is correlated to chain length and, thus, water solubility and viscosity.

The hierarchical clustering data of the mass spectra data showed that 3.5–5 kDa and 100 kDa MW fractions clustered separately. This validates their outlier MW, as they are both lower and higher than the average range of the other MW fractions, respectively. Given that the batch variants have a MW of approximately 15 kDa, it is expected that the MW derivatives of 15 kDa (F2) and 20 kDa (F3) are similar to the batch variants (D1, D2, and D3) and cluster

together. The 20-99 kDa (F4) MW derivative was also in cluster 3, which indicates that the ion peaks detected for this derivative were closer to 20 kDa than 100 kDa (F5) as F5 was in a separate cluster with greater dissimilarity. D3 was the most similar to the MW derivatives (15 kDa, 20 kDa, and 20–99 kDa), which is to be expected as the MW variants are derived from D3 and indicates that D3 is most likely a copolymer within that MW range.

As mentioned, it can be inferred that DP, DDA, and MW are correlated and fundamental features that directly influence the physiochemical and biological properties of aminochitosan. Thus, even though the biopolymers in cluster three share identical or similar DPs, they may exhibit distinct biological properties owing to variations in DDA, FA, and PA. Therefore, the properties of aminochitosan batches and various MW fractions may differ even though they may have the same DP, as isomers of a particular homolog with different sequences of D and A may have the same DP (e.g., D_2A_1 compared to D_1A_2) (Liaqat & Eltem, 2018). According to the definitions of oligomers and low MW by the reviews of Lodhi et al., (2014) and Verlee, Mincke & Stevens, (2017), the aminochitosan batches as well as F1 (3.5-5 kDa) and F2 (15 kDa) are therefore all low MW oligomers as the MW is ≤ 16 kDa and DP ≤ 20 (Lodhi et al., 2014; Verlee, Mincke & Stevens, 2017).

The DDA of aminochitosan synthesized using the same methods has previously been observed to be > 96% using Nuclear Magnetic Resonance Spectroscopy (NMR), specifically, ^{1}H, and ^{13}C -NMR (Sayed, 2018). The DDA of the current aminochitosan batches and fractions were therefore inferred to possess the same or similar DDA. However, future work on aminochitosan should in addition to the above, perform the aforementioned structural analysis assays to confirm the structural properties of each batch of aminochitosan synthesized. Furthermore, future ESI TOF MS analysis on aminochitosan should ideally be coupled with chromatography (e.g., size exclusion or liquid chromatography) to allow for a more in detail analysis on retention time, relative abundancies of the mass fragments (monomers vs oligomers) and the intensity counts. The literature on the optimal MW, DDA, DP and PA is vast with many conflicting results as complex mixtures of aminochitosan make identifying the key contributors to the effects seen rather challenging (Mourya & Inamdar, 2011; Liaqat & Eltem, 2018; Li et al., 2020).

This image was created with the assistance of DALL.E 2.

Chapter 4: A proteomic analysis on the resistance mechanisms of aminochitosan in the tomato/*Botrytis cinerea* pathosystem

4.1 Abstract

In Chapter 3, the interaction between tomato, *B. cinerea* and aminochitosan was assessed *in planta* by phenotyping and quantifying temporal stress responses using qualitative and quantitative chlorophyll fluorescence imaging, and DAB assays coupled with microscopy. We demonstrated that aminochitosan induces a significant resistant phenotype mediated through a combination of enhanced F_v/F_m and ChlIdx. We also observed that the resistant phenotype potentially occurs in a ROS-independent manner at higher concentrations due to the severity of direct inhibition. Consequently, leaf senescence, hypersensitive responses and therefore necrosis are mitigated, suggesting that aminochitosan primes defence responses in both mock and *B. cinerea* inoculated leaves. In this chapter, we attempt to identify proteins and pathways that contribute to aminochitosan-mediated resistance to *B. cinerea* infection early after treatment, with or without infection, by using a label-free quantitative proteomic approach. Moreover, we attempt to validate the observations demonstrated in Chapter 3.

We observed that 1 mg/mL of aminochitosan treatment differentially regulates proteins as early as 6 hpi with some of the induced responses being sustained up to 9 hpi. These proteins were related to signal transduction, defence response, photosynthesis and ROS homeostasis and included DNA and chromatin, cell wall, cell membrane, H^+-ATPase activity, chlorophyll biosynthesis and consequently the redox/ROS specific proteins. Finally, several of the proteins were oppositely regulated between aminochitosan pretreatment and *B. cinerea* infection, indicating differential regulation patterns between the “primed state” and the “triggered state”. The proteomic data therefore partially validated the ‘priming’ capacity of aminochitosan in 5-week-old tomato leaves, specifically diamino 3 when used as a foliar spray at a concentration of 1 mg/mL. This allowed us to identify potential key molecular mechanisms underpinning the aminochitosan primed states both with and without *B. cinerea* infection at 6 and 9 hpi.

4.2 Introduction

The characterization of molecular mechanisms involved in plant defence and their contribution to biotic and abiotic stress tolerance is a key step in the fields of plant breeding, biotechnology, and metabolic engineering, towards bridging the lab to farm gap thereby enhancing agricultural productivity and food security (Yang et al., 2021). Therefore, investigating the effects of biopolymers on these molecular mechanisms is essential for optimizing their application in agriculture. The advent of multi-omics approaches, including genomics, transcriptomics, proteomics, metabolomics, ionomics, and phenomics (**Figure 4.1**) have provided comprehensive insights into the molecular processes involved in plant-pathogen interactions and the factors that modulate defence response (Yang et al., 2021; Diwan, Rashid & Vaishnav, 2022). This is aided by the simultaneous development of enhanced analytical technologies for high-resolution and high-throughput use, increased sensitivity, reduced costs, and advances in computational, statistical and bioinformatic tools needed to analyze the resulting large datasets (Yang et al., 2021; Diwan, Rashid & Vaishnav, 2022). These 'omics techniques have been applied in important crops and associated pathosystems including wheat, maize, grapes, papayas, sugarcane, cotton, barley, soybean, millet, rice, and tomato (Sergeant & Renaut, 2010; Rampitsch & Bykova, 2012; Ashwin et al., 2017; Tan, Lim & Lau, 2017; Yang et al., 2021, and the references therein). The majority of the proteins identified in these plant pathogen studies have been categorized as signal transduction, defence responses, metabolism, energy production, and photosynthesis related proteins.

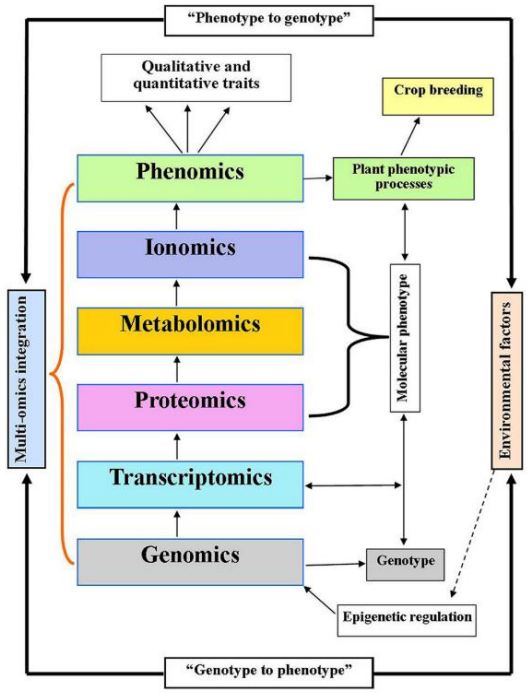

Figure 4.1: The role of 'omics in linking genotype to phenotype and vice-versa. Adapted from Yang et al., (2021).

Historically, transcriptomics has been the preferred technique because of its accessibility and relatively lower costs. However, alterations in the genome and transcriptome do not fully represent a plant's regulatory processes. As such, proteomics (and metabolomics) provides a more comprehensive understanding of the system's response, considering that not all genes are transcribed or translated (Sergeant & Renaut, 2010). Additionally, temporal scales of translation, protein turnover, degradation rates, and metabolite formation can vary significantly. Thus, changes in the transcriptome may not align with the proteome, necessitating the use of other 'omics approaches to reduce the phenotype-genotype disparity. (Figure 4.1) (Feussner & Polle, 2015).

The common basis for proteomic approaches is to extract, separate, cleave, detect and quantify the total proteins expressed in an organism/organ under certain conditions and at specific time points (Feussner & Polle, 2015; Fillinger & Elad, 2016; Kumar, Kumar, et al., 2021). Proteomics may be used to characterize the sequence, structure, function/activity, localization, post-translational modifications, rate of synthesis/turnover, protein-protein interactions or expression of proteins detected (Feussner & Polle, 2015; Fillinger & Elad, 2016; Kumar, Kumar, et al., 2021). Advantageously, expression proteomics, the "quantitative analysis of protein expression", has the potential to elucidate host-pathogen interactions that are otherwise not possible with genomics The proteomic methodologies used are categorized into

three groups: gel-based (involving protein separation through gel electrophoresis, followed by quantification, protein spot digestion, and MS identification), gel-free (involving protease degradation of the protein mixture, followed by LC separation and MS identification), and gel-free quantitative (using isobaric tags). These approaches extract, separate, cleave, detect and quantify the total proteins expressed in an organism/organ under certain conditions and at specific times (Feussner & Polle, 2015; Fillinger & Elad, 2016; Kumar, Kumar, et al., 2021).

Proteins and their interactions represent one of the final outcomes of regulatory processes and participate in regulating biochemical and signaling responses, and the biosynthesis of compounds necessary for growth or defence. During a plant-pathogen interaction, proteins involved in susceptibility or resistance undergo activation or deactivation through post-translational modifications like phosphorylation, acylation, or glycosylation. This in turn initiates signaling cascades that influence the plant's tolerance or susceptibility (Feussner & Polle, 2015).

Recent publications have clearly demonstrated the capacity of proteomic technologies to elucidate the roles played by specific proteins in various biological processes (Fillinger & Elad, 2016). Of these, several proteomic studies have investigated the plant molecular mechanisms of CHT-induced defence responses in a range of pathosystems. These pathosystems include *Arabidopsis thaliana* cell suspension cultures treated with 5.3 mg/mL CHT (crab shells, dissolved in 0.1 M acetic acid, pH 6.5) and infected with *F. verticillioides* (Ndimba et al., 2003); *Vitis vinifera* plantlets treated with 1.75% v/v chitogel and infected with *B. cinerea* (Ait Barka et al., 2004); *V. vinifera* cell suspensions treated with 50 mg/mL chitosan (dissolved in 0.1% (v/v) acetic acid, 76–139 kDa; low viscosity, Ferri et al., 2009); rice seeds treated 50, 100 and 200 µg/mL of CHT oligosaccharide and infected with Southern rice black-streaked dwarf virus (Yang et al., 2017); *V. vinifera* treated with 0.03% CHT (shrimp shell, low viscosity, Bavaresco et al., 2017); *A. thaliana* leaves treated with 50 mg/L CHT oligosaccharide (DP 2-10, 95% DDA) and infected with *Pseudomonas syringae* pv. tomato DC3000 (Pst) (Jia et al., 2020); strawberries infected with *Rhodotorula mucilaginosa* that was first cultured with 0.5% CHT (90% DDA, Gu et al., 2021); and *Cannabis sativa* roots and shoots treated with 0.1%, 0.2% and 0.5% w/v of chitin and CHT (in Hoagland's solution, Suwanchaikasem et al., 2023). These studies have elucidated some of the elements involved in complex PTI signaling of the CHT-induced 'primed state'.

As stated in Martinez-Medina et al., (2016), the primed state compared to the non-primed state can be understood by two sequential stimuli, the priming stimuli, and the triggering stimuli, which induces defence-related phenotypic, molecular, and biochemical traits in a robust manner in primed plants. Furthermore, the defence response is also longer-lasting in primed plants upon a triggering stimuli than in non-primed pants. Some of the defence responses may include alterations to defence signaling/compounds/processes like chromatin and PRR, the accumulation of glucosinolates, ROS, lignin phytoalexins, phenolics or plant volatiles (Martinez-Medina et al., 2016). Despite the aforementioned publications, of the crops accounting for 58% of all phyto-pathoproteomics related publications between the years of 2000 and August 2016, tomato only accounted for 8% of those publications (Ashwin et al., 2017). Furthermore, no proteomic studies have been conducted on CHT treatment in the tomato/*B. cinerea* pathosystem. As such, this is to our knowledge, the first label-free quantitative proteomics study to assess the temporal priming and resistance inducing mechanisms of CHT, specifically aminochitosan, in the tomato/*B. cinerea* pathosystem.

4.3 Methods

4.3.1. Aminochitosan and *Botrytis cinerea*

Preparations of the biopolymer used in this chapter, diamino 3 (D3), are as previously described in Chapter 3, Section 3.3.3. A 1 mg/mL solution was prepared in distilled water directly before use. The growth and solutions of *B. cinerea* used were as described in Chapter 3, Section 3.3.2.

4.3.2. Plant material and the application of diamino 1

Tomato (*Solanum lycopersicum* L.*)* cv. Moneymaker variety seeds were collectively germinated before being transplanted into individual pots containing potting soil. Seedlings were grown in a growth chamber at 23 °C with a photoperiod cycle of 8-h dark/16-h light (Audenaert, De Meyer & Höfte, 2002). Five-week-old plants, consisting of five tertiary leaves with five leaflets, were randomized and sprayed with D3 or water until run-off, 24 h before *B. cinerea* inoculation (**Figure 4.2**). Twenty-four h after spraying, whole leaves were excised at the base of the petiole before being wrapped in paper towels and placed on a tray. The leaves were then suspended above wet paper towels, with the stems immersed in distilled water. Individual leaflets were inoculated with two 10 µL droplets of either *B. cinerea* spore suspension or mock solution on

either side of the midrib. The trays were then sealed with transparent lids to ensure a high-humidity environment and grown under a 16-h light/8-h dark cycle. The samples were allocated into different time groups, where the infection was allowed to establish for either 6 or 9 hpi before being harvested using liquid N_2.

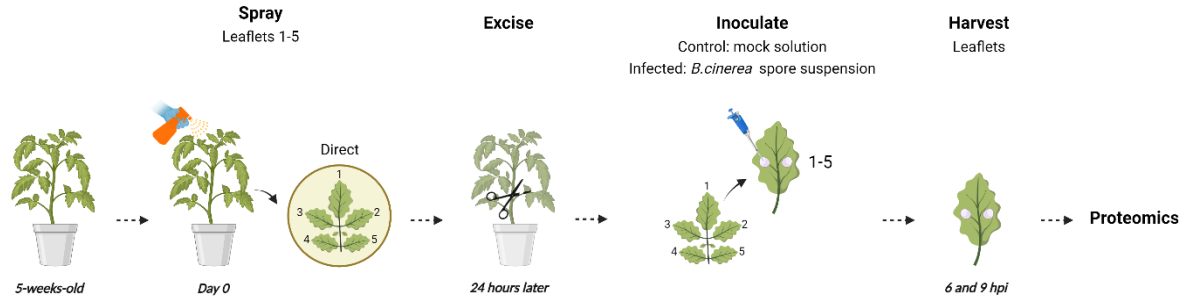

Figure 4.2: Schematic of the experimental set-up used for the proteomic analysis. 5-week-old tomato plants were treated with a foliar spray of aminochitosan at a concentration of 1 mg/mL or water. After 24h, leaves were excised and inoculated with either a solution of *B. cinerea* spore suspension (1 x 10^6 spores/mL containing 0.01 M glucose and 6.7 mM KH_2PO_4) or mock solution (water containing 0.01 M glucose and 6.7 mM KH2PO4). Leaflets were harvested at 9 and 9 hpi and flash frozen in liquid nitrogen before being stored at -80 °C for use. This figure was created with BioRender.com.

4.3.3 Label-free quantitative proteomics using liquid-chromatography mass spectrometry (LC-MS/MS)

4.3.3.1 Protein extraction, reduction, alkylation, and digestion

Samples were crushed into fine powder using liquid N_2 before being sent to the Centre for Proteomic and Genomic Research (CPGR) for proteomic analysis. Protein extraction, reduction, alkylation, and digestion was performed by CPGR according to the following protocols as provided by CPGR. Protein was extracted using a solution containing 4% sodium dodecyl sulfate (Sigma-Aldrich, United States) and 100 mM triethylammonium bicarbonate (TEAB, Sigma-Aldrich, United States) at 95 °C for 10 min followed by 10 min of centrifugation at 10 000 x *g*. The supernatants were transferred to a new tube and washed with 400 µL of cold acetone at 21 000 x *g* for 15 min at 4°C. This was repeated for two wash steps. Digestion was performed using the MagReSyn HILIC method with on-bead digestion as in Rossouw et al. (2021) with the following amendments: Two wash steps were performed before being resuspended in loading buffer at a concentration of 2.5 mg/mL (Rossouw et al., 2021). Each sample, amounting to approximately 20 µg, was then transferred in a volume of 10 µL to a protein LoBind plate (Merck, Germany).

The protein was reduced and alkylated by the addition of a solution containing 20 mM dithiothreitol (Sigma-Aldrich, United States) and 30 mM iodoacetamide (Sigma-Aldrich, United States) and incubated at 95 °C for 10 min. MagReSyn® HILIC magnetic beads were added at a ratio of 5:1 total protein and at equal volumes to that of the sample. Following which, plate incubation was performed as per Rossouw et al. (2021) with the amendment of a 2-h incubation at 45°C. Digestion was carried out using trypsin in 50mM TEAB at a ratio of 1:20 total protein and LysC (Pierce Biotechnology, Thermo Fisher Scientific, United States) and was added at a ratio of 1:250 total protein. After digestion, the supernatant was removed and dried before being resuspended in liquid chromatography loading buffer containing 0.1% formic acid (Sigma-Aldrich, United States) and 2.5% acetonitrile (Burdick & Jackson, United States).

4.3.3.2 Label-free LC-MS/MS

LC-MS/MS data dependent acquisition-based label-free quantitation was performed using a Q-Exactive quadrupole-Orbitrap mass spectrometer (Thermo Fisher Scientific, USA) coupled to a Dionex Ultimate 3000 nano-UPLC system mass spectrometer. Peptides were dissolved in 0.1% formic acid (FA, Sigma 56302), 2% acetonitrile (ACN, Burdick & Jackson BJLC015CS) and loaded on a C18 trap column (PepMap100, 9027905000, 300 µm × 5 mm × 5 µm). The dissolved peptides were trapped onto the column and washed for 3 min before the valve was switched and peptides eluted onto the analytical column as described hereafter. Chromatographic separation was performed with a Waters nanoEase (Zenfit) M/Z Peptide CSH C18 column (PepMap100, 300 µm × 5mm × 5 µm) where approximately 400 ng of peptide was injected for each sample. The methods and parameters as in Rossouw et al., (2021) was used for analysis with no amendments.

The solvent system employed was solvent A: LC water (Burdick and Jackson BJLC365), 0.1% FA and solvent B: ACN, 0.1% FA. All data acquisition was obtained using Proxeon stainless steel emitters (Thermo Fisher TFES523). The multi-step gradient) for peptide separation was generated at 300 nL/min as follows: time change 5 min, gradient change: 2-5% Solvent B, time change 40 min, gradient change 5-18% Solvent B, time change 10 min, gradient change 18-30% Solvent B, time change 2 min, gradient change 30-80% Solvent B. The gradient was then held at 80% Solvent B for 10 min before returning it to 2% Solvent B for 15 min. The mass

spectrometer was operated in positive ion mode with a capillary temperature of 320°C. The applied electrospray voltage was 1.95 kV. Data was acquired using Xcalibur v4.1.31.9, Chromelean v6.8 (SR13), Orbitrap MS v2.9 (build 2926) and Thermo Foundations 3.1 (SP4).

4.3.3.3 Data analysis

Peptide and protein identification was performed by CPGR. Database interrogation was performed with Byonic Software v2.6.46 (Protein Metrics, United States) using a tomato reference proteome sourced form UniProt (www.uniprot.org, accessed 24/11/2021). Protein search configurations are detailed in **Table 4.1**. Relative quantification was conducted using Progenesis QI for Proteomics v2.0.5556.29015 (Nonlinear Dynamics, UK). Data processing included peak picking, run alignment and normalisation (singly charged spectra were removed from the processing pipeline). Protein quantitation was run using the "relative quantitation using non-conflicting peptides" method. Valid proteins were filtered to remove reverse hits, common contaminants and singly charged ions. Proteins containing at least two unique peptides were selected and protein IDs converted to UniProtKB IDs.

Table 4.1: Detailed UniProt search parameters used for the data analysis.

Rule	Value
Protein database	Tomato_RefProt_34652prot_ UP000004994_241121.fasta
Spectrum-level FDR	Auto cut
Cleavage residues	RK
Digest cutter	C-terminal cutter
Peptide termini	Fully specific
Maximum number of missed cleavages	2
Precursor tolerance	10.0 ppm
Fragment tolerance	frag:qtof_hcd 20.0 ppm
Fragment tolerance version	2
Charges applied to charge-unassigned spectra	1, 2, 3
Precursor mass max	10 000
N-glycan search	None
O-glycan search	None
Off by x isotopes	-2, -1, 0, +1, +2
Contaminants added	TRUE
Decoys added	TRUE
Disulfide Enable	FALSE
Trisulfide Enable	FALSE
Custom Crosslink Enable	FALSE
DSS Crosslink Enable	FALSE
Wildcard Enable	0
Combyne cut off score	auto
Protein FDR cutoff	1%
Focused DB created	FALSE

Export mzIdentML	TRUE
Score version	2
Precurson_assignment__flags	2
po_NumberMonosReturn	1
Lock Mass list	None
common_modifications_max	1
rare_modifications_max	1
Carbamidomethyl/+57.021464 @ C	fixed
Oxidation / +15.994915 @ M	common2
Deamidated/ +0.984016 @ N, Q	common2
Product version	PMI-Byonic-Com:v3.8.13

4.3.3.4. Bioinformatics: Gene-ontology, enrichment, pathway, and network analysis

The bioinformatic analysis stated below were not conducted by CPGR. The pipeline followed in the following bioinformatic analysis are summarized in **Figure 4.3**. Differentially expressed proteins (DEPs) were identified using the Linear Models for Microarray Data (limma) package version 3.46.0 through R/Bioconductor project (http://www.R- project.org) for group pairwise comparisons of treatment:time:infection between chosen experimental groups and control groups (13 comparisons). The p-values were obtained using the Empirical Bayes (eBayes) function included in the package.

Gene Ontology (GO) annotation and enrichment analysis (by EASE Score, a modified Fisher Exact p-val) for the categories of biological process (BP), molecular function (MF) and cellular component (CC) were conducted using the Database for Annotation, Visualization, and Integrated Discovery (DAVID) database, version December 2022 (https://david.ncifcrf.gov/home.jsp). The total number of proteins identified in this study were used as the background/reference. GO terms with an FDR-corrected p-value < 0.05 were selected to identify over- and under-represented GO terms for each pairwise comparison.

The most representative GO terms were selected using REVIGO (http://revigo.irb.hr/) to remove GO term redundancy using the SimRel semantic similarity measurement. GO terms with a dispensability of < 0.05 were selected as the representative GO terms for each pairwise comparison. Pathway enrichment analysis was carried out in DAVID using the Kyoto Encyclopaedia of Genes and Genomes (KEGG) pathway annotation for the selected DEPs.

Protein-protein interactions (PPI) were investigated using Search Tool for the Retrieval of Interacting Genes (STRING) database (https://string-db.org/) for proteins of interest. Protein

interactions with a combined score of more than 0.4 were considered significant. GO and KEGG heatmaps as well as UpSet plots (made in R Studio using ggplot2 and upsetR respectively) were used to visualize the results.

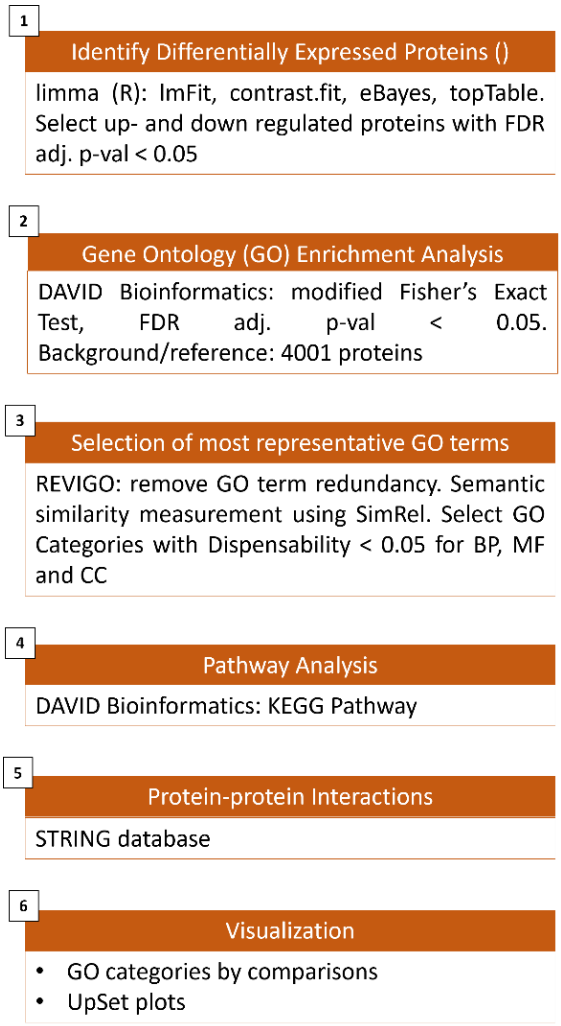

Figure 4.3: Steps followed in the bioinformatic analysis towards identifying and annotating DEPs and assigning GO terms. Adapted from Bonnot, Gillard and Magel, (2019).

4.4 Results

4.4.1 Exploratory data analysis

The proteome of tomato leaves treated with D3 and inoculated with *B. cinerea* was analysed to identify the mechanisms underpinning the efficacy of aminochitosan as a priming agent of resistance in the tomato/*B. cinerea* pathosystem at 6 and 9 hpi. These time points were chosen based on the accumulation of H_2O_2 in water-treated + infected leaves as early as 12

hpi (Chapter 3, Section 3.4.4) to evaluate the time points preceding the extensive accumulation of H_2O_2.

A total of 2663 proteins were quantified in all 40 samples consisting of eight treatment groups with 5 biological replicates each. The treatment groups consisted of a combination of three variables: infection, treatment, and time. The variables were as follows:

- infection by inoculation with water (control/Con) OR a *B. cinerea* spore suspension (infected/Inf)
- treatment with D3 (polymer/pol) OR water
- harvest at time points 6 hpi and 9 hpi

The eight treatment combination groups were as follows:

1. mock inoculated + D3 treated + 6 hpi (ConPol_6h)
2. mock inoculated + D3 treated + 9 hpi (ConPol_9h)
3. mock inoculated + water-treated + 6 hpi (ConWater_6h)
4. mock inoculated + water-treated + 9 hpi (ConWater_9h)
5. *B. cinerea* inoculated + D3 treated + 6 hpi (InfPol_6h)
6. *B. cinerea* inoculated + D3 treated + 9 hpi (InfPol_9h)
7. *B. cinerea* inoculated + water-treated + 6 hpi (InfWater_6h)
8. *B. cinerea* inoculated + water-treated + 9 hpi (InfWater_9h)

These treatment groups were compared to a control group of choice in a pairwise manner.

Exploratory data analysis was performed on all 40 samples to gain insight into the underlying patterns and relationships within the data, and to identify potential outliers by means of hierarchical clustering and Principal Component Analysis (PCA). The hierarchical clustering dendrogram of all 40 samples in **Figure 4.4A** highlighted natural groupings of the samples concurrently with the outliers identified by the PCA plot in **Figures 4.4C.**

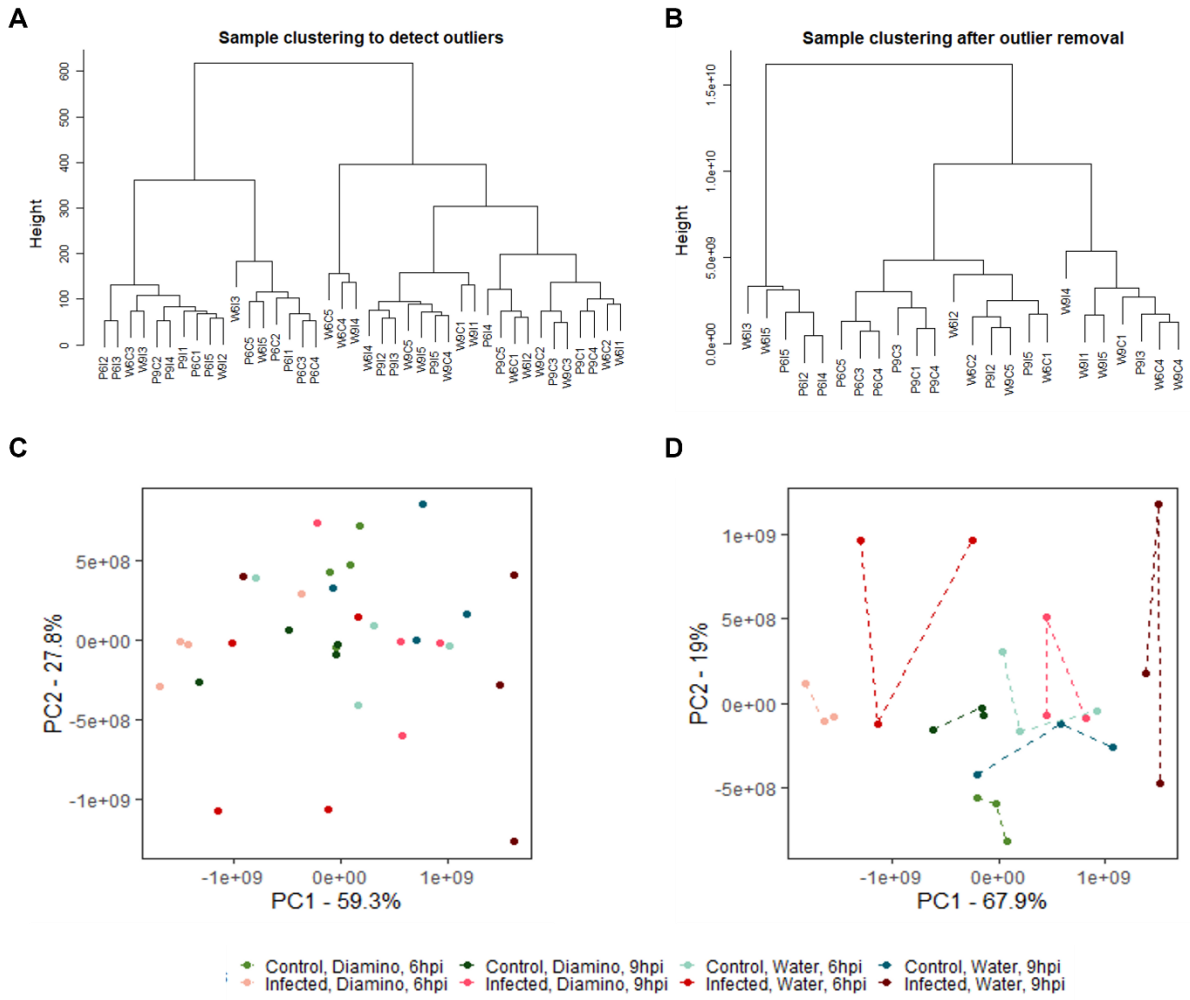

Figure 4.4: (A) A hierarchical clustering dendrogram of the 40 samples before outlier removal. (B) A hierarchical clustering dendrogram of the 24 samples after outlier removal. The letters found below the dendrogram indicate the following: P and D denote the treatments, polymer or water; 6 or 9 denote the time points as hours post inoculation; I or C denote the infection status as control or infected and the numbers at the end denote the biological replicate number. Hierarchical clustering analysis was conducted using Euclidean distance and Ward's linkage method. (C) PCA of 2663 normalized protein abundances in 40 samples for 5 biological replicates. (D) PCA of 2663 normalized protein abundances in 24 samples for 3 biological replicates after outlier removal. Samples were grouped by treatment, infection, and time point.

Subsequent analysis focussed on assessing the impact of different combinations of outlier removal on the grouping within the dataset. As seen in **Figures 4.4B and D**, 2 outlier samples were removed from each group combination resulting in a more refined dataset and groupings. Twenty-four samples consisting of eight treatment groups with three biological replicates were used in all further analyses. The expression profiles of the top 100 differentially expressed proteins (DEPs) under treatments, infection and time points are shown by the heatmap in **Figure 4.5**. Two clusters of proteins can be seen along with clear

differences in the regulation of the proteins for ConPol at 6 and 9 hpi (P6C and P9C respectively) and InfPol at 6 hpi (P6I).

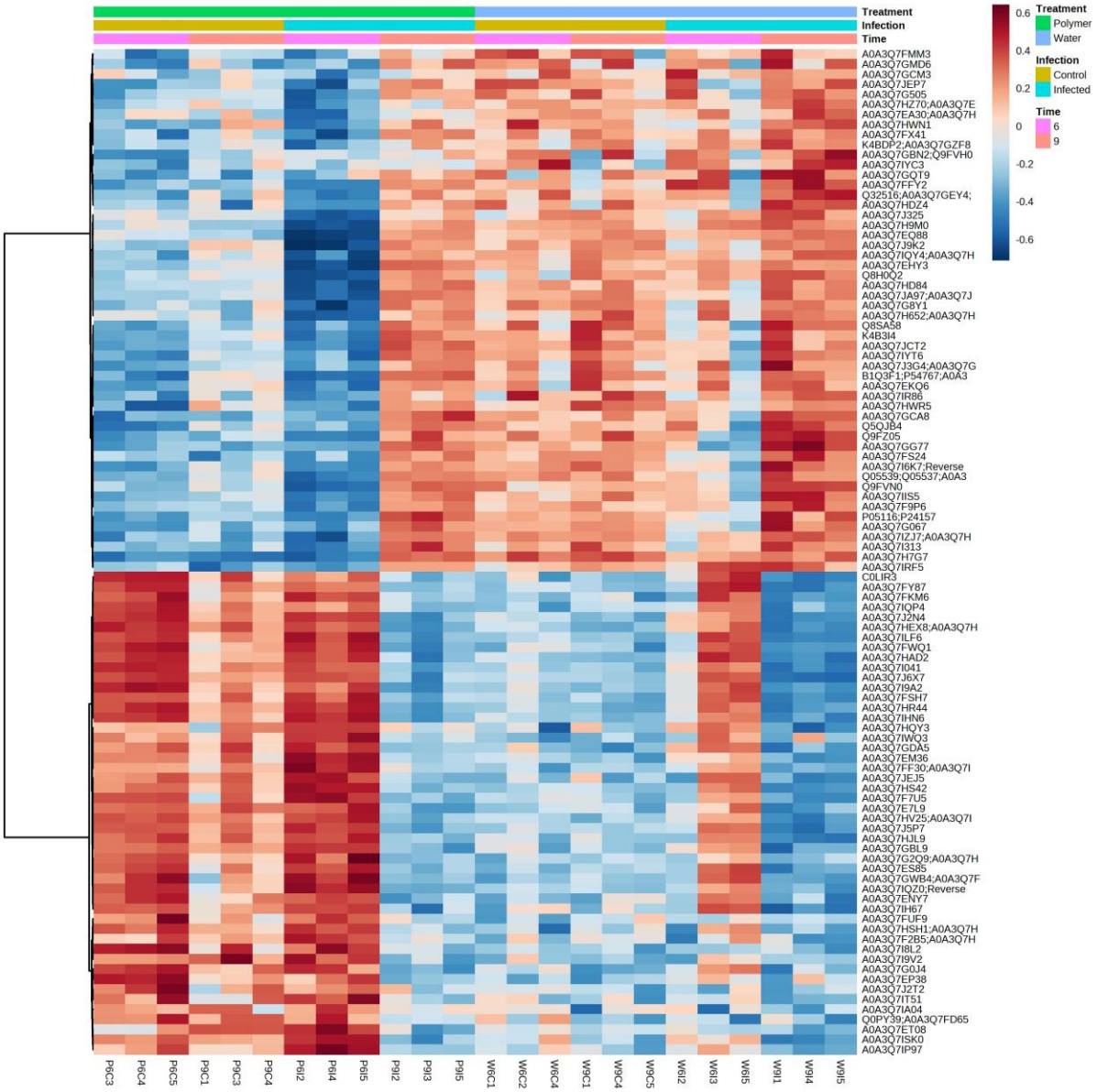

Figure 4.5: A heatmap showing the top 100 differentially expressed proteins (rows) determined using limma package, FDR-corrected P-value < 0.05) clustered by expression. Samples are organized (in columns) by treatment (aminochitosan/water) and infection (infected/mock) for the time points (6 and 9 hpi). The letters found below the dendrogram indicate the following: P and D denote the treatments, polymer or water; 6 or 9 denote the time points as hours post inoculation; I or C denote the infection status as control or infected and the numbers at the end denote the biological replicate number. The data was $\log_{10}$ transformed and normalized (range scaled). The dendrogram shows hierarchical clustering using Euclidean distance and Ward.D2 linkage method. This plot was created in Metaboanalyst.

4.4.2 Quantitative proteomic analysis

To identify DEPs regulated by treatment, infection or time, protein abundances were compared using limma and eBayes for each pairwise group comparison considering that three biological replicates were to be used in the subsequent analyses.

A pairwise group comparison contrasted a treatment group to a control group of choice either within a time point or between time points (**Table 4.2**). Proteins were considered differentially expressed if the FDR-corrected p-value was < 0.05, independent to the magnitude of the log_2FC. Proteins were not excluded based on log_2FC to allow for the inclusion of biologically relevant changes in underrepresented proteins with lower log_2FC magnitudes of which may be important in relevant pathways or regulatory roles.

Table 4.2: Differentially expressed proteins (DEPs) identified using limma, FDR-corrected p-value < 0.05, fold enrichment > 1, for each comparison (experimental/control). DEPs were selected after DAVID and REVIGO.

Time	Pairwise comparison	Up	Down	Over/under-represented GO terms	Unique DEPs	Total unique DEPs	Total exclusive DEPs
6 hpi	ConPol vs ConWater	74	147	23	221	758	665
	InfPol vs ConWater	278	173	26	451		
	InfPol vs ConPol	94	197	22	291		
	InfPol vs InfWater	77	173	21	250		
	InfWater vs ConWater	2	0	1	2		
9 hpi	ConPol vs ConWater	13	5	4	18	109	13
	InfPol vs InfWater	0	0	0	0		
	InfWater vs ConWater	0	0	0	0		
	InfPol vs ConPol	46	59	18	105		
9 hpi vs 6 hpi	ConPol vs ConPol	13	17	10	40	550	550
	ConWater vs ConWater	0	2	2	2		
	InfPol vs InfPol	272	171	19	443		
	InfWater vs InfWater	103	76	14	179		

Con = mock inoculated, Inf = *B. cinerea* inoculated, Pol = D3 treatment, Water = mock treatment. Unique DEPs: proteins occurring for both groups in a pairwise comparison is considered duplicates and were removed. Exclusive DEPs: proteins that are exclusive to the specific group and do not reoccur in another group.

Up-regulated and down-regulated proteins for each group comparison with an FDR-corrected p-value < 0.05 were selected as shown in (**Table 4.2**). Out of the 13 comparisons made between groups, 11 yielded DEPs. Interestingly, at 6 hpi, there were DEPs identified in five pairwise comparisons, whereas only two pairwise comparisons yielded DEPs at 9 hpi (**Table**

4.2). Furthermore, the number of DEPs identified at 6 hpi was greater than at 9 hpi (**Table 4.2).** The water treatment comparisons yielded two up-regulated proteins at 6 hpi (InfWater vs ConWater) and none at 9 hpi. When comparing treatments at 9 hpi to 6 hpi, 2 DEPs (down-regulated) were identified for the comparison of ConWater at 9 hpi to 6 hpi whereas 179 DEPs when comparing InfWater at 9 hpi to 6 hpi (103 up-regulated and 76 down-regulated) (**Table 4.2**).

In contrast, numerous DEPs were identified when comparing the polymer treatments to water treatments, for both control and infected samples at 6hpi, 9 hpi and 9 hpi vs 6 hpi (**Table 4.2**). The number of DEPs in polymer treated + infected samples were significantly greater than the number of proteins in water-treated + infected samples. Furthermore, the polymer treated + control samples were also significantly greater than the water-treated + infected samples (**Table 4.2**).

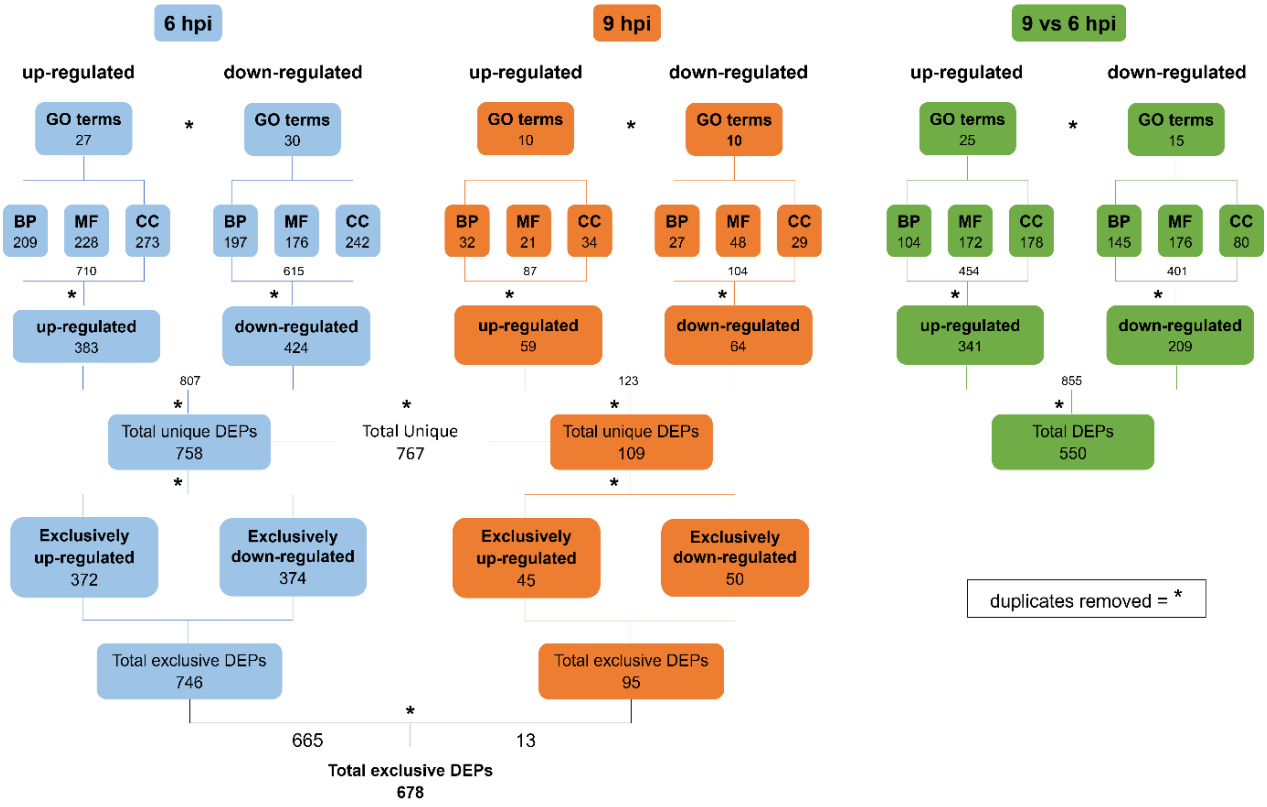

Figure 4.6: Flow diagram delineating the process of determining up- and down-regulated, unique, and exclusive proteins per time point for all of the group comparisons. * Indicates where duplicate proteins were removed.

In this study, a protein was considered unique if it appeared in a specific sample or experimental condition but was not exclusive to that sample (e.g. may be shared across

different time points, group comparisons or between up/down regulated proteins). Consequently, proteins were considered exclusive if they only occurred in one specific time point/regulation without reoccurring. This distinction allowed for proteins to be categorized based on their temporal regulatory patterns or if they were exclusively up-regulated or down-regulated (**Figure 4.6**).

When combining the results for the groups at 6hpi, a total of 758 proteins were unique (up = 383, down = 424, 50 shared) and 748 were exclusive (up = 372, down = 374) to 6 hpi. In contrast to this, 9 hpi yielded fewer DEPs with 109 unique proteins (up = 59, down = 64, 14 shared) and 95 proteins (up = 45, down = 50) exclusive to 9 hpi (**Figures 4.6 and 4.7**). Across 6 and 9 hpi, a total of 767 proteins were unique and 678 proteins were exclusive, with 665 (up = 324, down = 341) belonging to 6 hpi and 13 (up = 7, down = 6) to 9 hpi (**Figures 4.6 and 4.7**). When comparing the same groups at 9 hpi to 6 hpi (e.g. ConPol at 9 hpi to ConPol at 6 hpi), a total of 550 DEPs were observed, of which 341 were up-regulated with 34 shared between 9 hpi up-regulated and 6 hpi down-regulated proteins and 209 down-regulated with 44 shared between 9 hpi down-regulated and 6 hpi up-regulated proteins (**Figures 4.6 and 4.7**).

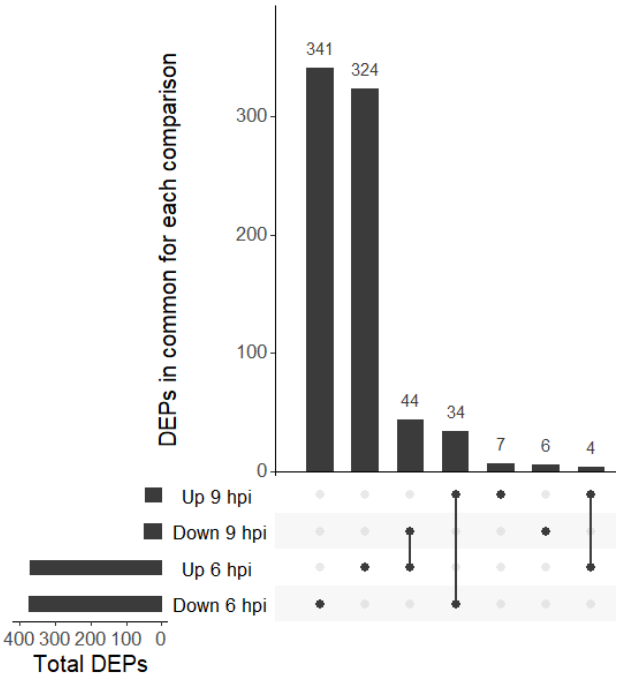

Figure 4.7: UpSet plot showing the unique and exclusive proteins for the different time points. The lines between dots indicate 'unique' proteins while the individual dots represent the 'exclusive' proteins.

4.4.3 GO and KEGG enrichment analysis of aminochitosan treatment and *B. cinerea* infection at 6 hpi

To explore the significance of the DEPs, pathways and networks involved, the proteins were functionally categorized using Gene Ontology (GO) and Kyoto Encyclopaedia of Genes and Genomes (KEGG) enrichment analysis. The proteins were assigned to three GO categories: biological process (BP), molecular function (MF), and cellular component (CC). A range of DEPs were multifunctional and were assigned to more than one category, hence the duplicates between categories, group comparisons and time points.

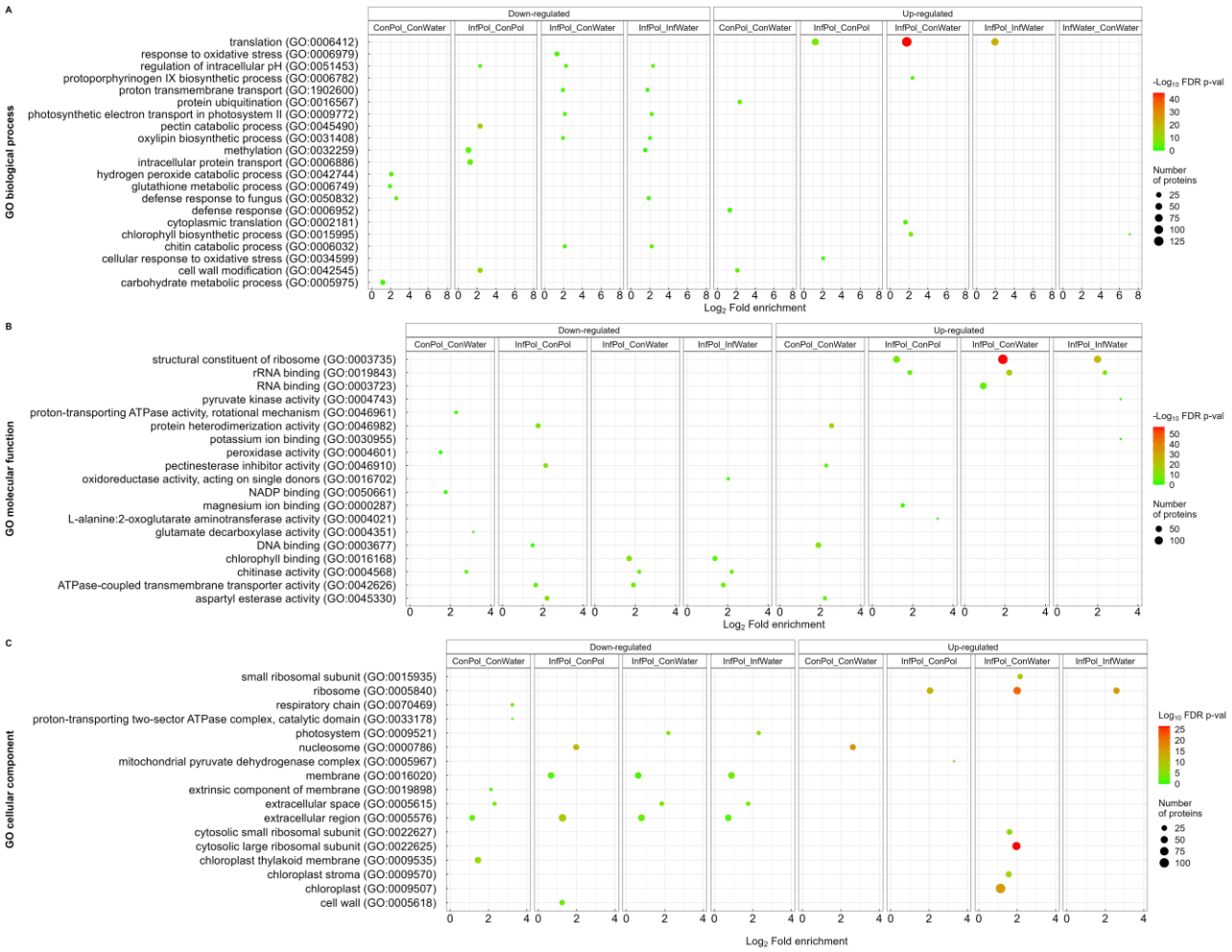

Figure 4.8: Functional analysis of the significantly up- and down-regulated proteins at 6 hpi. Classification of the over- and under-represented GO terms included biological process, molecular function, and cellular component. The dot size indicates the number of proteins associated with the term and the dot color indicates the statistical significance ($p < 0.05$).

At 6 hpi, a total of 93 GO terms were identified; duplicate GO terms across the group comparisons were removed resulting in a final total of 57 terms. Of these 57 terms, 30 terms

were categorized as down-regulated and 27 as up-regulated, with most of the GO terms belonging to the InfPol_InfWater (11 terms), InfPol_ConWater (8 terms), and ConPol_ConWater (7 terms) group comparisons (**Figures 4.6 and 4.8**), highlighting the potential benefits of aminochitosan pretreatment.

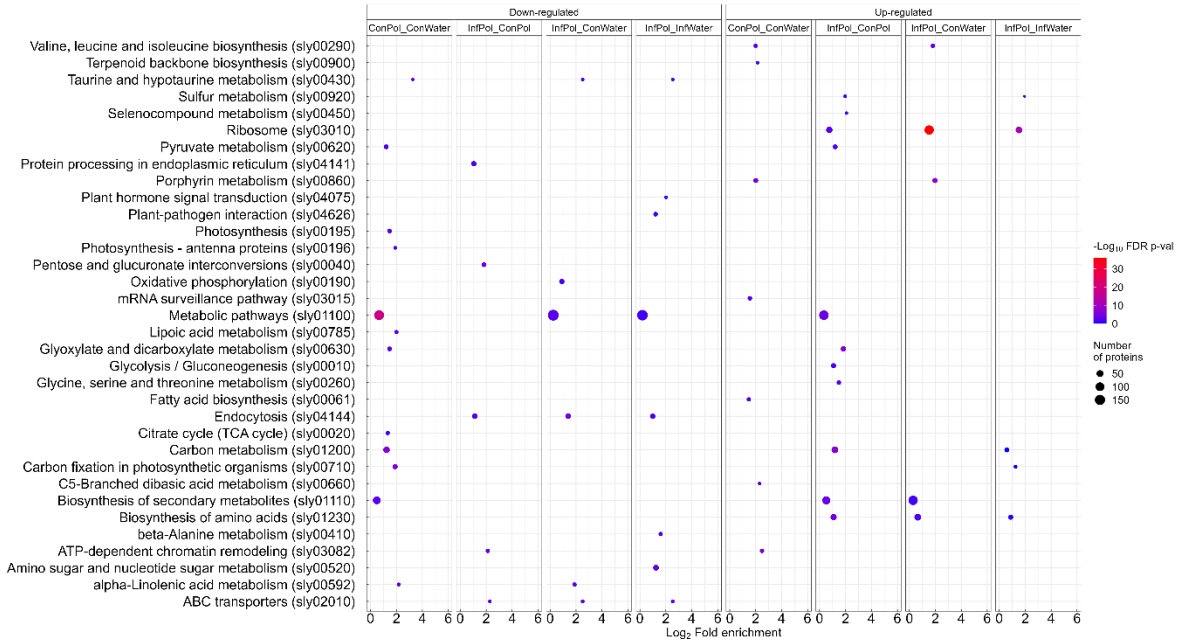

Figure 4.9: KEGG enrichment analysis of the differentially expressed proteins at 6 hpi. Size of each point represents the number of genes enriched in a particular pathway.

The most biologically relevant and notable regulated proteins (**Table S4.2**), GO terms (**Figure 4.8)** and KEGG features (**Figure 4.9**) for select group comparisons are mentioned below with the full dataset summarized in the figures mentioned.

4.4.3.1 The effects of aminochitosan in uninfected leaves at 6 hpi: ConPol vs ConWater

The ConPol vs ConWater group comparison assessed the effects of aminochitosan in mock inoculated (uninfected) leaves compared to the water treatment. The comparison identifies how aminochitosan treatment by itself influences protein expression in the absence of *B. cinerea* inoculation. This provides a baseline for the effects of aminochitosan treatment in a non-infected context, potentially highlighting primed proteins and pathways.

Table S4.2 displays the top 5 up- and down-regulated proteins that are unique or shared between group comparisons at each time point (6, 9) or between time points (9_6). From this, the top 5 up-regulated proteins for ConPol_ConWater were a GTP-binding protein

(A0A3Q7GBL9, logFC 3.93 increase), a threonine dehydratase 1 biosynthetic, chloroplastic (A0FKE6, logFC 3.86 increase), a magnesium chelatase (A0A3Q7G0W1, logFC 3.80 increase), a CHD3-type chromatin-remodelling factor PICKLE (A0A3Q7IH67, logFC 3.67 increase) and an NADPH-protochlorophyllide oxidoreductase (A0A3Q7IBI0, logFC 3.50 increase). The top 5 down-regulated proteins were a peroxidase (A0A3Q7E8T9, logFC 3.96 decreases), an inositol-3-phosphate synthase (A0A3Q7GNM9A0A3Q7H7G7, logFC 3.73 decrease), an uncharacterized protein (A0A3Q7FQP4, logFC 3.48 decrease), an alpha-amylase (A0A3Q7GDE1, logFC 3.32 decrease), and an acidic 26 kDa endochitinase (Q05539, logFC 3.19 decrease). Of these proteins, 4 up- and 3 down-regulated proteins were shared with other group comparisons.

The up-regulated proteins (**Figures 4.8** and **4.10**) were enriched in the BP category for 'protein ubiquitination' (GO:0016567, 13 proteins), 'pectinesterase inhibitor activity' (GO:0046910, 14 proteins), 'cell wall modification' (GO:0042545, 14 proteins) and 'defence response' (GO:0006952, 17 proteins). The up-regulated proteins in the MF category were enriched for 'protein heterodimerization activity' (GO:0046982, 26 proteins) and 'DNA binding' (GO:0003677, 35 proteins) while only one term was enriched in the CC category for 'nucleosome' (GO:0000786, 30 proteins).

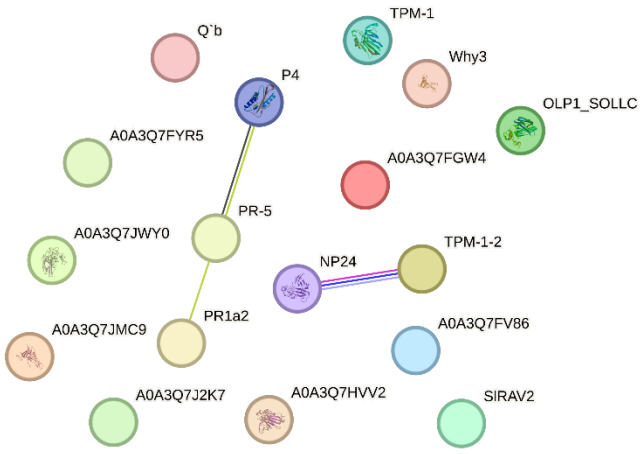

Figure 4.10: Protein-protein interactions of the proteins associated with the GO terms 'defence response' (GO:0006952, 17 proteins) in the ConPol_ConWater group comparison at 6 hpi.

In contrast, the down-regulated proteins were enriched in more than 3 GO terms per category. The enriched GO terms in the BP category were 'defence response to fungus '(GO:0050832, 9 proteins), 'hydrogen peroxide catabolic process' (GO:0042744, 15 proteins),

'glutathione metabolic process' (GO:0006749, 11 proteins) and 'carbohydrate metabolic process' (GO:0005975, 21 proteins). The down-regulated proteins in the MF category were enriched for 'glutamate decarboxylase activity' (GO:0004351, 5 proteins), 'chitinase activity' (GO:0004568, 11 proteins) and 'peroxidase activity' (GO:0004601, 13 proteins). The enriched CC terms were 'respiratory chain (GO:0070469, 7 proteins), 'extracellular space' (GO:0005615, 10 proteins), 'extrinsic component of membrane' (GO:0019898, 6 proteins) and chloroplast thylakoid membrane (GO:0009535, 37 proteins) (**Figure 4.8**).

Figure 4.9 displays the KEGG enrichment analysis which showed that the up-regulated proteins were significantly associated with 19 pathways, of which the most notable were 'biosynthesis of secondary metabolites' (73 proteins), 'porphyrin metabolism' (13 proteins), 'valine, leucine and isoleucine biosynthesis' (7 proteins), 'pentose and glucuronate interconversions' (7 proteins), 'citrate cycle' (9 proteins), 'biosynthesis of amino acids' (19 proteins) and 'terpenoid backbone biosynthesis' (6 proteins). The down-regulated proteins were significantly associated with 'carbon metabolism' (28 proteins), 'photosynthesis' (14 proteins), 'glyoxylate and dicarboxylate metabolism' (11), 'carbon fixation in photosynthetic organisms '(11 proteins), 'biosynthesis of secondary metabolites' (52 proteins), 'taurine and hypotaurine metabolism' (5 proteins) and 'photosynthesis - antenna proteins' (5 proteins).

4.4.3.2 The effects of aminochitosan in infected vs uninfected leaves at 6 hpi: InfPol vs ConPol

The InfPol vs ConPol group comparison assessed the impact of aminochitosan in *B. cinerea* inoculated (infected) leaves compared to aminochitosan-treated but uninfected leaves. Proteins identified in this comparison are associated with the combined effects of aminochitosan and *B. cinerea* infection and provides insights into how aminochitosan modulates tomato's response to *B. cinerea* after pretreatment with aminochitosan at 6 hpi.

From **Table S4.2**, 2 of the top 5 up-regulated proteins and 4 of the down-regulated proteins were shared with other group comparisons. The top 5 up-regulated proteins were three uncharacterized proteins (Q53U36, A0A3Q7IIQ1 and A0A3Q7GM48, logFC of 5.13, 4.37 and 3.79 increase respectively), isochorismatase domain-containing protein (K4ASZ0, logFC 3.92 increase), and 4-coumarate CoA ligase (A0A3Q7G3R4, logFC 3.81 increase). The top 5 down-regulated proteins were an ABC transporter B family member 25 (A0A3Q7FSS8), a 7-

dehydrocholesterol reductase (A0A3Q7E9H9), a cytochrome P450 (A0A3Q7H9W3), and two uncharacterised proteins (A0A3Q7F3X3 and A0A3Q7F7H4).

The up-regulated proteins in the BP category were enriched most notably in 'cellular response to oxidative stress' (GO:0034599, 9 proteins); the MF category in L-alanine:2-oxoglutarate aminotransferase activity (GO:0004021, 4 proteins), rRNA binding (GO:0019843, 21 proteins), 'magnesium ion binding' (GO:0000287, 15 proteins) and in the CC category are 'mitochondrial pyruvate dehydrogenase complex' (GO:0005967, 4 proteins) and 'ribosome' (GO:0005840, 37 proteins). The down-regulated proteins in the BP category were most notably enriched in the 'cell wall modification' (GO:0042545, 28 proteins), 'regulation of intracellular pH' (GO:0051453, 8 proteins), and 'methylation' (GO:0032259, 33 proteins); the MR category in 'aspartyl esterase activity' (GO:0045330, 23 proteins) and 'DNA binding '(GO:0003677, 33 proteins); and the CC category in the 'nucleosome' (GO:0046982, 25 proteins), 'extracellular region' (GO:0005576, 55 proteins) and ''membrane (GO:0016020, 36 proteins) (**Figure 4.8**).

The KEGG pathways significantly associated (**Figure 4.9**) with the up-regulated proteins were 'porphyrin metabolism' (17 proteins) while the down-regulated proteins are significantly associated with 'metabolic pathways' (144 proteins) and 'oxidative phosphorylation' (23 proteins).

4.4.3.3 The effects of aminochitosan in infected vs uninfected leaves at 6 hpi: InfPol vs ConWater

The InfPol vs ConWater group comparison assessed the effects of aminochitosan in *B. cinerea* inoculated (infected) leaves compared to the control, water-treated and uninfected leaves. This comparison highlights the impact of aminochitosan in modulating a response to infection and differs to InfPol_ConPol as it compares to a healthy untreated leaf and not a potentially "primed" leaf as in ConPol.

The top 5 up-regulated and down-regulated proteins revealed that all 10 proteins were shared with the other group comparisons (**Table S4.2**). The top 5 up-regulated were a GTP-binding protein (A0A3Q7GBL9, logFC 4.90 increase), a CHD3-type chromatin-remodelling factor PICKLE (A0A3Q7IH67, logFC 4.05 increase), an aromatic amino acid beta-eliminating

lyase/threonine aldolase domain-containing protein (A0A3Q7FWX0, logFC 4.04 increase) and 4-coumarate CoA ligase (A0A3Q7G3R4, logFC 3.91 increase). The top 5 down-regulated proteins are an ABC transporter B family member 25 (A0A3Q7FSS8, logFC 5.09 increase), a PMR5N domain-containing protein (A0A3Q7F572, logFC 4.74 increase), mitochondrial phosphate transporter (A0A3Q7FQP4, logFC 4.69 increase), a 7-dehydrocholesterol reductase (A0A3Q7E9H9, logFC 4.55 increase), and an acidic 26 kDa endochitinase (Q05539, log FC 4.27 increase).

The up-regulated proteins in the BP category were notably enriched for 'protoporphyrinogen IX biosynthetic process' (GO:0006782, 9 proteins) and 'chlorophyll biosynthetic process' (GO:0015995, 15 proteins); the MF category was notably enriched for 'rRNA binding' (GO:0019843, 40 proteins) and 'RNA binding' (GO:0003723, 62 proteins); and the CC category was notably enriched for 'chloroplast stroma' (GO:0009570, 31 proteins) and 'chloroplast' (GO:0009507, 104 proteins). The down-regulated proteins in the BP category were notably enriched for 'regulation of intracellular pH' (GO:0051453, 8 proteins), 'chitin catabolic process '(GO:0006032, 10 proteins), 'photosynthetic electron transport in photosystem II' (GO:0009772, 10 proteins), 'oxylipin biosynthetic process' (GO:0031408, 8 proteins), 'proton transmembrane transport' (GO:1902600, 12 proteins) and 'response to oxidative stress (GO:0006979, 19 proteins); the MF category was notably enriched for 'chitinase activity' (GO:0004568, 14 proteins) and 'chlorophyll binding' (GO:0016168, 34 proteins); and the CC category was notably enriched for 'photosystem' (GO:0009521, 11 proteins), 'extracellular region' (GO:0005576, 42 proteins) and 'membrane' (GO:0016020, 37 proteins) (**Figure 4.8**).

From **Figure 4.8**, the KEGG pathways significantly associated with the up-regulated proteins were 'carbon fixation in photosynthetic organisms'(16 proteins), 'carbon metabolism' (33 proteins), 'biosynthesis of secondary metabolites' (64 proteins) and 'glycine, serine and threonine metabolism' (12 proteins) while the down-regulated pathway was associated with 'pentose and glucuronate interconversions' (15 proteins).

4.4.3.4 The effects of aminochitosan in infected leaves at 6 hpi: InfPol vs InfWater

The InfPol vs InfWater comparison highlights the specific effects of aminochitosan during *B. cinerea* infection by comparing it directly to another infected condition with the control water treatment. This provides insights into how aminochitosan modulates the host response during

B. cinerea infection, allowing for a direct comparison between two infected conditions with different treatments.

The top 5 up-regulated proteins were an uncharacterized protein (Q53U36, logFC 4.15 increase), a 4-coumarate-CoA ligase (A0A3Q7G3R4, logFC 4.14 increase), 60S ribosomal protein (Q3SC85, logFC 4.05 increase), a non-symbiotic haemoglobin class 1 protein (Q9AWA9, 3.61 logFC increase) and an aromatic amino acid beta-eliminating lyase/threonine aldolase domain-containing protein (A0A3Q7FWX0, logFC 3.11 increase). The top 5 down-regulated proteins were an ABC transporter B family member 25 (A0A3Q7FSS8, logFC 4.66 decrease), an uncharacterized protein (A0A3Q7F3X3, logFC 4.43 decrease), a dehydrocholesterol reductase (A0A3Q7E9H9, logFC 4.16 decrease), a cytochrome P450 (A0A3Q7H9W3, logFC 4.04 decrease) and a PMR5N domain-containing protein (A0A3Q7F572, logFC 3.40 decrease). From **Table S4.2**, all 3 up- and 4 down-regulated proteins were shared between other group comparisons.

From **Figure 4.8**, the up-regulated proteins in the BP category were notably enriched for 'translation' (64 proteins). The down-regulated proteins in the BP category were notably enriched for 'regulation of intracellular pH 8' (GO:0051453, 8 proteins), 'chitin catabolic process' (GO:0006032, 10 proteins), 'photosynthetic electron transport in photosystem II' (GO:0009772, 10 proteins), 'oxylipin biosynthetic process' (GO:0031408, 8 proteins), 'defence response to fungus' (GO:0050832, 11 proteins), 'proton transmembrane transport' (GO:1902600, 10 proteins), and 'methylation' (GO:0032259, 13 proteins); the MF category was notably enriched for 'chitinase activity' (GO:0004568, 14 proteins), 'oxidoreductase activity, acting on single donors' (GO:0016702, 8 proteins), and 'chlorophyll binding' (GO:0016168, 27 proteins); and the CC category was significantly enriched for 'photosystem' (GO:0009521, 11 proteins), and 'membrane' (GO:0016020, 41 proteins).

The KEGG pathway significantly associated with the up-regulated proteins was 'ribosome' (45 proteins) and the KEGG pathway significantly associated with the down-regulated proteins was 'amino sugar and nucleotide sugar metabolism' (23 proteins).

4.4.4 GO and KEGG enrichment analysis of aminochitosan treatment and *B. cinerea* infection at 9 hpi

In contrast to 6 hpi, the 9 hpi time point yielded overall, fewer significant group comparisons and DEPs were identified at 9 hpi.

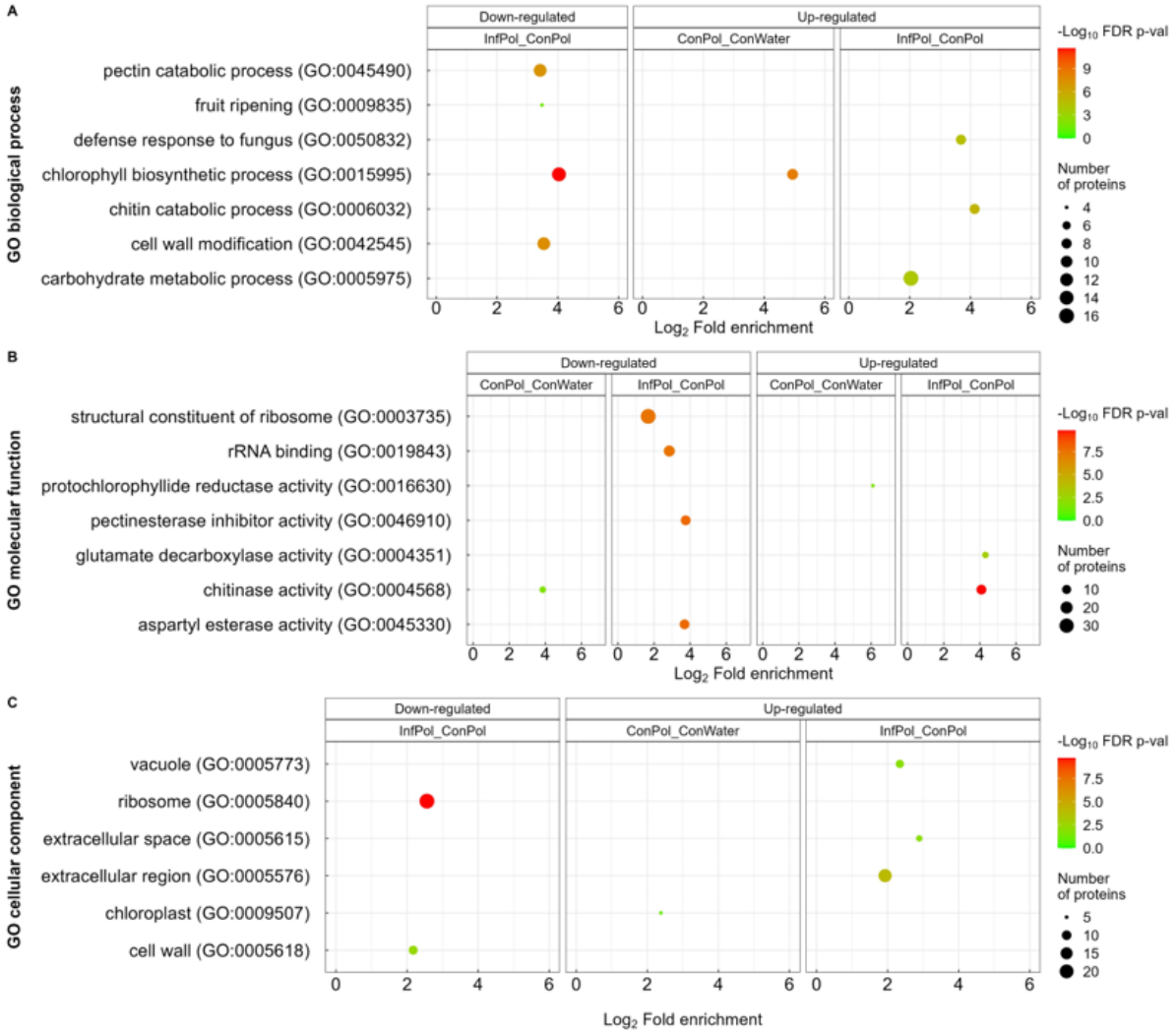

Figure 4.11: Functional analysis of the significantly up- and down-regulated proteins at 9 hpi. Classification of the over- and under-represented GO terms included biological process, molecular function, and cellular component. The dot size indicates the number of proteins associated with the term and the dot color indicates the statistical significance ($p < 0.05$).

At 9 hpi, a total of 22 GO terms were identified; duplicate GO terms across the group comparisons were removed resulting in a final total of 20 (**Figures 4.6**). Of the final 20 terms, 10 GO terms were categorized as down-regulated and 10 as up-regulated, with the GO terms belonging to the InfPol_ConPol (15 terms) and ConPol_ConWater (5 terms) group comparisons (**Figures 4.6 and 4.11**).

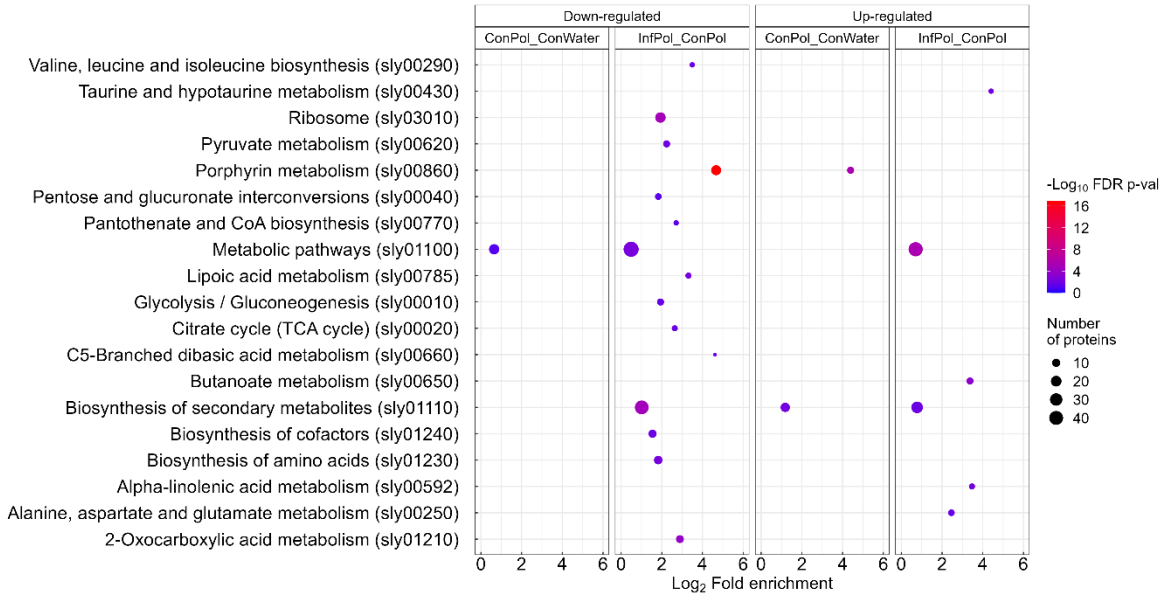

Figure 4.12: KEGG enrichment analysis of the differentially expressed proteins at 9 hpi. Size of each point represents the number of genes enriched in a particular pathway.

4.4.4.1 The effects of aminochitosan at 9 hpi: ConPol_ConWater

From **Table S4.2**, 5 up- and 4 down-regulated proteins were shared with other group comparisons. The top 5 up-regulated proteins were a 4-coumarate CoA ligase (A0A3Q7G3R4, logFC 3.79 increase), a GTP-binding protein OBGC2 (A0A3Q7GBL9, logFC 3.46 increase), a GUN4 domain-containing protein (A0A3Q7H247, logFC 3.30 increase), magnesium chelatase (A0A3Q7G0W1, logFC 2.92 increase), and a NADPH-protochlorophyllide oxidoreductase (A0A3Q7IBI0, logFC 2.60 increase). The top 5 down-regulated proteins were an inositol-3-phosphate synthase (A0A3Q7GNM9, logFC 4.33 decrease), an REF/SRPP-like protein (A0A3Q7GG77, logFC 2.70 decrease), a mitochondrial phosphate transporter (A0A3Q7FQP4. logFC 2.26 decrease), a PMR5N domain-containing protein (A0A3Q7F572, logFC 1.91 decrease) and a dirigent protein (A0A3Q7JCT2, logFC 1.79 decrease). From Table S4.2, 4 up- and 4 down-regulated proteins are shared with the other group comparisons.

The up-regulated proteins in the BP, MF and CC category were notably enriched for ‘chlorophyll biosynthetic process‘(GO:0015995 , 9 proteins), ‘protochlorophyllide reductase activity’ (GO:0016630, 3 proteins), and ‘chloroplast’ (GO:0009507, 5 proteins) respectively. The down-regulated proteins were enriched for ‘chitinase activity’ (GO:0004568, 5 proteins) (**Figure 4.11**). From **Figure 4.12**, the KEGG pathways significantly associated with the up-regulated proteins was porphyrin metabolism’ (7 proteins).

4.4.4.2 The effects of aminochitosan at 9 hpi: InfPol_ConPol

The top 5 up-regulated proteins were an inositol-3-phosphate synthase (A0A3Q7GNM9, logFC 4.19 decrease), an REF/SRPP-like protein (A0A3Q7GG77, logFC 3.58 decrease), a mitochondrial phosphate transporter (A0A3Q7FQP4. logFC 2.81 decrease), a subtilisin-like protease SBT1.7 (A0A3Q7HVI4, logFC 2.41 increase), and a Glucan endo-1,3-beta-glucosidase A (Q01412, logFC 2.30 increase). The top 5 down-regulated proteins were a GTP-binding protein OBGC2 (A0A3Q7GBL9, logFC 4.32 decrease), a GUN4 domain-containing protein (A0A3Q7H247, logFC 4.12 decrease), an uncharacterized protein (A0A3Q7F3X3, logFC 3.39 decrease), a superoxide dismutase [Cu-Zn] (P14831, logFC 3.20 decrease), and a magnesium chelatase (A0A3Q7G0W1, logFC 3.19 decrease). From **Table S4.2**, 3 up- and 4 down-regulated proteins were shared with other group comparisons.

The up-regulated proteins (**Figure 4.11**) in the BP category were notably enriched for 'chitin catabolic process' (GO:0006032, 8 proteins), 'defence response to fungus' (GO:0050832, 8 proteins) and 'carbohydrate metabolic process' (GO:0005975, 16 proteins); MF category was notably enriched for 'glutamate decarboxylase activity' (GO:0004351, 5 proteins) and 'chitinase activity' (GO:0004568, 12 proteins); and the CC category was notably enriched for 'extracellular space' (GO:0005615, 6 proteins) and 'extracellular region' (GO:0005576, 18 proteins). The down-regulated proteins in the BP category were notably enriched for 'chlorophyll biosynthetic process' (GO:0015995, 14 proteins), and 'cell wall modification' (GO:0042545, 12 proteins); the CC category was enriched for 'ribosome' (GO:0005840, 23 proteins) and 'cell wall' (GO:0005618, 9 proteins).

The KEGG pathways significantly associated with the up-regulated proteins was 'butanoate metabolism' (7 proteins), 'taurine and hypotaurine metabolism' (4 proteins), 'alpha-Linolenic acid metabolism' (5 proteins) and 'alanine, aspartate and glutamate metabolism' (6 proteins). The KEGG pathway significantly associated with the down-regulated proteins was 'porphyrin metabolism' (13 proteins) (**Figure 4.12**).

4.4.5 GO and KEGG enrichment analysis of aminochitosan treatment and *B. cinerea* infection: 9 hpi vs 6 hpi

The comparison of identical groups across the time points aimed at identifying temporal changes. It is important to note, however, that the experiments at 6 and 9 hpi were conducted on independent leaves within the same experiment.

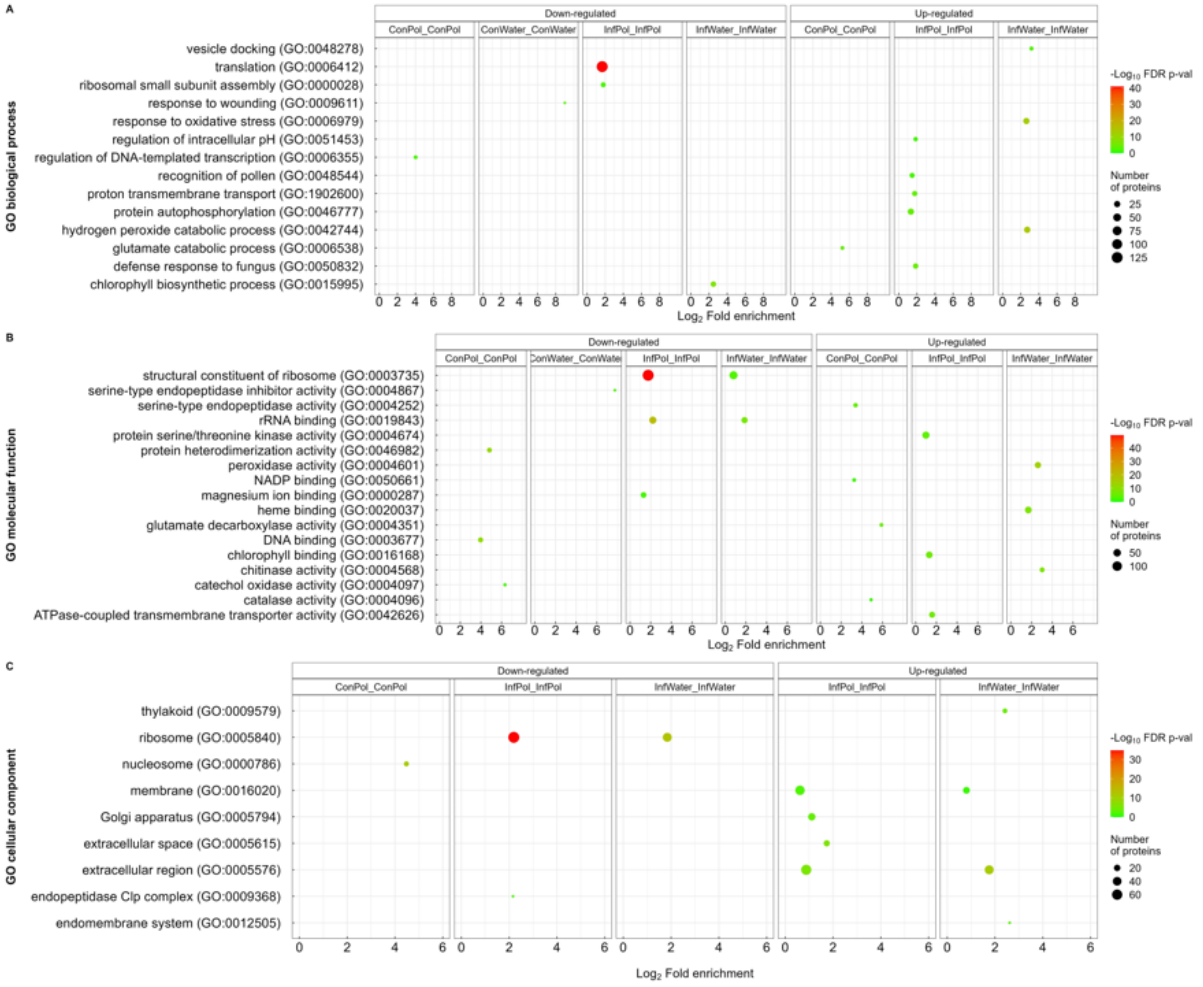

Figure 4.13: Functional analysis of the significantly up- and down-regulated proteins from the same groups at 9 hpi compared to 6 hpi. Classification of the over- and under-represented GO terms included biological process, molecular function, and cellular component. The dot size indicates the number of proteins associated with the term and the dot color indicates the statistical significance ($p < 0.05$).

When comparing the proteins at 9 hpi to 6 hpi for the same groups, a total of 45 GO terms were identified; duplicate GO terms across the group comparisons were removed resulting in a final total of 40 (**Table 4.6**). 25 GO terms were categorized as down-regulated and 15 as up-regulated, with the GO terms belonging to the InfPol at 9 hpi vs InfPol at 6 hpi (19 terms) and InfWater at 9 hpi vs InfWater at 6 hpi (14 terms) group comparisons (**Figures 4.6 and 4.13**).

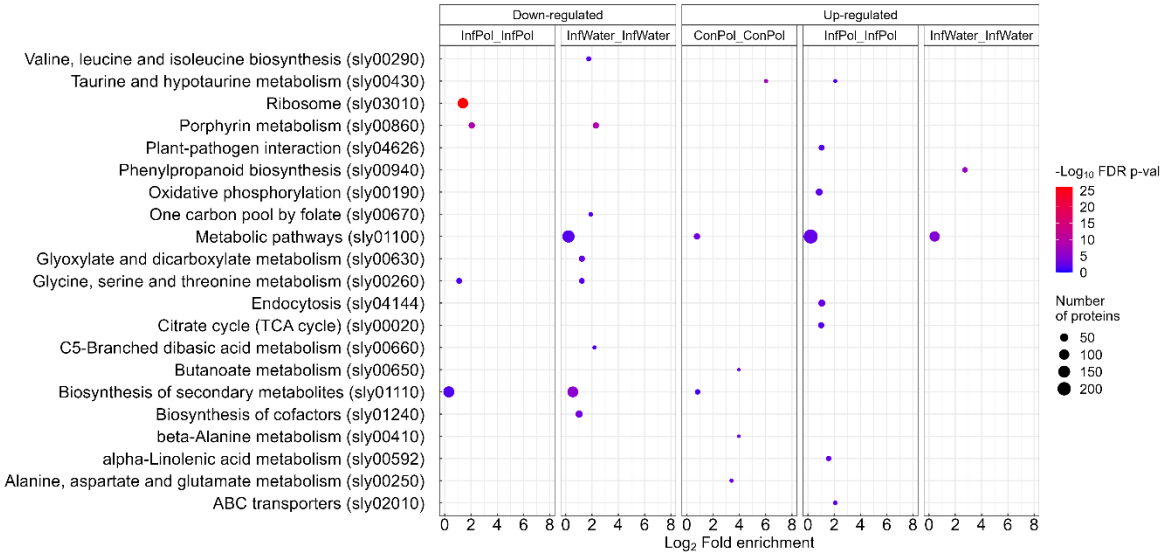

Figure 4.14: KEGG enrichment analysis of the differentially expressed proteins at 9 hpi compared to 6 hpi. Size of each point represents the number of genes enriched in a particular pathway.

4.4.5.1 The effects of aminochitosan at 9 hpi compared to 6 hpi: InfWater_InfWater

This comparison serves as a baseline for understanding the temporal response to *B. cinerea* without the effects of aminochitosan and may help in contextualizing the effects of aminochitosan and distinguishing treatment-specific responses from the inherent changes occurring during the course of infection.

From **Table S4.3**, only 1 up- and 3 down-regulated protein are shared with other groups. The top 5 up-regulated proteins were two peroxidases (A0A3Q7E8T9 and A0A3Q7FFR5, logFC 4.10 and 3.34 increase, respectively), REF/SRPP-like protein (A0A3Q7GG77, logFC 4.09 increase), Snakin-2 (E5KBY0, logFC 3.57 increase), and an SCP domain-containing protein (A0A494GA45, logFC 3.39 increase). The top 5 down-regulated proteins were an acid phosphatase (A0A3Q7GVG1, logFC 5.75 decrease), CHD3-type chromatin-remodelling factor PICKLE (A0A3Q7IH67, logFC 525 decrease), GTP-binding protein OBGC2 (A0A3Q7GBL9, logFC 4.53 decrease), an uncharacterized protein (A0A3Q7F3X3, logFC 4.23 decrease) and a magnesium chelatase (A0A3Q7G0W, logFC 4.07 decrease).

The up-regulated proteins in the BP category were enriched for ‘hydrogen peroxide catabolic process’ (GO:0042744, 26 proteins) and ‘response to oxidative stress’ (GO:0006979, 25 proteins); the MF category was enriched for ‘chitinase activity’ (GO:0004568, 13 proteins), and ‘peroxidase activity’ (GO:0004601, 28 proteins); and the CC category was enriched for the

'endomembrane system' (GO:0012505, 7 proteins), 'extracellular region' (GO:0005576, 43 proteins) and 'membrane' (GO:0016020, 22 proteins). The down-regulated proteins in the BP category were enriched for 'chlorophyll biosynthetic process' (GO:0015995, 16 proteins); the MF category was enriched for 'rRNA binding' (GO:0019843, 28 proteins); and the CC category was enriched for 'ribosome' (GO:0005840, 43 proteins) (**Figure 4.13**).

4.4.5.2 The effects of aminochitosan at 9 hpi compared to 6 hpi: InfPol_InfPol

This comparison evaluates how the proteomic profile changes over time during *B. cinerea* infection with aminochitosan treatment. Proteins identified as differentially expressed between these two time points indicate temporal dynamics in the host response to *B. cinerea* in the presence of aminochitosan. It provides insights into how the treatment-induced proteomic changes are modulated during the course of infection.

The DEPs for the InfPol group at 9 hpi was compared to the InfPol group at 6 hpi. As such, the top 5 up-regulated proteins were a PMR5N domain-containing protein (A0A3Q7F572, logFC 5.75 increase), an SCP domain-containing protein (0A494GA45, logFC 5.69 increase), a mitochondrial phosphate transporter (A0A3Q7FQP4, logFC 5.65 increase), an ABC transporter B family member 25 (A0A3Q7FSS8, logFC 5.39 increase) and a 7-dehydrocholesterol reductase (A0A3Q7H0B6, logFC 5.23 increase). The top 5 down-regulated proteins were a GTP-binding protein OBGC2 (A0A3Q7GBL9, logFC 6.29 decrease), a non-symbiotic hemoglobin class 1 (Q9AWA9, logFC 6.25 decrease), CHD3-type chromatin-remodeling factor PICKLE (A0A3Q7IH67, logFC 5.29 decrease), an uncharacterized proteins (A0A3Q7IIQ1, logFC 4.41 decrease) and GUN4 domain-containing protein (A0A3Q7H247, logFC 4.19 decrease). From **Table S4.3**, only 2 down-regulated protein are shared with other groups.

The up- and down regulated KEGG pathways are shown in **Figure 4.14** where the up-regulated proteins at 9 hpi compared to 6 hpi in the BP category were notably enriched for 'defence response to fungus' (GO:0050832, 15 proteins), 'regulation of intracellular pH' (GO:0051453, 8 proteins), and proton transmembrane transport' (GO:1902600, 14 proteins); the MF category was enriched for 'ATPase-coupled transmembrane transporter activity' (GO:0042626, 24 proteins), and 'chlorophyll binding' (GO:0016168, 34 proteins); the CC category was enriched for 'extracellular space' (GO:0005615, 18 proteins), and 'Golgi apparatus' (GO:0005794, 27 proteins). The down-regulated regulated proteins at 9 hpi

compared to 6 hpi in the BP, MF and CC category were notably enriched for 'translation' (GO:0006412, 129 proteins), 'rRNA binding (GO:0019843, 43 proteins) and 'ribosome' (GO:0005840, 70 proteins) respectively.

4.5 Discussion

In Chapter 3, we deduced that foliar application of aminochitosan primed a significant resistant phenotype that was mediated through a combination of enhanced and sustained photosynthetic parameters namely, PSII activity (F_v/F_m) and ChlIdx (chlorophyll content), at 4 and 6 dpi. We suggested that sustaining photosynthesis for as long as possible was a key aspect of the plant's defence strategy. However, we observed that at 2.5 mg/mL, aminochitosan may be cytotoxic when sprayed directly onto leaves. As such, we observed that foliar anthocyanins were primed to avoid excess carbon and sugar accumulation that mitigated possible "sugar-induced leaf senescence" caused by enhanced photosynthetic activity after application of high concentrations of aminochitosan.

As stated in Martinez-Medina et al. (2016), the ideal method of assessing defence priming is through both phenotypic and molecular analysis of the state of a plant before and after challenge with the a/biotic stress. This would include 1) naïve, 2) primed, 2) naïve-and-triggered, and 4) primed-and-triggered plants (Martinez-Medina et al., 2016). In this chapter, we specifically focused on these 4 plant states and the application of 1 mg/mL of aminochitosan; a concentration with significant efficacy and little to no *in planta* phytotoxicity as previously observed in Chapter 3.

DEPs were identified by treatment, infection or time, and protein abundances compared using limma and eBayes for each pairwise group comparison considering that three biological replicates were to be used in the subsequent analyses. Due to the Limma uses a moderated t-statistic and an Empirical Bayes framework, enabling a powerful statistical analysis by borrowing information across proteins by using the full dataset to reduce the sample variances towards a pooled estimate. This improves sensitivity to detecting true biological differences, even when the number of replicates are limited (Schwämmle, León & Jensen, 2013; Kammers et al., 2015). This process yielded significantly more DEPs for aminochitosan treated samples, for both control and infected samples at 6hpi, 9 hpi and 9 hpi vs 6 hpi. Furthermore, the number of DEPs at 6 hpi were significantly greater than at 9 hpi. This

suggests that pretreatment with aminochitosan or/and *B. cinerea* infection induced significant changes to the proteome earlier after treatment with fewer significant changes occurring at 9 hpi.

This discussion will not be exhaustive and will instead highlight key observations for each time point, and the effects of this specific concentration of aminochitosan with and without the presence of *B. cinerea*. Moreover, some crossover between the sub-headings may occur due to the interconnectedness of the observations and pathways.

4.5.1 Differential priming of plant defence in mock inoculated leaves at 6 and 9 hpi

4.5.1.1 Proteins related to DNA and chromatin

In Chapter 3, direct D1 and D2 treatment in mock inoculated leaves displayed significant increases in the average F_v/F_m, ChlIdx and mAriIdx values at 1 mg/mL. Aminochitosan was also shown to accumulate in the cell membranes, due to permeabilization of the cell membrane.

We have stated previously that aminochitosan is a polycationic polymer that when distributed across or within cells, will bind to negatively-charged components, such as the negatively-charged phosphates of DNA/nuclear proteins/histones, or generally within its vicinity by virtue of this charge affinity resulting in relaxed chromatin structure and transcription (Isaac et al., 2009; Hadwiger & Tanaka, 2018). CHT-treated pea tissue was shown to generate an mRNA patterns similar to that of pea tissue treated with *Fusarium solani* f. sp. *Phaseoli*, indicating this affinity(Loschke, Hadwiger & Wagoner, 1983).

As stated in Hadwiger (2013, 2017), the potential number of signaling routes are unlimited as a result of the positive charges along the length of the polymer and negatively-charged molecules within a cell (Hadwiger, 2013; Hadwiger & Tanaka, 2017). Moreover, the plant plasma membrane and nuclear chromatin have been suggested as potential targets for CHT and is proposed to induce gene activity through interacting directly with DNA by i) inserting into the minor grooves of DNA or chromatin not bound by nuclear proteins, ii) by inducing the removal of histones H2A and H2B, iii) by single strand cleavage, and iv), by competing “with histones for sensitive DNA sites to allow stalled DNA polymerase complexes to continue to transcribe through the open reading frames of PR genes” (Strand et al., 2005; Ma et al., 2009;

Hadwiger, 2013; Hadwiger & Tanaka, 2017). For example, another study on pea endocarp tissue treated with CHT demonstrated DNA fragmentation within 2.5 h of CHT treatment, indicating that CHT indeed altered the DNA *in planta* (Hadwiger, 2015). Therefore, CHT treatment results in the reduction of the compact nucleosome structure by competing with histones (Hadwiger, 2015). Furthermore, the induction of PR genes is said to occur within nucleosomes, especially in non-host resistance (a lack of co-evolutionary association between the host and pathogen), to which aminochitosan treatment may be recognized as elicitors/effectors of pathogen origin and can activate DNA-specific signals (Jones & Dangl, 2006; Isaac et al., 2009). As discussed in Hadwiger & Tanaka (2017), this resistance model "with chromatin as a receptor offers flexibility to account for many of the multiple interactions between plants and their pathogens". They suggest that for their studies on peas, the "major receptors targeted by effectors/elicitors released by these fungi may lie directly within the DNA and proteins of pea chromatin" (Isaac et al., 2009; Hadwiger & Tanaka, 2018). Similar to how effectors can initiate signaling pathways to engage transcription factors and promote gene expression, DNA/chromatin-specific agents can enhance transcription through direct conformational changes which are otherwise typically silent, stalled, or partially suppressed. This suppressed state of DNA regions can be altered by various agents, including DNA intercalators and histone modifications, transitioning them to a transcriptionally active state. Among these agents are single-strand cleaving DNases, which are released by pathogens and transferred to the host nucleus during the nonhost resistance response in peas (Isaac et al., 2009; Ding & Wang, 2015).

The protruding histone tails, extending from the compact nucleosome core, undergo a variety of post-translational modifications that play crucial roles in the modulation of chromatin structure and gene expression by influencing nucleosome stability and positioning (Ding & Wang, 2015; Kang et al., 2022). In this chapter, the ConPol_ConWater group comparison at 6 hpi showed a significant up-regulation of proteins related to the GO terms 'nucleosome' and 'DNA binding' proteins (Q42877/*RPB2*, Q2MIB0/*rpoC2*, P25469/*HTA6*, A0A3Q7HFW0) that function in 'DNA binding', 'histone binding', 'chromatin organization' and the 'regulation of double-strand break repair'. Furthermore, 'protein ubiquitination' was also significantly up-regulated at 6 hpi for the ConPol_ConWater group comparison. A study by Isaac et al., (2009), found that when attempting to monitor the phosphorylation of nuclear proteins, including

histones H2A/H2B, the proteins were undergoing elimination from chromatin through ubiquitination, in addition to alterations in phosphorylation. This allowed for the removal of these nuclear proteins and enabled the movement of transcription machinery and the induction of signaling cascades through pathogenesis-related (PR) genes (Isaac et al., 2009; Hadwiger & Tanaka, 2017). PR genes and proteins are induced shortly after pathogen attack, concomitantly with the accumulation of phytohormones associated with plant defence and have been shown to increase host resistant to a wide spectrum of pathogens (Ali et al., 2018 and the references therein). Furthermore, modifications to chromatin have been suggested to result in PR gene activation of which CHT (1 mg/mL) has been shown to be an elicitor (Isaac et al., 2009).

The proteins significantly up-regulated and associated with 'protein ubiquitination' in this study were several 'cullin family profile domain-containing proteins, (A0A3Q7EZL6, A0A3Q7J197, A0A3Q7H324, A0A3Q7EFN8, A0A3Q7EGC2, A0A3Q7FGL5) whose functions are associated with the 'Cullin-RING ubiquitin ligase complex' and 'ubiquitin protein ligase binding' as well a 'TATA-binding protein interacting (TIP20) domain-containing protein' (A0A3Q7F9Q3) whose function is associated with 'SCF complex assembly' (A0A3Q7JMC9). Both the multi-subunit family of Cullin-RING Ligases and SKP1/Cullin1/F- box (SCF) play important roles in protein ubiquitination by acting as a scaffold and adaptor for the target protein, respectively. These proteins have also been suggested as predominant mediators of plant immune signaling in both rice and peas (Furniss & Spoel, 2015; Hadwiger & Tanaka, 2017). Thus, early regulation of the defence response in mock inoculated leaves may be regulated through DNA and chromatin binding and the removal of histones through ubiquitination at 6 hpi. Noteworthy, post-translational modification of H2B has been shown to play a pivotal role in non-host resistance. Through ubiquitination, H2B contributes to resistance against pathogens such as *B. cinerea* and *Alternaria brassicola* by modulating SA-mediated responses in *Arabidopsis* (Dhawan et al., 2009).

However, for ConPol at 9 hpi compared to ConPol at 6 hpi, the GO terms relating to 'nucleosome', 'regulation of DNA-templated transcription' and 'DNA binding' were significantly down-regulated. This suggests that the interaction between aminochitosan with chromatin/DNA is tightly regulated in a relatively short timeframe. Isaac et al. (2009) explored the non-host disease resistance response in peas by investigating both host and non-host

pathogens response to 1 mg/mL of chitosan and as mentioned earlier highlighted noteworthy changes in the phosphorylation patterns of nuclear proteins, including histones H2A/H2B, thus emphasizing the crucial role of ubiquitination in the removal of these proteins from chromatin during the non-host disease resistance mechanism in peas. As stated in Isaac et al. (2009), the normal recycling of cellular proteins eventually leads to a decline in these proteins, disrupting regular nucleosome organization. However, the study also notes that infection with non-host pathogens accelerates this process, causing a deficit in histone proteins within a shorter period of 6 h. This accelerated depletion contributes to a faster immune response against non-host pathogens, leading to a more rapid termination of their growth. In contrast, the immune response to host pathogens, despite a slower initiation, allows for more extensive penetration and generates a total tissue PR gene response with elevated phytoalexin accumulation (Isaac et al., 2009).

Therefore, the disparity in the temporal and negative regulation of the DNA/chromatin/ubiquitination response at 9 hpi may be attributed to a similar occurrence as seen with the non-host pathogen in peas where the modifications to chromatin/DNA by aminochitosan (e.g., ubiquitination) mimics the gene activating actions of a non-host pathogenic fungus. However, a key difference in this activation is that aminochitosan results in a more intense induction in the early hours of infection than infection with *B. cinerea*, thus resulting in an early cessation due to the depletion of histones and nucleosomes generally necessary for normal/baseline functionality.

Similar to the aforementioned studies, PR proteins relating to the GO term ‘defence response (GO:0006952)’ were significantly up-regulated for the ConPol_ConWater group comparison at 6 hpi. The significantly up-regulated PR proteins were PR4 (Q04108), PR5 (A0A3Q7HTH3), PR1a2 (A0A3Q7HXW1) and Bet v1 domain containing proteins (A0A3Q7FGW4, A0A3Q7FV86, A0A3Q7FYR5) which are associated with PR10. The “global changes in chromatin” are posited as a more comprehensive explanation for triggering the diverse transcription of PR genes compared to modifications in specific transcription factors targeting individual PR gene promoters (Isaac et al., 2009 and the references therein).

4.5.1.2 Proteins related to cell wall and membrane modifications

The plant cell wall structure is complex and is composed of various proteins and polysaccharides including cellulose, lignin, hemicellulose and pectin, whose composition ratios change as needed during growth and development for dynamic support (Ziv et al., 2018). They also serve as a control point for the exchange of molecules and the relay of signals and signaling molecules, as well as primary chemical and physical barriers to biotic and abiotic stresses (Ziv et al., 2018). As such, plants are capable of sensing pathogens and cell wall integrity upon which the cell wall undergoes dynamic changes during plant-pathogen interactions, when necessary, to prevent pathogen invasion and disease (Bellincampi, Cervone & Lionetti, 2014). Studies have shown that CHT adheres to the plant cell wall and interacts with the plant cell membrane to exert its biological activity (Xing et al., 2015). This is due to its polycationic properties as CHT is likely to interact readily with negatively-charged residues exposed on the cell surface, leading to significant alterations in membrane composition (El-Ghaouth et al., 1992).

One mechanism regulating the membrane composition is that of pectin methylesterases (PMEs). They catalyze the demethyesterification of pectin in the plant cell wall and are regulated by PME inhibitors (PMEIs, invertase inhibitors). PMEIs function by inhibiting PMEs, resulting in an elevated degree of methylesterification in pectin. This increase in methylesterification enhances resistance to invading pathogens such as *B. cinerea* (Lionetti et al., 2007). PMEIs have also inhibited invading pathogens that secrete pectinases (cell wall hydrolases) as a means of aiding their entry into plants during the early stages of infection (Marzin et al., 2016; Liu et al., 2018; Gu et al., 2021). The overexpression of PMEIs in *Arabidopsis* results in lower levels of PME activity, higher degrees of pectin esterification and an overall reduced susceptibility to *B. cinerea* and *Pectobacterium carotovorum* (Lionetti et al., 2007). Similarly, a study on strawberries infected with *R. mucilaginosa* cultured in a medium amended with 0.5% (w/v) CHT (90% DDA) observed enhanced resistance to pectinase activity with the concomitant increase in the expression of a pectinesterase inhibitor (Gu et al., 2021).

In this study, the GO terms relating to ‘pectinesterase inhibitor activity’ and the proteins P14280 (PME1.9), P09607 (PME2.1), Q96575(PME2.2), Q96576 (PME3) were significantly up-

regulated for ConPol_ConWater at 6 hpi. When considering the aforementioned studies, it appears that aminochitosan primes plant defence by significantly increasing PMEIs (as seen by the above up-regulated proteins) which act to reduce PME activity. This contributes to elevated esterification of plant cell walls, thus increasing the cell wall integrity and reducing the probability of being degraded by pectinases released by invading pathogens. Alternatively, partial degradation of cell walls prior to PMEI activity may act as DAMPs and subsequently, elicitors of plant defence (Marzin et al., 2016). One such example is that, the majority of plant-derived methanol is a product of PME activity and serve as DAMPs, a signaling mechanism for plant resistance during cell wall damage or other stresses, as well as priming agents for increased plant immunity in neighbouring uninfected leaves or plants (Dorokhov, Sheshukova & Komarova, 2018; Hou et al., 2019).

However, proteins that were related 'cell wall macromolecule catabolic process' and the GO terms 'defence response, GO:0050832', 'chitinase activity', 'chitin catabolic activity' were significantly down-regulated for the group comparison of ConPol_ConWater at 6 hpi and included CHI3 (Q05539), CHI14 (Q05537), K4D1G8, K4D1M8, A0A3Q7IIY2, and A0A3Q7JDH4). At 9 hpi, the proteins related to the GO term, 'chitinase activity', were still significantly down-regulated. Chitinases, enzymes that break down chitin and related compounds, are essential components of plants' defence systems against fungal pathogens. They are strongly induced in response to pathogen stress and play different roles. Apoplastic chitinases directly inhibit hyphal growth while cellular chitinases are released upon hyphal penetration, affecting cell integrity and possibly triggering downstream defence pathways by releasing fungal elicitors (Ding & Wang, 2015). The aforementioned results are in contrast to a study by Samarah et al., (2020) where seed treatment of bell peppers with CHT (0.01, 0.05, 0.1, 0.3, and 0.5 %) resulted in the increase of chitinase activity in both seeds and seedlings compared to untreated seeds (Samarah et al., 2020). Another study by Roby, Gadelle & Toppan, (1987) also demonstrated increased local and systemic chitinase activity within 6 h of CHT treatment in melon plants that were maximal between 12-24 h (Roby, Gadelle & Toppan, 1987). In this study, both CHI3 and CHI14 exhibit glycoside hydrolase activity as endochitinases, effectively breaking down cell wall polysaccharides such as chitin and CHT, cellulose, pectin, and other proteins. Their function involves catalyzing the hydrolysis of β-1,4-glycoside bonds within these compounds. (Minic & Jouanin, 2006; Grover, 2012). As such, the down-regulation of these proteins

indicates reduced cell wall biodegradability and therefore, a cell wall primed for pathogen attack. This in combination with the increase in the PMEI activity suggests that aminochitosan in uninfected leaves acts to increase the integrity of the cell wall, the physical barrier on the frontline of defence.

4.5.1.3 Proteins related to defence response

Terpenoids are secondary metabolites derived from isoprenoids (5 carbon molecules) and may exist as volatile or non-volatile antimicrobial compounds. Terpenoid phytoalexins are defined as “low molecular weight, antimicrobial compounds that are both synthesized and accumulated in plants after exposure to micro-organisms or abiotic agents” (VanEtten et al., 1994). The pathways that synthesize these terpenoids occur in distinct cellular compartments and are the mevalonate (MVA) pathway in the cytoplasm and the 2-C-methyl-D-erythritol 4-phosphate (MEP) pathway in plastids. The products of these pathways include quinones and sterols and the isoprenoid based phytohormones cytokinin, gibberellins, brassinosteroids, strigolactones, and abscisic acid (Block et al., 2018).

We found that proteins related to the GO term ‘defence response, GO:0006952’ and KEGG term ‘terpenoid backbone biosynthesis’ were significantly up-regulated at 6 hpi in ConPol_ConWater. In this study, the up-regulated terpenoid proteins (Q8GZR6, A0A3Q7FSD7, A0A3Q7IB68, O65004, and A0A3Q7FSH7) are associated with the MEP sub-pathways, including monoterpenoid, diterpenoid, carotenoid, indole diterpene alkaloid, and ubiquinone/quinone. Aminochitosan may therefore prime terpenoid-related compounds with antimicrobial and defence related properties, despite not actually being exposed to a pathogen. One plausible explanation is that the leaves initially recognize aminochitosan as a biotic stress given that chitin is found in the cell walls of several fungal species (Terkula Iber et al., 2022).

As mentioned in 4.5.1.1, the GO term ‘defence response’ was significantly up-regulated for the ConPol_ConWater group comparison at 6 hpi and included ‘thaumatin-like’ (A0A3Q7JWY0, A0A3Q7HVV2) and ‘osmotin-like’ (A0A3Q7HVV0, Q41350, Q01591) proteins in addition to the PR proteins (PR1a2 and PR4). Both osmotin- and thaumatin-like proteins belong to the PR5 family which have been shown to be SA-dependent and a contributor to disease resistance in wheat and tobacco overexpressing lines in response to broad range of

pathogens (Liu et al., 2012; Zhang et al., 2017; Ali et al., 2018; Hakim et al., 2018). Additionally, osmotin has exhibited antifungal properties by inhibiting spore germination, hyphal growth, spore lysis and spore viability by increasing the cell wall permeability of pathogens (Chowdhury, Basu & Kundu, 2015; Hakim et al., 2018). In contrast to the above, PR4 however has been shown to be associated with the JA pathway (Ali et al., 2017, 2018). A study by Jia et al., (2018) has however demonstrated that both JA and SA pathways are effective, required and up-regulated for resistance in the *Arabidopsis*/*P. syringae* pathosystem pretreated with CHT oligosaccharides (Jia et al., 2018). As highlighted in Ramirez-Prado et al. (2018), the interplay among hormonal pathways, particularly JA/ET and SA, is influenced by the levels and signalling of additional hormones such as gibberellins, auxin, cytokinins, and brassinosteroids. This intricate balance leads to situations where the antagonism between SA and JA/ET is not absolute, enabling a precise and pathogen-specific adjustment of responses.

Other defence related proteins related to the GO term 'defence response, GO:0050832', different to the aforementioned 'defence response, GO:0006952', were significantly down-regulated for ConPol_ConWater at 6 hpi. These proteins included 'chitinases' as mentioned in Section 4.5.1.2 as well as PR2 and an allene-oxide cyclase (Q9LEG5/aoc). PR2 is a β-1,3-glucanase and catalyzes the cleavage of β-1,3-glucosidic bonds in β-1,3-glucans (cellulose) (Jain & Khurana, 2018). Therefore, the down-regulation of PR2 at 6 hpi corresponds with the regulation of PMEIs at 6 hpi towards the reinforcement of the cell wall integrity in the ConPol group. Allene oxide cyclase (EC 5.3.99.6) catalyzes the precursor of JA and has been shown to be induced after wounding of tomato leaves with a concomitant increase in JA levels (Ziegler et al., 2000). Therefore, the significant down-regulation of *aoc* in this study for ConPol may indicate that certain elements of the JA pathway are down-regulated at 6 hpi while others are up-regulated (PR4 and thaumatin-like proteins), like the aforementioned study by Jia et al., (2018).

4.5.1.4 Proteins related to photosynthesis and carbon metabolism

The decline of photosynthesis after pathogen and insect attack is well researched and evidenced in several reviews including that of Bilgin et al. (2010) and the references therein. As stated therein, "Strong convergence in the response of transcription suggests that the universal downregulation of photosynthesis-related gene expression is an adaptive response

to biotic attack." They hypothesize that "slow turnover of many photosynthetic proteins allows plants to invest resources in immediate defence needs without debilitating near term losses in photosynthetic capacity" (Bilgin et al., 2010). However, studies demonstrating the compensatory stimulations of photosynthesis have been published (Bilgin et al., 2010).

Proteins related to the GO terms, 'respiratory chain,' 'chloroplast thylakoid membrane,' and 'carbohydrate metabolic process' as well as the KEGG terms, 'Photosynthesis - antenna proteins,' 'Photosynthesis,' 'Carbon fixation in photosynthetic organisms' and 'Carbon metabolism' were significantly down-regulated in the ConPol_ConWater group comparison at 6 hpi. Some of the down-regulated proteins involved in the above terms were 'Chlorophyll a-b binding' proteins, P12360 (CAB6A), P27489 (CAB13), P14279 (CAB5); 'Oxygen-evolving enhancer' proteins P29795 (PSBP) and P23322 (PSBO); 'Photosystem II reaction center protein H', Q2MI72 (psbH); 'Cytochrome b6', Q2MI71 (petB); ''Photosystem I iron-sulfur center', Q2MI49 (psaC); Catalase isozyme 1', P30264 (CAT1); and 'Ferredoxin', A0A3Q7IIT3. With the down-regulation of photosynthesis, a corresponding reallocation of resources and reorientation of metabolism towards the mounting of defence repones is expected (Bilgin et al., 2010) and was demonstrated in Sections 4.5.1.1 – 4.5.1.3.

In an analogous manner to the published consensus of Bilgin et al., (2010), it appears that at 6 hpi, tomato pre-emptively down-regulates photosynthesis and carbon metabolism as an adaptive response to aminochitosan treatment while up-regulating defence systems. This suggests that in the early hours of treatment, aminochitosan is perceived as a biotic stress and resources are allocated to defence instead of growth as photosynthesis represents a hidden cost (Bilgin et al., 2010). However, at 9 hpi, the GO terms 'protochlorophyllide reductase activity', 'chlorophyll biosynthetic process' and 'chloroplast' were significantly up-regulated for the ConPol_ConWater group comparison, suggesting a stimulatory effect of aminochitosan at later time points when the polymer is no longer recognized as a threat or biotic stress.

When comparing ConPol at 9 hpi to ConPol at 6 hpi, the GO terms 'glutamate decarboxylase activity' and 'glutamate catabolic process' as well as the KEGG term 'Alanine, aspartate and glutamate metabolism' were significantly up-regulated. Glutamate metabolism plays a role in nitrogen transportation, cellular redox regulation, and tricarboxylic acid cycle-dependent energy reprogramming (Seifi et al., 2013). Glutamate decarboxylase (GAD) catalyzes the

conversion of glutamate to gamma-aminobutyric acid (GABA) which is an enzyme in plants involved in stress responses (redox buffer or signaling molecule), nitrogen storage, and in the regulation of carbon and nitrogen (C/N) metabolism via the GABA shunt (Seifi et al., 2013). The GABA shunt controls the ratio of C:N in order to replenish the tricarboxylic acid (TCA) cycle with carbon through source/sink remobilization (Fagard et al., 2014). This process would allow for excess carbon to be recycled in the ConPol leaves at 9 hpi, given the increase in photosynthesis as mentioned above. Alternatively, as suggested in Janse van Rensburg, Limami & Van den Ende (2021), GABA may be produced directly from the foliar application of aminochitosan or polyamines through intracellular oxidation, resulting in positve feedback loop that promotes endogenous GABA production through the up-regulation of GAD (Janse van Rensburg, Limami & Van den Ende, 2021). The increase in GABA may therefore also serve as a preemptive scavenger for reactive oxygen species; reducing the likelihood of oxidative stress at later time points, as seen in Chapter 3, by the low to absent levels of H_2O_2. Furthermore, glutamate metabolism during pathogen interactions is regulated in a manner that results in a metabolic state known as ‘endurance’ where cell viability is preserved, or an opposing state called "evasion," which facilitates cell death is avoided. Regulations associated with endurance confers resistance to necrotrophic pathogens but increase susceptibility to biotrophs. On the other hand, alterations linked to evasion provide resistance to biotrophic pathogens but enhance susceptibility to necrotrophs (Seifi et al., 2013). Overall, variations in host glutamate metabolism in response to different pathogenic scenarios play dual roles: supporting the ongoing defence strategy to establish an effective resistance response or being exploited by the pathogen to promote and facilitate infection (Seifi et al., 2013). Thus, aminochitosan in untreated tomato leaves may be regulating the glutamate metabolism in favour of an ‘endurance’ metabolic state.

4.5.1.5 Proteins related to ROS homeostasis

H_2O_2 and other ROS serve as critical regulators of programmed cell death (PCD), growth, development, and stress adaptation. Oxidative stress arises from the imbalance between ROS production and the cell's antioxidant defence mechanisms, with key antioxidants like catalase (CAT) playing crucial roles in mitigating oxidative damage (Tran & Jung, 2020). Pathogen perception typically leads to transient increases in ROS production, which function as secondary messengers and may induce hypersensitive response (HR) in infected tissues. The

specificity of ROS signals depends on factors such as their localization, chemical identity, and abundance, with interactions between organelle-derived ROS and defence gene expression being complex and pathogen-dependent. Peroxisomes, particularly, are significant sources of oxidative signals and are implicated in biotic interactions, and can interact with NADPH oxidases to induce SA-mediated defence and resistance (Kangasjarvi et al., 2012). Despite generally facilitating necrotrophic colonization, the timely induction of H_2O_2-dependent defences in the epidermal cell wall have been shown to effectively impede the development of *B. cinerea* (Asselbergh et al., 2007).

Increasing focus has been given to exploring the antioxidant properties of CHT. Sun et al. (2008) evaluated the antioxidant capacities of N-carboxymethyl chitosan oligosaccharides with different degrees of substitution (NA: 0.28, NB: 0.41, and NC: 0.54), finding that antioxidant activity increased with higher substitution levels but was still dependent on the charge properties of substituting groups. Another study reported that CHT oligomers (DDA 92.7%) of lower MW (2.3-6.12 kDa) displayed superior antioxidant activity against hydroxyl radicals and superoxide anions compared to the oligomer with the highest MW (15.25 kDa) (Sun et al., 2007). The molecular mechanisms underlying CHT's scavenging capacity are not fully elucidated, but it is proposed that the amino groups react with free radicals to form stable radicals (Liaqat & Eltem, 2018). Moreover, the antioxidant capacity is influenced by the DDA and MW, exhibiting increased activity at lower MW (Liaqat & Eltem, 2018).

In this study, at 6 hpi, the GO terms associated with oxidative stress namely, ‘hydrogen peroxide catabolic process’, ‘glutathione metabolic process’, ‘NADP binding’ and ‘peroxidase activity’ were down-regulated for the ConPol_ConWater group comparison. This implies that within the initial 6 hpi, aminochitosan treatment may initiate the defence response independently of ROS accumulation (as demonstrated at later time points in Chapter 3) and/or aminochitosan itself may function as an antioxidant. Considering diamino 3’s degree of substitution of 0.63 and its heightened positive charge, it is conceivable that it exhibits robust antioxidant properties similar to those demonstrated by Sun et al. (2008). However, when comparing the regulation of proteins for ConPol at 9 hpi to ConPol at 6 hpi, the GO terms ‘catalase activity’ and ‘serine-type endopeptidase’ and ‘catechol activity’ were up-, up- and down-regulated, respectively. Catalase, primarily located in peroxisomes but also present in mitochondria and the cytoplasm, serves as a key scavenger of H_2O_2 generated during

photorespiration, mitochondrial electron transport, and the oxidation of fatty acids, respectively. (Sharma & Ahmad, 2014). In photorespiration, it is responsible for scavenging H_2O_2, the byproduct of glycolate oxidation, in an attempt at preventing carbon loss in plants by recycling carbon (Kangasjarvi et al., 2012). Additionally, the changes in redox-cycling linked to photorespiration may alter the rate of ROS production in the mitochondrion and chloroplast through altered NAD(P) redox states. Therefore, the up-regulation of catalase may be as a result of the enhanced photosynthesis at 9 hpi (also in Section 4.5.1.4 and Chapter 3) and may serve as sink/means for dissipating the excess energy, preventing any damage to photosynthetic machinery. Alternatively, changes to the C/N ratio and metabolism results in oxidative stress in the peroxisomes (Willekens, 1997). Numerous studies have demonstrated that the down-regulation of catalase contributes to the general increase in ROS and the activation of the SA-related defence cascade, including PCD, that is induced during biotrophic interactions (Kangasjärvi et al., 2012 and the references therein). Although *B. cinerea* has been defined quite clearly as a necrotrophic pathogen in tomato, the lifestyle in the early stages of disease establishment remains unclear; whether it includes the suppression of autophagy and a brief 'biotrophic' or rather, a non-destructive phase before the transition to necrotrophy, or whether an immediate induction of regulated cell death is induced (Bi et al., 2022). In this chapter, we assessed the early non-destructive stages of infection before the phase of necrotrophy where according to the chlorophyll fluorescence and phenotyping data, aminochitosan delays or prevents both senescence and necrosis.

Furthermore, the down-regulation of 'catechol oxidase activity' and the proteins 'polyphenol oxidase F, and E, chloroplastic' and 'catechol oxidase' were observed for ConPol at 9 hpi compared to ConPol at 6 hpi. Polyphenol oxidases (PPOs) are enzymes located in both chloroplasts and mitochondria that catalyzes the oxidation of phenolics to quinones, which through redox cycling, may result in the production of ROS (Mayer, 2006). Therefore, the down-regulation of PPO E and F after aminochitosan treatment may be used as a means of maintaining lower levels of ROS by reducing the pathways that result in ROS production. In the study conducted by Thipyapong et al. (2004), the impact of varied PPO expression levels on tomato plants under drought stress was investigated. Transgenic plants with suppressed PPO exhibited improved drought tolerance, as evidenced by higher F_v/F_m values and total chlorophyll content. This contrasted with the responses observed in both overexpressing and

non-transformed plants within the experimental conditions (Thipyapong et al., 2004). The transgenic plants with suppressed PPO also displayed greater photosynthesis which they suggested as a reason for the lower rate of ROS production. A comparison can be drawn between this study and our study on aminochitosan treatment specifically with the relevance of Chapter 3 where photosynthetic parameters such as F_v/F_m and chlorophyll content were elevated along with an absence of H_2O_2 accumulation. Additionally, despite Thipyapong et al.'s (2004) focus on abiotic stress, other similarities emerge with the significant reduction in PPO activity noted in this chapter.

Finally, the significant up-regulation of 'serine-type endopeptidase activity' and its proteins namely the 'Subtilisin-like protease' (A0A3Q7F322, A0A3Q7F302 and A0A3Q7HKM1) for ConPol at 9 hpi compared to ConPol at 6 hpi was observed. Subtilisin-like proteases (SBTs) are extracellular plant serine proteases which have been shown to be induced by both exogenous SA treatment and biotic stress in tomato (Hou et al., 2019 and the references therein). Similarly, a study by van Aubel et al. (2016) demonstrated through leaf proteomic and RT-qPCR analysis that COS-OGA, an elicitor comprising cationic chitosan oligomers (COS) and anionic pectin oligomers (OGA), protected tomato against *Leveillula taurica* (powdery mildew). They showed significant accumulation of subtilisin-like proteases in addition to PR proteins and genes associated with SA-related genes, while genes linked to JA/ET exhibited no significant expression. They suggested that the induction of subtilisin following COS-OGA indicates a SA-dependent MoA and are also likely to involve epigenetic control given the increase in other related proteins including DNA/RNA remodeling enzymes. Furthermore, subtilisin-like proteases are frequently associated with SA, and chitinases (PR3 or CHI3 and CHI9) to JA as according to Wu & Bradford (2003), the expression of CHI9 and PR2a in leaves is significantly increased with ET and methyl jasmonate but not with SA treatment (Wu & Bradford, 2003; Ahmad, Shafique & Shafique, 2014; van Aubel et al., 2016). Lastly, the *Arabidopsis* subtilisin orthologue, SBT3.3, is associated with priming and induced resistance through a rapid response to H_2O_2, without an HR response or high accumulation (Ramírez et al., 2013). Similarly in Chapter 3 of this dissertation, little to no H_2O_2 or HR response was visible with 1 mg/mL of aminochitosan treatment. Given the modulation of DNA/chromatin in Section 4.5.1.1 and the above subtilisin activity combined with the lack of H_2O_2 accumulation, it

appears that the biological activity of aminochitosan is potentially mediated through SA pathways at 6 hpi.

4.5.2 Differential priming of plant defence in *B. cinerea* inoculated leaves at 6 and 9 hpi

4.5.2.1 Proteins related to RNA, DNA, and chromatin

As discussed in length by Kang et al., (2022) and Ding & Wang (2015), several studies have demonstrated the significant involvement of chromatin regulation in the activation of defence-related genes for rapid and suitable physiological immune reaction (Ding & Wang, 2015; Kang et al., 2022).

The GO terms 'DNA binding', 'protein heterodimerization', and 'methylation' were significantly down-regulated in the 'nucleosome', for the group comparisons of InfPol to ConPol at 6 hpi, and 'methylation' for the group comparison of InfPol to InfWater at 6 hpi. The proteins associated with these GO terms were 'methyl-CpG-binding domain-containing protein 11 (A0A3Q7GWR6)', 'BED-type domain-containing protein (A0A3Q7J3N8)' and several 'S-adenosylmethionine-dependent methyltransferase (A0A3Q7FF29)' proteins which were collectively associated with the histones, H2A.1, H2B and H3. In various contexts, histone methylation can serve as either an activator or inhibitor of transcription, depending on the specific targets involved (Ramirez-Prado et al., 2018).

Methyl-CpG-binding domain-containing (MBD) proteins have been suggested as the proteins responsible for CpG methylation-induced formation of compact chromatin as they recognize methylated CpG sites and recruit chromatin-modifying enzymes to regulate the chromatin structure. The *Arabidopsis* model is proposed to be induced by AtMBD7 which is methylated by a histone arginine methyltransferase at relevant arginine sites, thereby increasing AtMBD7 affinity for methylated CpG sites. Subsequently, transcriptional co-repressor and/or histone deacetylases that induce/maintain compact chromatin are sequestered (Grafi, Zemach & Pitto, 2007). Therefore, in this study for aminochitosan pretreated and infected leaves, S-adenosylmethionine transferase (SAMT) may play a crucial role in histone methylation as SAMT activity is downregulated along with MBD proteins and the subsequent recruitment of histone modifying enzymes. The alterations thereafter in histone methylation patterns could

allow for a more open chromatin configuration and increased accessibility for an increase in gene expression. Furthermore, the downregulation of H2B in *N. benthamiana* infected with potato virus has been shown to reduce the time and titer of infection as well as induce the accumulation of SA (Yang et al., 2019).

Lastly, as highlighted earlier, a BED-type domain-containing protein was significantly down-regulated for InfPol to ConPol and InfPol to InfWater at 6 hpi. Methyl-CpG-binding domain-containing (Zuluaga et al. 2020 and the references therein). Zuluaga et al., (2020) demonstrated that transiently overexpressed Zn-finger BED domains in *N. benthamiana* was capable of inducing ROS and a cell death phenotype after 4-5 days (Zuluaga et al., 2020). Therefore, the down-regulation of the BED-type domain-containing protein may be another attempt at evading excessive ROS accumulation.

4.5.2.1 Proteins related to protein homeostasis

Proteins related to ribosomal structure, translation, protein turn-over, post-translational modification and biogenesis pathways were found to be differentially regulated. For the group comparison of InfPol compared to ConPol at 6 hpi, the GO terms ‘rRNA binding’, ‘ribosome’, ‘translation’ and ‘structural constituent of ribosome’ were significantly up-regulated and ‘intracellular protein transport’ were significantly down-regulated. Similarly, the GO terms relating to ‘rRNA binding’, ‘small ribosomal subunit’, ‘ribosome‘, ‘cytosolic large ribosomal subunit’, ‘structural constituent of ribosome’, ‘translation’, ‘cytoplasmic translation’, ‘cytosolic small ribosomal subunit’ were significantly up-regulated for the InfPol compared to ConWater at 6 hpi group comparisons. However, at 9 hpi for InfPol compared to ConPol, the GO terms that were significantly up-regulated were now significantly down-regulated and also included ‘ribosomal small subunit assembly’ and ‘translation‘ with ‘vacuole’ and proteins associated with vacuole protein processing being significantly up-regulated. At 6 hpi for InfPol, it appears that protein biogenesis is favoured over transport with transport being more important at 9 hpi, specifically in the vacuole. This is furthered by the group comparison for InfPol at 9 hpi compared to 6 hpi, where the GO terms ‘protein autophosphorylation’, and ‘Golgi apparatus’ were significantly up-regulated and ‘endopeptidase Clp complex’ significantly down-regulated. Here, proteins related to transport and modifications were up-regulated and proteins related to protein turnover, down-regulated. Self-compartmentalizing proteases like

ATP-dependent Clp proteases and proteasomes play a crucial role in degrading misfolded or damaged proteins. Under various stress conditions, the levels of misfolded proteins degraded rise, enabling cells to maintain feedback regulations in response to cellular signals and adapt to changing environmental conditions (Ali & Baek, 2020). Comparatively, for the group comparison of InfPol to InfWater at 6 hpi, the terms relating to 'translation', 'ribosome', 'structural constituent of ribosome' and 'rRNA binding' were significantly up regulated. This was sustained at 9 hpi as these GO terms, and the associated proteins were down-regulated for InfWater at 9 hpi compared to InfWater 6 hpi.

Given that a broad activation of defence has been suggested in Section 4.5.1, it is to be expected that the priming of the defence response by pretreatment with aminochitosan requires an enhancement of proteins related to protein homeostasis which include biosynthesis, translation, modification, degradation, and transport. Similarly seen in Jia et al., (2020), 68 proteins related to protein homeostasis were differently expressed in *Arabidopsis* pretreated with COS and/or Pst DC3000 infection. They suggested that this significant regulation of proteins related to protein homeostasis with COS and/or Pst DC3000 infection are capable of reprogramming protein homeostasis processes which may contribute to an enhanced defence response and increased survival during infection (Jia et al., 2020). Therefore, it stands to reason that a similar observation may be true for aminochitosan as the up-regulation of proteins related to 'translation' and general protein homeostasis indicates that translation processes were primed by aminochitosan treatment in the priming interval before the infection and up to 6 hpi, unlike in the InfWater treatment where proteins and GO terms associated with protein homeostasis were significantly down-regulated at both 6 and 9 hpi.

4.5.2.2 Proteins related to cell wall and membrane modifications

In response to pathogen attack or elicitors, one of the earliest responses involves changes in membrane permeability and activation of ion channels, allowing the influx of $Ca2^{+}$ and H^{+} and the efflux of K^{+}. This triggers rapid shifts in transmembrane potential, often causing membrane depolarization. Following this, plants undergo an oxidative burst, produce phytoalexins, and activate defence genes (Rossard et al., 2006 and the references therein). The down-regulation of the GO terms 'membrane', 'regulation of intracellular pH', 'proton transmembrane

transport' and 'ATPase-coupled transmembrane transporter activity' and the proteins 'Cation-transporting P-type ATPase N-terminal domain-containing protein', 'P-type H(+)-exporting transporter' and 'Plasma membrane ATPase ('LHA1' and 'LHA2') were observed for InfPol_ConWater at 6 hpi, InfPol_ConPol at 6 hpi, and InfPol_InfWater at 6 hpi.

Stomatal closure represents one of the earliest reactions initiated upon the identification of pathogens or elicitor molecules and can be observed even within minutes (Czékus et al., 2021). Plant H^+-ATPases are the primary proton pumps in the plant plasma membrane and are responsible for establishing a membrane potential. They do this by pumping protons from the cytosol to the extracellular space (extracellular acidification and intracellular alkalinization), resulting in a H^+ potential gradient that facilitates ion/solute exchange across the membrane. As H^+-ATPases are not significantly altered at the transcript level in response to biotic/abiotic stresses, their change in activity is suggested to be under post-translational control (Elmore & Coaker, 2011). The down-regulation of plasma membrane H^+-ATPase activity during PTI has been shown to be necessary for certain immune responses. Keinath et al. (2010) demonstrated that *Arabidopsis* with a mutation in the plasma membrane H^+-ATPase, AHA1, treated with flg22 resulted in a reduction of ROS, consistent with the notion that H^+-ATPases function in early immune signaling (Keinath et al., 2010). Furthermore, the inhibition of H^+-ATPases have been shown to be important for ABA-mediated stomatal closure in plant-pathogen interactions (Merlot et al., 2007). Therefore, the reduced H^+-ATPase activity contributes to the hypothesis that aminochitosan primes a defence response predominantly in a ROS-independent manner that is sustained up to 72 hpi and that other defence response systems are key contributors to the priming and resistance phenotype observed in Chapter 3. Moreover, this phenomenon can be interpreted as priming, given its substantial down-regulation in comparison to both ConPol and InfWater. This suggests that following the second trigger (*B. cinerea*), a more pronounced and rapid down-regulation occurred. This hypothesis was partially validated by Gonugunta, Srivastava & Raghavendra, (2009) who showed that cytosolic alkalinization is a common and early component of stomatal closure that is induced by ABA, methyl jasmonate and CHT (5 µg/mL). This was also shown to precede the production of the signaling molecules ROS and nitric oxide during induced stomatal closure but was followed by the positive regulation of the secondary messenger, Ca^{2+} (Gonugunta, Srivastava & Raghavendra, 2009).

However, for InfPol at 9hpi compared to InfPol at 6 hpi, 'membrane', 'regulation of intracellular pH', 'proton transmembrane transport' 'extracellular region' and 'ATPase-coupled transmembrane transporter activity' were significantly up-regulated. The proteins related to these terms included PR2 (P32045), PR4 (Q04108), PR-5x (Q8LPU1), PR23 (P12670), and CHI14 (Q05537). As seen with aminochitosan treatment, Schaller & Oecking (1999) reported that the up-regulation of H^+-ATPase was coupled with the activation of pathogen defence signaling pathways with the accumulation of SA and PR gene expression in tomato plants. Conversely, the accumulation of defence proteins (defined here as "proteases, inhibitors of serine, cysteine, and aspartic proteases, and components of the wound signaling pathway") was coupled with the inhibition of H^+-ATPase activity. Therefore, it was suggested that the regulation of plasma membrane H^+-ATPase activity serves as a switch between elicitor recognition/response to wounding and pathogen defence signaling pathways (Schaller & Oecking, 1999). This observation was also noted by Amborabe et al., (2008) who deduced that early in the interaction between CHT and *Mimosa pudica* motor cell, CHT directly induced membrane depolarization (much like other fungal elicitors) by inhibition of H^+-ATPase and subsequent influx of H^+. They concluded that CHT curative treatments requires careful consideration due to its potential to increase cell permeability, which could facilitate fungal entry and infection. However, for elicitation purposes (preventative treatment), this concern regarding cell permeability and fungal entry was not applicable (Amborabe et al., 2008). Other studies in *Arabidopsis*, *Commelina communis* and *Pisum sativum* have demonstrated that CHT, by SHAM-sensitive peroxidases, ABA and methyl jasmonate, induced ROS and nitric oxide production in guard cells, resulting in stomatal closure (Khokon et al., 2010).

Furthering the H^+-ATPase hypothesis, the GO terms 'chitinase activity' and 'chitin catabolic activity' were significantly down-regulated for the group comparisons for InfPol_ConWater and InfPol_InfWater at 6 hpi and included the proteins PR2 (P32045), PR4 (Q04108), PR-5x (Q8LPU1) and CHI3 (Q05539), CHI17 (Q05540), CHI14 (Q05537). This observation is congruent with the aforementioned theory where the down-regulation of H^+-ATPase activity is related to the reduction in PR activity and given that chitinases are a class of PR proteins, it stands to reason that these two observations are related. Interestingly, throughout all of the group comparisons in both infected and control leaves, 'chitinase activity' has consistently been down-regulated for all aminochitosan treatments except for InfPol_ConPol at 9 hpi and

InfWater at 9 hpi compared to InfWater at 6 hpi where it was significantly up-regulated. It can be argued that 'chitinase activity' is not a defence mechanism commonly induced by aminochitosan early in the defence response to *B. cinerea*. Moreover, between 6 and 9 hpi, the defence response appears to switch from 'elicitor recognition and response to wounding' and 'defence signaling pathways' (Schaller & Oecking, 1999; Amborabe et al., 2008).

As stated by Amborabe et al., (2008), given the inhibitory nature on the plasma membrane H^+-ATPase activity, downstream process regulated by this activity are expected to be disturbed after aminochitosan treatment. Other proteins and GO terms related to cell wall were 'cell wall modification', 'pectin catabolic process', 'aspartyl esterase activity', 'pectinesterase inhibitor activity', 'extracellular region', 'cell wall', 'membrane' and 'fruit ripening' which were down-regulated for InfPol_ConPol at both 6 and 9 hpi. The above observation may indicate a shift in the expense of resources from modulating both the cell wall and cell membrane towards other defence response systems, specifically after the permeabilization of the cell membrane by aminochitosan. Young, Köhle & Kauss, (1982) stated that the treatment of suspension-cultured *Glycine max* cv Harosoy 63 cells with a soluble CHT resulted in an increase in the membrane permeability of the host cell in the presence of CHT when contact with the cell wall was made but that this increase permeability could facilitate and enhance infection (Young, Köhle & Kauss, 1982).

4.5.2.3 Proteins related to defence response

CHT as an elicitor induces typical PTI responses that include the up-regulation of SA and JA-mediated signaling pathways (Jia et al., 2020). In this study, the GO term 'oxylipin biosynthetic process' and the related GO terms 'lipid oxidation', 'response to wounding' and 'jasmonic acid biosynthetic process' were significantly down-regulated for InfPol_ConWater and InfPol_InfWater at 6 hpi. The proteins associated with oxylipin biosynthesis were 'fatty acid hydroperoxide lyase, chloroplastic (K4CF70, LeHPL/Cytochrome P450 of the CYP74B subfamily)', 'LoxF' (A0A3Q7E8Z0), 'TomloxC (A0A3Q7ERA8)', '12-OPDA-reductase 3 (Q9FEW9, LeOPR3)', 'allene oxide synthase 2, chloroplastic (Q9LLB0, LeAOS2)' and 'allene oxide synthase 1, chloroplastic (K4BV52, LeAOS1)'. Plant oxylipins form part of alpha linolenic acid metabolism and are biologically active lipid metabolites derived from the oxidation of polyunsaturated fatty acids by lipoxygenases, lipases and a subfamily of cytochrome (Howe &

Schilmiller, 2002; Mosblech, Feussner & Heilmann, 2009). The most researched molecules synthesized by this pathway include JA, methyl jasmonate and methyl ester but also include the precursors to these molecules, some of which have been reported to be biologically active signals important for wound signaling induced defence (Howe & Schilmiller, 2002). Oxylipins are not generally pre-formed and instead are produced *de novo* in response to biotic stress such as pathogen attack or herbivory. Of the proteins mentioned above, AOS results in JA signaling and hydroperoxide lyase in pathogen defensive volatiles and divinyl ether synthases (Griffiths, 2015). Therefore, the significant down-regulation of proteins involved in oxylipin biosynthesis is further evidence that the priming mechanisms are potentiated through SA-mediated pathways at 6 hpi.

As mentioned in Section 4.5.2.2, JA has been implicated in signaling and defence pathways after CHT treatment in *Arabidopsis*, rice, tomato, strawberry, grape, and oilseed rape to name a few which makes the aminochitosan inhibition of JA related pathways and proteins at 6 hpi noteworthy (Rakwal et al., 2002; Yin et al., 2006; Suarez-Fernandez et al., 2020; Peian et al., 2021). Additionally, this down-regulation is only noted for the group comparisons against the water treatments with/without an infection. However, it is important to acknowledge that the types of CHT applied and the timing of measurements after application and infection across different studies vary. This variability contributes to a range of results, making comparisons challenging.

Additional defence related proteins that were differentially regulated were related to the GO term ‘defence response to fungus (GO:0050832)’. Proteins that were significantly upregulated for InfPol_ConPol at 9 hpi, InfPol_ConPol at 9 hpi and InfPol at 9 hpi compared to 6 hpi while down-regulated for InfPol_InfWater at 6 hpi were ‘chitinase (EC 3.2.1.14) (A0A3Q7JDH4)’, ‘Glycoside hydrolase family 19 catalytic domain-containing protein (K4D1G8)’, ‘Basic endochitinase (EC 3.2.1.14) (Q05537/CHI14)’, ‘Acidic 26 kDa endochitinase (EC 3.2.1.14) (Q05539/CHI3)’ and ‘allene-oxide cyclase (EC 5.3.99.6) (Q9LEG5/aoc)’. These proteins suggest that at 9 hpi, chitinase activity and proteins associated with the JA-mediated response are up-regulated while from the previous sections, it appears that at 6 hpi, the defence response is associated with an SA-mediated response. However, a further 2 proteins were only up-regulated for the two 9 hpi group comparisons and included SA-mediated defence proteins namely, ‘Pathogenesis-related leaf protein 6 (P6) (P04284/PR1B1) and ‘Pathogenesis-related

protein P2 (P32045)'. Therefore, although it appears that SA-mediated pathways are up-regulated at 6 hpi and JA-mediated pathways at 9 hpi, the involvement and crosstalk with other hormones as proteins responsive to both SA and JA have been shown to accumulate at 9 hpi. Instead, 'SA and JA antagonism is in fact dose-dependent and synergy between the two hormones can appear especially at low concentrations' (Tornero et al., 1997; van Aubel et al., 2016). It is important to highlight that the complex interplay among different hormonal pathways poses significant challenges in understanding the specific roles of individual hormones in precisely regulating the expression of genes (Gururani, Mohanta & Bae, 2015).

4.5.2.4 Proteins related to ROS homeostasis

As a signaling molecule for oxidative stress and signaling cascades and a byproduct of other aerobic metabolism, ROS, H_2O_2 in particular, has been shown to be induced by CHT in several plants species as an early defence response to both biotic and abiotic stress (Mejía-Teniente et al., 2013; Malerba & Cerana, 2016). An imbalance between ROS generation and enzymatic/nonenzymatic detoxification generates oxidative stress and is well characterized being detrimental to plants. H_2O_2 accumulation has been shown to accumulate within 1-24 h after various concentrations of CHT application and with/without biotic and abiotic stress in *Arabidopsis* cell suspension cultures, sycamore cultured cells, sweet peppers and tomatoes (Ndimba et al., 2003; Jabeen & Ahmad, 2013; Mejía-Teniente et al., 2013; Lopez-Moya et al., 2017).

In Chapter 3, little to no H_2O_2 accumulation was visible at between 4-72 hpi for 1 mg/mL of aminochitosan treatment. In this chapter, the GO term 'cellular response to oxidative stress' was significantly up-regulated for InfPol_ConPol at 6 hpi while 'response to oxidative stress' and 'oxidoreductase activity, acting on single donors' were significantly down-regulated for InfPol_ConWater and InfPol_InfWater at 6 hpi, respectively. The up-regulated proteins for InfPol_ConPol at 6 hpi were also distinct from the down-regulated proteins associated with InfPol_ConWater and InfPol_InfWater at 6 hpi. The significantly up-regulated proteins for InfPol_ConPol at 6 hpi were localized in the chloroplast and cytoplasm were 'peptide-methionine (S)-S-oxide reductase (G3K2M3 and G3K2M4)', 'Plant heme peroxidase family profile domain-containing protein (A0A3Q7GX85)', 'Peroxiredoxin Q, chloroplastic (A0A3Q7H8S0)', and 'Glutaredoxin-dependent peroxiredoxin (Q7Y240/TPx1)'. H_2O_2 produced

in a specific organelle may either integrate signals that are independent of the H_2O_2 production site or that are dependent on the production site. As such, H_2O_2 generated in chloroplasts promotes the induction of genes linked to responses to pathogen attack and wounding. These genes encompass early signaling responses, such as transcription factors and the biosynthesis of secondary messengers (Sewelam et al., 2014).

Once reactive oxygen species bypass cellular scavenging mechanisms, specific damaged proteins may undergo repair. Methionine (Met) is particularly susceptible to oxidative damage by free radicals that escape the scavenging mechanisms. As such, Met residues that are oxidized may be reduced back to Met sulfoxide by peptide methionine sulfoxide reductase (PMSR). This reversible oxidation/reduction poses an attractive alternative repair or scavenging mechanism for oxidative damage before the onset of damage. It has been hypothesized that the Met residues therefore act as additional ROS sinks and that the reduction back to its original state allows for these residues to be used as scavengers for ROS, all at the expense of NADPH; "a novel antioxidant role for proteins containing surface exposed Met residues" (Weissbach et al., 2002). Interestingly, after exposure to different biotic and abiotic stresses, an *Arabidopsis* cytosolic PMSR gene was found to display low expression. However, after leaves were exposed for an extended period of 2-3 weeks to cauliflower mosaic virus, there was a strong induction of PMSR expression levels. Hence, the upregulation of PMSR observed at 6 hpi suggests an aminochitosan primed response which exhibits an antioxidant effect and an overall appearance of low levels of ROS accumulation.

CHT treatment has been shown to enhance antioxidant enzyme activities in various fruits and vegetables, including strawberries (catalase, glutathione-peroxidase, guaiacol peroxidase, dehydroascorbate reductase, monodehydroascorbate reductase), pears (ascorbate peroxidase, glutathione reductase), sweet peppers (superoxide dismutase, catalase, peroxidase), guavas (superoxide dismutase, catalase, peroxidase), table grapes (peroxidase), sweet cherries (peroxidase), oranges (peroxidase, superoxide dismutase, ascorbate peroxidase, catalase), tomatoes (peroxidase), and potatoes (peroxidase) (Romanazzi et al., 2017 and the references therein). However, the effects of CHT on litchi fruit and table grape tissues were mixed, with some studies reporting decreased activity and others reporting increased activity when combined with certain treatments (Romanazzi et al., 2017).

In contrast, the proteins down-regulated by InfPol_ConWater and InfPol_InfWater at 6 hpi were localized to the extracellular region, 'membrane', cytosol, and peroxisome. These proteins included 'peroxidase (EC 1.11.1.7) (A0A3Q7IJN4)', 'Catalase isozyme 1 (EC 1.11.1.6) (CAT1)', 'Catalase core domain-containing protein (A0A3Q7EP36)', and 'Glutathione peroxidase (A0A3Q7H2Q7)'. As H_2O_2 produced in peroxisomes has been demonstrated to elevate transcripts associated with protein refolding, repair, and degradation, it implies that H_2O_2 production in peroxisomes induces stress acclimation and/or tolerance responses (Sewelam et al., 2014). Therefore, the reduced levels of antioxidant-related proteins observed in both InfPol_ConWater and InfPol_InfWater at 6 hpi may be attributed to the potent direct antifungal effects of 1 mg/mL of aminochitosan, the overall diminished eliciting nature of *B. cinerea* infection, and as a result, the decreased demand for ROS scavenging systems. Moreover, as highlighted in Chapter 3, aminochitosan bears similarity to the effects of polyamines (PA) such as spermidine and putrescine. PAs modulate ROS homeostasis by scavenging free radicals thereby promoting the degradation of ROS as well as enhancing antioxidant enzymes (Gupta et al., 2016). Furthermore, free PAs are associated with neutralizing both superoxide anions and H_2O_2 while conjugated PAs likely assist in scavenging other ROS (Gupta et al., 2016 and the references therein). However, PAs also facilitate ROS production through PA catabolism in the apoplast.

Therefore, given the reduced chitinase activity observed in Sections 4.5.2.2-4.5.2.3 and reduced antioxidant enzymes in this section, it is possible that aminochitosan present in the apoplast (Chapter 3) is not degraded by chitinases and does not contribute significantly to the overall increase in ROS and shows little to no visible accumulation (Chapter 3). Additionally, this observation appears to be sustained up to 9 hpi as no significant ROS homeostasis related proteins or GO terms were identified at 9 hpi. Lucini et al. (2018) reported a reduced accumulation of peroxidases in their proteomic analysis of foliar CHT application on grapes. As plant peroxidases rely on H_2O_2 for the formation of apoplastic structural protein bonds and lignin polymerization, they are necessary for restoring the cell wall after mechanical damage and fortifying it against microbial attacks (Daou & Faulds, 2017). This in turn correlates well with the reduced cell wall modifications observed at 6 hp for InfPol. However, the InfWater at 9 hpi compared to InfWater at 6 hpi displayed a strong and significant up-regulation of the GO terms 'hydrogen peroxide catabolic process', 'response to oxidative stress', 'peroxidase

activity' and 'heme binding' and included the proteins 'Catalase isozyme 1 (EC 1.11.1.6) (P30264/CAT1)', 'Catalase (EC 1.11.1.6) (A0A3Q7JD73)', 'Ascorbate peroxidase (EC 1.11.1.11) (Q52QQ4)', 'Peroxidase (EC 1.11.1.7) (A0A3Q7F0H1)', 'Glutathione peroxidase (A0A3Q7HK83)' and 'Thylakoid lumenal 29 kDa protein, chloroplastic (Q9THX6/CLEB3J9)'.

The lower levels of ROS observed have not consistently correlated well with an increase in antioxidant enzymes as would be expected from the literature on CHT and plant-pathogen interactions. One would expect to see comparable results to Turk et al. (2019) who observed lower levels of ROS with a concomitant increase in CHT-induced GPX, CAT, and APX activity. However, they too concluded that CHT improves plant defence by maintaining reducing ROS levels via the inhibition of the production of the O^{2-}, alternative respiration and antioxidant scavenging mechanisms (Turk, 2019). Lastly, similar to ConPol at 9 hpi vs 6 hpi in Section 4.5.1.2, the InfPol at 9 hpi vs 6 hpi also displayed a significant up-regulation of the GO term 'glutamate decarboxylase activity'. This supports the hypothesis that foliar application of 1mg/mL of aminochitosan induces a state of 'endurance', preserving cell viability by limiting the production of ROS.

4.5.2.5 Proteins related to photosynthesis and carbon metabolism

Chloroplasts play a crucial role in orchestrating cellular functions during stress responses, aiding in the plant's survival against environmental challenges (Gururani, Mohanta & Bae, 2015). They are also recognized for their role in initiating signaling processes that suppress the expression of nuclear genes via retrograde signaling. Retrograde signaling constitutes a complex network of signals categorized into "biogenic control" from plastid development and "operational control" in response to environmental changes. Acting as an environmental sensor, the chloroplast communicates with the nucleus/other organelles during both biogenesis and normal operation, altering the expression of numerous pathways including ROS, tetrapyrroles, heme, and proteins to modulates gene expression and RNA turnover (Chan et al., 2016; Hernández-Verdeja & Strand, 2018). This adaptive behavior also serves as a defence mechanism, influencing carbohydrate metabolism in stressed plant tissues. By adapting to biotic and abiotic stresses, plants can allocate resources to necessary defence responses without detrimentally impacting overall plant health (Gururani, Mohanta & Bae, 2015; Landi et al., 2017).

The biosynthesis of tetrapyrroles, which take place almost exclusively in plastids, is essential for the biosynthesis of chlorophyll (Chl), heme and siroheme. The process starts with 5-aminolevulinic acid (ALA), the precursor of all tetrapyrroles which is converted into a into a cyclic porphyrin, protoporphyrin IX and finally, chlorophyll (a or b) or heme. The Chl branch of the pathway consists of the insertion of $Mg2^{+}$ into Proto IX for Chl a biosynthesis, or the interconversion between Chl a and Chl b (Tanaka, Kobayashi & Masuda, 2011). These tetrapyrrole intermediates, being photosensitizers, pose a risk of generating radicals and ROS, especially in light, despite the biosynthetic process requiring light. Therefore, plants regulate tetrapyrrole biosynthesis and degradation pathways to manage ROS, focusing on the rate-limiting step, ALA synthesis. Excess energy in photosynthesis can be transferred to molecular oxygen, causing harm if protective components such as antioxidant enzymes fail to detoxify the ROS generated (Inzé & Montagu, 1995; Papenbrock et al., 2000; Tripathy & Oelmüller, 2012).

For the group comparisons of InfPol_ConWater at 6 hpi, the GO terms 'protoporphyrinogen IX biosynthetic process', 'chlorophyll biosynthetic process', 'chloroplast stroma' and 'chloroplast' were significantly up-regulated with the associated proteins 'NADPH-protochlorophyllide oxidoreductase (A0A3Q7IBI0)', 'Mg-protoporphyrin IX chelatase (A0A3Q7FY87)', 'Glutamate-1-semialdehyde 2,1-aminomutase (Q40147/GSA-AT)', 'Uroporphyrinogen-III synthase (A0A3Q7GAE5)', 'Protoporphyrinogen oxidase (A0A3Q7EHA7)', 'Uroporphyrinogen decarboxylase (A0A3Q7GR78)', 'Delta-aminolevulinic acid dehydratase (A0A3Q7ILF6)', 'coproporphyrinogen oxidase (A0A3Q7I9A2)', 'Mg protoporphyrin IX methylester (A0A3Q7IJU8)' and 'hydroxymethylbilane synthase (A0A3Q7HGD7)'. These proteins are enzymes involved in tetrapyrrole metabolism, specifically in Chl biosynthesis. Notably, while heme, specifically protoporphyrin IX, serves as the common precursor for both heme and Chl, it undergoes magnesium chelation by Mg chelatase during Chl synthesis, a process that was up-regulated. Alongside this, uroporphyrinogen III, when oxidized, can lead to phototoxic reactions, highlighting the intricate processes of tetrapyrrole metabolism. (Inzé & Montagu, 1995; Mochizuki et al., 2010; Tripathy & Oelmüller, 2012).

High-pH conditions can drastically reduce leaf chlorophyll content, impacting photosynthetic rates and plant tolerance to stress. Given the potential of cytosolic alkalinization due to the inhibition of H^{+}-ATPase activity described in Section 4.5.2.2, such conditions may decrease

enzymatic activity in chlorophyll biosynthesis and enhance oxidative stress, leading to chloroplast injury (Khan et al., 2019). Therefore, the increase in chlorophyll biosynthesis may be a counteractive measure to prevent the loss of chlorophyll. The significant accumulation of porphyrin intermediate proteins may be due to a temporary dysregulation in chlorophyll metabolism which could lead to PCD. However, At 9 hpi, the 'chlorophyll biosynthetic process' was significantly down-regulated. This suggests that tetrapyrrole intermediates were regulated in a timely manner, enabling them to function not as toxic intermediates but as chloroplast-derived signaling molecules, ROS and Mg-Proto IX participate in chloroplast-to-nucleus retrograde signaling, stress responses, and PCD, conveying the porphyrin pathway's status to the nucleus, regulating levels of light-harvesting chlorophyll-binding proteins (Tran & Jung, 2020). Tran & Jung et al. (2020) reported that *Pseudomonas syringae* pv. tomato infection in tobacco leaves resulted in a decrease in chlorophyll at 48 hpi while Proto IX, Mg-Proto IX, Mg-Proto methylester, and protochlorophyllide were strongly reduced as early as 24 hpi. They suggested that the rapid degradation of photosensitizing porphyrin intermediates contributed to the reduction in cellular damage at the initial stages of *Pseudomonas syringae* pv. tomato induced PCD. However, a regulatory role for tetrapyrroles in higher plants is currently ambiguous.

Understanding the regulation and dynamics of tetrapyrrole pathways sheds light on plant responses to biotic and abiotic stresses, emphasizing the importance of coordinated metabolic processes in plant survival and adaptation (Tripathy, Mohapatra & Gupta, 2007). Despite the up-regulation of chlorophyll biosynthesis, ‘photosynthetic electron transport in photosystem II’ and ‘chlorophyll binding’ were significantly down-regulated for InfPol_ConWater and InfPol_InfWater at 6 hpi. The proteins associated with these terms were ‘Chlorophyll a-b binding protein CP24 10A (P27524/LHCP)’, ‘Chlorophyll a-b binding protein 8 (P27522/LHCI type III)’, ‘Chlorophyll a-b binding protein 13 (P27489/LHCII type III)’, ‘Photosystem II CP47 reaction center protein (Q2MI75/psbB)’, ‘Photosystem II D2 protein (Q2MIA5/psbD)’, ‘Photosystem II CP43 reaction center protein (Q2MIA4/psbC)’, ‘Photosystem I P700 chlorophyll a apoprotein A2 (Q2MIA1/psaB)’,, ‘Photosystem I P700 chlorophyll a apoprotein A1 (Q2MIA0/psaA)’‘Photosystem II protein D1 (Q2MIC0/psbA)’, and ‘Chlorophyll a-b binding protein 7 (P10708/LHCI type II)’.

The aforementioned light harvesting proteins are key components of the light harvesting antennae PSI and PSII. Therefore, in response to infection and foliar application of aminochitosan, the observed significant reduction at 6hpi in the light harvesting components indicates a down-regulation of photosynthesis. The up-regulation of genes related to protoporphyrinogen IX, and chlorophyll biosynthetic processes suggests a defensive strategy, as chlorophyll not only facilitates photosynthesis but also may participate in plant defence mechanisms by retrograde signaling. Concurrently, the down-regulation of proteins associated with photosynthetic electron transport in PSII, and chlorophyll binding may signify the plant's reallocation of resources to activate defence-related compounds, temporarily reducing photosynthetic efficiency (trade-off). Contrastingly, InfPol at 9 hpi compared to 6 hpi displayed significant up-regulation of 'chlorophyll binding' with the aforementioned associated proteins. This indicates a potential swift shift from defence to recovery as the plant adapts to the infection more rapidly after aminochitosan application, aiming to restore normal physiological functions, including photosynthesis. From Chapter 3, we know that the increase in chlorophyll content is sustained up to 4 dpi. This is in contrast to Tran & Jung (2020) who found that the decline in photosynthetic efficiency was indicated by the reduction in ethylene, F_v/F_m, and chlorophyll and a complete disappearance of porphyrin intermediates. However, the relationship between the accumulation of tetrapyrrole intermediates, which often leads to ROS production, and alterations in protein expression following aminochitosan treatment is not straightforward. Any potential involvement of ROS is likely to be influenced by nuanced temporal and spatial signals. The disruption of tetrapyrrole synthesis may also influence other recognized plastid signaling pathways. For instance, the redox state of plastids plays a role in regulating nuclear gene expression, and changes in tetrapyrrole metabolism are expected to impact the redox status as well. Lastly, in contrast to InfPol at 9 hpi vs6 hpi, InfWater at 9 hpi vs 6 hpi, displayed significant down-regulation of 'chlorophyll biosynthetic process' with the same aforementioned associated proteins.

4.6 Conclusions

Chapter 4 used a label-free proteomics approach to characterize the molecular mechanisms of priming observed in Chapter 3, with a specific focus on the effects at earlier time points after the application of diamino 3 at a concentration of 1 mg/mL. Furthermore, we analyzed

four plant states namely, naïve, primed, naïve-and-triggered, and primed-and-triggered. As defence priming results in positive cost benefit, we assessed the consequences of both activating (6 hpi) and maintaining a primed state (9 hpi). To our knowledge, this represents the first proteomic study on aminochitosan in the tomato/*B. cinerea* pathosystem. We identified differential regulation of the proteome that could be separated into five categories namely, DNA and chromatin, cell wall and membrane, defence response, photosynthesis and carbon metabolism, and ROS homeostasis.

ConPol: A look at the aminochitosan primed and non-triggered state

In the ConPol leaves at 6 hpi, it appears that early regulation of the defence response may be regulated through DNA and chromatin binding and the removal of histones through ubiquitination, a mechanism of action that has been shown to play a pivotal role in non-host resistance. However, the interaction between chromatin/DNA is tightly regulated in a relatively short timeframe as it is negatively regulated at 9 hpi; another phenomenon that is indicative of non-host resistance as this accelerated depletion contributes to a faster immune response against non-host pathogens, leading to a more rapid termination of their growth. However, a key difference in this activation is that aminochitosan results in a more intense induction in the early hours of infection than infection with *B. cinerea*, thus resulting in an early cessation due to the depletion of histones and nucleosomes generally necessary for normal functioning. Changes to physical barriers, the cell wall and membrane, were also observed for ConPol at 6 and 9 hpi where aminochitosan appeared to significantly increase the esterification and decrease the chitinase activity of plant cell walls, thus increasing the cell wall integrity and reducing the probability of being degraded by invading pathogens.

Defence related proteins including terpenoid-related compounds with antimicrobial and defence related properties were positively regulated despite not actually being exposed to a pathogen indicating that the leaves initially recognize aminochitosan as a biotic stress, another extension of non-host resistance. A positive and negative regulation of both JA- and SA-associated PR proteins was also observed which in turn validates the modifications to chromatin conclusion as global changes to chromatin are posited as a more comprehensive explanation for triggering the diverse transcription of PR genes (Isaac et al., 2009). The significant down-regulation of allene oxide at 6 hpi may indicate that certain elements of the

JA pathway are down-regulated at 6 hpi while others are up-regulated (PR4 and thaumatin-like proteins). Similarly, the up-regulation of PR1a2 and subtilisin-like proteases and down-regulation of PR2 indicate an intricate balance where the antagonism between SA and JA/ET is not absolute, enabling a precise and pathogen-specific adjustment of responses.

From the little to no accumulation of H_2O_2 in Chapter 3, we expected to see a similar occurrence in Chapter 4. At 6 hpi for ConPol, it appeared that aminochitosan treatment indeed initiated the defence response independently of ROS accumulation and/or aminochitosan itself functioned as an antioxidant. Considering diamino 3's degree of substitution of 0.63 (Chapter 3) and its heightened positive charge, it is possible that it exhibited robust antioxidant properties. Additionally, the down-regulation of catechol oxidase activity (PPO) may be used as a means of maintaining lower levels of ROS by negatively regulating the pathways that result in ROS production. Therefore, as the negative regulation of PPO activity has been shown to occur concurrently with an increase in F_v/F_m and increase in chlorophyll content and an absence of H_2O_2 accumulation, the work in Chapter 3 is simultaneously validated.

The down-regulation of photosynthesis at 6 hpi, and corresponding reallocation of resources and reorientation of metabolism towards the mounting of defence repones was expected. It appears that at 6 hpi, tomato pre-emptively down-regulates photosynthesis and carbon metabolism as an adaptive response to aminochitosan treatment while up-regulating defence systems. This suggests that in the early hours of treatment, aminochitosan is perceived as a biotic stress and resources are allocated to defence instead of growth as photosynthesis represents a hidden cost. However, at 9 hpi, the up-regulation of catalase coupled with chlorophyll biosynthesis may serve as sink/means for dissipating the excess energy of enhances photosynthesis, preventing any damage to photosynthetic machinery. This suggests a stimulatory effect of aminochitosan at later time points when the polymer is no longer recognized as a threat or biotic stress.

Glutamate decarboxylase activity was also positively regulated at 9 hpi, allowing for excess carbon to be recycled in the ConPol leaves given the increase in photosynthesis as mentioned above. Alternatively, GABA may be produced directly from the foliar application of aminochitosan (as aminochisoan is a polyamine) through intracellular oxidation, resulting in

positve feedback loop that promotes endogenous GABA production through the up-regulation of GAD. The increase in GABA may therefore also serve as a preemptive scavenger for reactive oxygen species; reducing the likelihood of oxidative stress at later time points, as seen in Chapter 3, by the low to absent levels of H_2O_2. Furthermore, glutamate metabolism was regulated in a manner that resulted in the 'endurance' metabolic state where cell viability is preserved. Regulations associated with endurance confer resistance to necrotrophic pathogens but increase susceptibility to biotrophs. Thus, aminochitosan in untreated tomato leaves may be regulating the glutamate metabolism in favour of an 'endurance' metabolic state at 9 hpi.

InfPol: A look at the aminochitosan primed and *B. cinerea*-triggered state

Similar to ConPol at 6 hpi, modification to histones were observed for InfPol at 6 hpi as the activity S-adenosylmethionine transferase (SAMT) was significantly and methyl-CpG-binding domain-containing proteins were significantly down-regulated. The coupled potential downregulation of histone methylation and recruitment of histone modifying enzymes could allow for a more open chromatin configuration and increased accessibility for the modulation of gene expression.

It was suggested that the regulation of plasma membrane H^+-ATPase activity serves as a switch between elicitor recognition/response to wounding and pathogen defence signaling pathways. At 6 hpi, the negative regulation of H^+-ATPase activity and chitinase activity (PR2, PR4, PR5x, CHI3, CHI14, CHI17) contributes to the hypothesis that aminochitosan primes a defence response predominantly in a ROS-independent manner and that other defence response systems are key contributors to the priming and resistance phenotype observed in Chapter 3. However, at 9 hpi, the up-regulation of H^+-ATPase was coupled with the activation of pathogen defence signaling pathways (PR2, PR4, PR5x, PR23 and CHI14). Therefore, between 6 and 9 hpi, the defence response appears to switch from 'elicitor recognition and response to wounding' and 'defence signaling pathways'. Given the inhibitory nature on the plasma membrane H^+-ATPase activity, downstream process regulated by this activity are expected to be disturbed after aminochitosan treatment which included cell wall modifications which may indicate a shift in the expense of resources from modulating both

the cell wall and cell membrane towards other defence response systems, specifically after the permeabilization of the cell membrane by aminochitosan.

At 6 hpi, the significant down-regulation of proteins involved in oxylipin biosynthesis is further evidence that the priming mechanisms are potentiated through SA-mediated pathways. Additionally, this down-regulation is only noted for the group comparisons against the water treatments with/without an infection. Contrastingly at 9 hpi, chitinase activity and proteins associated with the JA-mediated response are up-regulated. However, a further 2 proteins were up-regulated and included SA-mediated defence proteins. Therefore, although it appears that SA-mediated pathways are up-regulated at 6 hpi and JA-mediated pathways at 9 hpi, the involvement and crosstalk with other hormones as proteins responsive to both SA and JA have been shown to accumulate at 9 hpi. Instead, 'SA and JA antagonism' is in fact dose-dependent and crosstalk between the two hormones can appear especially at low concentrations of elicitors.

The upregulation of peptide methionine sulfoxide reductase observed at 6 hpi suggests a primed response triggered by aminochitosan which exhibits an antioxidant effect. Additionally, the reduced levels of antioxidant-related proteins observed at 6 hpi may be attributed to the potent direct antifungal effects of 1 mg/mL of aminochitosan, the overall diminished eliciting nature of *B. cinerea* infection, and as a result, the decreased demand for ROS scavenging systems. Thus, the overall and apparent low levels of ROS accumulation.

Given the reduced chitinase activity and antioxidant enzymes, it is possible that aminochitosan present in the apoplast (Chapter 3) is not degraded and does not contribute significantly to the overall increase in ROS as seen by the little to no visible accumulation of H_2O_2 (Chapter 3). Additionally, this observation appears to be sustained up to 9 hpi as no significant ROS homeostasis related proteins or GO terms were identified at 9 hpi. Lastly, similar to ConPol at 9, the InfPol at 9 hpi also displayed a significant up-regulation of glutamate decarboxylase activity. This furthers the hypothesis that foliar application of 1mg/mL of aminochitosan induces a state of 'endurance', preserving cell viability by limiting the production of ROS. The lower levels of ROS observed have not consistently correlated with an increase in antioxidant enzymes as would be expected from the literature on CHT and plant-pathogen interactions. However, aminochitosan may improve plant defence by maintaining

reduced ROS levels via the inhibition of the production of the O^{2-}, alternative respiration and it acting as an antioxidant.

Given the potential of cytosolic alkalinization due to the inhibition of H^{+}-ATPase activity at 6 hpi, such conditions may decrease enzymatic activity in chlorophyll biosynthesis and enhance oxidative stress, leading to chloroplast injury. Therefore, the increase in chlorophyll biosynthesis at 6 hpi may be a counteractive measure to prevent the loss of chlorophyl and suggests a defensive strategy, as chlorophyll not only facilitates photosynthesis but also may participate in plant defence mechanisms by retrograde signaling. The significant accumulation of porphyrin intermediate proteins may be due to a temporary dysregulation in chlorophyll metabolism. Concurrently, the down-regulation of proteins associated with photosynthetic electron transport in PSII, and chlorophyll binding may signify the plant's reallocation of resources to activate defence-related compounds, temporarily reducing photosynthetic efficiency (trade-off). However, at 9 hpi, 'chlorophyll biosynthetic process' was significantly down-regulated indicating that the tetrapyrroles intermediates were regulated in a timely manner so that instead of being toxic intermediates, function as chloroplast-derived signaling molecules. The up-regulation of chlorophyll binding at 9 hpi indicates a potential swift shift from defence to recovery as the plant adapts to the infection more rapidly after aminochitosan application, aiming to restore normal physiological functions, including photosynthesis. From Chapter 3, we know that the increase in chlorophyll content is sustained up to 4 dpi.

Lastly, proteins related to ribosomal structure, translation, protein turn-over, post-translational modification and biogenesis pathways were found to be differentially regulated. Given that a broad activation of defence, it is to be expected that the priming of the defence response by pretreatment with aminochitosan requires an enhancement of proteins related to protein homeostasis which include biosynthesis, translation, modification, degradation, and transport. Therefore, it stands to reason that a similar observation may be true for aminochitosan as the up-regulation of proteins related to 'translation' and general protein homeostasis indicates that translation processes were primed by aminochitosan treatment in the priming interval before the infection and up to 6 hpi unlike in the InfWater treatment where proteins and GO terms associated with protein homeostasis was significantly down-regulated at both 6 and 9 hpi.

Overall, the present data highlights that aminochitosan affects the DNA and chromatin, cell wall, membrane, and H^+-ATPase activity, chloroplasts and consequently the redox/ROS status as early as 6 hpi with some of the induced responses being sustained up to 9 hpi. This resulting regulation of transcription in the nuclear genome, which includes up-regulation of defence-related proteins and down-regulation of chitinases, occurs in a ROS-independent manner. Finally, several of the proteins were oppositely regulated between aminochitosan pretreatment and *B. cinerea* infection, indicating different regulation patterns between the "primed state" and the "triggered state". In conclusion, our proteomic data validated the 'priming' capacity of aminochitosan in 5-week-old tomato leaves, specifically diamino 3 at a concentration of 1 mg/mL, allowing us to identify key molecular mechanisms underpinning the primed states both with and without *B. cinerea* infection at 6 and 9 hpi

4.8 Addendum: Supplementary data

Table S4.1: The number of DEPs identified using limma and varying parameters. FDR adj. p-val and biological replicates were adjusted between 0.01 and 0.05 and 5,4,3 respectively. DEPs were selected using the parameters of 3 biological replicates and FDR adj. p-val < 0.05.

Comparisons		**Biological replicates**	**3**	**3**	**4**	**3**	**5**
		FDR adj. p-val	**< 0.05**	**< 0.01**	**< 0.05**	**< 0.05 & LFC > 1.5**	**< 0.05**
Within time points	6 hpi	ConPol vs ConWater	674	240	166	104	108
		InfPol vs InfWater	700	392	1	110	0
		InfWater vs ConWater	2	0	0	2	0
		InfPol vs ConPol	771	447	115	116	0
		InfPol vs ConWater	976	623	0	182	0
	9 hpi	ConPol vs ConWater	123	46	0	19	0
		InfPol vs InfWater	0	0	0	0	0
		InfWater vs ConWater	0	0	0	0	0
		InfPol vs ConPol	249	122	0	39	0
Between time points	9 hpi vs 6 hpi	ConPol vs ConPol	61	1	2	0	0
		ConWater vs ConWater	2	1	0	0	0
		InfPol vs InfPol	1178	794	1	0	0
		InfWater vs InfWater	733	299	2	0	0

Table S4.2: The top 5 up- and down-regulated proteins that are unique or shared between group comparisons between time points (9_6). Up-regulated proteins are highlighted in green and down-regulated proteins are highlighted in blue. The log_2FC column is highlighted according to a green-yellow-red colour scale indicating the levels of expression (low to high).

Time	Comparison	Protein accession	log_2FC	adj.P.Val
6	InfPol_ConPol_6	A0A3Q7E9H9	-4.352	2.82E-05
6	InfPol_ConWater_6		-4.549	8.86E-06
6	InfPol_InfWater_6		-4.161	3.82E-05
6	InfPol_ConPol_6	A0A3Q7F3X3	-4.316	1.21E-09
6	InfPol_InfWater_6		-4.431	7.49E-10
9	ConPol_ConWater_9		3.791	1.88E-08
9	InfPol_ConPol_9		-3.386	1.39E-07
6	InfPol_ConWater_6	A0A3Q7F572	-4.732	2.59E-09
6	InfPol_InfWater_6		-3.404	2.24E-07
9	ConPol_ConWater_9		-1.907	1.41E-03
6	ConPol_ConWater_6	A0A3Q7FQP4	-3.478	2.19E-04
6	InfPol_ConWater_6		-4.678	1.22E-06
9	InfPol_ConPol_9		2.820	1.26E-03
9	ConPol_ConWater_9		-2.258	1.21E-02
6	InfPol_ConPol_6	A0A3Q7FSS8	-4.633	1.01E-10
6	InfPol_ConWater_6		-5.087	1.91E-11
6	InfPol_InfWater_6		-4.662	9.01E-11
6	InfPol_ConWater_6	A0A3Q7FWX0	4.044	1.61E-05
6	InfPol_InfWater_6		3.109	4.02E-04
6	ConPol_ConWater_6	A0A3Q7G0W1	3.797	1.94E-05
6	InfWater_ConWater_6		2.451	3.25E-02
9	ConPol_ConWater_9		2.927	5.06E-04
9	InfPol_ConPol_9		-3.180	1.02E-04
6	InfPol_ConPol_6	Q53U36	5.128	5.10E-03
6	InfPol_InfWater_6		4.158	2.08E-02
6	ConPol_ConWater_6	A0A3Q7GBL9	3.903	1.03E-03
6	InfPol_ConWater_6		4.909	3.13E-05
9	ConPol_ConWater_9		3.456	6.74E-03
9	InfPol_ConPol_9		-4.327	6.58E-04
9	InfPol_ConPol_9	A0A3Q7GG77	3.580	1.66E-04
9	ConPol_ConWater_9		-2.699	4.14E-03
6	ConPol_ConWater_6	Q05539	-3.192	2.27E-04
6	InfPol_ConWater_6		-4.272	1.37E-06
9	ConPol_ConWater_9	A0A3Q7H247	3.301	5.06E-04
9	InfPol_ConPol_9		-4.106	3.21E-05
6	ConPol_ConWater_6	A0A3Q7GNM9	-3.729	1.81E-07

9	InfPol_ConPol_9		4.192	2.26E-08
9	ConPol_ConWater_9		-4.330	1.26E-08
6	InfPol_ConPol_6	A0A3Q7H9W3	-3.959	7.21E-04
6	InfPol_InfWater_6		-4.041	6.42E-04
6	ConPol_ConWater_6	A0A3Q7IBI0	3.503	1.94E-05
9	ConPol_ConWater_9		2.597	7.06E-04
6	ConPol_ConWater_6	A0A3Q7IH67	3.673	2.23E-02
6	InfPol_ConWater_6		4.046	7.96E-03
6	InfPol_ConPol_6	A0A3Q7IIQ1	4.372	8.61E-03
6	InfPol_ConWater_6		4.346	7.25E-03
6	ConPol_ConWater_6	A0FKE6	3.857	3.98E-03
6	ConPol_ConWater_6	A0A3Q7GDE1	-3.318	2.21E-02
6	ConPol_ConWater_6	A0A3Q7E8T9	-3.963	2.80E-03
9	ConPol_ConWater_9	A0A3Q7JCT2	-1.793	1.56E-02
6	InfPol_ConPol_6	K4ASZ0	3.922	7.21E-04
6	InfPol_ConPol_6	A0A3Q7GM48	3.788	9.03E-03
6	InfPol_ConPol_6	A0A3Q7F7H4	-3.297	1.24E-03
6	InfPol_ConPol_6	A0A3Q7G3R4	3.809	9.50E-12
9	InfPol_ConPol_9	Q01412	2.296	5.48E-03
9	InfPol_ConPol_9	Q7XAV2	-3.195	9.52E-03
9	InfPol_ConPol_9	A0A3Q7HVI3	2.409	6.35E-04
6	InfPol_ConWater_6	A0A3Q7G3R5	3.908	6.20E-12
6	InfPol_InfWater_6	Q3SC85	4.051	4.44E-02
6	InfPol_InfWater_6	Q9AWA9	3.611	1.48E-03
6	InfPol_InfWater_6	A0A3Q7G3R6	4.143	1.94E-12
6	InfWater_ConWater_6	A0A3Q7J565	1.605	3.25E-02

Table S4.3: The top 5 up- and down-regulated proteins that are unique or shared between the same group comparisons at 9 hpi vs 6 hpi. Up-regulated proteins are highlighted in green and down-regulated proteins are highlighted in blue. The log_2FC column is highlighted according to a green-yellow-red colour scale indicating the levels of expression (low to high).

Comparison	Protein accession	log_2FC	adj.P.Val
ConPol_ConPol	A0A3Q7E8T9	4.028	3.19E-02
InfWater_InfWater		4.102	1.95E-03
ConWater_ConWater	A0A3Q7F3X3	-3.612	8.89E-08
InfWater_InfWater		-4.227	5.29E-09
ConPol_ConPol	A0A3Q7G0W1	-1.823	3.73E-02
InfWater_InfWater		-4.065	7.64E-06
InfPol_InfPol	A0A3Q7GBL9	-6.295	8.48E-07
InfWater_InfWater		-4.534	2.70E-04
InfPol_InfPol	A0A3Q7IH67	-5.290	7.29E-04
InfWater_InfWater		-5.246	2.52E-03
ConPol_ConPol	A0A3Q7H0U0	-1.741	2.78E-02
ConPol_ConPol	A0A3Q7HVI4	1.632	3.73E-02
ConPol_ConPol	A0A3Q7HWR5	1.449	8.66E-03

ConPol_ConPol	A0A3Q7IA80	-2.290	4.33E-02
ConPol_ConPol	G1DEX3	-1.536	3.07E-02
ConPol_ConPol	K4C627	1.679	3.44E-02
ConPol_ConPol	Q40143	1.424	3.19E-02
ConPol_ConPol	A0A3Q7FT32	-1.630	4.33E-02
ConWater_ConWater	A0A3Q7I877	-3.546	2.32E-02
InfPol_InfPol	A0A3Q7H247	-4.185	1.29E-06
InfPol_InfPol	A0A3Q7IIQ1	-4.410	5.02E-03
InfPol_InfPol	A0A494GA45	5.691	6.22E-05
InfPol_InfPol	Q9AWA9	-6.249	1.85E-06
InfPol_InfPol	A0A3Q7E9H9	5.229	7.31E-07
InfPol_InfPol	A0A3Q7F572	5.752	6.74E-11
InfPol_InfPol	A0A3Q7FQP4	5.653	4.45E-08
InfPol_InfPol	A0A3Q7FSS8	5.388	6.00E-12
InfWater_InfWater	A0A3Q7GG77	4.092	3.73E-05
InfWater_InfWater	A0A3Q7GVG1	-5.748	1.84E-02
InfWater_InfWater	A0A494GA46	3.395	1.32E-02
InfWater_InfWater	E5KBY0	3.570	4.00E-02
InfWater_InfWater	A0A3Q7FFR5	3.339	1.25E-02

This image was created with the assistance of DALL.E 2.

Chapter 5: Investigating the efficacy of aminochitosan in the maize/*Fusarium verticillioides* pathosystem

Parts of the following chapter were published in:

Lambarey, H., Moola, N., Veenstra, A., Murray, S. & Suhail Rafudeen, M. 2020. Transcriptomic Analysis of a Susceptible African Maize Line to *Fusarium verticillioides* Infection. *Plants*. 9(9):1112.

Veenstra, A., Moola, N., Wighard, S., Korsman, J., Christensen, S.A., Rafudeen, M.S. & Murray, S.L. 2019. Kauralexins and zealexins accumulate in sub-tropical maize lines and play a role in seedling resistance to *Fusarium verticillioides*. *European Journal of Plant Pathology*. 153(1):223–237.

The only work of the above publications that were included in this chapter were conducted by me. I have been granted permission by all co-authors to use the data and results generated by me.

5.1 Abstract

In the previous chapters, the effects of aminochitosan in the dicotyledonous tomato/*Botrytis cinerea* pathosystem were characterized. This chapter attempts to further characterize aminochitosan as a treatment in the monocotyledonous maize/*Fusarium verticillioides* pathosystem. Maize is a staple crop in South Africa, used for both human and animal consumption. *Fusarium verticillioides* is a toxigenic species responsible for *Fusarium* ear rot in maize with moderate to severe consequences including reduced yield and grain quality, and the accumulation of mycotoxins that may result in adverse health effects in humans and animals.

In this chapter, we first demonstrated the effects of *F. verticillioides* infection on the defence response of the susceptible maize line, CML144 by measuring the prevalence of fungal growth *in planta* by qPCR, the accumulation of fumonisins by LC-MS and the expression and accumulation of phytoalexins by RT-qPCR and LC-MS respectively. We showed that fungal growth and phytoalexin accumulation were positively co-regulated with the phytoalexin genes biosynthetic genes in 14-day old maize roots. Furthermore, fumonisins, specifically FB_1, were significantly accumulated in the roots of 14-day old maize roots. Overall, the roots of maize seedlings were preferentially affected compared to the shoot tissue.

Thereafter, the effects of aminochitosan were investigated by assessing the direct effects on *F. verticillioides growth* and plant defence elicitor properties *in planta* on maize roots and shoots. Aminochitosan, D1, displayed significant antifungal activity on both radial growth and sporulation at a minimum concentration of 1 mg/mL. The oligomer, HD1, however did not exhibit any antifungal activity potentially due to a high concentration of salt or due to the molecular weight (MW) and degree of polymerisation (DP) of the oligomer. D1 and HD1 were then assessed as preventative or curative treatments in maize seedlings infected with *F. verticillioides* at two time points. In the preventative treatment, SA accumulated during the early stages of infection (biotrophic phase) whereas in the curative treatment, JA accumulated during the necrotrophic phase.

5.2 Introduction

5.2.1 Maize: the significance of a South African staple

Globally, the production of primary crops increased by 52% (9.3 billion tonnes) between 2000-2020, of which maize is the second largest crop contributor at 12% (1.2 billion tonnes). (FAOSTAT, 2022). Despite South Africa being defined as an upper-middle-income country by the World Bank, food insecurity and food safety remain a challenge for a large proportion of South Africans (Statistics South Africa, 2020; Ala-Kokko et al., 2021).

Field crops are important for food security in South Africa and account for the largest portions of cultivated land (Statistics South Africa, 2020). Maize (*Zea mays L.)* is considered a staple crop and accounted for the second largest use of cultivated land between 2000-2017 at 89.4% of planted area (Statistics South Africa, 2020). Moreover, maize production increased by 46.5 % (3.9% annually or 3.4 million tonnes) between 2007-2017 (Statistics South Africa, 2020). Despite this, hunger vulnerability was faced by 11.6% (2.1 million people) in 2021 and inadequate to severe food vulnerability by 15% (2,6 million people) and 6 percent (1,1 million people) respectively (Statistics South Africa, 2020, 2021). As a result, households are being encouraged to participate in producing their own food through subsistence farming (Statistics South Africa, 2021).

The primary goal of subsistence farming is to grow crops sufficient for household use with little emphasis on trading any surplus produce (Baiphethi & Jacobs, 2009). This type of farming is acknowledged as a significant contributor to alleviating food insecurity and poverty in South Africa and is part of a distinct cultural diet and ethnic tradition (Shephard et al., 2007; Baiphethi & Jacobs, 2009; Pienaar & Traub, 2015). However, subsistence farmers lack the appropriate resources and as such, their crops are often severely affected by the likes of pest damage and fungal infections (Ncube et al., 2011). Given that maize is a staple crop, the average consumption of maize in South Africa far surpasses international average daily consumption in both urban and rural areas (Shephard et al., 2002; Burger et al., 2010). The quality of maize cultivated and consumed by subsistence farmers holds significant importance as maize produced within this system is under constant threat of pre- and post-harvest damage with the likes of fungal pathogens being a particularly pressing concern for its economic and livelihood impacts (Ncube et al., 2011).

5.2.2 *Fusarium verticillioides*

The most common fungal pathogens individually or synergistically affecting maize seeds, roots, stems, ears, or silks of maize globally are listed in **Table 5.1**. Of the fungal species listed, the *Fusarium* genus is the dominant genus affecting maize grain in South Africa with *F. verticillioides* (warmer areas) being most prevalent followed by *F. subglutinans* (cooler areas) and *F. proliferatum* as determined by Ncube et al. (2011) over two seasons (Viljoen, 2003; Ncube et al., 2011; Beukes et al., 2017; Schoeman et al., 2018).

Table 5.1: Common pathogen interactions with maize that lead to disease of varying severity. The following table was adapted from Lamichhane & Venturi (2015) and Thompson & Raizada (2018) with references to be found therein.

Disease	Organism
Gibberella Ear Rot	*Fusarium graminearum*
Fusarium Ear Rot	*F. verticillioides, F. proliferatum, F. subglutanis, F. temperatum,*
Aspergillus Ear Rot	*A. flavus* Link*, A. parasitics* Speare
Corn Smut	*Ustilago maydis**
Stenocarpella/Diplodia Ear Rot	*Stenocarpella maydis* (previously *Diplodia maydis*)
Root and stalk rot	*Trichoderma* sp.*, Penicillium* sp.*, Pyrenochaeta indica, F. verticillioides*, *F. graminearum,* and *F. oxysporum, F. solani* species complex,
Crown and root rot	*F. graminearum, F. boothii*, and *F. meridionale*

**U. maydis* does not produce mycotoxins but may facilitate infections with other toxigenic fungi.

Fusarium verticillioides (formerly *Fusarium moniliforme*) is a facultative endophyte/hemi-biotroph that is most commonly associated with South African maize and causes severe symptomatic infection in the form of root rot, ear rot (FER), stalk rot and seedling blight (Munkvold & Desjardins, 1997; Schoeman et al., 2018; Omotayo et al., 2019). However, an infection may also present as asymptomatic biotrophic infection that is actually physiologically active (Bacon et al., 2001).

As *F. verticillioides* is a facultative endophyte of maize; it infects both during biotrophic endophytic association which may present as asymptomatic or by a pathogenic phase facilitated by environmental saprophytic growth. The fungus is thus transmitted vertically and horizontally to subsequent generations (Bacon et al., 2001). Horizontal infection generally occurs by plant debris and is the contagious spreading by “saprophytic colonization of soil

debris and insect vectors" to external plant organs such as roots and silks and can be mitigated by application of fungicides (Bacon et al., 2001).

The vertical endophytic transmission occurs by infection from infected seeds and may proceed as an asymptomatic and systemic infection. This is noteworthy as it remains the source for infection and mycotoxin biosynthesis generationally making fungicidal management challenging (Bacon et al., 2001)**.** The infection cycle of *F. verticillioides* is detailed in **Figure 5.1** and highlights both horizontal and vertical transmission. During systemic infection, endophytic conidia spread from roots to stalks, to cobs, and kernels, causing stalk rot. Spores are able to survive winter and infect silks during flowering (airborne spores or by splashing), leading to FER - the most common and damaging disease (Omotayo & Babalola, 2023).

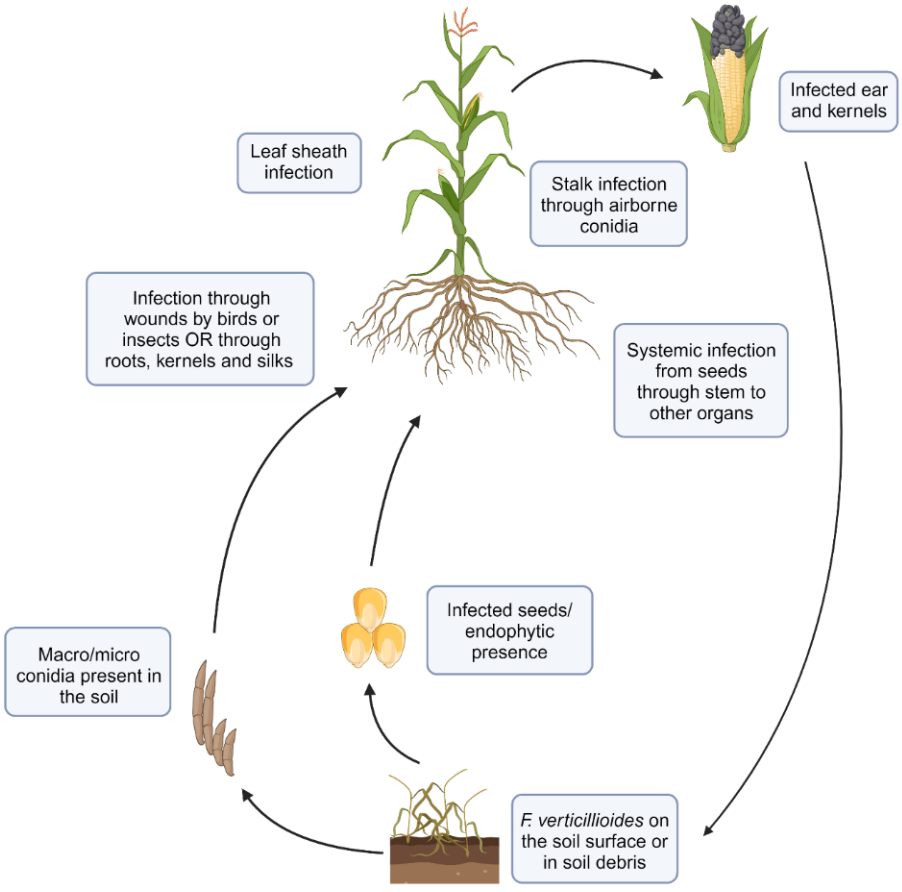

Figure 5.1: The infection cycle of *F. verticillioides* in maize adapted from Munkvold & Desjardins (1997) and Omotayo et al. (2019). This figure was created in BioRender.com.

5.2.3 Mycotoxins: Fumonisins

In addition to the economic impacts of infection, many of the fungal pathogens produce mycotoxins; toxic secondary metabolites that pose significant threat to both human and

animal health (Alshannaq & Yu, 2017). **Table 5.2** displays the common toxigenic *Fusarium* species affecting maize and their associated toxins. As shown in **Table 5.2**, *F. verticillioides* produces a range of mycotoxins of which fumonisins are the most naturally abundant in maize infected with *F. verticillioides* (Desjardins & Plattner, 2000).

Table 5.2: Toxigenic *Fusarium* species associated with South African maize. The following table was adapted from Beukes et al. (2017) with references to be found therein.

Species	Associated mycotoxins
F. boothi	15-ADON
F. dimerum	-
F. globosum	BEA, FUM
F. graminearum	3-ADON, 15-ADON, NIV, ZEA, DAS
F. incarnatum-equiseti species complex	BEA, DON, MON, NIV, ZEA
F. meridionale	NIV
F. oxysporum	BEA, FA, FUM, MON, ZEA
F. poae	BEA, Fx, HT-2, NIV,
F. proliferatum	BEA, FUM, MON
F. solani species complex	DON, FUM, T-2, ZEA
F. subglutinans	BEA, FA, FUM, MON
F. temperatum	BEA, FUM, MON
F. verticillioides	BEA, FusaC, FUM, MON

BEA, beauvericin; DON, deoxynivalenol; HT-2, HT-2 toxin; MON, moniliformin; T-2, T-2 toxin; FUM, fumonisins; FusaC, fusarin C; NIV, nivalenol; Fx, fusarenon-X; ZEA, zearalenone; FA, fusaric acid; 15-ADON, 15-acetyldeoxynivalenol; 3-ADON, 3-acetyldeoxynivalenol; DAS, diacetoxyscirpenol.

Fumonisins are polyketide mycotoxins, structurally resembling sphingoid bases such as sphinganine and phytosphinganine, which are intermediates in sphingolipid biosynthesis. The structural similarity allows for sphingolipid metabolism disruption through competitive inhibition of the ceramide synthase resulting in the accumulation of sphingoid bases (Arias et al., 2016). This ultimately results in fumonisin-induced mycotoxicoses in animals and plants cells (Arias et al., 2016).

The wild-type (WT) strains of *F. verticillioides* primarily produce the B-series fumonisins (FB_1, FB_2, FB_3, and FB_4). FB_1 is the most abundant, making up 70% of the total content with the other B-series fumonisins occurring in lesser amounts (Desjardins & Plattner, 2000; Ncube et al., 2011; Han et al., 2014; Nji et al., 2022).

5.2.4 Fumonisins and the consequences for plants

Studies have shown that the production of fumonisins in root and shoot tissue is not dependent on fungal colonization of the respective tissue. Instead, the toxins can be transported to sites distal from the site of entry, infection and/or synthesis (Bacon et al., 2001; Arias et al., 2012, 2016; Zeng, Li & Yao, 2020). A close correlation between the FB_1 levels in roots, the increase in spingoid bases and the occurrence of leaf lesions are consistent with fumonisins inducing seedling disease (Williams et al., 2007).

Sphingolipids function as structural components of the plasma membranes and cellular signalling (Zeng, Li & Yao, 2020). The disruption of sphingolipid metabolism in plants affects their ability to respond to a/biotic stressors as well as growth and development inducing programmed cell death (PCD) via multiple signalling pathways as seen in **Figure 5.2** (Arias et al., 2016 and the references therein). FB_1 has the potential to modify the physiology of the host plant thus diminishing defence responses and favouring fungal infections (Arias et al., 2016; Zeng, Li & Yao, 2020). Arias et al. (2012) demonstrated that exogenous application of fumonisin concentrations to resistant and susceptible maize line seedlings acted as pathogenic factors at higher concentrations or triggered plant detoxification mechanisms at lower concentrations (Arias et al., 2012).

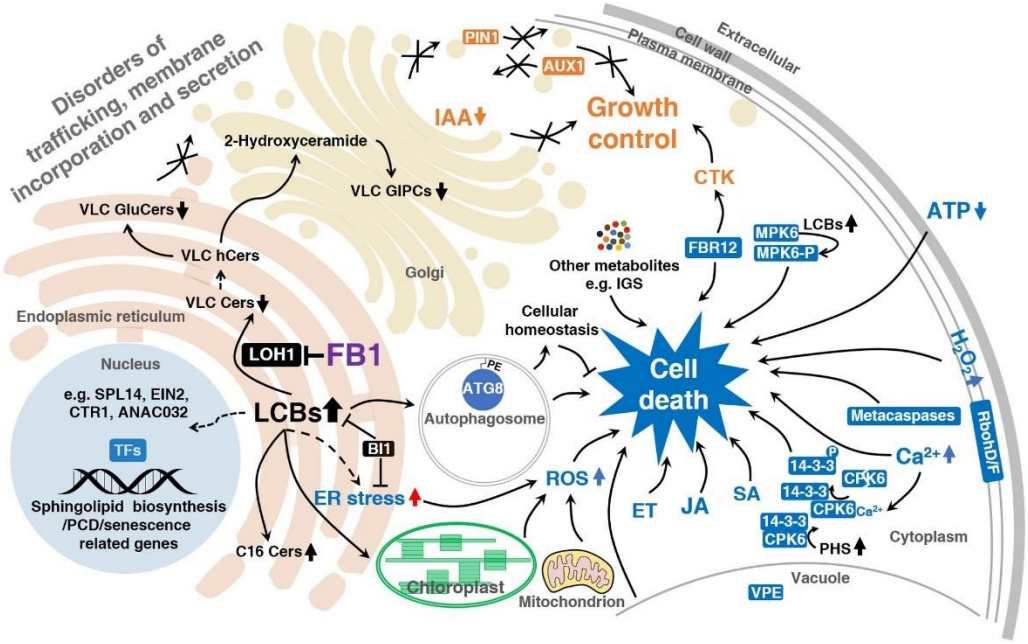

Figure 5.2: A summary of the mechanisms in which FB_1 disrupts plant systems and kills plant cells. The solid arrows indicate established links, and the dashed arrows indicate putative links. This figure was sourced from Zeng, Li & Yao, (2020).

This suggests a threshold for FB_1 of which plants can sufficiently induce detoxification mechanisms and beyond which the plant's immune system cannot effectively manage FB_1 toxicity. Furthermore, the detoxification process has been described as the storage of toxic compounds in the vacuoles or the permanent chemical binding to cell walls for permanent storage in plant tissue to root exudation respectively (Arias et al., 2016 and the references therein).

The roles of phytohormones in mediating FB_1 induced PCD was summarized in Zeng, Li & Yao, (2020) and the references therein (**Figure 5.2**). It was stated that FB_1 "hijacks the JA pathway to initiate PCD" and "induces JA-responsive defence genes but represses growth-related and JA biosynthesis-related genes, thereby reducing JA contents in plants" (Zeng, Li & Yao, 2020). This suggests that FB_1 hijacks the JA pathway to coordinate PCD (Zhang et al., 2015). In addition to JA, FB_1 induced SA-elicited PCD by suppressing the JA signalling pathway. In summary, FB_1-induced PCD is mediated through JA, SA, and ethylene (Zeng, Li & Yao, 2020). In addition to PCD, FB_1 has the potential to induce additional responses similar to hypersensitive response, such as the production of ROS, deposition of phenolic compounds and callose, the expression of PR proteins and the accumulation of phytoalexins (Wolpert et al., 2002).

5.2.5 The implications of fumonisins for South Africans are significant

The disruption of sphingolipid metabolism is now widely acknowledged as a significant mechanism involved in FB_1 toxicity within both animal and plant cells as summarized in **Figure 5.3**. FB_1 has thus been linked to a range of diseases of varying severity in both humans and animals as detailed in Jackson, DeVries & Bullerman, 1996 (Jackson, DeVries & Bullerman, 1996). The World Health Organisation identified the consumption of maize contaminated with fumonisins as a major health risk to both humans and animals with subsistence farming communities being the most at risk due to the quality and quantity of contaminated crops. (Nji et al., 2022).

In the context of South Africa, maize intended for eating and production of traditional umqombothi beer naturally contaminated with high levels of FB_1 was directly linked to the high incidences of oesophageal cancer in humans from subsistence farms in the former

Transkei region of the Eastern Cape as well as the province of Limpopo (Sydenham et al., 1990; Rheeder, 1992; Phoku et al., 2012).

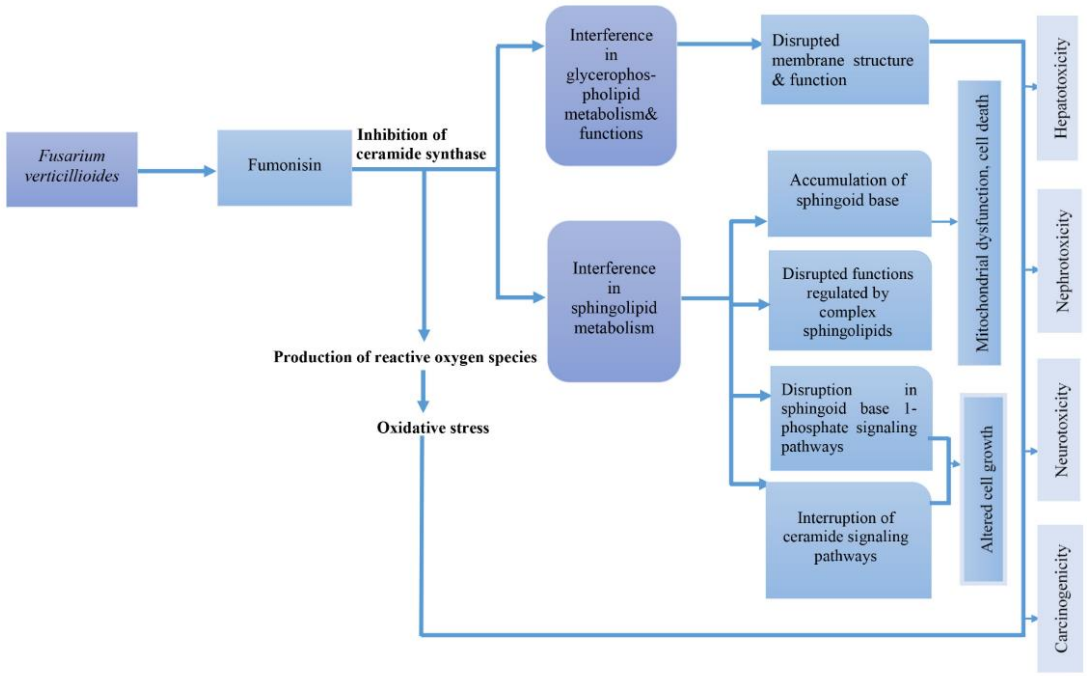

Figure 5.3: The mechanisms of action of fumonisins. Sourced from (Omotayo & Babalola, 2023).

This suggests that FB_1 is present in the staple diet of people at high risk in Transkei. Furthermore, the study noted that mean levels of FB_1 and FB_2 were significantly higher in samples of both asymptomatic and symptomatic home-grown maize from the high incidence area of cancer compared to samples from a low incidence area of cancer during 1985 and 1989 (Rheeder, 1992; Rheeder et al., 2016). This highlights one of the risks faced by the South African population, specifically those in rural areas.

Considering global risk evaluations, numerous nations have implemented risk mitigation measures by establishing regulatory maximum levels for fumonisins and other mycotoxins in maize and other foods. As of September 2016, the permitted levels of fumonisins in foods set by the Codex Alimentarius Commission have been adopted into South African health regulations (Regulations, 2016). The Codex Alimentarius Commission set the levels of fumonisins at 4000 µg/kg for raw maize and 2000 µg/kg for maize flour and maize meal. These regulations are expected to significantly increase South Africans' (especially subsistence farmers) exposure to fumonisins, potentially surpassing the provisional maximum tolerable daily intake of 2 mg/kg body weight/day, depending on the area or province (Alberts et al., 2017, 2019; Shephard et al., 2019). As stated in Matumba et al. 2017, the enforcement of

regulations are appropriate for the exportation of commercial crops but has little relevance for subsistence farmers given that access to testing facilities are limited or inaccessible (Matumba et al., 2017; Misihairabgwi et al., 2019).

5.2.6 The antifungal effects of chitosan against *F. verticillioides*

Considering the impacts of maize contaminated with fumonisins on human and animal health as well as economic losses, strategies to mitigate the aforementioned are key. The benefits of environmentally friendly fungicides such as CHT and aminochitosan for its antifungal activity have been extensively elaborated on Chapter 2 and Chapter 3. Furthermore, the effects of aminochitosan on *B. cinerea* were shown to be significant in Chapter 3.

In brief, the fungicidal activity of CHT has been documented against a range of fungal pathogens; with minimal inhibitory concentrations differing based on the derivatives of CHT (Mukarram et al., 2023). Maximal activity is achieved at its pKa (pH 6.0) as suboptimal pH affects the solubility of chitosan (Kong et al., 2010). Studies have demonstrated the fungicidal or fungistatic effects of CHT and derivatives by means of fungal inhibition assays against a variety of fungal pathogens including the following *Fusarium* species: *F. verticillioides*, *F. graminearum*, *F. proliferatum, F. oxysporum* f. sp. *cubense*, *F. oxysporum* f. sp. *niveum, F. oxysporum* f. sp. *vasinfectum*. These derivatives were assessed for their antifungal activity at various developmental stages including sporulation, germination and mycelial growth and were found to significantly inhibit the aforementioned (Guo et al., 2006; Tikhonov et al., 2006; Liu et al., 2007; Xu et al., 2007; Al-Hetar et al., 2011; Saharan et al., 2013; Luan et al., 2018; Zachetti et al., 2019).

Additionally, differences in the fungal exterior structural morphology were noted and included excessive branching, changes in hyphal size, mycelial swelling, and abnormal mycelial shapes. Further changes in cell morphology included cells with no cytoplasm in the mycelium, large vesicles and cytoplasm aggregation (Benhamou & Thériault, 1992; El-Ghaouth et al., 1992; Al-Hetar et al., 2011). The antifungal activity of aminochitosan has previously been reported for *Aspergillus niger*, *F. oxysporum* f. sp. *cucumerium*, *F. oxysporum* f. sp. *niveum*, *Phomopsis asparagi, F. graminearum*. The results demonstrated that aminochitosan had a higher degree of inhibitory activity compared to CHT against the fungal pathogens tested (Yang et al., 2012; Luan et al., 2018). However, a limitation to be noted with the use of aminochitosan in these

studies is that the polymer was only soluble in a 0.35-1% acetic acid solution. As noted from the list above, direct fungal inhibition of *F. verticillioides* by the water-soluble aminochitosan has not been investigated yet.

5.2.7 Chitosan: a cereal killers killer *in planta*

Studies on cereal crops have not only investigated derivatives of CHT but also different methods of treatment and concentrations across a range of plants (Kocięcka & Liberacki, 2021). Common methods of applications stated in the review of Kocięcka & Liberacki (2021) include seed soak (short period, 0-6 h), seed soak (long) until germination, foliar spray, soil treatment/fertilizer, seed soak + foliar spray and seed soak + soil treatment. The results from testing different methods of application, both within a single type of crop and across different crops, showed varied outcomes due to the inconsistency in the variables across studies (Kocięcka & Liberacki, 2021).

Nonetheless, irrespective of the method of application and as stated in Chapter 2, CHT and its derivatives have been shown to induce physiological changes by promoting plant growth and development as well as eliciting plant defence responses both locally and systemically in monocots and dicots. This includes the synthesis of secondary metabolites, such as phytohormones and phytoalexins which have been shown to be involved in the signalling pathways/network (Iula et al., 2022; Mukarram et al., 2023).

Interestingly, a meta-analysis on 58 published articles by Ji et al. (2022) reported that CHT treatment significantly increased phytohormones by 26.9% (Ji et al., 2022). A variety of studies have shown that CHT treatment increased the following: GA3 and IAA levels in peanut (Zhou et al., 2002); JA in rice (Rakwal et al., 2002); JA and ABA in *Phaseolus vulgaris* (Iriti & Faoro, 2008; Iriti et al., 2009); JA, ABA and ET in tomato (Iula et al., 2022), SA in *Arabidopsis thaliana*, ABA in rubber tree (*Hevea brasiliensis*); a JA-mediated defence required kinase gene, JA synthase gene, two ethylene responsive element binding protein genes and an ethylene receptor gene in rapeseed (Yin et al., 2006) and benzylaminopurine, IAA and 1-napthol acetic acid in cucumber (Jogaiah et al., 2020).

Furthermore, CHT was shown to increase phytoalexins in pea cells (Hadwiger & Beckman, 1980), soybean cells (Köhle, Young & Kauss, 1984), rice suspension cultures (Kuchitsu, Kikuyama & Shibuya, 1993; Yamada et al., 1993), grapevine (Jeandet et al., 1995; Aziz et al.,

2006a,b; De Bona et al., 2021), potatoes (Vasyukova et al., 2001), tomato plants (Vasyukova et al., 2001; Iula et al., 2022), cotton seeds (Awadalla & Mahamoud, 2005) and grape (Lucini et al., 2018). However, the effects of aminochitosan on the induction of phytoalexins, phytohormones and phytohormone-mediated defence pathways have not been investigated in maize to date.

Additionally, studies assessing the effects of CHT on mycotoxin production, specifically fumonisins, are limited. No studies have investigated the effects of aminochitosan on fumonisin production in maize. However, a study by Ferrochio et al. (2014) on maize-based media assessed the impact of CHT (3.42 kDa, 77.6% DDA in both humans and animals as detailed in Jackson, DeVries & Bullerman, 1996) at varying concentrations (0.5, 1.0, 2.0, and 3.0 mg/mL) under different water availabilities (0.995, 0.99, 0.98, 0.96, and 0.93) on the lag phase, growth rate, and fumonisin production of *F. verticillioides*. At a concentration of 0.5 mg/mL, the combined effects of CHT and water availability were demonstrated a significant reduction in both the growth rate and fumonisin production on maize-based media. The maximum levels of reduction for both parameters were achieved at the highest doses tested (Ferrochio et al., 2014). A later study by Zachetti et al. (2019) also reported that low MW CHT (3.42 kDa, DDA > 70%) reduced fumonisins production on irradiated maize and wheat at the lowest concentration of 0.5 mg/g (approximately 0.6 mg/mL).

5.3 Materials and Methods

5.3.1 Biopolymers

The biopolymers, preparations, and concentrations used in this chapter are the same as previously described in Chapter 3, Section 3.3.3, with the following amendments. Aminochitosan, specifically diamino 1 (D1), underwent a hydrolysis process (performed by Dr Shakeela Sayed, Department of Chemistry, UCT) to yield hydrolyzed diamino 1 (HD1, 5 kDa - 14 kDa). Hydrolyzed chitosan with excess salts (CHT + salts) and hydrolyzed CHT from which the salts were removed (CHT - salts) were used in addition to CHT. The hydrolysis process yielded oligosaccharides)/oligomers; low MW polymers with a MW < 16 kDa that generally range between 0.2-3 kDa and a DP < 20 (Lodhi et al., 2014; Verlee, Mincke & Stevens, 2017). This chapter does not assess the MW fractions, however, the batch-to-batch variants, diamino 2 (D2) and diamino 3 (D3), were assessed. The range of aminochitosan concentrations was

expanded on from those previously examined in Chapter 3 (0.5, 1, and 2.5 mg/mL) to include 5, 7.5, and 10 mg/mL. Furthermore, an additional acetic acid control was introduced at a concentration of 0.15% (v/v) for further investigation.

5.3.2 *F. verticillioides*

Fusarium verticillioides MRC826 strain (Gelderblom et al., 1988) obtained from Pannar Seed (Pty) Ltd. in South Africa was grown on potato dextrose agar (PDA) for 14 days at room temperature under 12 h dark/12 h combined UVA and UVC light conditions (2x TUV 8W T5 and 1x TL 8W BLB, Philips, the Netherlands). Control (mock) and spore suspensions were made in 2% (v/v) Tween 20, with 1 x 10^6 spores/mL of *F. verticillioides* (spore suspension) or distilled water (mock solution). For large quantities of spore suspensions, *F. verticillioides* was grown in mung bean broth (MBB). The MBB was made by boiling 40 g of mung beans in 1L of distilled water for 15 min followed by filtration through four layers of Mira cloth and autoclaving at 121 °C for 20 min. The MBB was then inoculated and left to shake for 7 days after which spore suspensions were harvested by filtering the mycelia and conidia through Mira cloth.

5.3.3 GFP-transformed *F. verticillioides*

5.3.3.1 Transformation of *F. verticillioides* protoplasts with *GFP*

The green fluorescent protein (GFP) encoding gene with its promoter were cloned from pRFHUE-GFP (addgene: #89469) into the plasmid pII99 (Addendum **Figure S5.3**) by Dr Jiang Tan (Tan, 2021). The following protocols used for isolating protoplasts and transformation was adapted from Tan et al. (2020) and Ammar et al. (2013). To isolate the protoplasts, the spores of *F. verticillioides* grown on PDA for 7 days (see Section 5.8) were harvested in water and added to 100 mL of potato dextrose broth (Sigma-Aldrich). The final spore suspension containing 1 x 10^7 spores/mL was incubated for 16 h at 25 °C and shaking at 175 rpm. The spores were collected on sterile filter paper and transferred to 20 mL of a protoplast mix containing 500 mg Driselase (Sigma-Aldrich), 1 mg Chitinase (Sigma-Aldrich), 100 mg lysing enzyme of *Trichoderma harzianum* (Sigma-Aldrich) and 0.8 M KCl. The solution was gently stirred at room temperature for 30 min and then filter sterilized using 0.45 µM Millex-HA filters and a 20 mL syringe. The solution was incubated for 4 h at 30 °C with 100 rpm shaking. The protoplasts were then isolated by centrifugation for 10 min at 1500 *g* and then suspended in

2 mL of STC buffer containing 1.2 M sorbitol (Sigma-Aldrich), 10 mM Tris/HCl (Sigma-Aldrich) and 50 mM $CaCl_2$ (Sigma-Aldrich) (Abou Ammar et al., 2013; Tan et al., 2020).

For the transformation, a solution containing 100 µL of 2 x 10^7 protoplasts/mL, 50 µL PEG buffer (30% (v/v) PEG 8000, 0.5 mM CaCl and 0.01 M Tris/HCl at pH 8), 100 µL of STC buffer and 10 µg of the pII99 plasmid DNA was gently shaken (20-25 rpm) for 20 min at 25°C. An additional 2 mL of 30% PEG buffer was added to the solution and shaken for a further 5 min. Following this, 4 mL of STC buffer was added and the solution inverted to homogenise. Following this, 600 µL of the solution was then added to 15 mL aliquots of warm regeneration medium (0.5 g/L yeast extract, 0.5 g/L casein hydrolysate, 5 g/L agar and 275 g/L sucrose) and poured in 90mm petri dishes. The plates were incubated for 18 h at 28°C. Following incubation, 15 mL of regeneration medium also containing hygromycin B (200 µg/ml) was overlayed and incubated for a further 3-5 days at 28 °C until colonies began to form. Colonies were randomly selected and transferred to a new PDA plate containing hygromycin B (100 µg/ml) and incubated for 4-5 days at 28°C. Mycelia from the transformed plates were visualized by fluorescence microscopy (Olympus BX-51 microscope) and compared to wild-type *F. verticillioides*. The K3/L4 filter cube with excitation between 470-490 nm and suppression at 515-560 nm was used for GFP fluorescence detection in mycelia. Transformants with the correct amplicon size was identified using PCR. DNA was extracted from the selected plates using the CTAB protocol and run on an agarose gel. Positive transformants were selected and grown on PDA for 14 days after which 30% (v/v) glycerol stocks were made.

5.3.3.2 Assessing the general fitness of the GFP transformants.

GFP-transformants were assessed for growth, sporulation, and pigment formation (see Section 5.3.4, **Figures S5.4** and **S5.5**) and virulence and effects on plant growth *in planta* (see Section 5.3.5, **Figures S5.6** and **S5.7**).

5.3.4 Antifungal assays

5.3.4.1 Mycelial radial inhibition

The direct effects of the biopolymers were assessed as in Section 3.3.6.1 with the following additions: the final concentrations of the amended media were 0.5, 1, 2.5, 5, 7.5 or 10 mg/mL. Unamended PDA, water (PDA dilution control), 0.1 and 0.15% (v/v) acetic acid and NaCl at

concentrations of 25, 50, 100, 200 and 300 mEq were used as controls. Radial growth measurements (expressed as an average mycelial area in mm^2) and macro-photos were taken post-initiation at days 1-5, and 11. Experiments were performed with between three to five biological replicates per treatment, per experiment, and repeated twice.

5.3.4.2 Sporulation

The direct effects of the biopolymers were assessed as in Section 3.3.6.2

5.3.5 *In planta* assays

5.3.5.1 Growth medium: sand sterilisation, sand: SAP mix and *F. verticillioides* inoculation

The following protocol was adapted from the protocol used by Dr Noēmi de Zutter (LAMP, Gent University) and Kyndt et al., (2017). Fine white sand was used for both germination and growth of maize seedlings throughout this chapter. The sand was first sterilised by base/acid treatment and washing. Prior to washing, the sand was treated with 0.5 % NaOH (1:1 of sand: NaOH), shaken for 1 h and washed twice with sterile distilled water. The sand was then treated with 5 % HCl (1:1 of sand: HCl) and washed twice with distilled water. Following base and acid treatment, the sand was decanted into a conical flask and washed with 4x with distilled water at a ratio of 1:1 sand: water (Kyndt et al., 2017). Following this, the sand was washed twice more with milli-Q water. On the second wash, the water was retained and the electrical conductivity of the water above the sand measured and compared to milli-Q water (< 3µs). The conical flask was then autoclaved and subsequently dried in a 60 °C oven for 1-2 days with shaking every few hours. The sterile sand was then stored in a sterile airtight container for later use.

Before being used, the sand was mixed with a synthetic absorbent polymer (SAP). Approximately 3 g of SAP (Aquaperla®, DCM, Belgium) was added to 300 mL of distilled water and left to sit for 2 h until the formation of a gel. The gel was then vigorously shaken, mixed into 2 kg of sterile sand and the sand: SAP mix allowed to dry for 2 days before use. To inoculate the sand: SAP mix for use, 2 kg of sand: SAP was inoculated with 200 mL of 1×10^7 *F. verticillioides* spores/mL to achieve a final concentration of 1×10^6 spores/g of white sand.

5.3.5.2 Growth medium: Murashige and Skoog (MS) media

1 L of MS media was made by combining 2.15 g of MS salts (Sigma-Aldrich) and 10 mL of MS vitamins (Sigma-Aldrich) in milli-q water. Subsequently, the pH was adjusted to 5.7 using KOH and 2.2 g of phytagel (Sigma-Aldrich) added. The mixture was heated until the salts were dissolved and then autoclaved before pouring the media into the tubs.

5.3.5.3 Plant material: seed sterilisation, inoculation, and germination

Seeds of the maize (*Zea mays L.*) lines CML144 (KALRO Arid and Range Lands Research Institute, Kenya), B104 (K2 Klein Karoo Seed Production, South Africa) and LG32017 were used. Seeds were sterilised using a protocol adapted from Oren et al. (2003) prior to further use. The seeds were shaken in 20 mL of 100% (v/v) ethanol for 1 min before being soaked in 20 mL of 50% (v/v) commercial bleach for 15 min. After soaking, the seeds were washed 5x with sterile water. If the seeds were to be inoculated before use, the seeds would be added to an appropriate volume of 1 x 10^6 spores/mL in Tween 20 (v/v) or mock solution of Tween 20 (v/v) and shaken for 15-30 min before being dried overnight on sterile filter paper in a sealed petri dish (Oren et al., 2003). The seeds were then subsequently grown collectively in a large tray of sand: SAP mix for 3 days until germination or planted in MS media for 14 days until use for phytoalexin and gene expression analysis.

5.3.5.4 Biopolymer testing: curative vs preventative treatment

Due to a limited stock and availability of the aminochitosan polymers, certain methods of application *in planta* were not possible and alternative methods that reduced the amount of polymer required were chosen. The *in planta* effects of the biopolymers were investigated using two different premises for application (**Figure 5.4**) with the following general overview. The primary objective of the therapeutic or curative method was to reduce the effects of an endophytic infection or subsequent infection. This entailed first soaking the seeds with an *F. verticillioides* spore suspension, followed by an inoculation with 2.5 mg/mL of D1 or water (control) 3 days later once the seed had germinated. The preventative method aimed to prevent an infection from establishing. This method entailed first inoculating the roots of a germinated seedling with 2.5 mg/mL of D1 or water, followed by transplantation to *F.*

verticillioides infected sand:SAP mix distributed in test tubes, grown in a specific set up (**Figure S5.8**).

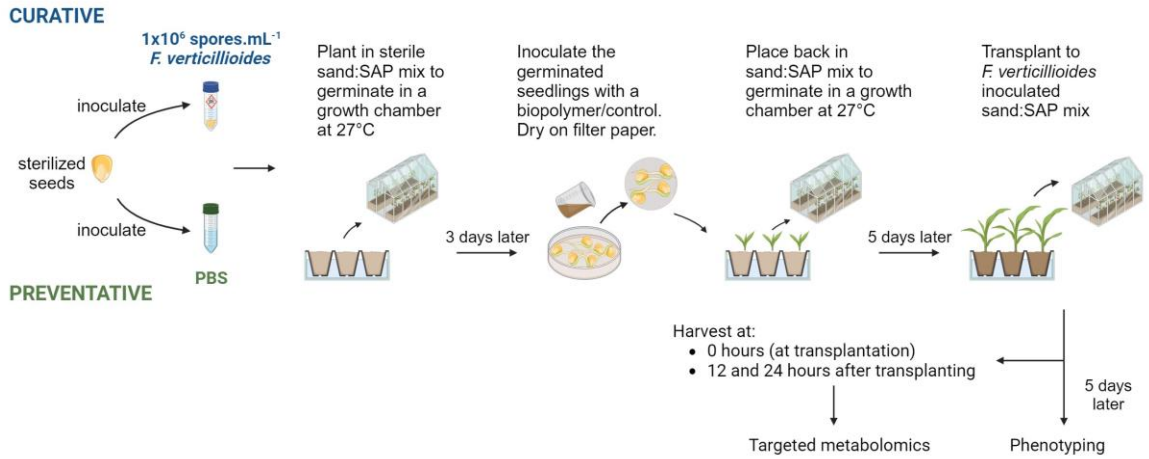

Figure 5.4: A diagram depicting the protocol used to inoculate the seeds or germinated seedlings with both *F. verticillioides* and biopolymer/control. Curative Treatment: sterilized seeds were inoculated with 1 x 10^6 spores/mL of *F. verticillioides*, allowed to dry on filter paper and subsequently planted in sterile white sand: SAP mix and grown in a growth chamber at 27°C. After 3 days, the germinated seedlings were inoculated with a concentration of a biopolymer/control by soaking the radicle and seed in a petri dish containing biopolymer/control for 1 min. After 1 min, the seedlings were dried on filter paper for 1 h and then replanted in the same sterile white sand: SAP mix and grown for a further 5 days in a growth chamber at 27°C. After 5 days, the 14-day old seedlings were transplanted to sand: SAP mix infected with *F. verticillioides* at a concentration of 1 x 10^6 spores/g sand: SAP. Root and shoot samples were harvested and phenotyped at transplantation (T0) as well as 12 (T12) and 24 (T24) h after transplanting.

5.3.5.5 Phenotyping

The phenotyping platform used in Chapter 3, Section 3.3.7.2 was used to phenotype the roots and shoots of the maize seedlings at 0, 12 and 24 h after transplantation. However, photosynthetic parameters of the shoots were not assessed. The GFP signal of GFP-tagged *F. verticillioides* was used as a marker for the presence of *F. verticillioides* in the roots.

5.3.6 Targeted metabolomics

To investigate the effects of curative and preventative biopolymer treatment at T0, T12 and T24, the following phytohormones and metabolites commonly associated with plant defence were selected for metabolomic analysis using U-HPLC-MS: indole-3-acetic acid (IAA), salicylic acid (SA), abscisic acid (ABA), jasmonic acid (JA) and deuterated 6 abscisic acid (d6-ABA, internal standard).

5.3.6.1 Sample preparation

The protocol described in Ameye et al. (2015) and Van Meulebroek et al. (2012) was used for sample preparation. The harvested root and shoot tissue were flash frozen and crushed using liquid nitrogen. Thereafter, 1 mL of cold (- 20°C) modified Bieleski extraction buffer composed of methanol, ultrapure water, and formic acid at a ratio of 75:20:5 (v/v/v) and of 100 pg/µL of the internal standard, deuterium-labelled d6-abscicic acid (OlChemIm, Olomouc, Czech Republic) was added to 200 mg of each sample. Following this, the samples were vortexed and subsequently left to cold extract at -20 °C for 12 h. The samples were then centrifuged and 500 µL of the supernatant transferred to a 30 kDa Amicon® Ultra centrifugal filter unit (Merck, USA) where the extract was reduced to a quarter of the volume by vacuum (Gyrovap) at 35 °C and subsequently transferred to an HPLC vial. Finally, 10 µL of each sample was injected directly into the column (Van Meulebroek et al., 2012; Ameye et al., 2015).

5.3.6.2 U-HPLC-MS

The following protocol was extracted from Ameye et al. (2015) and conducted by Lieven Van Meulebroek (Merelbeke, Gent University). “The U-HPLC-MS system consisted of an Accela U-HPLC pumping system (Thermo Fisher Scientific, San Jose, USA), coupled to an Exactive™ Orbitrap mass spectrometer (Thermo Fisher Scientific, San Jose, USA) and equipped with a heated electrospray ionization source (HESI), operating in both the positive and negative mode (switching polarity mode). Chromatographic separation of the compounds was achieved with a gradient elution program, using a reversed phase Nucleodur Gravity C18 column (1.8 µm, 50 mm × 2.1 mm ID) (Macherey-Nagel, Düren, Germany). The column oven temperature was set at 30 °C. The mobile phase consisted of a binary solvent system: 0.1% formic acid in ultrapure water (solvent A) and methanol (solvent B) at a constant flow rate of 300 µL min 1. A linear gradient profile with the following proportions (v/v) of solvent A was applied: 0–1 min at 98%, 1–2.50 min from 98 to 60%, 2.50–4 min from 60 to 50%, 4–5 min from 50 to 20%, 5–7 min at 20%, 7–7.10 min from 20 to 0%, 7.10–8 min at 0%, 8–8.01 min from 0 to 98%, followed by 2 min of re-equilibration. The instrumental parameters for HESI can be found in Van Meulebroek et al. (2012). The phytohormones were identified by their accurate masses and retention times relative to d6-ABA.

5.3.5.3 Data Analysis

Concentrations were determined by fitting the area ratios into a six-point calibration curve using separate root and shoot matrixes. The data underwent a normality check through the Shapiro-Wilk test, while equality of variances was assessed using Levene's test. Statistical significance between the different grouping variables were calculated using Dunn's *post hoc* test with $p < 0.05$. Soft Independent Modelling of Class Analogy (SIMCA) software (version 14.1 Umetrics; Umea, Sweden) was used for the principal component analysis (PCA).

5.3.7 Mycotoxin analysis: Fumonisins

The mycotoxin analysis was conducted in the laboratory of Prof. Marthe de Boevre. Prof. de Boevre supplied all chemicals, reagents, equipment, and protocols.

5.3.7.1 Chemicals and reagents

Acetonitrile (ACN), glacial acetic acid (LC-MS grade) and methanol (MeOH, LC-MS grade) were all analytical grade and obtained from Biosolve B.V. (Valkenswaard, The Netherlands). Analytical grade n-hexane was obtained from VWR International (Zaventem, Belgium). Purified Milli-Q water was obtained using a Milli-Q Gradient System (Millipore; Brussels, Belgium).

The analytical mycotoxin standards for Fumonisins included FB_1, FB_2 and zearalenone (ZAN) were obtained from Sigma-Aldrich (Bornem, Belgium) and FB_3 obtained from Promec Unit (Tygerberg, South Africa). The stock solutions of FB_1, FB_2, FB_3 and ZAN were prepared in MeOH at a concentration of 1 mg/mL. The working standard solutions of 100 ng/µL were made by diluting the stock standard solutions in MeOH. A FB mixture of FB_1, FB_2, FB_3 with a concentration of 40 ng/µL, 40 ng/µL and 25 ng/µL in the final standard mix were combined. The mixture was evaporated until dryness at 40 °C under gentle nitrogen flow before 1000 µL of MeOH was added. The solution was then vortexed and stored in the freezer until use. ZAN was prepared in MeOH at a concentration of 100 ng/µL.

5.3.7.2 Sample Extraction

The protocol was adapted from Centre of Excellence in Mycotoxicology and Public Health's protocol for the determination of mycotoxins in animal feed by LC-MS/MS for use given the low mass per sample. The samples were ground and spiked with 100 µL of the internal

standard, ZAN (± 10 µg/mL), and 50 µL of FB mixture and allowed to equilibrate in the dark for 15 min. Extraction was performed by adding 5 mL of extraction solvent containing ACN: water: acetic acid (79:29:1, v/v/v). The samples were then shaken for 1 h using an overhead shaker (Agitelec, Paris, France) and centrifuged for 15 min at 3300 x *g*. A C18 column was set up on a vacuum elution manifold and twice conditioned with 5 mL of acetonitrile/water/acetic acid (79/20/1, v/v/v) solvent. A 25 mL volumetric flask was placed below the column. The sample underwent extraction with the solvent, followed by vortexing and agitation for 10 min and centrifugation for 15 min at 4000 rpm. The resulting supernatant was applied to the C18 column, and the eluent was collected in the volumetric flask. The column was dried for 10 min under increased vacuum, and the eluent was adjusted to the grade mark with the extraction solvent. After careful vacuum release, the volumetric flask was removed from the vacuum elution manifold and closed, and its contents were mixed for subsequent analysis.

5 mL of the supernatant was removed and defatted by adding 2.5 mL of n-hexane, shaken for 15 min with the overhead shaker and centrifuged for 15 min at 4000 rpm. The upper n-hexane layer was then removed, and the remaining sample filtered and evaporated to dryness at 40 ◦C under a gentle nitrogen flow. The remaining residue was redissolved in 150 µL of the mobile phase (A: water/methanol/acetic acid (94/5/1, v/v/v) + 5 mM ammonium acetate and B: water/methanol/acetic acid (2/97/1, v/v/v) + 5mM ammonium acetate) centrifuged at 4000 rpm. The redissolved residue was then transferred to a centrifuge filter and centrifuged for 5 min at 10 000 rpm before being transferred to an HPLC vial.

5.3.7.3 Liquid chromatography-mass spectrometry (LC-MS)

The identification and quantification of fumonisins involved the utilization of a Waters Acquity UPLC system coupled with a Quattro Premier XE Tandem Mass Spectrometer (Waters, Milford, MA, USA). Chromatographic conditions outlined by the Centre of Excellence in Mycotoxicology and Public Health's protocol for the determination of mycotoxins in animal feed by LC-MS/MS. The protocol employed a C18 column (5µm 2.1 x 150 mm) preceded by a guard column (10 mm × 2.1 mm) of similar composition (Waters, Zellik, Belgium). An analyte injection volume of 10 µL was applied, with mobile phases A and B flowing at a rate of 0.3 mL/min in accordance with a gradient elution program and a total run time of 28 min.

Instrument control and data processing were executed using Masslynx version 4.1 and Quanlynx version 4.1 software (Manchester, UK).

5.3.8 Fungal quantification: DNA extraction and quantitative PCR (qPCR)

Ground root and shoot maize tissue as well as *F. verticillioides* mycelia were used for DNA extraction. DNA was extracted using a modified CTAB protocol and a qPCR protocol from Korsman et al. 2012. The plant membrane protein PB1A10.07c (*ZmMEP*) (Manoli et al., 2012) and the fungal gene elongation factor 1α (*FvEF1α*) (Nicolaisen et al., 2009) genes were used as reference genes for quantification (**Table 5.3**). Dilutions of *F. verticillioides* DNA in mock inoculated CML144 maize DNA were used to quantify FvEF1α levels and dilutions of mock inoculated CML144 maize were used to quantify *ZmMEP*. The qPCRs were performed using the FAST qPCR Master Mix (2X) Kit (Kapa Biosystems, Wilmington, USA) to set up 10 µL reactions and run on the Rotor-Gene™ 6000 (Corbett Life Science, Sydney, Australia) for 30 cycles: 95 °C for 3s, 60 °C for 20s, 72 °C for 1 s. Standard curves were obtained from the Rotor-Gene™ 6000 series software (version 1.7) and used to determine the ratio of fungal DNA in plant DNA (*F. verticillioides* DNA/maize DNA (ng/µg) (Korsman et al., 2012).

Table 5.3: Plant and fungal specific primers used for fungal quantification (qPCR) and gene expression (RT-qPCR).

	Gene name	Transcript ID	Forward (F) primer (5' – 3')	Reverse (R) primer (5' – 3')	Amplicon size (bp)	Reference
Candidate genes	*ZmAN2*	GRMZM2G044481	TGTTCTTGTGAAGGCAGTTC	CAGACACGTTTGCTTGTCATG	217	F primer: Schmelz et al., 2011; R primer: designed from sequence on MaizeGDB
	ZmCYP818A	GRMZM2G087875	TTTCAGCTCATCGCACGCTG	CGTCAAGAGGTGGTGGAGC	120	Designed from sequence on MaizeGDB
	ZmKO	GRMZM2G161472	GAAGCATCCAGGCAGTGAAC	GAGGTACACATGCAACGGGT	146	Christie et al., 2017
	ZmKSL2	AC214360.3_FG001	ACTCATCTCCGCTCACGAAT	ACCGGGGAGTTGATCTTCTT	89	Christie et al., 2017
	ZmKSL4	GRMZM2G016922	AGTTCAGCAGTGAGTCCAGC	CCGGTCTAGGGTGGTGTAGA	248	Moola, 2016
	ZmTPS1	GRMZM2G049538	CTCTCGCTGAAGGCGGTCTG	CTTGCTTTTGCCAGAGCTAACCTCA	156	Designed from sequence on MaizeGDB
	ZmTPS11	GRMZM2G127087	GAAATGCGACAAAGGGCT	TCTTGAAGGCATCTCGTAGTA	398	Huffaker et al., 2011
Reference genes	*ZmMEP*	GRMZM2G018103	TGTACTCGGCAATGCTCTTG	TTTGATGCTCCAGGCTTACC	203	Manoli et al., 2012
	ZmRpo1	GRMZM2G034326	AGCCAAAACGCTAAAGTGGA	TAAGTGACGAGCAAGGCAAA	175	Ma et al., 2006
	FvEF1α		CGTTTCTGCCCTCTCCCA	TGCTTGACACGTGACGATGA		Nicolaisen et al., 2009

5.3.9 Gene expression: RNA extraction and RT-qPCR

RNA was extracted from ground maize tissue using the PureLink® Plant RNA Reagent (Thermo Fisher Scientific, Waltham, USA) according to the manufacturers instructions for <100 mg tissue. The cDNA was synthesized from 1000 ng RNA/sample using the Maxima First Strand cDNA Synthesis Kit for RT-qPCR with dsDNase (Thermo Scientific, Waltham, USA) according to the manufacturer's instructions. Serial dilutions of the pooled RNA samples were made to generate a standard curve. The KAPA SYBR® FAST qPCR Master Mix (2X) Kit (Kapa Biosystems, Wilmington, USA) was used to set up 10 µL reactions where 1 µL unpooled cDNA of unknown concentration was added to each reaction. RT-qPCR analysis for gene expression was carried out on the Rotor-Gene™ 6000 (Corbett Life Science, Sydney, Australia) using the primers for the candidate and reference genes in **Table 5.3**. Samples were run for 40 cycles: 95 °C for 3 s, 60 °C for 20 s and 72 °C for 1 s. The Rotor-Gene™ 6000 series software, version 1.7 was used to obtain standard curves for relative gene expression measurements and for melt/dissociation curve analysis. Data was analysed using qBase+ software (Biogazelle, Zwijnaarde, Belgium – www.qbaseplus. com). Reference genes with a stability value (M) less than 1 and a coefficient of variation (CV) less than 0.5 were accepted as stable reference genes.

5.3.10 Phytoalexin accumulation: Gas chromatography-mass spectrometry (GC-MS)

Approximately 100 mg maize tissue of each replicate was finely ground in liquid nitrogen and was sent on dry ice for phytoalexin analysis at the Chemistry Research Unit, Centre for Medical, Agricultural, and Veterinary Entomology, United States Department of Agriculture–Agricultural Research Service (USDA–ARS) in Gainesville, USA. Phytoalexins were solvent extracted, methylated, collected on a polymeric adsorbent using vapor phase extraction (VPE), and analysed using GC/isobutene chemical ion mass spectrometry (CI-MS) as previously described (Schmelz et al., 2011). Metabolite quantification was based on U-13C-18:3 (Cambridge Isotope Laboratories, Inc., Tewksbury, MA, USA) as an internal standard.

5.4 Results

The effects of *F. verticillioides* infection on maize roots and shoots were first characterized in CML144 before the application of aminochitosan.

5.4.1 *F. verticillioides* grows preferentially in the roots of CML144 maize seedlings

As *F. verticillioides* is characterized by both its predominantly root affecting and asymptomatic presentation, the root and shoot tissue of the CML144 maize line were assessed for fungal growth at 10- and 14-days post inoculation (dpi) (**Figure S5.2)** by means of qPCR. **Figure 5.5** displays higher average *F. verticillioides* growth in roots at 10 dpi (52.6 ng/µg) than at 14 dpi (25 ng/µg). The fungal growth displayed significantly higher growth in the roots compared to the shoots at 14 dpi (3.04 ng/ µg) with no fungal growth in the shoots at 10 dpi. No growth was detected in the mock inoculated root or shoot tissue.

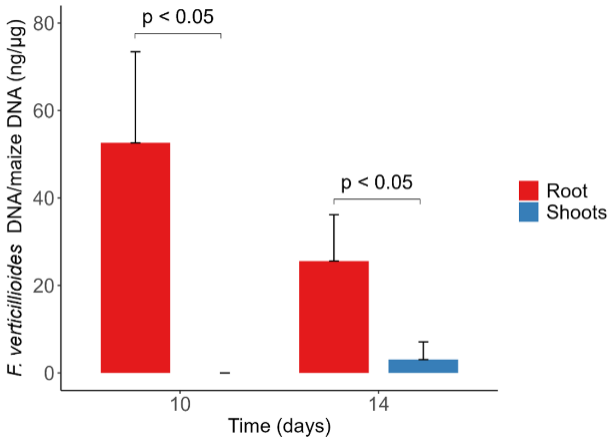

Figure 5.5: *In planta* quantification of *F. verticillioides* growth in 10 and 14-day old CML144 maize roots. Growth was quantified using FvEF1α and MEP primers and measured by qPCR of mock inoculated and *F. verticillioides* inoculated CML144 maize roots (mean + SD; n= 3). Statistical significance was determined by Kruskal-Wallis test followed by Dunn's *post hoc* test, $p < 0.05$.

5.4.2 Do fumonisins accumulate in the root tissue of CML144 and B104 seedlings?

Given that *F. verticillioides* growth was greater in the roots than the shoots at 10 and 14 dpi (Section 5.4.1), the accumulation of fumonisin B_1 (FB_1), fumonisin B_2 (FB_2) and fumonisin B_3 (FB_3) were quantified in the root tissue of mock and *F. verticillioides* inoculated root tissue of the maize lines, CML144 and B104 using LC-MS.

From **Table 5.4**, the mean accumulation of fumonisins in CML144 at 14 dpi was the greatest for FB_1 at 4098 ± 2925 µg/kg. FB_2 and FB_3 displayed significantly lower mean levels at 411 ±

178 µg/kg and 130 ± 92 µg/kg, respectively. In contrast to 14 dpi, 10 dpi displayed lower accumulation of the fumonisins with some of the replicates being below the LOQ. The accumulation of fumonisins in B104 was not consistent for all the biological replicates at 10 dpi, which was similarly seen for CML144 at 10 dpi. Therefore, 10 dpi appears to be a key turning point for fumonisin production (**Table 5.4**).

Table 5.4: The levels of *F. verticillioides* mycotoxins, namely, Fumonisin B1 (FB1), Fumonisin B2 (FB2) and Fumonisin B3 (FB3) in F. verticillioides inoculated root tissue of CML144 and B104 maize lines at 10- and 14-days post inoculation (dpi).

Maize line	Time (days)	Infection	FB_1 (µg/kg)	FB_2 (µg/kg)	FB_3 (µg/kg)
CML144	10	Mock	<LOQ	<LOQ	<LOQ
CML144	10	Mock	<LOQ	<LOQ	<LOQ
CML144	10	Mock	<LOQ	<LOQ	<LOQ
CML144	10	Infected	**350.40**	<LOQ	**29.23**
CML144	10	Infected	**89.28**	<LOQ	<LOQ
CML144	10	Infected	<LOQ	<LOQ	<LOQ
CML144	14	Mock	<LOQ	<LOQ	<LOQ
CML144	14	Mock	<LOQ	<LOQ	<LOQ
CML144	14	Mock	<LOQ	<LOQ	<LOQ
CML144	14	Infected	**7451.66**	**546.90**	**236.03**
CML144	14	Infected	**2071.02**	**208.60**	**71.35**
CML144	14	Infected	**2772.12**	**476.00**	**82.25**
B104	10	Mock	<LOQ	<LOQ	<LOQ
B104	10	Mock	<LOQ	<LOQ	<LOQ
B104	10	Mock	<LOQ	<LOQ	<LOQ
B104	10	Infected	**1266.49**	**216.60**	**93.62**
B104	10	Infected	**185.58**	**36.90**	<LOQ
B104	10	Infected	<LOQ	<LOQ	<LOQ
LOQ			**31.84**	**24.37**	**23.18**

5.4.3 Phytoalexins accumulate preferentially in *F. verticillioides* infected root tissue

CML144 maize roots and shoots were assessed for the accumulation of phytoalexins, prior to aminochitosan treatment, establishing basal levels of phytoalexins in these tissues. Maize seeds inoculated with *F. verticillioides* were grown on MS media in tubs for 10 and 14 dpi. The roots and shoots were assessed separately for phytoalexin accumulation by GC-MS (**Figures 5.6 and S5.1**).

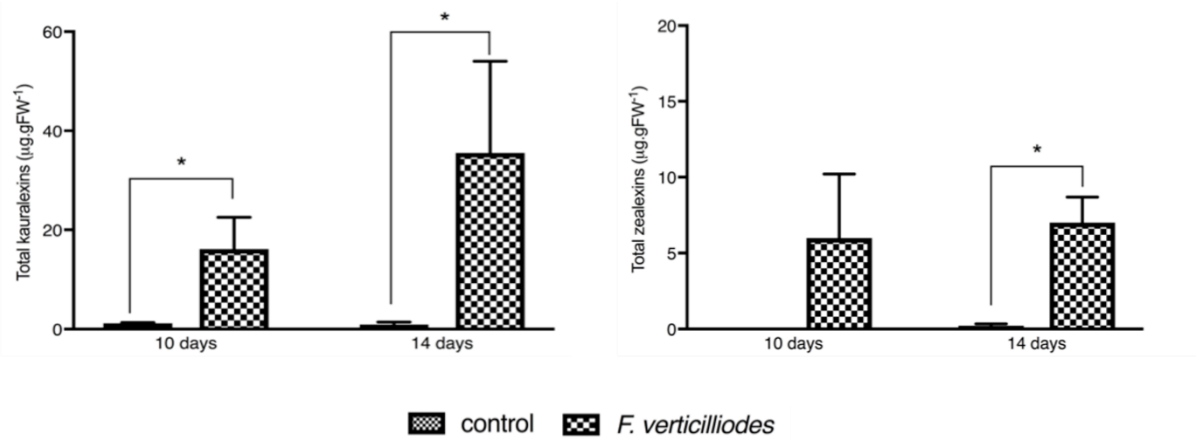

Figure 5.6: GC-MS analysis of total kauralexin accumulation in CML144 roots 10- and 14-days post *F. verticillioides* seed inoculation (dpi). Error bars indicate standard deviation (SD). An unpaired t test was performed on log10-transformed phytoalexin data to measure statistical significance between control and treatment *=p<0.05, n= 3.

Root and shoot tissue were analyzed for the accumulation of kauralexins and zealexins in **Figure 5.6** and **S5.1,** respectively. All six metabolites in the kauralexin A and B series were detected using GC-MS whereas only zealexins A1 (of A1, A2, A3, A4) and B1 could only be detected in root and shoot tissue (**Table S5.1** and **S5.1**). The total kauralexins and zealexins did not accumulate significantly in shoot tissue (**Figure S5.1** and **Table S5.2**). The total kauralexins (A and B) accumulated significantly at 10 dpi and 14 dpi whereas the total zealexins (A and B) only accumulated to significantly higher levels at 14 dpi in root tissue (**Figure 5.6** and **Table S5.1**). Furthermore, kauralexins accumulated at significantly higher levels in root mock samples at 10 and 14 dpi (1.17 and 0.90 µg/g FW respectively) than in shoot mock samples at 10 and 14 dpi (0.21 and 0.82 µg/g FW respectively) (**Table S5.1** and **S5.2**). The same was observed for root *F. verticillioides* inoculated samples at 10 and 14 dpi (16.14 and 35.51 µg/g FW respectively) compared to shoot *F. verticillioides* inoculated samples at 10 and 14 dpi (2.67 and 11.91 µg/g FW respectively) (**Table S5.1** and **S5.2**).

In both root and shoot tissue at 10 and 14 dpi, total kauralexins accumulated to higher levels than total zealexins (**Table S5.1** and **S5.2**). Moreover, higher accumulation of individual and total kauralexins and zealexins were observed at 14 dpi than at 10 dpi for the *F. verticillioides* inoculated roots while the mock inoculated roots displayed no difference between 10 and 14 dpi (**Table S5.1**). The average total kauralexin and zealexin accumulation levels following fungal inoculation was compared to *F. verticillioides* colonization levels (Section 5.4.1) and the highest CML144 ratio was at 14 dpi (0.7). Phenotypically at 14dpi, roots inoculated with *F. verticillioides* were stunted compared to the mock roots and appeared browner than mock

roots (**Figure S5.2**). The mock roots also exhibited a more diverse root network, consisting of many seminal and lateral roots compared to the *F. verticillioides* inoculated roots.

5.4.4 Putative phytoalexin biosynthetic genes accumulate significantly in *F. verticillioides* infected roots

In order to validate the kauralexin and zealexin accumulation observed in the root and shoot tissue at 14 dpi (see Section 5.4.3), the expression of the following candidate kauralexin and zealexin biosynthetic genes were analysed in the root and shoot tissue of mock/*F. verticillioides* inoculated seedlings at 14 dpi (**Figure 5.7**): copalyl diphosphate synthase gene, *ZmAn2*; Cytochrome p450 monooxygenases genes, *ZmCYP818A and ZmKO*; terpene synthase genes, *ZmTPS1* and *ZmTPS11* and putative kauralexin biosynthetic genes encoding kaurene synthase-like enzymes, *ZmKSL2* and *ZmKSL4.*

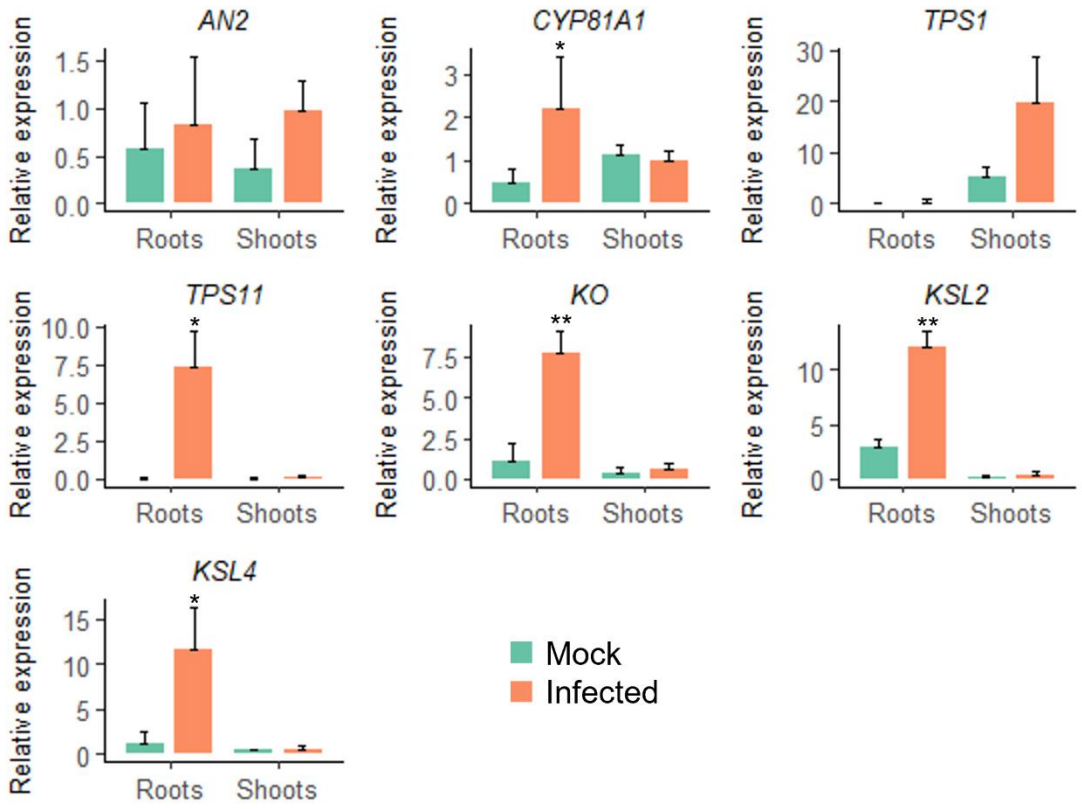

Figure 5.7: Gene expression of candidate phytoalexin biosynthetic genes in mock/*F. verticillioides* inoculated CML144 maize root and shoot tissue. *ZmMEP* and *ZmRPol* were used to normalization. Significance is denoted by * = $p < 0.05$ and ** + $p < 0.01$ (unpaired t-test, n = 3).

From **Figure 5.7**, *CYP818A*, *ZmTPS1, ZMKO*, *ZmKSL2* and *ZmKSL4* were significantly upregulated in *F. verticillioides* inoculated root tissue and not in shoot tissue. *ZmAn2* was not

significantly upregulated but did display elevated expression levels in *F. verticillioides* inoculated tissue in both roots and shoots. *ZmTPS1* was the only candidate gene to be significantly upregulated in *F. verticillioides* inoculated shoots and not roots (**Figure 5.7**).

5.4.5 Antifungal effects of aminochitosan: diamino 1 (D1) outperforms hydrolyzed diamino 1 (HD1)

The investigation into the effects of aminochitosan in the maize/*F. verticillioides* pathosystem preceded the work in Chapter 3 and preceded the synthesis of the batch-to-batch variants. Therefore, the investigation began with an exploratory analysis of the minimum concentration required for at least 50% inhibition of radial growth and sporulation.

The antifungal effects of aminochitosan, diamino 1 (D1) and hydrolyzed diamino 1 (HD1) were investigated for their antifungal effects on mycelial radial growth 5 days after incubation (dai) by analysing the percentage inhibition radial growth (PIRG%) and the percentage inhibition of sporulation (PIS%), 11 dai (**Figure 5.8** and **Table 5.6**). The effects on sporulation were assessed 11 dai due to the absence of spores on the PDA controls at 5 dai when the radial mycelial growth reached the edge of the plate.

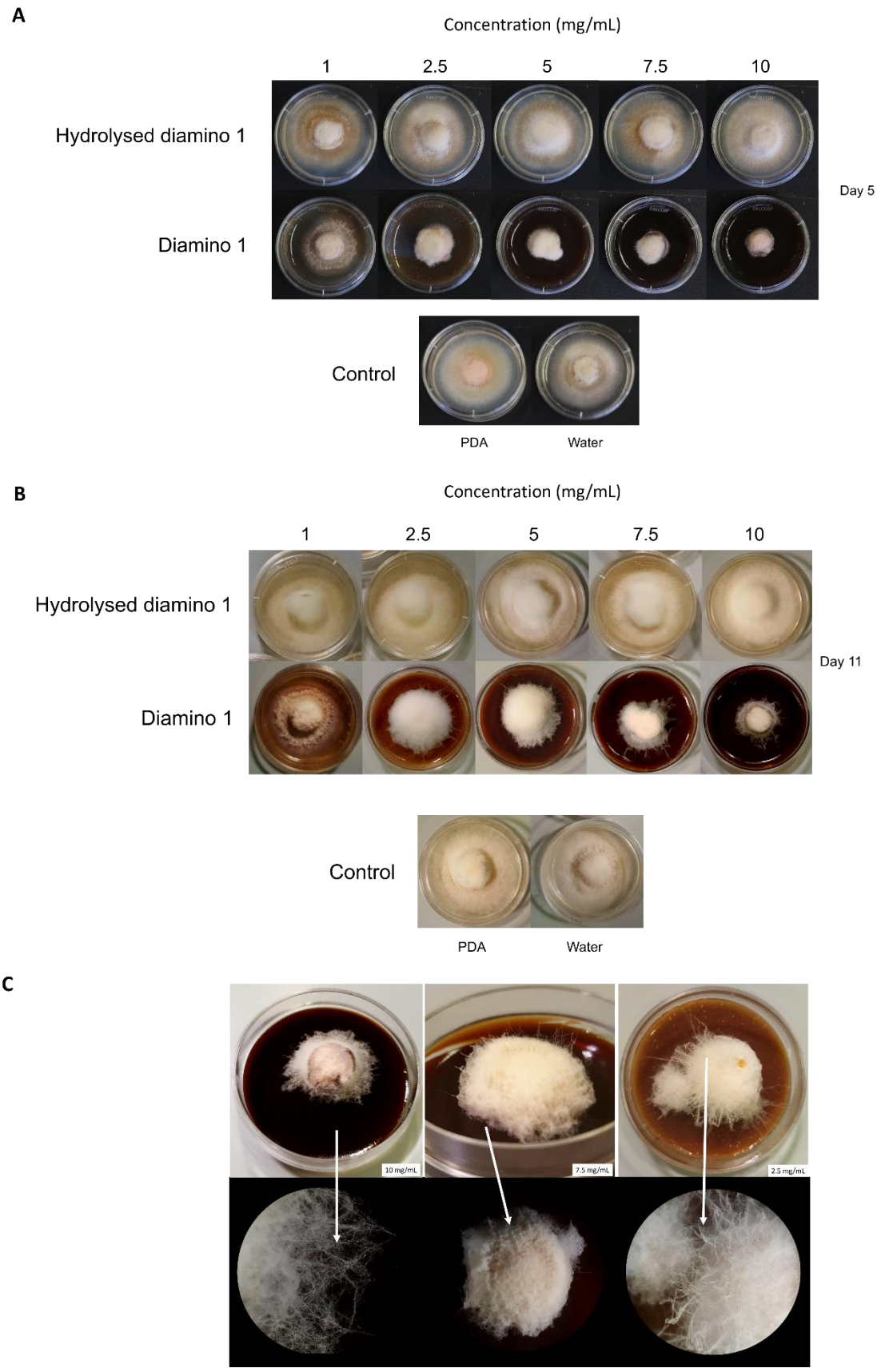

Figure 5.8: The direct antifungal effects of diamino 1 and hydrolyzed diamino 1 on *F. verticillioides* growth compared to the controls (unamended PDA and a water dilution control), 5 days after incubation (dai) (A) and

11 dai (B). The images represent one of five biological replicates. The experiment was repeated twice. (C) Close-up images of the radial growth on 2.5, 7.5 and 10 mg/mL of diamino 1 amended PDA. The images at the bottom were taken with a stereo microscope.

After 5 and 11 dai, a clear phenotypic difference between D1 and HD1 was visible in the mycelial radial growth and morphology as seen with an increase in the concentration (**Figure 5.8A** and **B**). As compared to the PDA control and HD1, excessive branching of mycelium with a "hair-like" appearance, extending upwards and outwards was observed for D1 (**Figure 5.8C**). At concentrations greater than 5 mg/mL of D1, the outward growth of the mycelia appeared to preferentially not touch the media. Instead, the mycelia appeared to be suspended above the media with sporadic lengthy projections anchored to the media. Over time and with an increase in condensation within the environment of the plate, the outward growth would eventually "drop" onto the media due to the moisture on the mycelia (**Figure 5.8C)**. No phenotypic differences were observed for HD1 compared to PDA at all concentrations evaluated at 5 and 11 dai.

In contrast to the effects induced by D1 and compared to the PDA control, no significant differences in the PIRG% and PIS% were observed for all concentrations of HD1 analyzed (**Table 5.5**). However, a significant increase in the number of spores/mL was observed for all concentrations of HD1 analyzed (**Table 5.5**). Overall, 1 mg/mL of D1 appeared to be the optimal concentration for greater than 50% inhibition in mycelia radial growth and sporulation while HD1 was not inhibitory at all concentrations evaluated.

Table 5.5: The effects of different concentrations of diamino 1 and hydrolyzed diamino 1 on the average mycelial radial inhibition and sporulation of *F. verticillioides* 11 days after incubation.

		Radial Inhibition		**Sporulation**	
Treatment	Concentration (mg/mL)	Growth area (mm^2) ± SD	PIRG (%)	Spores/mL ± SD	PIS (%)
PDA	0	490.87 ± 0.00	0^{a}	201 667 ± 47 082	0^{a}
Diamino 1	1	177.57 ± 43.43	64^{b}	116 667 ± 5 774	43^{b}
	2.5	17.2 ± 15.38	97^{b}	0.00 ± 0.00	100^{c}
	5	22.14 ± 20.28	96^{b}	0.00 ± 0.00	100^{c}
	7.5	12.81 ± 16.07	98^{b}	0.00 ± 0.00	100^{c}
	10	0.00 ± 0.00	100^{b}	0.00 ± 0.00	100^{c}
PDA	0	490.87 ± 0.00	0^{a}	201 667 ± 47 082	0^{a}
Hydrolyzed diamino 1	1	490.87 ± 0.00	0^{a}	648 334 ± 90 899	-204^{bc}
	2.5	490.87 ± 0.00	0^{a}	665 750 ± 129 119	-223^{bc}
	5	490.87 ± 0.00	0^{a}	828 750 ± 98 155	-308^{bc}
	7.5	490.87 ± 0.00	0^{a}	597 917 ± 146 650	-196^{b}
	10	490.87 ± 0.00	0^{a}	615 834 ± 142 449	-205^{c}

PIRG% = percentage inhibition of radial growth (PIRG), and PIS% = percentage inhibition of sporulation (PIS). A negative PIS% indicates growth greater than the control. Statistical significance was calculated between concentrations for each polymer. Means ± SD (standard deviation) followed by the same superscript letter are not significantly different from each other. Different letters indicate significant differences between concentrations. The presence of two letters indicates either similarity or difference across multiple concentrations for that polymer (Kruskal-Wallis test followed by Dunn's *post hoc* test, $p < 0.05$). The values shown are the average of three experiments.

5.4.6 Are salts affecting the antifungal activity?

Given the significant differences in the inhibitory properties of D1 and HD1, an investigation into the intrinsic properties of CHT was performed. It was hypothesized that the differences in the efficacy between D1 and HD1 was due to a high concentration of salt in HD1, thus reducing the accuracy of the concentrations assessed as majority of the dissolved solute would be salt. Moreover, the salt may contribute to the observed increase in sporulation. As a result, native CHT was compared to hydrolyzed CHT + salts (excess salts not removed) and hydrolyzed CHT - salts (salts removed). Due to the solubility challenges of CHT, the highest concentration of CHT assessed was 5 mg/mL. NaCl was used as a control for the minimum inhibitory salt concentration. From **Figure 5.9** and **Table 5.6**, 200 mEq of NaCl is the

concentration where a significant decrease in the PIRG% was observed. At 300 mEq of NaCl, complete inhibition was observed (**Figure 5.9** and **Table 5.6**). Conversely, a concentration-dependant increase in PIS% was observed between 25-200 mEq of NaCl, while no spores were observed at 300 mEq.

Figure 5.9: The radial inhibition effects of chitosan (CHT), hydrolyzed chitosan + salts (CHT + salts), hydrolyzed chitosan – salts (CHT – salts), and the controls (PDA, 0.15% (v/v) acetic acid, 0.1% (v/v) acetic acid and the salt control, NaCl) on the growth of *F. verticillioides*, 5 days after incubation (dai). The images represent one of five biological replicates. The experiment was repeated twice.

Table 5.6: The effects of different concentrations of diamino 1 and hydrolyzed diamino 1 on the average mycelial radial inhibition and sporulation of *F. verticillioides*, 5 and 11 days after incubation respectively.

		Radial Inhibition		**Sporulation**	
Treatment	Concentration (mg/mL)	Growth area (mm^2) ± SD	PIRG (%)	Spores/mL ± SD	PIS (%)
PDA	0	490.87 ± 0.00	0^{a}	201 667 ± 47 082	0^{a}
0,15% acetic acid	0	304.86 ± 16.77	38^{b}	56 667 ± 15 276	72^{b}
0.1% Acetic acid	0	327.26 ± 32.30	34^{b}	131 667 ± 68 405	35^{b}
Chitosan	0.5	346.3 ± 152.04	30^{ab}	195 900 ± 43 285	3^{a}
	1	63.09 ± 11.81	88^{cd}	107 063 ± 95 460	47^{ab}
	2.5	73.35 ± 18.4	86^{d}	133 188 ± 121 047	34^{abc}
	5	70.03 ± 8.54	86^{cd}	0.00 ± 0.00	100^{c}
PDA	0	490.87 ± 0.00	0^{a}	201 667 ± 47 082	0^{a}
NaCl (mEq)	25	383.87 ± 101.27	22^{ab}	145 667 ± 137 791	28^{b}
	50	490.87 ± 0.00	0^{a}	279 700 ± 76 801	-38^{ab}
	100	490.87 ± 0.00	0^{a}	362 534 ± 164 959	-79^{ab}
	200	207.19 ± 179.66	58^{b}	405 834 ± 20 208	-101^{b}
	300	0.00 ± 0.00	100^{bc}	0.00 ± 0.00	100^{c}
PDA	0	490.87 ± 0.00	0^{a}	201 667 ± 47 082	0^{a}
0,15% acetic acid	0	304.86 ± 16.77	38^{b}	56 667 ± 15 276	72^{b}
0.1% Acetic acid	0	327.26 ± 32.30	34^{b}	131 667 ± 68 405	35^{b}
Chitosan - salts	1	184.55 ± 25.26	63^{bc}	33 334 ± 17 225	84^{bcd}
	2.5	47.38 ± 15.52	91^{cd}	3 750 ± 6 275	99^{cd}
	5	15.62 ± 10.79	97^{d}	1 667 ± 2 797	100^{d}
PDA	0	490.87 ± 0.00	0^{a}	201 667 ± 47 082	0^{a}
0,15% acetic acid	0	304.86 ± 16.77	38^{b}	56 667 ± 15 276	72^{b}
0.1% Acetic acid	0	327.26 ± 32.30	34^{b}	131 667 ± 68 405	35^{b}
Chitosan + salts	1	365.49 ± 25.12	26^{b}	44 167 ± 37 739	79^{b}
	2.5	315.14 ± 45.80	36^{b}	54 584 ± 43 024	73^{b}

PIRG% = percentage inhibition of radial growth (PIRG), and PIS% = percentage inhibition of sporulation (PIS). A negative PIS% indicates growth greater than the control. Statistical significance was calculated between concentrations for each polymer. Means ± SD (standard deviation) followed by the same superscript letter are not significantly different from each other. Different letters indicate significant differences between concentrations. The presence of two letters indicates either similarity or difference across multiple concentrations for that polymer (Kruskal-Wallis test followed by Dunn's *post hoc* test, $p < 0.05$). The values shown are the average of three experiments.

While the inhibitory effect of CHT + salts was notably significant when compared to the PDA control, it did not exhibit the same level of inhibition when compared to CHT - salts and CHT (**Figure 5.9** and **Table 5.6**). This difference in efficacy becomes evident when comparing the

concentrations. Specifically, 5 mg/mL of CHT + salts displayed an inhibition level equivalent to that of 1 mg/mL of CHT - salts (**Table 5.6**). Furthermore, the PIRG% of the acetic acid controls compared to 1, 2.5 and 5 mg/mL were not significantly different to each other. Conversely to CHT + salts, CHT - salts displays similar efficacy to CHT across the concentrations (**Table 5.6**). When comparing the effects of treatment on PIS% however, CHT - salts were more effective at reducing the number of spores than CHT at the concentrations of 1 and 2.5 mg/mL.

The effects of acetic acid were significantly different to the PDA control at both 0.15% and 0.1% with a marginally greater difference at 0.15%. The acetic acid controls were not significantly different to 0.5 mg/mL on radial growth for CHT, hydrolyzed CHT +/- salts. The acetic acid controls were significantly inhibitory on sporulation when compared to CHT (1 and 2.5 mg/mL), CHT - salts (1 mg/mL) and CHT + salts (1, 2.5 and 5 mg/mL).

5.4.7 The antifungal effects of aminochitosan batch-to-batch variants: D2 and D3

In Chapter 3, it was established that differences in the efficacy of the batch-to-batch variants, D1 and D2, were notable. Due to those notable differences in the tomato/*B. cinerea* pathosystem, the efficacy of D2 and D3 were additionally assessed on the growth and sporulation of *F. verticillioides* and compared to the effects of D1 and CHT.

As observed in Sections 5.4.5 and 5.4.6, there were no statistically significant differences in PIRG% between the concentrations of 2.5 – 5 mg/mL. As such, D2 and D3 were only assessed at the concentrations of 0.5, 1, and 2.5 mg/mL. Phenotypic differences between 5 and 11 dai were visible and distinct for CHT, D2 and D3; much like in 5.3.1 and 5.3.2. These phenotypic differences were particularly different for the higher concentrations evaluated in **Figure 5.10** where an increase in radial inhibition with an increase in concentration was also visible.

Table 5.7 shows that D2 and CHT exhibited similar and significant PIRG% at 1 and 2.5 mg/mL. in contrast, D3 displayed a lower and nonsignificant PIRG% at 1 mg/mL but significant PIRG% with a similar magnitude at 2.5 mg/mL (**Table 5.7**).

Table 5.7: The effects of different concentrations of chitosan, diamino 1, diamino 2 and diamino 3 on the average mycelial radial inhibition and sporulation of *F. verticillioides*, 5 and 11 days after incubation respectively.

		Radial Inhibition		**Sporulation**	
Treatment	Concentration (mg/mL)	Growth area (mm^2) ± SD	PIRG (%)	Spores/mL ± SD	PIS (%)
PDA	0	490.87 ± 0.00	0^{a}	201 667 ± 47 082	0^{a}
0,15% acetic acid	0	304.86 ± 16.77	38^{b}	56 667 ± 15 276	72^{b}
0.1% Acetic acid	0	327.26 ± 32.30	34^{b}	131 667 ± 68 405	35^{b}
Chitosan	0.5	346.3 ± 152.04	30^{ab}	195 900 ± 43 285	3^{a}
	1	63.09 ± 11.81	88^{cd}	107 063 ± 95 460	47^{ab}
	2.5	73.35 ± 18.4	86^{d}	133 188 ± 121 047	34^{ab}
	5	70.03 ± 8.54	86^{cd}	0.00 ± 0.00	100^{b}
PDA	0	490.87 + 0.00	0^{a}	201 667 ± 47 082	0^{a}
Diamino 1	0.5	255.71 ± 53.12	28b	NA	NA
	1	177.57 + 43.43	64^{b}	116 667 ± 5 774	43^{b}
	2.5	17.2 + 15.38	97^{b}	0.00 ± 0.00	100^{c}
PDA	0	490.87 ± 0.00	0^{a}	201 667 ± 47 082	0^{a}
Diamino 2	0.5	450.6 ± 90.04	9^{a}	95 400 ± 25 300	53^{b}
	1	60.87 ± 38.32	88^{b}	116 100 ± 8 153	43^{b}
	2.5	27.63 ± 19.20	95^{b}	134 500 ± 22 961	34^{ab}
PDA	0	490.87 ± 0.00	0^{a}	201 667 ± 47 082	0^{a}
Diamino 3	0.5	422.74 ± 152.34	14^{a}	309 000 ± 116 947	-53^{a}
	1	342.75 ± 202.82	31^{a}	237 500 ± 42 764	-17^{a}
	2.5	60.77 ± 21.20	88^{b}	373 100 ± 187 912	-85^{a}

PIRG% = percentage inhibition of radial growth (PIRG), and PIS% = percentage inhibition of sporulation (PIS). A negative PIS% indicates growth greater than the control. Statistical significance was calculated between concentrations for each polymer. Means ± SD (standard deviation) followed by the same superscript letter are not significantly different from each other. Different letters indicate significant differences between concentrations. The presence of two letters indicates either similarity or difference across multiple concentrations for that polymer (Kruskal-Wallis test followed by Dunn's *post hoc* test, $p < 0.05$). The values shown are the average of three experiments.

Furthermore, the PIS% for D2 and CHT were similar at 1 mg/mL. However, a decrease in the PIS% with an increase in concentration was observed for D2 instead of an increase with increasing concentrations as seen for CHT (**Table 5.7**). Additionally, D2 displayed greater PIS% at 0.5 mg/mL than CHT at 0.5 mg/mL. Conversely to D2 and CHT, D3 did not display any

inhibition on sporulation at all concentrations evaluated and instead displayed an increase in sporulation (**Table 5.7**).

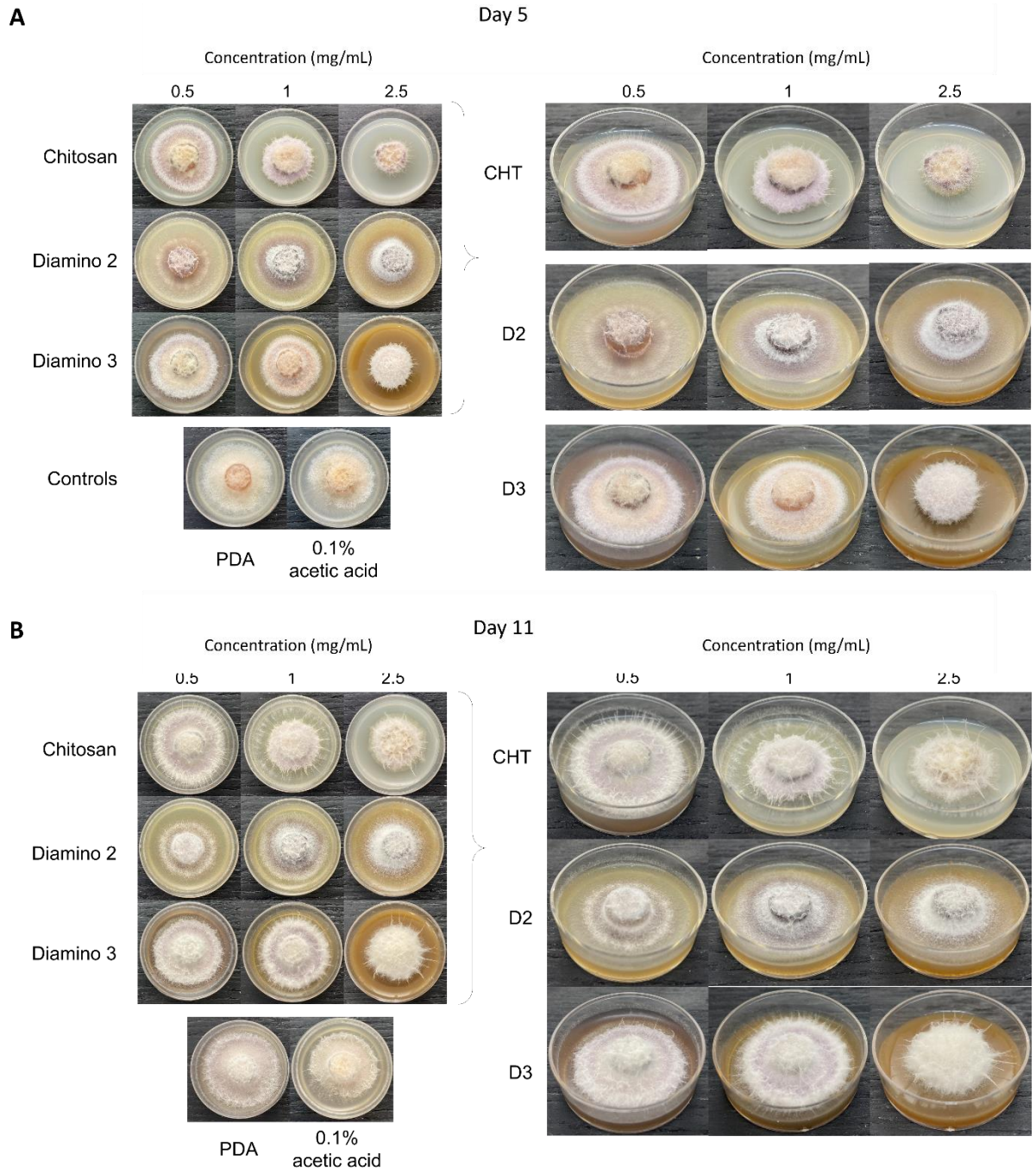

Figure 5.10: The direct effects of chitosan (CHT) and aminochitosan batches (diamino 2 (D2) and diamino 3 (D3)) on *F. verticillioides* growth at 5 days after incubation (dai) **(A)** and 11 dai **(B).** An overview of the phenotypic effects relative to the controls (PDA and 0.1% (v/v) acetic acid) and a more detailed image are shown. The images represent one of five biological replicates. The experiment was repeated once.

5.4.8 Phenotyping the *in planta* effects of diamino 1 in maize roots vs shoots

As no prior *in planta* plant studies on aminochitosan had been conducted, this was an exploratory analysis into the *in planta* effects of D1. HD1 was not assessed further given the

lack of antifungal activity while D1 was assessed at one concentration, 2.5 mg/mL, by two methods of application (**Figure 5.6**). The 2.5 mg/mL concentration was chosen for the analysis as the higher concentrations were not statistically different; they displayed the greatest inhibitory effects in the lower range of concentrations (Section 5.4.5).

The maize seedlings were treated "preventatively" with water or 2.5 mg/mL diamino 1 before being mock or *F. verticillioides* inoculated. **Figure 5.11** displays images captured by camera. Phenotypically, a change in the length of the shoots as well as the length and density of roots was visible with the establishment of an infection at 14 dpi (**Figure 5.11**). Roots were less dense and shorter with browning in successful infections. Additionally, seeds that were *F. verticillioides* inoculated displayed purple growth of *F. verticillioides* on the surface of the seed and a red discolouration.

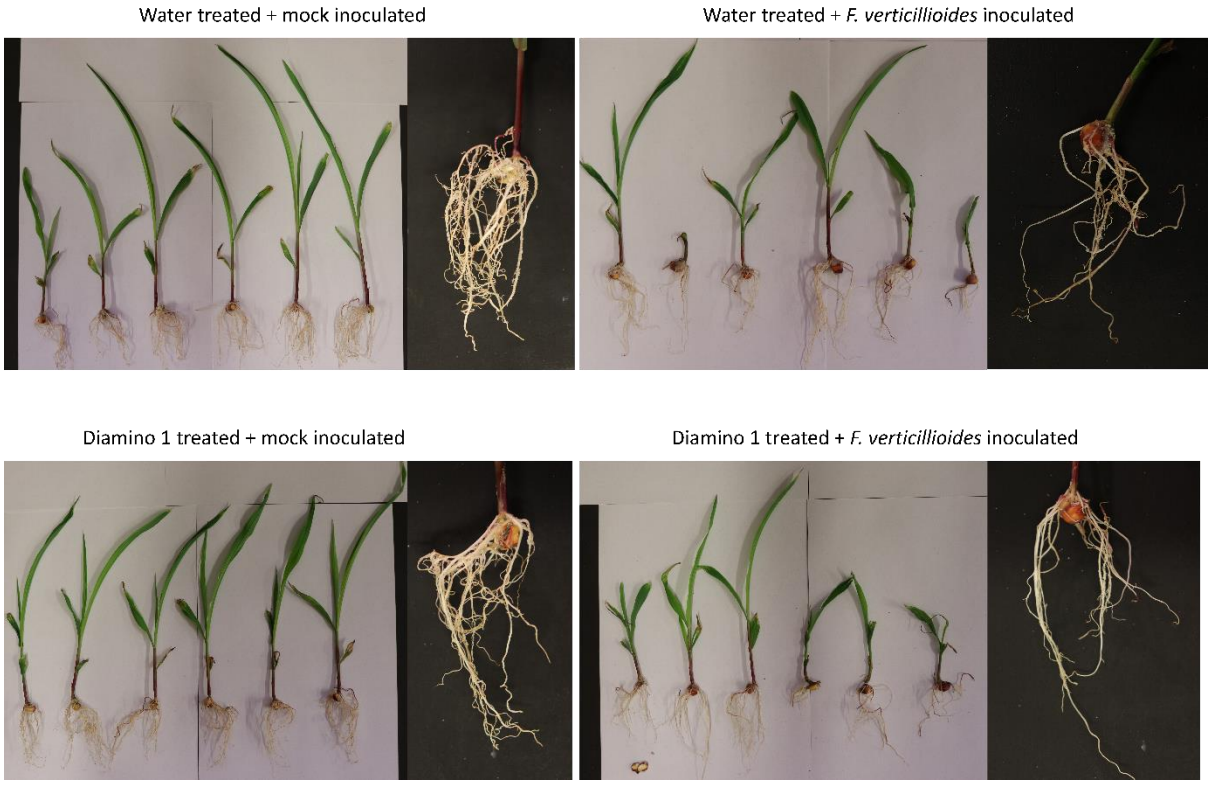

Figure 5.11: CML144 maize seedlings at 14 days post inoculation (dpi) after preventative treatment with water or diamino 1 and inoculation with water or *F. verticillioides*.

Furthermore, diamino 1 treated + mock inoculated shoots appeared consistent in shoot length whereas the water-treated + mock inoculated seedlings displayed variable shoot lengths. Compared to the water-treated + *F. verticillioides* inoculated seedlings, the diamino 1 treated + *F. verticillioides* inoculated seedlings displayed less stunting of growth with longer and more

dense roots. However, the above data is qualitative and was only conducted on 6 biological repeats.

5.4.9 Does aminochitosan modulate phytohormones production?

Two methods of aminochitosan applications were assessed at two time points to identify and understand the differences in defence response regulations with each method and the benefits thereof. To assess the effects of D1 and HD1 on the priming of plant hormones in root and shoot tissue, aminochitosan was applied preventatively and curatively (therapeutic) at a concentration of 2.5 mg/mL (**Figure 5.6**). The phytohormone analysis was conducted on the CML144 maize line.

Two independent targeted analyses were conducted on both root and shoot tissue. An initial trial analysis with 6 biological replicates was performed on 14-day-old root tissue for optimization of the extraction protocol. The following metabolites were targeted: indole-3-acetic acid (IAA), salicylic acid (SA), abscisic acid (ABA), jasmonic acid (JA), hexenylglucoside, zeatin, 2,4-Dihydroxy-7-methoxy-1,4-benzoxazin-3-one (DIMBOA) and deuterated 6 abscisic acid (d6-ABA, internal standard). The initial trial analysis displayed variation in the regulation of the hormones across the treatments between root and shoot tissue (data not displayed). Therefore, three time points, 0 h (T0), 12 h (T12) and 24 h (T24), were chosen to analyse the regulation and quantification by U-HPLC-MS of the above stated plant hormones at 3 earlier time points after treatment. T0 was subsequently excluded from the analysis as an error occurred during U-HPLC-MS process that resulted in the samples not being processed. The plant hormones, hexenyl glucoside, zeatin, and DIMBOA were excluded due to being lower than the limit of quantification.

Multivariate data analysis namely, Principal Component Analysis (PCA), was performed to determine any natural data groupings, relationships, or outliers with the inclusion of variables (metabolites) as vectors. These vectors indicate the direction and magnitude (by length) of each variable's correlation with PC1 and PC2. Variables that are closer to each other are strongly correlated and variables that are closer to a PC axis are more associated with that PC axis. The PCA score plots for T12 in **Figure 5.12A** do not show any clear groupings of treatments, infection, or methods of treatments due to large variations between the biological replicates (as only 3 biological replicates were used). The total variance explained by the two

PC axes is 64.1%. However, the PCA score plots for T24 show a marginally clearer separation of samples by infection and methods of treatment. In **Figure 5.12B**, D1 and HD1 applied by the preventative method + *F. verticillioides* inoculated samples cluster separately to the mock inoculated samples and curatively treated samples and have a positively corelated relationship with SA.

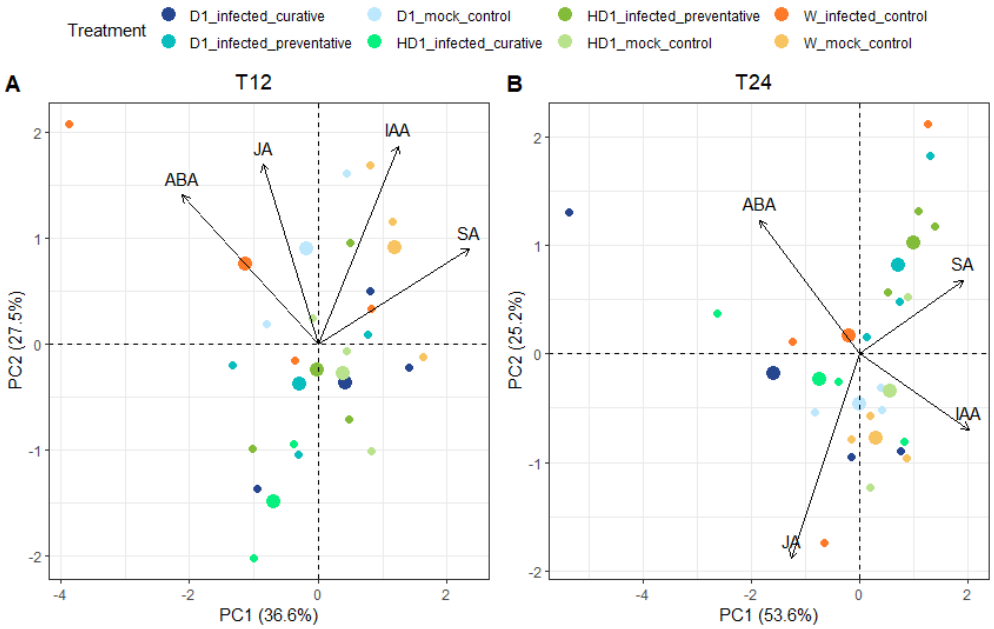

Figure 5.12: Principal component analysis (PCA) score plots of the metabolites (JA, SA, ABA and IAA) at different time points in root The plots represent the data points from different sampling time points: **A =** 12 h (T12), **B =** 24 h (T24). The plots also display the variables (metabolites) as vectors. They convey information about the relationship between the variables and the principal components. The data compares polymers and control (diamino 1, hydrolyzed diamino 1 and water), types of treatment (preventative, curative, control) and infection (mock, *F. verticillioides*).

Conversely, the mock inoculated samples of D1, HD1 and water, cluster separately from the above, but do cluster together with the HD1 and D1 curative method + *F. verticillioides* inoculated samples (**Figure 5.12B**). The JA vector is closer to the PC1 axis and is therefore more associated with it, and the total variance explained by PC1 and PC2 is 78.8 %.

From **Figure 5.13**, JA and SA are regulated antagonistically as seen by the inverse accumulation at 12 and 24 h. For both the curative and preventative methods, SA levels were higher at 12 h than 24 h while JA levels were lower at T12 and T24. At T24 for the preventative method, a significant fold change for JA was obserevd for HD1 and D1 at 4.09 and 3.55 respectively ($p < 0.05$) with a greater effect being seen for the preventative method compared to the curative method (**Figure 5.13**). No clear effect can be observed for SA and ABA at both T12 and T24 for

the curative and preventative methods or controls. For IAA, a significant fold change of 1 was observed at T12 for D1 treated + mock inoculated (control) samples relative to water.

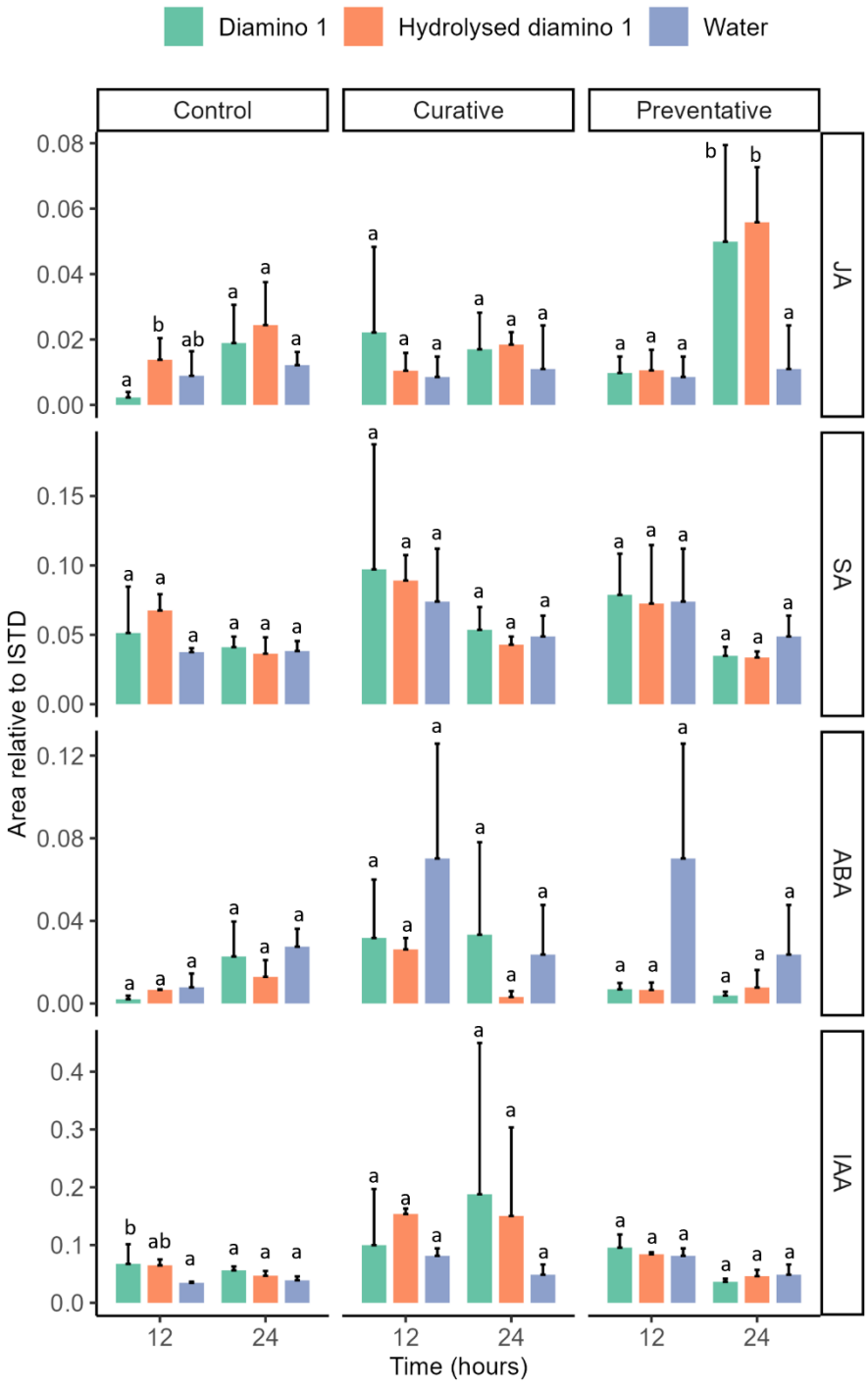

Figure 5.13: Analysis of plant hormones in tomato leaflets after treatment with the polymers using different methods (curative, preventative) at 12 and 24 h after *F. verticillioides* or mock inoculation (control). The peak area relative to the internal standard (ISTD, d-6 ABA) is shown. Abbreviations: jasmonic acid (JA), salicylic acid (SA), abscisic acid (ABA and indol-3-acetic acid (IAA). Significant differences between biopolymer treatments for each time point are shown with different letters. Significance was determined by Kruskal-Wallis test followed by Dunn's *post hoc* test, $p < 0.05$). Error bars represent SD for n = 3

5.5 Discussion

Due to COVID-19 and the lockdowns imposed during 2020-2021, experiments to determine the effects of aminochitosan on fungal quantification, fumonisin accumulation, phytoalexin accumulation and gene regulation of the phytoalexin genes in root and shoot tissue could not be conducted.

5.5.1 *F. verticillioides* preferentially accumulates in 10 and 14 dpi CML144 roots

As an endophyte of maize, *F. verticillioides* may present as asymptomatic through a growing season while existing as an intercellular biotrophic infection with the potential to become an intracellular infection with the appropriate environmental stresses. The early stages of *F. verticillioides* have been well characterized by Bacon et al. (2001), Oren et al. (2003) and Wu et al. (2011) who have demonstrated that an endophytic seed infection generally presents within the first 10 days after germination, typically by the second day, with systemic movement of the fungus to roots and aboveground tissue following thereafter (Bacon et al., 2001; Oren et al., 2003; Wu et al., 2011). However, the progression from crown to stalk tissue, and ultimately kernels, is the rate limiting step in the movement to above ground maize tissue with seed transmission of systemic infection to above ground tissue being significantly less effective than inoculated crowns, stalks and silks (Munkvold, McGee & Carlton, 1997).

In this chapter, quantification of fungal growth revealed higher *F. verticillioides* growth in roots than in shoots at 14 dpi, with no growth in 10 dpi shoots. This result is validated by previous studies using GFP- and Ds-red-tagged *F. verticillioides* to observe the spread of infection in maize seedlings where *F. verticillioides* growth was predominantly in root tissue of 14-day-old seedlings (Oren et al., 2003; Wu et al., 2011). Seed inoculation did not result in an obviously detectable infection while soil inoculation produced a more pronounced infection (Oren et al., 2003). Furthermore, minimal amounts of mycelia were detected by fluorescent microscopy in above-ground tissue at 14 dpi but, growth was observed from stems plated on minimal media. These results validate the movement of fungi to above-ground tissue in the initial stages of the interaction, yet minimal fungal biomass was formed during these early infection stages (Oren et al., 2003).

Wu et al. (2011) observed a decrease in the colony forming units (CFU) of *F. verticillioides* in root tissue over time but an increase in CFU in stem tissue over time thereby demonstrating the systemic movement of *F. verticillioides* to above-ground tissue instead of continual root propagation. Similar results were observed in this chapter as the biomass of *F. verticillioides* in the roots decreased between 10 and 14 dpi, coinciding with the increase in stem and shoot biomass. Furthermore, in this chapter, growth of GFP-tagged *F. verticillioides* in inoculated seedlings at 14 dpi was limited to root tissue as seen by the GFP signal in the elongation and differentiation zones (**Figure S5.6**). This result is consistent with Wu et al. (2011) who observed that during early stages of *F. verticillioides* infection, the elongation zones of the roots were mainly infected. Wu et al. (2011) and Oren et al. (2003) stated that their observations demonstrated a common mechanism of early colonization where *F. verticillioides* first attached to lateral roots and root hairs before penetrating the cuticle and epidermis to develop in intercellular spaces for varied lengths of time (Oren et al., 2003; Wu et al., 2011).

5.5.2 FB_1 predominantly accumulates in CML144 roots at 10 and 14 dpi

Earlier studies on fumonisin production assumed that fumonisins were produced late in the plant-pathogen interaction or on damaged/dead tissue during saprophytic growth. However, much evidence to support the presence of low-high concentrations of fumonisins in endophyte infected asymptomatic tissue as well as early production in maize seedlings has since been published thus proving that the asymptomatic endophytic growth stage is physiologically active (Bacon et al., 2001; Williams et al., 2007; Zitomer et al., 2010; Baldwin et al., 2014). Fumonisins contribute to disease expression and are necessary for the induction of leaf lesions in *F. verticillioides* maize seedling disease. However, root infection is necessary for FB_1 accumulation in leaves but colonization of the leaf itself is not necessary for the accumulation (Williams et al., 2007; Baldwin et al., 2014). Additionally, fumonisin levels were shown to be significantly higher in root than shoot tissue (Bacon et al., 2001; Williams et al., 2007).

Therefore, in this chapter, FB_1 was to be expected in root tissue and was detected at significantly higher levels at 14 dpi than at 10 dpi. Zitomer et al. (2010) demonstrated that FB_1 preferentially accumulated in roots over FB_2 and FB_3 which supports the data in this chapter. Owing to the impact of the COVID-19 pandemic, we were unable to conduct the experiments

aimed at evaluating the efficacy of aminochitosan in mitigating fumonisin levels in maize seedlings. However, Ferrochio et al. (2014) and Zachetti et al. (2019) demonstrated that the combined effects of CHT (3.42 kDa, DDA > 77%) and water activity on growth and mycotoxin production of *F. verticillioides*, *F. proliferatum* and *F. graminearum* in maize grain and maize media was positively inhibited at 2 mg/mL, 2 mg/mL, and 0.5 mg/mL respectively.

5.5.3 Phytoalexins and their biosynthetic genes accumulate preferentially in CML144 infected maize roots

Terpenoids are essential secondary metabolites for plant growth, development and in plant defence to biotic and abiotic challenges (Tholl, 2006). Terpenoid phytoalexins, specifically the diterpenoid kauralexins and sesquiterpenoid zealexins, have been shown to accumulate in both resistant and susceptible maize lines in response to abiotic (drought and salt) and biotic (*F. graminearum* infection, *Ostrinia nubilalis* herbivory, *Cochliobolus heterostrophus* and *U. maydis* infection) stressors as well as exhibit antimicrobial activity (Huffaker et al., 2011; Schmelz et al., 2011; Vaughan et al., 2015; Christie et al., 2017; Meyer et al., 2017). We analysed the effects of *F. verticillioides* infection in 10- and 14-day old CML144 maize roots and shoots.

In this chapter, phytoalexin accumulation was induced in response to *F. verticillioides* seed-inoculation in both the roots and shoots of the susceptible maize line CML144, but accumulation was significantly greater in the roots than shoots at 10 and 14 dpi. Furthermore, the total kauralexin accumulation was significantly greater than total zealexin accumulation in roots at 10 and 14 dpi. This contrasts with Vaughan et al. (2015) who observed higher total zealexin levels in 4-week-old roots of Golden Queen maize in response to *F. verticillioides* infection. Similarly, Meyer et al. (2017) reported higher levels of zealexins than kauralexins in maize leaves inoculated with *Cercospora zeina* in a *C. zeina* susceptible (RIL165) and *C. zeina* resistant (RIL387) maize line. However, it should be noted that this variation may arise from differences in the age of the roots, the maize genotype, and the inoculation methods employed. Although zealexins have previously been shown to accumulate in uninfected seedlings (Huffaker et al. 2011), they were not detected in the mock inoculated roots and shoots of CML144 at 10 dpi with extremely low accumulation at 14 dpi.

This chapter demonstrated that fungal growth and kauralexin accumulation were positively regulated with the kauralexin biosynthetic genes, *ZmKO*, *ZmKL2*, *ZmKSL4* and *CYP81A1* and zealexins with the zealexin biosynthetic gene, *ZmTPS11*. Kauralexins and zealexins have previously been shown to be coregulated in response to fungal infection with the expression of their biosynthetic genes and accumulation of metabolites increasing with an increase in fungal inoculum (Huffaker et al., 2011).

In this study, total kauralexins B accumulated to a higher level than kauralexins A at 10 and 14 dpi. This contrasts with Veenstra et al. (2018) and Meyer et al. (2017) were kauralexins A where more abundant in the resistant maize lines CML444 and RIL 387 and respectively. However, like Schmelz et al. (2011) and Meyer et al. (2017), we observed that KA3 and KB3 were the most abundant metabolites of the A and B series at 14 dpi with *F. verticillioides* infection. Schmelz et al. (2011) demonstrated that KB3 treatment directly reduced *F. verticillioides* and *Rhizopus microsporus* growth by 30% as well as *Colletotrichum graminicola* by 50-60 % at 10 µg/mL for both KA3 and KB3. However, the efficacy of both KA3 and KB3 appear to be pathogen-specific as KA3, at the same concentration (10 µg/mL), was not effective at reducing the growth of *R. microspores* (Schmelz et al., 2011).

5.5.4 High concentrations of aminochitosan causes excessive branching of mycelia

The inhibitory properties of CHT has been well documented with the results varying and dependent on the CHT derivative and fungal species analyzed (Goy, Britto & Assis, 2009). In this chapter, significant inhibition of radial growth and sporulation with D1 treatment was observed at a minimum concentration of 1 mg/mL at 5 dpi. However, unlike *B. cinerea* in Chapter 3, this was not sustained at 11 dai as seen by the significant changes in mycelia morphology with the increase in concentration between 2.5-5 mg/mL of D1. The fungal growth on D1 amended media displayed excessive branching of mycelia with a "hair-like" appearance, extending upwards and outwards without direct contact with the media. Comparable results for the change in mycelia morphology were observed for CHT. A review by Bautista-Baños et al. (2016) summarized the effects of CHT derivatives (different concentrations) on the morphology and ultrastructure of a range of fungi using light, confocal, scanning and transmission electron microscopy. Herein, *Fusarium* species treated with CHT

between 0.5-3 mg/mL displayed the following morphological changes to hyphae and conidia: abnormal shape with contortion, presence of vesicles, excessive vacuolation, empty cells and cytoplasm leakage with the exception of excessive branching (Bautista-Baños et al., 2016 and the references therein). However, studies on other genera including *B. cinerea* (1 and > 1.5 mg/mL), *Alternaria alternata* (0.5 m/mL), *Penicillium expansum* (1 mg.mL), *Sclerotinia sclerotiorum* (1, 2, 4 % w/v) and *Rhizopus stolonifer* (0.5-1.5 mg/mL) displayed excessive branching as well as swelling and abnormally shaped and reduced hyphae (Oliveira Junior, Melo & Franco, 2012; Bautista-Baños et al., 2016 and the references therein). The results for *B. cinerea* and *A. alternata* however were not consistent across studies with excessive branching specifically not being observed (El-Ghaouth et al., 1992). Therefore, morphology of conidia and mycelia appear to be differentially affected and is dependent on the fungal species, time of incubation, derivative, concentration, DP and FA of CHT (El-Ghaouth et al., 1992; López, Molina & Baños, 2004; Oliveira Junior, Melo & Franco, 2012; Bautista-Baños et al., 2016).

As previously mentioned in Chapters 2 and 3, aminochitosan bears similarity to polyamines (PA) in its physiochemical properties and effects as PAs are known to strongly induce the branching of hyphae in arbuscular mycorrhizal fungi. A study by Cheng et al. (2012) demonstrated that PAs acted as branching factors. They significantly stimulated, enhanced, and altered the branching of hyphae in a concentration-dependent manner. Moreover, they prolonged branching lifespan up to 10 and 11 days, unlike the control group where branching ceased by day 8 (Cheng et al., 2012). Therefore, the concentration-dependent change in the excessive branching until 11 dai may be as a result of aminochitosan acting as a branching factor in a comparable manner. Alternatively, the excessive branching may be a result of F. verticillioides utilizing aminochitosan as a nutrient source. There appears to be a preference for an increased number of amine groups in the concentration range of 2.5-5 mg/mL, which appear optimal for continued abnormal mycelia growth. However, an inhibitory effect is observed at 11 dai. This is in contrast to Chapter 3 where *B. cinerea* utilized amine groups preferentially at low concentrations of aminochitosan (Chapter 3, Section 3.4.1). As described earlier, CHT displays pleiotropic antifungal effects that are dependent on the genera of the fungi, their sensitivity and capacity to utilize CHT as well as detoxify or dispose thereof once inside the cell (Palma-Guerrero et al., 2007). However, further analysis on the effects of

aminochitosan on the ultrastructure of *F. verticillioides* mycelia, hyphae and spores is required to corroborate the above conjecture.

5.5.5 Hydrolyzed polymers lose antifungal efficacy due to high levels of salts

According to the definition of Lodhi et al., (2014), CHT oligomers are synthesized by chemical, physical or enzymatic hydrolysis of CHT to yield low MW oligomers of < 16 kDa that generally range between 0.2-3 kDa with a DP < 20 (Lodhi et al., 2014). Thus, following this definition, HD1 is theoretically an aminochitosan oligomer/oligosaccharide. Given the abolishment of all antifungal activity with HD1 treatment, we hypothesized that the differences in the efficacy between D1 and HD1 was possibly due to the following: the low MW of HD1 is non-functional/below the threshold for biological activity; the hydrolysis process yielded a polymer with a high concentration of salt thus reducing the accuracy of the concentrations assessed as the majority of dissolved solute would be salt; and that salt may contribute to the observed increase in sporulation. As a result, native CHT was compared to hydrolyzed CHT + salts (excess salts not removed), hydrolyzed CHT - salts (salts removed) and NaCl used as a control for the minimum inhibitory salt concentration.

In Chapter 3 Section 3.4.1, the MW range of 3.5-15 kDa (F1) appeared to be the most effective for antifungal activity (radial growth and sporulation) against *B. cinerea* at concentrations of 0.5, 1, and 2.5 mg/mL. In contrast to D1 treatment on *F. verticillioides* and F1 on *B. cinerea*, HD1 treatment on *F. verticillioides* did not display any antifungal activity at the concentrations of 1, 2.5, 5, 7.5 or 10 mg/mL. Furthermore, sporulation of *F. verticillioides* was positively regulated at all concentrations of HD1 assessed.

The results from this chapter showed that hydrolyzed CHT + salts treatment on *F. verticillioides* growth displayed similar results to HD1 where no significant antifungal activity was observed at 0.5, 1 or 2.5 mg/mL. However, hydrolyzed CHT - salts displayed antifungal activity that resembled that of CHT and D1 indicating that the removal of salts restored antifungal activity. The NaCl controls displayed no change in radial growth between 50-150 mEq. However, significant change in radial growth was observed between 200-300 mEq with 300 mEq inhibiting all radial growth. These results are validated by the Boumaaza, Benkhelifa & Belkhoudja (2015) study that compared the impact of sodium and calcium salts on *B. cinerea* growth and sporulation. They observed that concentrations up to 150 mEq of NaCl

significantly stimulated *B. cinerea* growth but that at concentrations of ≥ 300 mEq, mycelial growth was inhibited (Boumaaza, Benkhelifa & Belkhoudja, 2015).

Attjioui, et al. (2021) assessed the inhibition of *F. graminearum* with CHT (DP 300), the product of its hydrolysis with ~ DP 70 and two fractions of the hydrolysate (DP 90 and oligomers DP 2-17). They observed that CHT DP 300, its hydrolysis product (DP 70) and the larger fraction DP 90 had similar minimum inhibitory concentrations of 100 µg/mL (0.1 mg/mL). In contrast, the oligomer fraction displayed weaker activity with minimum inhibitory concentrations of 200 µg/mL (0.2 mg/mL). They hypothesized that oligomers display weaker antifungal activity as these fractions cannot disrupt the cell membrane and that synergy between long polymers and oligomers are necessary. Thus, long polymers destabilize the cell membrane allowing the oligomers (shorter polymers) to penetrate the cell and interact with the intracellular components (Attjioui et al., 2021; Lemke, Jünemann & Moerschbacher, 2022).

Furthermore, in this chapter, sporulation of the NaCl control displayed a concentration-dependent increase in sporulation up to 200 mEq with significant inhibition only observed at 300 mEq. Boumaaza, Benkhelifa, and Belkhoudja (2015) noted that in the absence of salt, B. cinerea isolates displayed a different conidial production profile compared to those stimulated by NaCl up to 300 mEq. This finding contrasts with the results presented in this chapter, where 300 mEq significantly inhibited sporulation. HD1 exhibited sporulation results similar to those of the NaCl control, where sporulation was stimulated. Conversely, CHT + salts showed only a moderate decrease in inhibitory effects compared to CHT - salts and CHT alone. This difference could potentially be attributed to variations in molecular weight and degree of polymerization following hydrolysis. The mechanisms by which sodium salts affect mycelial growth are unknown, but a study by Zahran (1997) postulated that hydric stress changes physiology and morphology in response to increased osmotic pressure citing “cells are usually elongated, swollen and showing shrinkage, in addition to changes in the cell and cytoplasmic volume” (Zahran, 1997). Therefore, the MW, DP, resulting absence of long polymers and high concentrations of salt for the oligomers, HD1 and hydrolyzed CHT + salts, may synergistically affect the antifungal efficacy of CHT. However, further analysis into the structural and chemical properties of the biopolymers are needed to corroborate the above statement.

5.5.6 Batch-to-batch variants: the antifungal effects on *F. verticillioides*

Due to the different sources, properties and variable polymer chain length of the starting material chitin and the processing methods for CHT synthesis, obtaining consistent and reproducible batch-to-batch CHT biopolymers is challenging (Croisier & Jérôme, 2013). These factors are potential limitations in the full application of CHT and obtaining aminochitosan with consistent physiochemical properties is key (Sayed, 2018).

The results from Chapter 3 highlighted the variations in the efficacy of the batch-to-batch variants, D2 and D3. In this chapter, both D2 and D3 displayed significantly similar inhibitory activity on radial growth for 0.5, 1 and 2.5 mg/mL but different effects on sporulation. D2 displayed significant antifungal activity from 0.5 mg/mL with a concentration-dependent decrease with an increase in the concentration. This contrasts with Chapter 3 Section 3.3.1 where D2 did not display any significant activity at 0.5 or 1 mg/mL but was instead only significantly inhibitory at 2.5 mg/mL. D3 in Chapter 3 Section 3.3.5.2 significantly inhibited sporulation at all concentrations assessed while in this chapter, D3 stimulated sporulation at all concentrations assessed.

Considering that D3 displayed the highest ratio of Nitrogen (10.10%) of the batch-to-batch variants and that nitrogen has been shown to support and enhance fungal growth, the difference in efficacy of D3 in this chapter may be due to the different microbial species and associated microbial factors or the agglomerative nature of CHT (Harper, Strange & Langcake, 1981; Kong et al., 2010; Lee, Koo & Park, 2016; Verlee, Mincke & Stevens, 2017). Furthermore, CHT sensitive and resistant fungi belong to different taxonomical groups that are based on their membrane fluidity; this affects the biological activity and mode of action of CHT (Palma-Guerrero et al., 2010). The study by Palma-Guerrero et al. (2010) demonstrated that the phospholipid fatty acid cell composition of cell membranes for sensitive fungi contained elevated levels of unsaturated fatty acids compared to resistant fungi. CHT resistant fungi are therefore unable to permeabilize the cell membrane and instead remain outside. Thus, due to its elevated fatty acid content, *B. cinerea* is classified as a CHT-sensitive fungus. While no classification has been made for *F. verticillioides*, *Fusarium oxysporum* f. sp*. radicis-lycopersici* and *Fusarium equiseti* have been classified as CHT sensitive (Palma-Guerrero et al., 2010).

5.5.7 Aminochitosan and the temporal induction of phytohormones

Phytohormones such SA and JA play a pivotal role in enhancing host resistance against both biotrophic and hemi-biotrophic pathogens (Glazebrook, 2005). These hormones can stimulate the synthesis of defence proteins, secondary metabolites, signalling pathways, and PCD, collectively limiting the pathogen's growth. However, a whole cohort of phytohormones that exhibit intricate crosstalk between each other are regulated by pathogens as part of plant defence (Pieterse et al., 2012). As such, a combination of JA and ET (Huffaker et al., 2011; Schmelz et al., 2011), and ABA (Vaughan et al., 2015) have been shown to induce terpenoid phytoalexins, specifically kauralexin accumulation, in maize roots (Schmelz et al., 2011, 2014; Meyer, Murray & Berger, 2016). Therefore, considering that SA and JA display antagonistic regulation (Pieterse et al., 2012; Thaler, Humphrey & Whiteman, 2012) and that *F. verticillioides* is a hemi-biotroph, the potential temporal priming of these defence pathways is key. Additionally, the impact of fumonisins on plant health and immunity characterized by the disruption of sphingolipid metabolism; and recognizing the significant influence of phytohormones in this context; it is important to investigate whether aminochitosan exerts any modulatory effects on phytohormones levels post-treatment or post-infection. This becomes particularly key in the context of fumonisin-induced impairment of plant immunity and PCD, where higher phytohormone levels may protect against the adverse effects of FB_1.

In this chapter, the mock inoculated D1, HD1 and water samples clustered separately to the *F. verticillioides* inoculated samples at T24 indicating the establishment of an infection and the differential regulation of phytohormones as a result. This is in keeping with the early establishment of an infection within 24 h after inoculation (Bacon et al., 2001; Oren et al., 2003). The mock inoculated sample of D1, HD1 and water do however cluster with the HD1 and D1 curatively treated + *F. verticillioides* inoculated samples at T24. This indicates that aminochitosan application after *F. verticillioides* inoculation potentially impedes the normal infection timeline either due to direct antifungal effects or potential differential regulation of JA and IAA, which was significantly upregulated at T12 in mock samples of HD1 and D1 respectively. In contrast to the analysis on antifungal activity, it appears that HD1 displays some efficacy *in planta*, highlighting the role of the plant physiology and defence in the bi-modal activity of aminochitosan. In addition, the combination of long polymers and short

oligomers may be more of a necessitating factor for antifungal activity than *in planta*, where oligomers retain their functionality.

Unlike the antifungal activity analysis of HD1, application of HD1 *in planta* displayed efficacy. D1 and HD1 preventatively treated + *F. verticillioides* inoculated samples clustered separately to the control, water-treated + *F. verticillioides* inoculated samples. This potentially indicates an effect of aminochitosan treatment on the regulation of phytohormones at T24, distinct from the effects of an establishing infection. Furthermore, D1 and HD1 preventatively treated + *F. verticillioides* inoculated samples, JA accumulated significantly at T24 compared to the water-treated samples. SA ad JA were antagonistically regulated at T12 and T24 for the controls, curative and preventative treatments. The correlation between SA/JA regulation and fumonisin accumulation should be analyzed in future with a more time point focused analysis on phytohormone accumulation. Beccaccioli et al. (2021) demonstrated that the "timing of hormone accumulation correlates with the transition from a biotrophic growth to a necrotrophic lifestyle for *F. verticillioides*" and " that the activation of the JA signalling pathway follows the activation of SA-mediated pathways" (Beccaccioli et al., 2021). Another study (Ding et al., 2011) reported observing higher concentrations of endogenous SA during the early stages of infection (first few hours) followed by an increase in the endogenous concentrations of SA as the infection and time progressed.

CHT oligosaccharides have been shown to activate both SA and JA when induing resistance to *Pseudomonas syringae* pv. tomato DC3000 infection in *Arabidopsis* (Jia et al., 2016, 2018). However, in this study the curative and preventative methods of treatment appear to be enhancing a differential regulation of SA and JA. The preventative method appears to be regulated as in Ding et al. (2011) where SA is upregulated at T12, followed by a rise in JA at T24, while the curative method is oppositely regulated at T12 and T24, with JA upregulated at T12 and SA at T24. The curative method of treatment seeks to treat an already "establishing infection" and it can thus be assumed that upon aminochitosan treatment, *F. verticillioides* has already entered its necrotrophic phase. In contrast, the preventative method of treatment aims to prime a defence response thereby reducing the incidence of infection. Therefore, in the preventative treatment, SA accumulation during the early stages of infection plays an important role in the biotrophic phase whereas in the curative treatment, JA is a key contributor to resistance during the necrotrophic phase. The switching between SA and JA

regulation at precise times, specifically at the onset of the necrotrophic phase, allows for a more efficient and effective defence response mounted against *F. verticillioides* (Ameye et al., 2015). Christensen et al. (2014) highlighted the importance of JA-mediated defence in maize against *F. verticillioides* infection by assessing a novel 9-LOX gene, *ZmLOX12,* in mutant plants. They showed increased susceptibility to infection coupled with reduced JA levels in mutant plants (Christensen et al., 2014). Another study by Ameye et al. (2017) demonstrated that Z-3-hexanyl acetate pretreatment of hormone-treated and inoculated seeds resulted in enhanced JA-dependent defences during the necrotrophic phase of *F. graminearum* infection with a suppression of SA during the biotrophic phase. However, more biological replicates as well as time points are needed for a robust analysis. Moreover, the methodology set-up for characterizing the curative vs preventative methods of treatment should be refined and improved upon as they are currently sub-optimally designed.

5.6 Conclusion

This chapter aimed at broadly investigating the effects of aminochitosan in a pathosystem comprising of a monocotyledon plant and toxigenic fungus namely, the maize/*F. verticillioides* pathosystem, and represents the first study investigating aminochitosan in this pathosystem. We first demonstrated the effects of *F. verticillioides* infection on the defence response of the susceptible maize line, CML144. We showed that fungal growth and phytoalexin accumulation were positively regulated with the kauralexin and zealexin biosynthetic genes in 14-day old maize roots. Furthermore, fumonisins, specifically FB_1, were significantly accumulated in the roots of 14-day old maize roots. Overall, the roots of maize seedlings were preferentially affected compared to the shoot tissue.

Aminochitosan, specifically D1, treatment resulted in significant inhibition of radial growth and sporulation at a minimum concentration of 1 mg/mL. The effects were concentration-dependent with an increase in efficacy as concentrations increased. Further antifungal effects were noted on the morphology of the mycelia after treatment with aminochitosan where mycelia displayed an increase in length and excessive branching with an increase in concentration. However, these effects were abolished when D1 was hydrolyzed into its oligomer derivative. The hydrolyzed polymer of D1, HD1, did not display any inhibitory efficacy and instead resulted in an increase in sporulation. By analysing hydrolyzed CHT with

and without salts, it was deduced that high concentrations of salt were a contributing factor to the reduced antifungal efficacy. However, further analysis is required to determine the contribution of MW and DP to the reduced functionality of HD1 in antifungal assays, allowing for a better understanding of aminochitosan oligomers, their functionality and optimal MW range.

Compared to D1, differences in the inhibition of sporulation for aminochitosan batch-to-batch variants, D2 and D3 were noted, with no differences in the radial growth inhibition. As such, all *in planta* analyses were only conducted on D1 and HD1. In contrast to the antifungal activity analysis, HD1 displayed some efficacy *in planta*, highlighting the role of the plant physiology and defence in the bi-modal activity of aminochitosan. The pre-treatment and post-inoculation treatment of leaves with D1 and HD1 resulted in different temporal regulation of SA and JA. The curative treatment resulted in an increase of JA at T12 and SA at T24 while the preventative treatment resulted in an increase of SA at T12 and JA at T24. Therefore, SA and JA were antagonistically regulated in the different methods of treatment. Thus, in the preventative treatment, SA accumulation during the early stages of infection plays an important role in the biotrophic phase whereas in the curative treatment, JA accumulation was a key contributor to resistance during the necrotrophic phase.

Future studies assessing the impact of aminochitosan on phytoalexin accumulation, phytoalexin gene expression and fumonisin accumulation will further the understanding of the mechanisms of action and efficacy of aminochitosan.

5.7 Addendum: Supplementary phytoalexin data

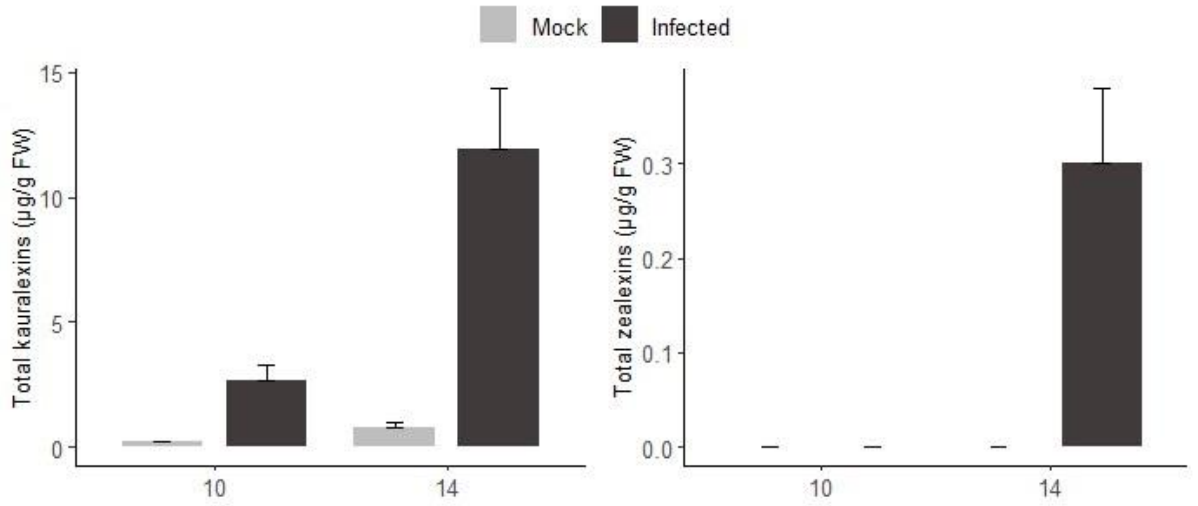

Figure S5.1: GC-MS analysis of total kauralexin accumulation in CML144 shoots 10- and 14-days post *F. verticillioides* seed inoculation (dpi). Error bars indicate standard deviation (SD), n = 3. No significant differences between mock/infected samples were observed.

Figure S5.2: The phenotype of mock and *F. verticillioides* inoculated root tissue 14 days post inoculation (dpi). Root browning, seed discoloration and fungal colonization of seeds are visible in the infected tissue compared to the mock inoculated roots.

Table S5.1: Accumulation of individual kauralexin A1, A2, A3, B1, B2, B3 compounds and zealexins A1 and B1 compounds in CML144 roots at 10 dpi and 14 dpi with *F. verticillioides*. Average values (n=3) are shown. An unpaired t test was performed on log_{10}-transformed phytoalexin data to measure statistical significance between inoculated and control tissue.

Metabolite (µg/g FW)	10 days		14 days	
	Mock	*F. verticillioides*	Mock	*F. verticillioides*
KA1	0.09	0.84	0.09	1.87
KA2	0.05	0.75	0.11	2.35
KA3	0.30	5.96	0.22	13.01
Total KA	0.44	7.55	0.42	17.23
KB1	**0.16**	**1.36**	0.12	2.88
KB2	**0.14**	**2.34**	**0.12**	**5.90**
KB3	0.42	4.89	0.24	9.50
Total KB	0.73	8.59	0.49	18.28
Total K	**1.17**	**16.14**	**0.90**	**35.51**
ZA1	0.00	1.38	0.05	1.26
ZB1	**0.00**	**4.08**	**0.10**	**4.51**
Total Z	0.00	5.46	**0.15**	**5.77**

Shaded blocks and bold numbers represent a significant difference in accumulation between treatment and control ($p<0.05$).

Table S5.2: Accumulation of individual kauralexin A1, A2, A3, B1, B2, B3 compounds and zealexins A1 and B1 compounds in CML144 shoots at 10 dpi and 14 dpi with *F. verticillioides*. Average values (n=3) are shown. An unpaired t test was performed on log_{10}-transformed phytoalexin data to measure statistical significance between inoculated and control tissue.

Metabolite (µg/g FW)	10 days		14 days	
	Mock	*F. verticillioides*	Mock	*F. verticillioides*
KA1	0	0.03	0	0.15
KA2	0.01	0.03	0.01	0.26
KA3	0.07	0.48	0.07	1.88
Total KA	0.08	0.54	0.08	2.28
KB1	0.02	0.23	0.13	0.8
KB2	0.03	0.31	0.11	2.11
KB3	0.08	1.59	0.51	6.72
Total KB	0.13	2.13	0.74	9.63
Total K	0.21	2.67	0.82	11.91
ZA1	0	0.01	0	0.05
ZB1	0	0.04	0	0.25
Total Z	0	0	0	0.3

No significant differences were observed due to large standard deviations in the accumulation of individual A and B metabolites.

5.8 Evaluating the fitness of GFP-transformed *F. verticillioides* transformants

The *F. verticillioides* GFP transformants that were selected for further use were analysed for fitness costs due to the GFP transformation process (**Figure S5.3**)

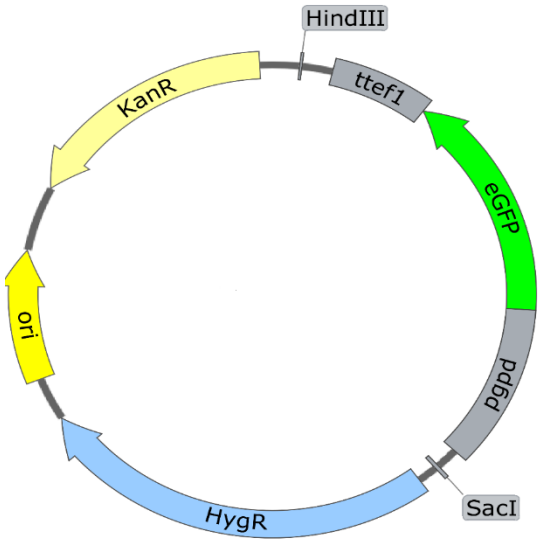

Figure S5.3: The plasmid pII99 containing the *GFP* gene. This figure was adapted from Jiang Tan, PhD thesis, Gent University, 2021.

Seven GFP-transformants were selected for further analysis and subsequently named: FvGFP 3, FvGFP 6, FvGFP 9, FvGFP 10, FvGFP 14, FvGFP 15 and FvGFP 16 (**Figure S5.4**)

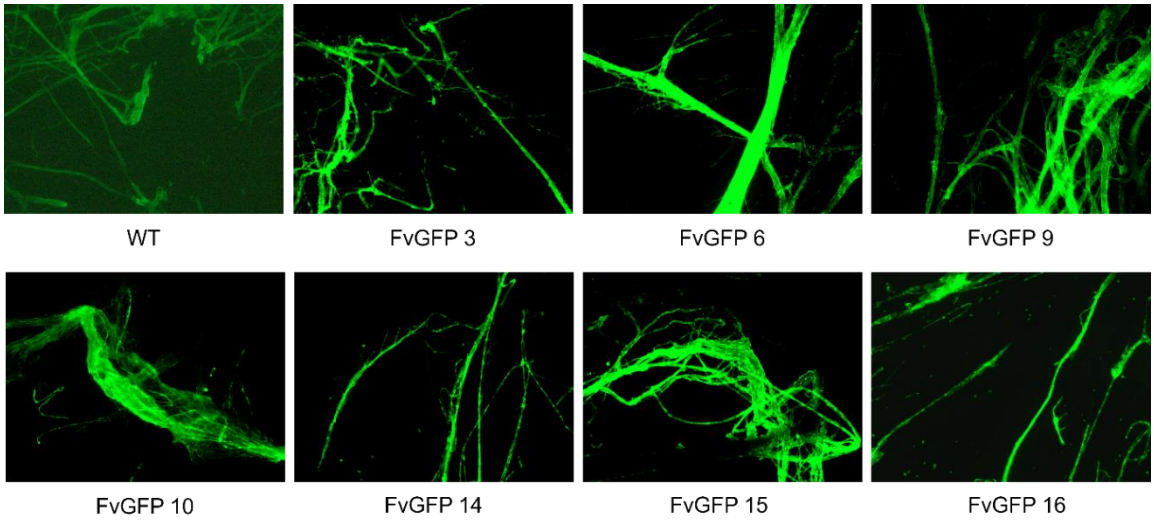

Figure S5.4: Fluorescent microscopy images of mycelia from the GFP-tagged *F. verticillioides* transformants compared to wild-type (WT) *F. verticillioides*.

The mycelia of GFP-transformants were analysed for GFP fluorescence and compared to wild-type (WT) *F. verticillioides* where the selected transformants showed clear GFP fluorescence compared to WT *F. verticillioides* (**Figure S5.5**). The selected transformants were subsequently grown on PDA for 7 days and the mycelial radial growth and sporulation measured (**Figure S5.5**). Significant differences for radial growth were only highlighted for the last day of the measurement period where the radial growth of FvGFP 3 was significantly lower than FvGFP 15 and FvGFP 16 (**Figure S5.5A**). However, none of the GFP-transformants displayed significantly different radial growth to WT radial growth (**Figure S5.5A**). Similarly, the sporulation data displayed no significant differences between the GFP-transformants and WT *F. verticillioides*, with the exception of FvGFP 15 which was significantly different to FvGFP 3 and 10 **(Figure S5.5B**).

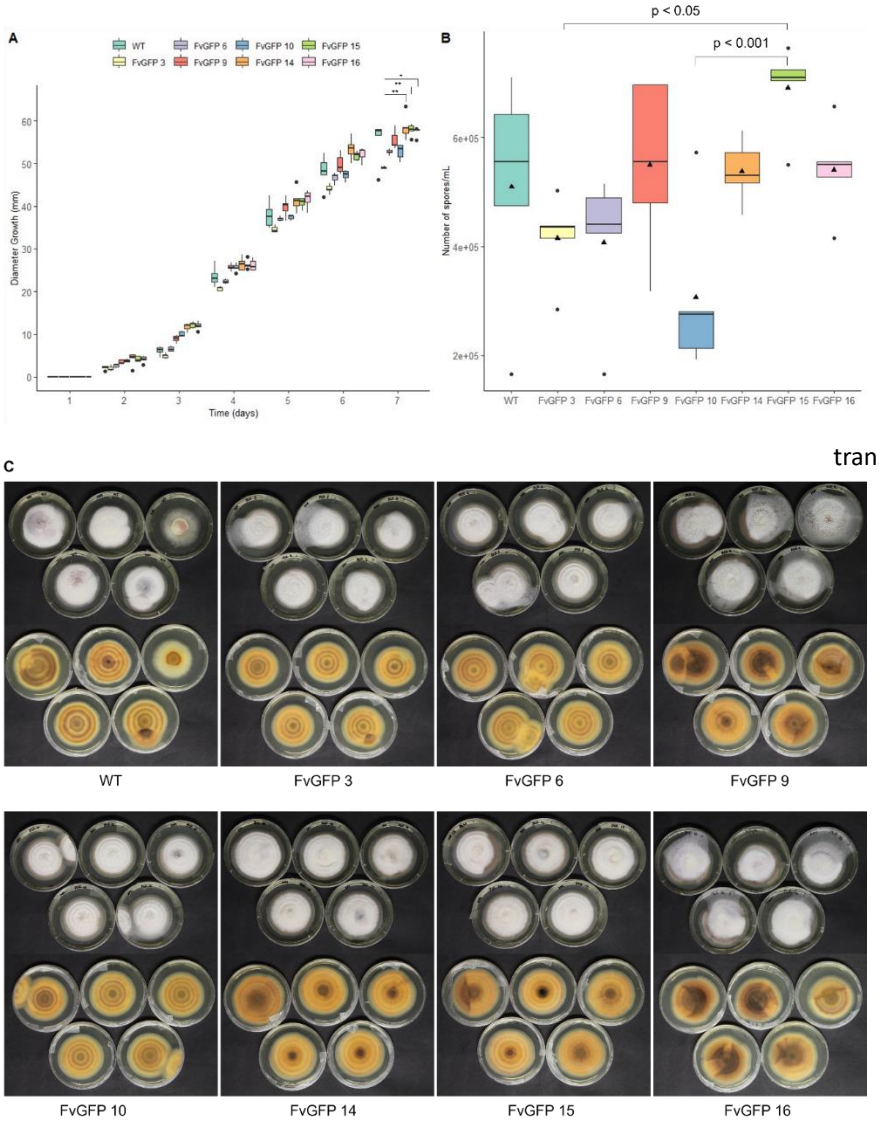

Figure S5.5: (A) The radial growth of GFP-tagged *F. verticillioides* transformants compared to wild-type (WT) *F. verticillioides* grown on PDA for 7 days. Statistical significance is indicated by an asterisk (*). * < 0.05 and ** < 0.01 (Kruskal-Wallis test followed by Dunn's *post hoc* test, p < 0.05, n = 5). **(B)** The number of spores for GFP-tagged *F. verticillioides* transformants compared to wild-type (WT) *F. verticillioides* measured at 7 days. The triangle indicates the average number of spores for each transformant. Statistical significance was determined by Kruskal-Wallis test followed by Dunn's *post hoc* test, p < 0.05, n = 5. **(C)** GFP-tagged *F. verticillioides* transformants compared to wild-type (WT) *F. verticillioides.*

Following the fitness tests, the GFP-transformants were tested *in planta* for root colonization and the effects thereof. As displayed in the colur images of **Figure S5.6**, the effects of *F. verticillioides* inoculation is visible in both WT and GFP-tagged *F. verticillioides* inoculated roots when compared to the water-treated + mock inoculated seedling. Furthermore, the GFP signal was visible in the GFP image of the GFP *F. verticillioides* inoculated seedling and not in the WT or mock inoculated seedlings (**Figure S5.6**).

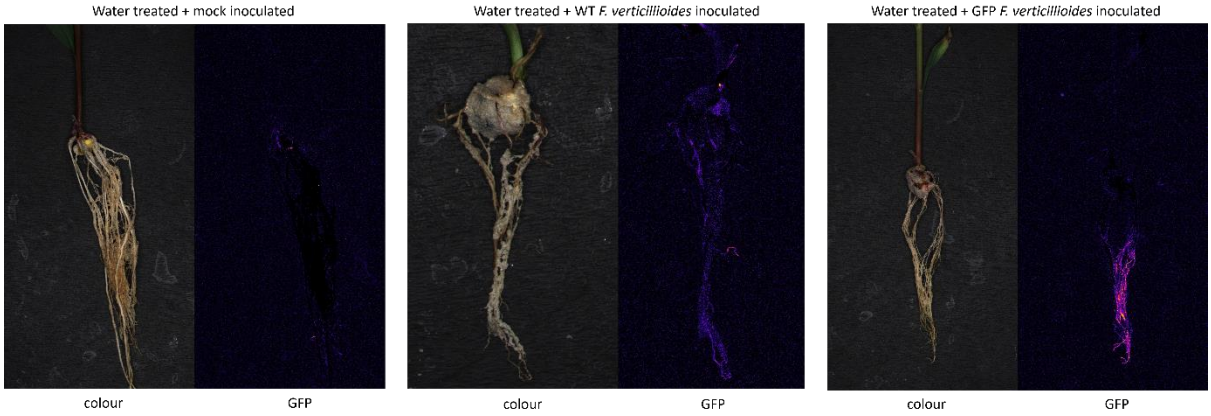

Figure S5.6: Colour and GFP signal images of wild-type (WT) and GFP-tagged *F. verticillioides* inoculated roots, 14 days post inoculation. The images represent one of six biological replicates. The WT *F. verticillioide*s images represented here were generated by inoculating germinated seedlings (preventative) and the GFP *F. verticillioides* images represented here were generated by inoculating the seed + sand: SAP growth medium (curative).

The effects of the different treatment and inoculation methods were analysed to observe if any significant differences in root and shoot growth were noticeable between the methods. From **Figure S5.7**, it can be seen that no significant differences were noticed between the different methods used.

Figure S5.7: Images comparing the effects of different inoculation systems assessed in mock and *F. verticillioides* inoculated germinated seedling (preventative) or seed + sand: SAP inoculated seedlings (curative). Three of six biological replicates represented here.

5.9 Addendum: Maize growth system

The growth methods described in **Figure 5.4** was conducted in glass tubes filled with mock or *F. verticillioides* inoculated sand: SAP mix (**Figure S5.8B)** that were placed in a box that protected the roots from light (**Figure S5.8A**). The box systems were designed and kindly provided by Dr Noēmi de Zutter and Dr Waldo Deroo.

Figure S5.8: The system used to germinate and grow maize seedlings. Glass tubes were filled with mock or *F. verticillioides* inoculated sand: SAP mix. Root browning, fungal growth in the medium and stunted shoot growth are visible.

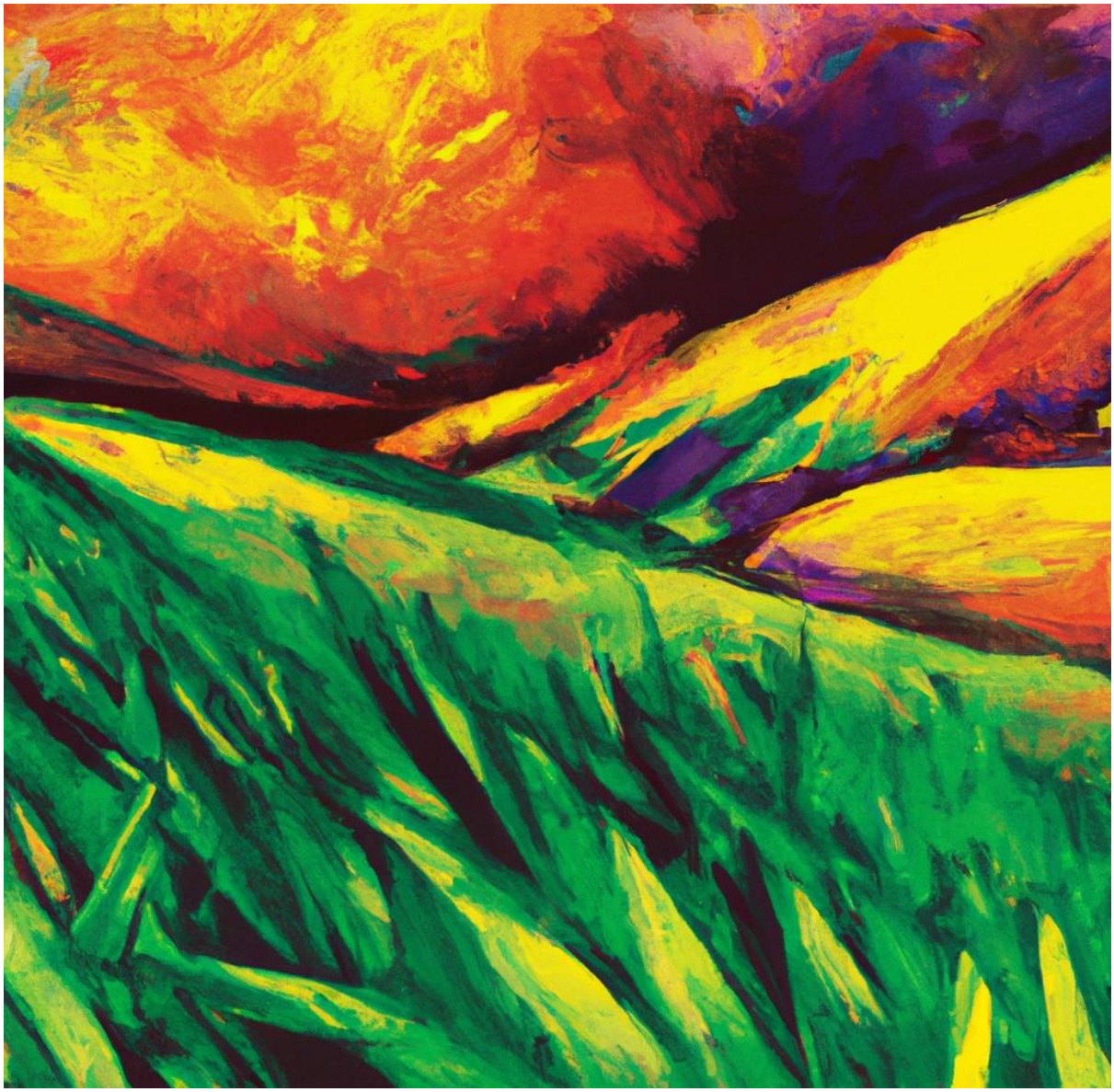

This image was created with the assistance of DALL.E 2.

Chapter 6: General discussion, limitations, and future perspectives

6.1 Introduction

This thesis focused on investigating the effects of aminochitosan both for its antifungal and *in planta* efficacy to elucidate the molecular mechanisms underpinning its bioactivity in a monocotyledon and dicotyledon pathosystem. As such, we **hypothesized that aminochitosan exhibits superior bioactivity to native chitosan, and that it results from a combination of priming and direct antifungal activity**. Given that this was the first investigation into the effects of aminochitosan and its batch-batch variability in synthesis, **we hypothesized that there would be minor variations in the efficacy of the batches that the aminochitosan MW fractions would display differing efficacies, with the lower MW fractions demonstrating the highest efficacy.**

We achieved this by reviewing the current literature on chitosan's defining physiochemical properties and mechanisms of action in a plant-pathogen context (**Chapter 2**). **Chapter 3** and **4** focussed on aminochitosan in the dicotyledonous tomato/*B. cinerea* pathosystem. **Chapter 3** specifically examined the bioactivity and priming capacities of the batch-to-batch and MW fractions, towards obtaining the optimal working concentration and MW for antifungal and *in planta* efficacy. Chapter 3 also aimed to identify any chemical differences between the biopolymers by doing a chemical analysis. **Chapter 4** focussed on elucidating the temporal and molecular mechanisms of priming by using a label-free proteomic analysis. **Chapter 5** further characterized aminochitosan in the monocotyledonous maize/*F. verticillioides* pathosystem, similarly to Chapter 3.

In this concluding chapter, we will provide responses (derived from our results) to the research questions, draw parallels with existing literature and highlight any challenges/limitations that were faced. The research questions will be answered across the various headings and overlap between them may exist. Finally, we will briefly address some future perspectives.

6.2 Batch-to-batch variations

1) ***What are the contributing factors and the effects thereof?***
2) ***Is there an optimal MW for direct antifungal and/or* in planta *use?***

Given that discrepancies in batch-to-batch products pose a challenge to achieving consistent data (physiochemical properties and biological activity), we sought to assess the level of

variability in the synthesis of aminochitosan batches. This was achieved in Chapter 3 by antifungal, *in planta,* and chemical analysis. Initially, only two batches of aminochitosan were synthesized namely, diamino 1 (D1) and diamino 2 (D2), of which D2 showed a clear and noticeable contrast in the ease of dissolution. D1 was easily dissolved by stirring whereas D2 required overnight stirring and subsequent sonication. It was decided thereafter to prepare all of the solutions in this standardized method. The differences between the ease of dissolving the polymers was attributed to chitosan's property of 'swelling' in solution due to the hydrogen bonds between it and the water molecules, the presence of impurities in the sample and the crystallinity of the polymer (Sayed, 2018). Due to the differences in the solubility, a third batch namely, D3 was synthesized. As the batches of aminochitosan were synthesized independently (**Figure 6.1**), it was anticipated that there would be slight variations in their physiochemical properties, which would potentially be exacerbated by the process used to obtain CHT.

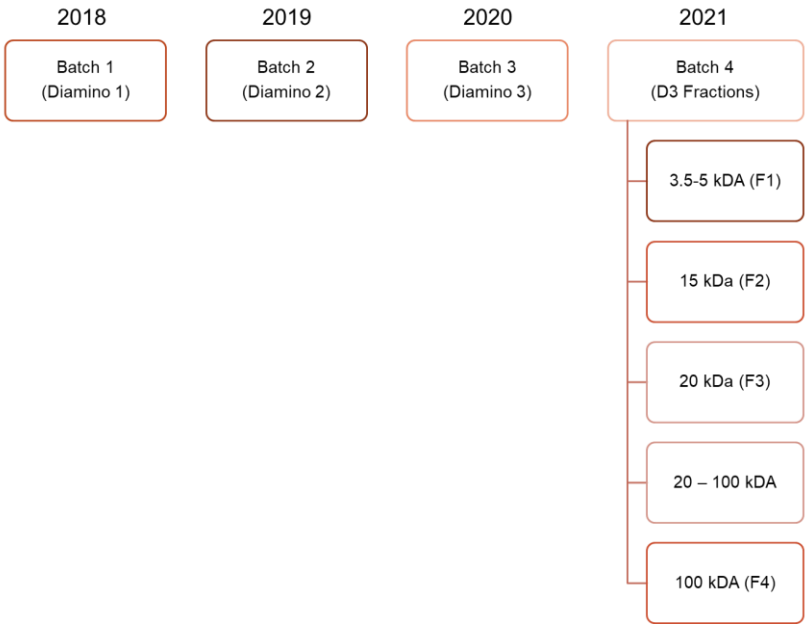

Figure 6.1: The year of synthesis for the batch-to-batch and MW fractions.

As a consequence of the processing methods, CHT does not possess a single molecular structure and may exhibit heterogeneity or homogeneity regarding the composition of D and A units, which correlates with varying DDA and MW. Moreover, these homogeneous or heterogeneous polymers may also have varied DP, polydispersity, pattern (PA), and fraction of N-acetylated groups (FA). Therefore, the observed difference in the solubility of D2 may be attributed to these factors, as DP is linked to chain length and, therefore, water solubility and

viscosity. It is important to note that batches were not synthesized within the same time period (**Figure 6.1**) or with the same starting batch material (i.e. they were all synthesized from crab, but not the same batch of crab). As has been discussed in this thesis, the starting chitin material is a source of variation for the physiochemical properties.

The antifungal activity analysis showed small but non-significant variations in the antifungal activity of D1, D2 and D3 with respect to the inhibition of radial growth. Larger differences between were noted for D2 when compared to D1 and D3 for sporulation at all concentrations tested. However, D1 did exhibit an overall greater inhibition of both metrics at a concentration of 1 mg/mL and higher. The *in planta* analysis showed that foliar application of D1 and D3 performed significantly better than native CHT and in priming direct and systemic resistance to *B. cinerea* infection by maintaining elevated PSII activity (F_v/F_m) and chlorophyll content (ChlIdx) at 4 dpi and 6 dpi for all concentrations tested. D2 also performed significantly better but only up to 4 dpi.

The differences in efficacy between the batch concentrations, albeit non-significant, were important to analyze for quality control and the ability to routinely synthesize consistent polymer batches. Thus, to properly understand the properties differentiating the batches, the third batch of polymer, D3, was fractionated to allow for chemical and biological characterization of different MWs. Elemental analysis, used to determine whether varying efficacies of the batches, showed that the nitrogen content between the batches differed slightly but agreed with the DS values reported in the literature on aminochitosan. Therefore, it was assumed that the differences in efficacy were not due to their elemental composition and proportions and were instead potentially due to MW differences as the efficacy and biological activity of CHT (by extension, aminochitosan) is intricately correlated with its chemical structure (Verlee, Mincke & Stevens, 2017). ESI TOF-MS analysis of the batches and MW fractions showed that the mass fragments and hierarchical clustering separated as we expected with the lowest MW (3.5-5 kDa) and highest MW (100 kDa) clustering separately with a high dissimilarity. The 15 and 20 kDa fractions also clustered closely with the batch variants as expected, given that the batches are approximately 15 kDa. Consequently, despite the polymers having identical or similar DPs, they may demonstrate diverse biological

characteristics due to differences in DDA, FA, and PA. However, further analysis is needed to deduce the FA and PA.

In summary, it is challenging to identify the key contributors to the observed results. The elemental analysis and mass fragment analysis are similar for the batches and the MW fractions. The batches and MW fractions display minor variations in their chemical composition with bigger variations seen in their biological efficacy. The potential largest contributor to the noticeable differences is the different batches of starting material and the process of alkaline deacetylation which as stated, generates a polymer of random MW. To obtain a more uniform polymer, enzymatic synthesis of aminochitosan should be investigated as the MW and DP can be controlled with high specificity and the overall process is environmentally friendly (Hamed, Özogul & Regenstein, 2016; Liaqat & Eltem, 2018; Cord-Landwehr & Moerschbacher, 2021).

It is also worth noting that the biological assays were conducted over the span of 3 years due to the COVID-19 pandemic which leads to questions on the shelf life of aminochitosan, which have not been evaluated to date and may pose a confounding factor to the results obtained. Future investigations on aminochitosan should include structural analysis assays to validate the structural properties of each synthesized batch (may not necessarily be feasible). Additionally, future ESI TOF MS analysis on aminochitosan should ideally integrate chromatography (e.g., size exclusion or liquid chromatography) to enable more detailed analysis on retention time, relative abundances of the mass fragments (monomers vs. oligomers), and intensity counts.

6.3 Aminochitosan vs 'native' chitosan

Does aminochitosan perform better than native CHT?

The term 'native CHT' is not an accurate representation of CHT but was instead used as a representative term for the insoluble CHT used to a large extent in the literature and this study. As good practice and for literature cohesion, each batch and derivative of CHT should at least be distinguished by its source, modifications (if any), concentration, solvent for dissolution (including concentration) and its physiochemical properties including DDA, MW, DP, and elemental composition (Verlee, Mincke & Stevens, 2017). The absence of one of the

aforementioned properties makes comparisons between studies challenging as CHTs bioactivity is largely dependent on these properties, as has been evidenced throughout this thesis. The only available details for the CHT used in this thesis was that it was of crab origin and had a DDA > 90%.

In Chapter 3, a concentration-dependent increase in the antifungal activities of CHT, D1, D2 and D3 was observed for radial growth and sporulation compared to the PDA control. Maximum inhibition for the batch variants and CHT were seen between the 2.5 and 5 mg/mL concentrations. We did not anticipate no significant differences between the batch variants and native CHT as was observed in the antifungal efficacy. However, we feel it important to reiterate that the antifungal activity of CHT was confounded by the use of acetic acid as a solvent for CHT on account of acetic acid displaying significant radial growth inhibition at a concentration of 0.1%. Furthermore, these results were no different from the effects of the 0.5 and 1 mg/mL concentrations of CHT, indicating a protective effect of 0.1% acetic acid. This result extended to the *in planta* analysis and was evident in the necrotic lesions at both 16 hpi and 4 dpi and photosynthetic parameters (F_v/F_m, chlorophyll index and anthocyanin index). The *in planta* analysis also showed that foliar application of D1 performed significantly better than native CHT and in priming direct and systemic resistance to *B. cinerea* infection by maintaining elevated PSII activity (F_v/F_m) and chlorophyll content (ChlIdx) at 4 dpi and 6 dpi for all concentrations tested. D2 also performed significantly better but only up to 4 dpi.

In Chapter 5, similar results were observed in the maize/*F. verticillioides* pathosystem. D1, D2 and D3 treatment resulted in significant inhibition of radial growth that were comparable to CHT at 2.5 mg/mL. For the inhibition of sporulation, D1 and D2 performed similarly to CHT at all concentrations while D3 displayed opposite results to D1, D2 and CHT. The hydrolyzed oligomers, D1 (HD1) and CHT (CHT + salts), displayed the same lack of radial inhibition but differed in their inhibition of sporulation. CHT displayed a concentration-dependent increase in the inhibition of sporulation whereas HD1 displayed no inhibition of sporulation. By analysing hydrolyzed CHT with and without salts, it was deduced that high concentrations of salt were a contributing factor to the reduced antifungal efficacy of HD1. However, further analysis is required to determine the contribution of MW and DP to the reduced antifungal efficacy of HD1 compared to CHT - salts to better understand the functionality of aminochitosan oligomers and the optimal MW range as it is likely that the MW range of CHT

– salts differed greatly to HD1. As CHT and HD1 were not assessed *in planta* in this pathosystem, no comparisons can be made.

In summary, contrary to what we hypothesized, aminochitosan does not display superior antifungal activity to native CHT (used in this thesis) to *B. cinerea* and *F. verticillioides* and instead displays bioactivity that is similar. However, aminochitosan does induce superior resistance and photosynthetic parameters to CHT in the tomato/*B. cinerea* pathosystem at concentrations of 0.5-2.5 mg/mL for up to 6 dpi.

6.4 Exploring the dichotomy: dicots, monocots, or both?

1) ***Does aminochitosan offer dual protection against* B. cinerea *and* F. verticillioides *at equal concentrations?***
2) ***What is the lowest concentration that achieves maximum biological activity, and do they differ for antifungal and* in planta *immunostimulatory uses?***
3) ***Is aminochitosan effective both as a direct and systemic inducer of resistance?***

Given the existing literature on the direct antifungal effects of aminochitosan against other pathogens (Yang et al., 2012; Luan et al., 2018), we hypothesized that aminochitosan would display efficacy against both *B. cinerea* and *F. verticillioides*. This section will propose answers to these questions as a collective. The values presented below are summarized in **Tables 6.1-6.3** for ease of viewing.

Antifungal activity

From the tomato/*B. cinerea* pathosystem in Chapter 3, we deduced that a concentration-dependent increase in antifungal effects were observed for all aminochitosan batches, but that maximum radial growth and sporulation inhibition occurred between 2.5-5 mg/mL. The lowest concentration of aminochitosan batch variants that could be used to still obtain 50% inhibition of both radial growth and sporulation was 1 mg/mL. However, when assessing the effects of D1 on germination *in planta*, a concentration-dependent increase in the inhibition of germination and germ tube length was sustained up to 72 hpi. From this assay, 1 mg/mL of D1 already displayed a maximal inhibitory phenotype indicating that spores were more sensitive than a spores and mycelia mixture (used in the *in vitro* plate assays). This indicated the possibility of a bimodal mechanism of action as well as the difference in efficacy against a

spore and mycelia + spore mixture. For the MW fractions, an increase in the efficacy of the concentrations with a decrease in the MW was observed which indicates a trend between MW and biological activity. The MW range of 3.5-15 kDa displayed the greatest efficacy for antifungal activity at the maximum concentrations of 2.5 mg/mL. The lowest concentration of 3.5-15 kDa MW fraction that could be used to still obtain 50% inhibition of both radial growth and sporulation was similarly 1 mg/mL.

For the maize/*F. verticillioides* pathosystem in Chapter 5, we deduced that aminochitosan exhibited maximal effects at 2.5 mg/mL with a similar concentration-dependent increase in efficacy. The lowest concentration of D1 and D2 that could be used to still obtain 50% inhibition of both radial growth and sporulation was 1 mg/mL and 2.5 mg/mL for D3. HD1 displayed no antifungal efficacy both radial growth and sporulation. We wish to emphasize that each and every one of the antifungal assays were conducted over a 3-year period with the experiments on the efficacy of D2 and D3 for *F. verticillioides* being conducted last. Therefore, the large standard deviations for experimental repeats may be a result of the polymer shelf life. Additionally, we explored the variation in efficacy between the oligomers, hydrolyzed diamino 1 (HD1) and hydrolyzed CHT (CHT + salts). From the antifungal acitivty analysis, we identified that efficacy for both HD1 and CHT+ salts were lost and instead resulted in an increase in sporulation. By analysing hydrolyzed CHT with and without salts, it was deduced that high concentrations of salt were a contributing factor to the reduced antifungal efficacy. However, further analysis is required to determine the contribution of MW and DP to the reduced antifungal efficacy of HD1 to better understand the functionality of aminochitosan oligomers and the optimal MW range.

In summary, from the antifungal assay results, it appears that the optimal aminochitosan concentration for maximum efficacy is 2.5 mg/mL and can be considered standardized and applicable to both *B. cinerea* and *F. verticillioides*. However, for an efficacy of at least 50% inhibition, 1 mg/mL would be sufficient for *B. cinerea* while 2.5 mg/mL would be necessary for *F. verticillioides* due to the variable batch variant results. More data and experimental repeats are needed to verify the aforementioned recommendations and these experiments should ideally be performed within the same time period. Furthermore, we would like to emphasize that microbial factors such as the amount of polyunsaturated fats in the cell membrane that play a significant role in determining the efficacy of CHT (Chapter 2).

Therefore, we would expect a nuanced outcome for the recommended concentrations for *B. cinerea* and *F. verticillioides* with *B. cinerea* being more sensitive to lower concentrations of aminochitosan due to its high polyunsaturated fatty acid content. As stated by Poznanski, Hameed & Orczyk, (2023), the physiochemical properties of CHT drastically affects it antifungal activity between batches of CHT available commercially. Moreover, the bioactivity of a particular batch is highly dependent on the species (Palma-Guerrero et al., 2010).

In planta

The direct and systematic effects of aminochitosan were only evaluated in the tomato/*B. cinerea* pathosystem of Chapter 3 through both a qualitative and quantitative phenotyping assessments. When visually assessing the number of resistant lesions after direct pre-treatment with the batch variants, maximum inhibition was achieved at 2.5 mg/mL whereas the concentration that still achieved at least 50% direct inhibition was much lower at 0.5 mg/mL. The MW fractions varied in comparison with the 15-20 kDa variants displaying maximum direct inhibition at 1 mg/mL and at least 50% direct inhibition at 0.5 mg/mL. 3.5-5 kDa displayed the lowest performance with maximum direct inhibition at 2.5 mg/mL and at least 50% direct inhibition at 1 mg/mL.

The photosynthetic measurements were only assessed for D1 and D2 and will be reported as collective values (mock inoculated and *B. cinerea* inoculated). In contrast to the measurement of resistant lesions, the photosynthetic parameters namely, F_v/F_m and ChlIdx as well the stress index, mAriIdx, highlighted a potential negative side effect of 2.5 mg/mL of aminochitosan sprayed directly onto leaves. At 2.5 mg/mL, a decrease in F_v/F_m for both mock and *B. cinerea* inoculated leaves was noted, indicating that the observed effects were not due to the establishment of an infection but rather to the concentration of the treatment, or as stated in Goy et al. (2009), the free amino groups that are charged and have the capacity to bind to the surface of fungal cells are reduced with an increase in concentration of CHT applied as the chains form clusters and aggregates while in solution. This finding was also noted to vary with time, as no signs of toxicity were detected up to 72 hpi, with indications only appearing at 4 dpi. However, at 2.5 mg/mL, the mAriIdx stress index displayed higher accumulation values in mock-inoculated (uninfected leaves) than in *B. cinerea* inoculated leaves at the site of infection.

For maximum systemic inhibition as measured by the resistant lesions, 2.5 mg/mL was the most effective concentration for all 3 batch variants. However, to achieve at least 50% inhibition, 1, 2.5 and 0.5 mg/mL was needed for D1,D2 and D3 respectively. The MW fractions displayed a similar systemic efficacy to the direct efficacy with the 15-20 kDa variants displaying maximum direct inhibition at 1 mg/mL and at least 50% direct inhibition at 0.5 mg/mL. However, the 3.5-5 kDa variant displayed the lowest performance with maximum direct inhibition at 2.5 mg/mL and at least 50% direct inhibition at 0.5 mg/mL. Based on the aforementioned variables relating to F_v/F_m and mArIdx values, the photosynthetic parameters displayed maximum *in planta* inhibition at a concentration of between 1-2.5 mg/mL and displayed at least 50% *in planta* inhibition at 1 mg/mL. These values are applicable to both direct and systemic application.

In Chapter 5 we did not assess the effects of aminochitosan on the qualitative and quantitative phenotype of maize. We also did not assess the occurrence of resistant lesions as *F. verticillioides* was investigated as a root affecting pathogen. However, we would like to highlight that despite HD1 having no antifungal efficacy, some effects were observed when analysing the temporal accumulation of phytohormones. Although we do not specifically know the MW of HD1 and CHT + salts, we do know that it is < 15 kDa. This observation highlights the necessity of determining the effects of a polymer of a 'single' MW (i.e. 5 kDa) and one composed of a range of MWs (i.e. 3.5-25 kDa) as there appears to be a MW threshold beyond which antifungal efficacy is lost. It is therefore of interest to identify the equivalent *in planta* MW threshold value.

In summary, if we are to combine both the qualitative and quantitative data, 2.5 mg/mL of the batch variants appears ideal for maximum efficacy *in planta*, and 1 mg/mL for at least 50% inhibition *in planta*. These concentrations are applicable for both direct and systemic efficacy. However, if we assess the specific MW fractions, specifically 15-20 kDa, 1 mg/mL appears ideal for maximum efficacy *in planta*, and 0.5 mg/mL for at least 50% inhibition *in planta*. Based on our *in planta* data, we propose a lower concentration of 1 mg/mL as the optimal concentration for *in planta* use with a high efficacy for inhibiting germination of spores *in planta* and was shown to provide full protection up to 30 dpi when applied both directly and systemically. This is due to spores (ungerminated conidia) displaying higher sensitivity to treatment (Palma-Guerrero et al., 2009). We would not recommend 0.5 mg/mL as we have demonstrated that

the fungi are capable of using aminochitosan as a nitrogen source at low concentrations (sporulation data).

Finally, we suggest an aminochitosan variant with a MW range of 15-20 kDa OR 3.5-20 kDa as the optimal biopolymer for dual and approximately equal antifungal and *in planta* efficacy (Figure 6.2). This conclusion is supported by Poznanski, Hameed & Orczyk, 2023 who showed that high molecular weight CHT disrupts fungal cell membranes, causing intracellular component leakage, while low molecular weight CHT fractions exhibit minimal antifungal impact as they fail to destabilize membranes. However, a blend of high and low molecular weight CHT fractions demonstrate potent antifungal activity by leveraging the membrane destabilization caused by high molecular weight fractions to enable penetration and disruption of fungal cell processes by low molecular weight fractions.

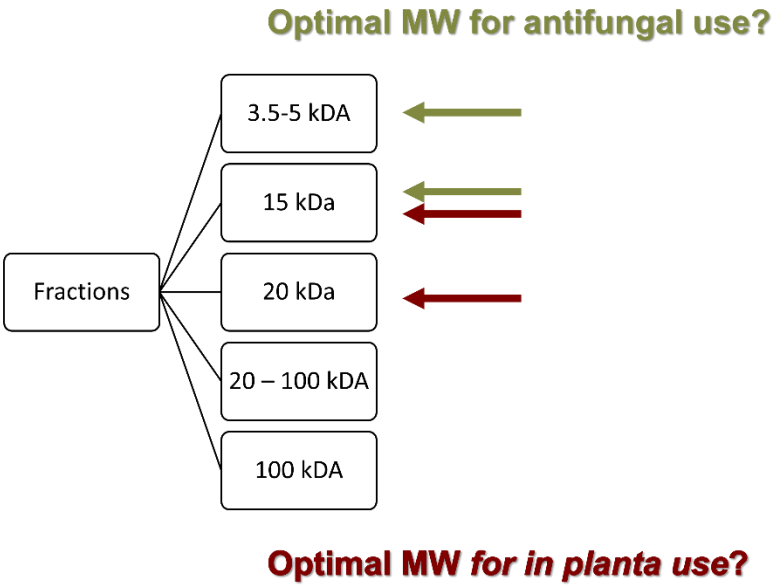

Figure 6.2: Identifying the ideal MW for dual antifungal and *in planta* efficacy.

We recommend avoiding the highest concentration due to our preliminary results indicating potential cytotoxicity at 2.5 mg/mL. Previous studies suggest that the cytotoxic effect of CHT varies with applied concentrations. Amborabe et al. (2008) proposed two explanations for these effects: 1) CHT acts as an elicitor, inducing HR and H_2O_2 accumulation, and 2) higher concentrations of CHT exhibit mixed results, ranging from no cytological alterations/toxicity at 37.5 mg/mL to destabilization of the cell membrane, electrolyte and protein leakage, and disrupted cell organization at 200-1000 mg/mL (Amborabe et al. 2008 and the references therein). The leakage of internal material results from CHT's polycationic property, forming

pores upon binding to negatively-charged cell components, contributing significantly to dose-dependent cytotoxicity. Amborabe et al. (2008) cautioned against using high concentrations of CHT due to membrane destabilization, which could facilitate pathogen entry, suggesting instead the use of concentrations that maintain normal physiology. Understanding the effective concentration after external treatment is complex, relying on absorption capacity, transport systems, and CHT's binding ability to the cell.

Table 6.1: Concentration (mg/mL) of aminochitosan that provides maximum inhibition of both radial growth and sporulation for *B. cinerea* . The data below is adapted from Chapter 3.

	in vitro: B. cinerea		***in planta: B. cinerea***				
			Direct			Systemic	
	Radial inhibition	Sporulation	Germination	Resistant lesions	Photosynthetic parameters	Resistant lesions	Photosynthetic parameters
Diamino 1	2.5	2.5	2.5	2.5	0.5-1	2.5	1-2.5
Diamino 2	5	5	NA	2.5	1	2.5	1-2.5
Diamino 3	5	5	NA	2.5	NA	2.5	NA
3.5-5 kDa	2.5	2.5	NA	2.5	NA	2.5	NA
15 kDa	2.5	2.5	NA	1	NA	1	NA
20 kDa	2.5	2.5	NA	1	NA	1	NA

Maximum inhibition is defined as the PIRG% and PIS% inhibition for each polymer, independent of other polymer efficacies based off experimental repeats. NI = Not inhibitory, NA = Not Applicable as no measurements were assayed for this polymer.

Table 6.2: Concentration (mg/mL) of aminochitosan that provides at least 50% inhibition of both radial growth and sporulation B. cinerea . The data below is adapted from Chapter 3.

	in vitro: B. cinerea		***in planta: B. cinerea***				
			Direct			Systemic	
	Radial inhibition	Sporulation	Germination	Resistant lesions	Photosynthetic parameters	Resistant lesions	Photosynthetic parameters
Diamino 1	1	1	1	0.5	1	1	1
Diamino 2	1	1	NA	0.5	1	2.5	1
Diamino 3	1	1	NA	0.5	NA	0.5	NA
3.5-5 kDa	1	1	NA	1	NA	0.5	NA
15 kDa	1	1	NA	0.5	NA	0.5	NA
20 kDa	1	1	NA	0.5	NA	0.5	NA

Maximum inhibition is defined as the PIRG% and PIS% inhibition for each polymer, independent of other polymer efficacies based off experimental repeats. NI = Not inhibitory, NA = Not Applicable as no measurements were assayed for this polymer.

Table 6.3: The concentration (mg/mL) of aminochitosan that provides maximum inhibition of both radial growth and sporulation for *F. verticillioides*. The data below is adapted from Chapter 5.

	in vitro: F. verticillioides			
	Maximum inhibition		**±50% inhibition**	
	Radial inhibition	Sporulation	Radial inhibition	Sporulation
Diamino 1	2.5	2.5	1	2.5
Diamino 2	2.5	0.5	1	0.5
Diamino 3	2.5	NI	5	NI
Hydrolyzed diamino 1	NI	NI	NI	NI

Maximum inhibition is defined as the PIRG% and PIS% inhibition for each polymer, independent of other polymer efficacies based off experimental repeats. NI = Not inhibitory, NA = Not Applicable as no measurements were assayed for this polymer.

6.5 A bimodal mechanism of action

1) ***Does priming occur in tomato and maize?***
2) ***If priming occurs, what defence systems are induced after treatment with/without infection?***

To start with, it is important to highlight that the priming capacity of aminochitosan in Chapter 3 was assessed at 0.5, 1 and 2.5 mg/mL, Chapter 4 at 1 mg/mL and Chapter 5 at 2.5 mg/mL. Furthermore, Chapter 3 focused on D1, D2, and D3, Chapter 4 on D3 and Chapter 5 on D1 and HD1. Hence, drawing comparisons between Chapters 3 and 4 with Chapter 5 is not a possibility. We recognize this factor as a major limitation and recommend that future studies assess relative concentrations and polymer batches. Furthermore, the data presented in Chapter 3 and 4 offer only a brief snapshot within a specific timeframe of the intricate changes in photosynthetic parameters caused by infection. In this section, we will not differentiate between the batches of aminochitosan and will instead refer to aminochitosan as a singular.

6.5.1 The takeaways from Chapter 3

The primary conclusions from Chapter 3 were that aminochitosan applied as a foliar spray in 5-week-old tomato leaves was a successful direct and systemic preventative treatment to *B. cinerea* infection up to up to and including 72 hpi at 1 and 2.5 mg/mL, 1 and 2.5 mg/mL for 4 and 6 dpi and 1 and 2.5 mg/mL for 30 dpi (15-20 kDa MW fractions). The successful priming

of a resistant response systemically highlighted the benefits of a rapid and intense induction of the innate immune system globally. The observed resistant phenotype was determined to be mediated through sustained and elevated photosynthetic parameters namely, PSII activity (F_v/F_m) and chlorophyll content (ChlIdx) up to 4 and 6 dpi. Therefore, prior to 4 dpi, 2.5 mg/mL of aminochitosan proved advantageous for the leaves; however, its effectiveness diminished at later time points (refer to Section 6.4). Similarly, anthocyanin accumulation (mAriIdx) was observed to decrease with an increase in the concentration of aminochitosan at the site of *B. cinerea* inoculation. We hypothesized that the mechanisms of protection were likely due to a severe direct antifungal inhibition at higher concentrations, resulting in lower ROS production, less oxidative stress (HR-like response), and lower anthocyanin production.

Conversely, in aminochitosan-treated but uninfected leaves, anthocyanins were primed and accumulated in response to higher concentrations. This observation coupled with the enhanced $F_{v/}F_m$ values and thereby enhanced photosynthetic activity observed in these leaves indicated an increase in starch and sugar production. We hypothesized that anthocyanin accumulation may act as a mechanism for regulating sugar content in an attempt to circumvent early senescence elicited by high sugar levels in source tissue. Therefore, anthocyanins function as potential alternative sinks that avoid excess carbon and sugar accumulation mitigating possible "sugar-induced leaf senescence" induced by enhanced photosynthetic activity after application of a high concentration of diamino chitosan (Landi et al., 2015). Given that the enhanced photosynthesis was visible in both the inoculation droplet site and in the surrounding areas, the sustained elevated photosynthetic activity was hypothesized to be due to priming a stronger and more rapid elicitation of the defence systems at earlier time points, resulting in an unsuccessful infection. Unexpectedly, the resistance phenotype was not mediated by a strong accumulation of H_2O_2 between 4-72 hpi. Instead, a decrease in H_2O_2 accumulation with an increase in aminochitosan concentration was observed. These results corroborated the aforementioned anthocyanin data and direct *in planta* germination observation to suggest that aminochitosan functions in a ROS-independent manner, especially at higher concentrations where direct inhibition take precedence. Hence, lower concentrations may be favoured due to its low and slow increase in H_2O_2 levels, resulting in maintained PSII functionality compared to the decrease seen at 2.5 mg/mL.

ACRE genes encode signalling pathways, protein kinases, and ubiquitination pathway-related proteins. They have been shown to be induced in ROS gene-independent early plant defence responses and be primed by a water-soluble CHT for a faster and stronger expression after infection with *B. cinerea* (Durrant et al., 2000; De Vega et al., 2021). We observed that aminochitosan primes ACRE75 accumulation both in direct and systemically treated leaves with/without *B. cinerea* inoculation. Moreover, *ACRE75* was positively regulated with an increase in concentration at 6 hpi indicating a concentration-dependent response at the earlier time points. This suggested that lower concentrations of aminochitosan were sufficient for priming systemic accumulation of *ACRE75* and that the protection was sustained up to and including 96 hpi.

Lastly, when assessing the *in planta* effects of aminochitosan on germination, we observed an aminochitosan accumulating in the epidermal cells. We concluded that aminochitosan acts to increase the membrane permeability of cells after foliar spray thereby allowing the permeation of aminochitosan into the cell membranes and cells. These observations corroborate the notion that polymers such as aminochitosan can exert their effects in a bimodal mechanism, exerting both direct mechanisms of inhibition and indirect immunostimulatory mechanisms.

In summary, we suggest that direct and systemic foliar application of aminochitosan primed the defence response of mock and *B. cinerea* inoculated leaves by increasing the membrane permeability, the photosynthetic properties, and ACRE75 gene expression, all in a manner that required little to no H_2O_2 accumulation as a signalling molecule. Although the MW fractions were not discussed individually here, we feel it important to highlight that the H_2O_2 accumulation data for the fractions was variable. However, this experiment was only conducted once, unlike the experiments on D1, and therefore requires additional repeats to determine the true H_2O_2 phenotype for each MW fraction. Sun et al. (2007) reported that CHT oligomers (DDA 92.7%) of lower MW (2.3-6.12 kDa) displayed superior antioxidant activity against hydroxyl radicals and superoxide anions compared to the oligomer with the highest MW (15.25 kDa). This further highlights the importance of characterizing the optimal ranges of MW for maximum biological activity. We also recognize that the methods used to assess

the systemic capacity could be improved upon by testing distal leaves and not distal leaflets for a more accurate representation of systemic priming.

6.5.2 The link between Chapters 3 and 4: connecting the phenotyping and proteomics data

In this section, we will specifically focus on the ROS-independent and enhanced photosynthesis hypotheses.

6.5.2.1 Examining the ROS-independent hypothesis in the aminochitosan primed and non-triggered state (ConPol compared to ConWater)

From the proteomics analysis of the aminochitosan treatment leaves, we suggest that aminochitosan initiated the defence response in a ROS-independent manner at 6 hpi by: **1)** functioning as an antioxidant. **2)** Catalase 1 was significantly down-regulated at 6 hpi indicating a reduced necessitation of antioxidants. **3)** The down-regulation of chitinase activity.

The ROS-independent induction of defence response was continued up to 9 hpi by: **4)** The continued down-regulation of chitinase activity indicating that aminochitosan present in the apoplast (Chapter 3) is not degraded by chitinases and does not contribute significantly to the overall increase in ROS and shows little to no visible accumulation up to 72 hpi as seen in Chapter 3. **5)** The down-regulation of catechol oxidase activity at 9 hpi as a means of maintaining lower levels of ROS by negatively regulating the pathways that result in ROS production which have previously been shown to occur concurrently with an increase in F_v/F_m and increase chlorophyll content with the simultaneous absence of H_2O_2 accumulation. **6)** Positive regulation of GAD which promotes endogenous GABA production and also serves as a preemptive scavenger for ROS; reducing the likelihood of oxidative stress at later time points, as seen in Chapter 3, by the low to absent levels of H_2O_2 up to 72 hpi, therefore inducing a state of 'endurance', preserving cell viability by limiting the production of ROS. **7)** The up-regulation of catalase activity may serve as a H_2O_2 scavenger.

6.5.2.2 Examining the ROS-independent hypothesis in the aminochitosan primed and *B. cinerea*-triggered state (InfPol)

When assessing the primed and triggered state, we suggest that low to no accumulation of ROS at 6hpi was achieved by **1)** The negative regulation of H^+-ATPase activity across the cell wall at 6 hpi which resulted in reduced ROS, validated by Gonugunta, Srivastava & Raghavendra (2009) and Keinath et al. (2010). **2)** Furthering on from both the H^+-ATPase hypothesis and chitinase activity hypothesis, chitinase was significantly down-regulated at 6 hpi. The down-regulation of H^+-ATPase activity has been shown to be coupled with the reduction in PR activity (chitinases are PR proteins). **3)** The upregulation of peptide methionine sulfoxide reductase at 6 hpi to facilitate the reduction of oxidized methionine residues back to methionine, which are particularly susceptible to oxidative damage by free radicals. These therefore act as additional ROS sinks and scavengers. **4)** The down-regulation of a DNA binding BED-type domain containing protein at 6 hpi which has been shown to be capable of inducing ROS and a cell death phenotype after 4-5 days (Zuluaga et al., 2020). **5)** The down-regulation of antioxidant proteins at 6 hpi namely In 'peroxidase (EC 1.11.1.7), Catalase isozyme 1 (EC 1.11.1.6) and 'Glutathione peroxidase (A0A3Q7H2Q7) indicates a general reduced need for stress acclimation and/or tolerance responses in the peroxisomes and may be attributed to the potent direct antifungal effects of 1 mg/mL of aminochitosan, the overall diminished eliciting nature of *B. cinerea* infection, and as a result, the decreased demand for ROS scavenging systems. As highlighted in Chapter 3, aminochitosan shares characteristics with polyamines (PAs) which have been shown to regulate ROS levels by scavenging free radicals, promoting ROS degradation, and boosting antioxidant enzymes (Gupta et al., 2016). Free PAs also neutralize superoxide anions and H_2O_2, while conjugated PAs probably aid in scavenging other ROS (Gupta et al., 2016). **6)** Glutamate decarboxylase activity was significantly up-regulated also supporting the hypothesis that foliar application of 1mg/mL of aminochitosan induces a state of 'endurance', preserving cell viability by limiting the production of ROS and upregulating GABA, a H_2O_2 scavenger.

In summary, Chapter 4 in part validates the ROS-independent hypothesis and the molecular mechanisms underpinning it. However, given the variable H_2O_2 results for the MW fractions, an alternative to the ROS- independent hypothesis is that aminochitosan triggers a level of

ROS accumulation that is lower than pathogen-induced ROS upon first spray, priming the antioxidant system to rapidly respond upon a second trigger (pathogen inoculation), avoiding an oxidative burst or HR response. However, this swift scavenging response may occur earlier than our investigated 6-h time point. Several of these conclusions are extrapolations and further experiments on quantitative phenotyping, analysis of antioxidant levels, glutamate metabolism and H^+-ATPase activity on the equivalent time points are needed for a true validation.

6.5.2.3 Examining photosynthesis in the aminochitosan primed and non-triggered state (ConPol compared to ConWater)

1) At 6 hpi, tomato pre-emptively down-regulates photosynthesis and carbon metabolism as an adaptive response to aminochitosan treatment while up-regulating defence systems. Given that Chapter 3 does not look at the quantitative photosynthetic parameters in the early hours of infection, this could not be corroborated. **2)** At 9 hpi, the up-regulation of catalase coupled with chlorophyll biosynthesis and glutamate decarboxylase may be as a result the enhanced photosynthesis and may serve as sink/means for dissipating the excess energy, preventing any damage to photosynthetic machinery. Glutamate decarboxylase is involved in the regulation of carbon and nitrogen (C/N) metabolism via the GABA shunt which controls the ratio of C:N in order to replenish the tricarboxylic acid cycle with carbon through source/sink remobilization (Seifi et al., 2013; Fagard et al., 2014). This process would allow for excess carbon to be recycled, given the increase in photosynthesis as highlighted in Chapter 3. GAD also promotes the state of "endurance" as mentioned earlier which validates the observation that aminochitosan primes and by maintaining enhanced photosynthesis for as long as possible.

6.5.2.4 Examining photosynthesis in the aminochitosan primed and *B. cinerea*-triggered state (InfPol)

1) The increase in chlorophyll biosynthesis at 6 hpi may be a counteractive measure to prevent the loss of chlorophyl and suggests a defensive strategy, as chlorophyll not only facilitates photosynthesis but also may participate in plant defence mechanisms by retrograde signaling. **2)** At 6 hpi, the down-regulation of proteins associated with photosynthetic electron transport in PSII, and chlorophyll binding may signify the plant's reallocation of resources to activate

defence-related compounds, temporarily reducing photosynthetic efficiency (trade-off). **3)** At 9 hpi, chlorophyll biosynthesis was significantly down-regulated indicating that the tetrapyrroles intermediates were regulated in a timely manner so that instead of being toxic intermediates, function as chloroplast-derived signaling molecules. **3)** The up-regulation of chlorophyll binding at 9 hpi indicates a potential swift shift from defence to recovery as the plant adapts to the infection more rapidly after aminochitosan application, aiming to restore normal physiological functions, including photosynthesis. From Chapter 3, we know that the increase in chlorophyll content is sustained up to 4 dpi.

In summary, the aforementioned results at 9 hpi partially validate the enhanced and sustained photosynthesis seen up to 72 hpi in Chapter 3. Furthermore, the combination of the ROS-independent hypotheses and enhanced photosynthesis indicate an immune system headed towards a state of 'endurance' as seen in Chapter 3. However, conducting a time trial experiment incorporating the time points not addressed here would provide stronger assurance for reaching this conclusion.

6.5.3 Deciphering priming from induced resistance

Finally, to conclude that aminochitosan indeed primes a defence response, it is essential to differentiate between priming and induced resistance, aptly demonstrated by Ameye (2017). We have assessed this based on criteria as per Ameye (2017) and Martinez-Medina et al. (2016).

The definition of priming defined by Martinez-Medina et al. (2016) is "defence responses deployed in a faster, stronger, and/ or more sustained manner following the perception of a later challenging signal (the triggering stimulus); that is, in times of stress". They also highlight that priming is a low-cost defensive mechanism that it not or only partially or transiently activated after being primed by a stimulus; a key differentiating factor to induced resistance (**Figure 6.3**).

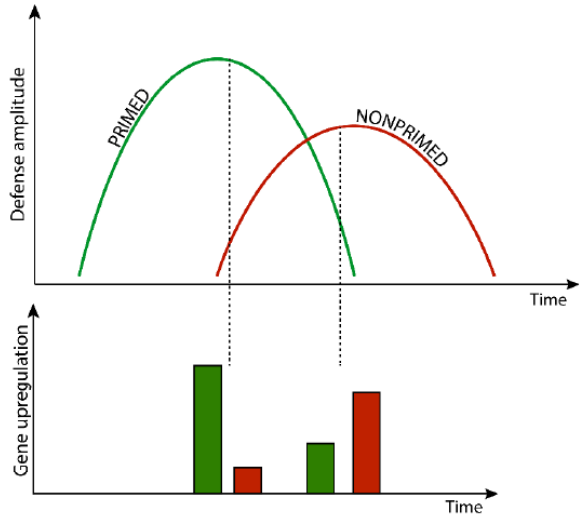

Figure 6.3: A hypothetical model adapted from Ameye (2017) that depicts the time course of a primed and non-primed defence response. Green represents the primed defence response and red the non-primed defence response.

Priming can arise from exposure to chemical, pathogens and pests, and environmental signals with the mechanisms of priming varying based on the type of stimulus and stressor involved. Irrespective of the specific triggers, defence priming consistently displays certain features, as outlined by Martinez-Medina et al. (2016), who proposed essential criteria for identifying priming in plants and include: i) memory, ii) low fitness costs, iii) more robust defence, iv) broad spectrum activity, and vi) low ecological costs.

(i) Memory in plants involves the transient and low-level maintenance of a primed state post-priming until a biotic attack occurs. As highlighted above in Section 6.5.2, we believe this criterion is met.

(ii) Low fitness costs are defined as requiring fewer overall costs than the activation of direct defence responses. Some allocation costs are to be incurred due to physical changes (e.g. histone modifications), however, the benefits of priming become obvious after a second stress when primed plants perform better than non-primed plants. As highlighted above in Section 6.5.2, we believe this criterion is met.

(iii) A more robust defence response is defined as a stronger and more rapid elicitation of defence after a triggering stress than in non-primed plants. As highlighted above in Section 6.5.2, we believe this criterion is met.

(iv) Broad spectrum activity is defined as enhanced defence to both biotic and abiotic stresses. As we did not effectively assess this in the maize/*F. verticillioides*

pathosystem, we cannot positively confirm this *in planta*. However, as highlighted in Section 6.4, aminochitosan does display antifungal activity to both *B. cinerea* and *F. verticillioides*.

(v) Low ecological costs are defined as effects on mutualists or inter species competition. Determining these effects are more challenging and we did not assess this.

An insightful observation was articulated by Ameye (2017) who stated that demonstrating the additional criteria of broad-spectrum activity and low ecological costs poses significant challenges due to the multitude of antagonistic signaling pathways. These pathways, likely influencing each other negatively, between different pathogens and the environment, may ultimately undermine the validation of these two supplementary criteria. In conclusion, based on criteria i-iii, we have demonstrated the short-term priming properties of aminochitosan in plants and propose a hypothetical model of aminochitosan induced molecular alterations in Figure 6.3 which summarizes key findings of this PhD thesis.

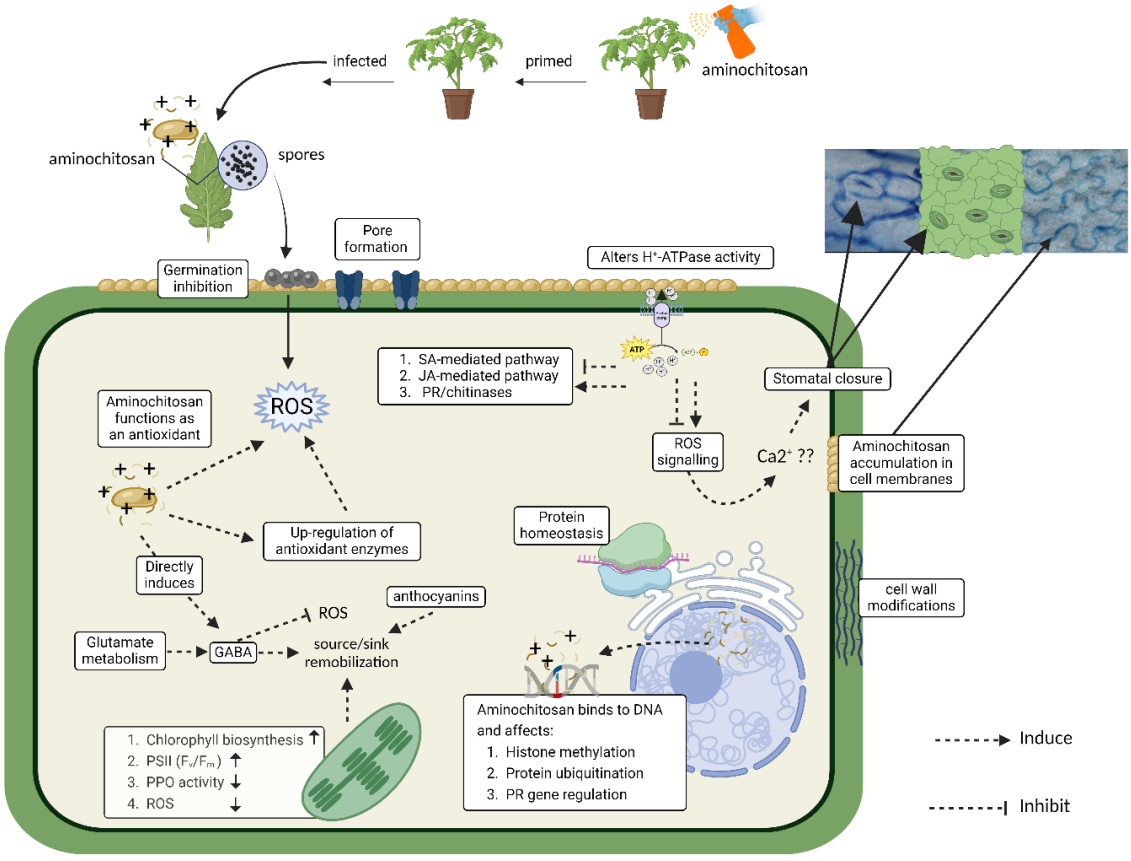

Figure 6.4: An overview of the hypothetical model of primed defence mechanisms elicited by 1 mg/mL foliar application of aminochitosan. Created in Biorender.com.

6.5.3 Future work

This PhD thesis represents the first insight into the molecular mechanisms and bioactivity of 6-deoxy-6-aminochitosan short interval priming in the tomato/*B. cinerea* pathosystem, and the maize/*F. verticillioides* pathosystems. As such, this served as a preliminary investigation into primary questions such as the method of application, optimal concentrations for direct antifungal efficacy and *in planta* immunostimulatory efficacy, potential cytotoxicity, and MoA. However, several questions remain unanswered with further questions arising from this research's limitations. Some of the primary limitations in brief were the short priming interval of 24 h, the narrow concentration range tested, low number of biological replicates, lack of experiment replication for some of the assays, design of the systemic treatment method, unmatched time comparisons, testing of one growth stage, lack of network and protein-protein interaction analysis of proteomic dataset, and lastly, COVID-19 restrictions. Some of the outstanding questions highlighted below represent different categories of future research to be undertaken based on the limitations of this study. The ultimate goal for this research is to bridge the lab-to-market gap as biopolymers represent a large potential for sustainable agriculture.

Unanswered Questions:

1. Is aminochitosan efficacious in maize?
2. Does it regulate the defense response as in tomato?
3. Does aminochitosan reduce the occurrence of mycotoxins?

1. In combination, what is the ideal dosage, interval between applications and number of applications?
2. What is the ideal length of time for assessing the primed interval?
3. Are there any negative effects of multiple rounds of priming?

1. What are the risks associated with field application?
2. Can it be used with other Integrated Pest Management strategies?
3. What are the ecological costs?
4. How will climate change and other abiotic factors affect the efficacy?
5. Does it retain its efficacy when applied as a seed coat, soil drench or other mechanisms of application?
6. How does run off of foliar application affect soil health?

1. What are the barriers to commercialization?
2. Is there any prohibitive legislature?
3. Can aminochitosan be both a biostimulant and a plant protectant product?

1. Can it be synthesized enzymatically to reduce the use of toxic solvents?
2. Does insect based aminochitosan have the same efficacy as crustacean based aminochitosan?
3. Are aminochitosan nanoparticles more efficacious than aminochitosan ?
4. Can we consistently synthesize aminochitosan with the required physiochemical properties?

Integrating information across physiological, molecular, ecological, educational, policy, and commercial domains will enhance our understanding of aminochitosan's functionality and its potential as an alternative, sustainable solution to address challenges in food security, environmental safety, and climate change.

References

Abou Ammar, G., Tryono, R., Döll, K., Karlovsky, P., Deising, H.B. & Wirsel, S.G.R. 2013. Identification of ABC transporter genes of *Fusarium graminearum* with roles in azole tolerance and/or virulence. *PLoS ONE*. 8(11):e79042. DOI: 10.1371/journal.pone.0079042.

Adamakis, I.-D.S., Sperdouli, I., Hanć, A., Dobrikova, A., Apostolova, E. & Moustakas, M. 2020. Rapid Hormetic Responses of Photosystem II Photochemistry of Clary Sage to Cadmium Exposure. *International Journal of Molecular Sciences*. 22(1):41. DOI: 10.3390/ijms22010041.

Ahmad, A., Shafique, S. & Shafique, S. 2014. Intracellular interactions involved in induced systemic resistance in tomato. *Scientia Horticulturae*. 176:127–133. DOI: 10.1016/j.scienta.2014.07.004.

Ait Barka, E., Eullaffroy, P., Clément, C. & Vernet, G. 2004. Chitosan improves development, and protects *Vitis vinifera L.* against *Botrytis cinerea*. *Plant Cell Reports*. 22(8):608–614. DOI: 10.1007/s00299-003-0733-3.

Al-Hetar, M.Y., Zainal Abidin, M.A., Sariah, M. & Wong, M.Y. 2011. Antifungal activity of chitosan against *Fusarium oxysporum* f. sp. *cubense*. *Journal of Applied Polymer Science*. 120(4):2434–2439. DOI: 10.1002/app.33455.

Ala-Kokko, K., Lanier Nalley, L., Shew, A.M., Tack, J.B., Chaminuka, P., Matlock, M.D. & D'Haese, M. 2021. Economic and ecosystem impacts of GM maize in South Africa. *Global Food Security*. 29:100544. DOI: 10.1016/j.gfs.2021.100544.

Alberts, J., Rheeder, J., Gelderblom, W., Shephard, G. & Burger, H.M. 2019. Rural subsistence maize farming in South Africa: Risk assessment and intervention models for reduction of exposure to fumonisin mycotoxins. *Toxins*. 11(6):1–20. DOI: 10.3390/toxins11060334.

Alberts, J.F., Lilly, M., Rheeder, J.P., Burger, H.M., Shephard, G.S. & Gelderblom, W.C.A. 2017. Technological and community-based methods to reduce mycotoxin exposure. *Food Control*. 73:101–109. DOI: 10.1016/j.foodcont.2016.05.029.

Ali, M.S. & Baek, K.-H. 2020. Protective Roles of Cytosolic and Plastidal Proteasomes on Abiotic Stress and Pathogen Invasion. *Plants*. 9(7):832. DOI: 10.3390/plants9070832.

Ali, S., Mir, Z.A., Tyagi, A., Bhat, J.A., Chandrashekar, N., Papolu, P.K., Rawat, S. & Grover, A. 2017. Identification and comparative analysis of *Brassica juncea* pathogenesis-related genes in response to hormonal, biotic and abiotic stresses. *Acta Physiologiae Plantarum*. 39(12):268. DOI: 10.1007/s11738-017-2565-8.

Ali, S., Ganai, B.A., Kamili, A.N., Bhat, A.A., Mir, Z.A., Bhat, J.A., Tyagi, A., Islam, S.T., et al. 2018. Pathogenesis-related proteins and peptides as promising tools for engineering plants with multiple stress tolerance. *Microbiological Research*. 212–213:29–37. DOI: 10.1016/j.micres.2018.04.008.

Alshannaq, A. & Yu, J.-H. 2017. Occurrence, Toxicity, and Analysis of Major Mycotoxins in Food. *International Journal of Environmental Research and Public Health*. 14(6):632. DOI: 10.3390/ijerph14060632.

Amborabe, B.-E., Bonmort, J., Fleurat-Lessard, P. & Roblin, G. 2008. Early events induced by

chitosan on plant cells. *Journal of Experimental Botany*. 59(9):2317–2324. DOI: 10.1093/jxb/ern096.

Ameye, M. 2017. Uncovering the Priming Potential of the Green Leaf Volatile Z-3-Hexenyl Acetate : Towards a New Disease Control Tool. Ghent University. Available: http://hdl.handle.net/1854/LU-8525800.

Ameye, M., Audenaert, K., De Zutter, N., Steppe, K., Van Meulebroek, L., Vanhaecke, L., De Vleesschauwer, D., Haesaert, G., et al. 2015. Priming of Wheat with the Green Leaf Volatile Z -3-Hexenyl Acetate Enhances Defense against *Fusarium graminearum* But Boosts Deoxynivalenol Production. *Plant Physiology*. 167(4):1671–1684. DOI: 10.1104/pp.15.00107.

Ana Niurka Hernández-Lauzardo. 2011. Current status of action mode and effect of chitosan against phytopathogens fungi. *African Journal of Microbiology Research*. 5(25):4243–4247. DOI: 10.5897/AJMR11.104.

Aranega-Bou, P., de la O Leyva, M., Finiti, I., GarcÃ-a-AgustÃ-n, P. & GonzÃ¡lez-Bosch, C. 2014. Priming of plant resistance by natural compounds. Hexanoic acid as a model. *Frontiers in Plant Science*. 5:1–12. DOI: 10.3389/fpls.2014.00488.

Arias, S.L., Theumer, M.G., Mary, V.S. & Rubinstein, H.R. 2012. Fumonisins: Probable Role as Effectors in the Complex Interaction of Susceptible and Resistant Maize Hybrids and *Fusarium verticillioides*. *Journal of Agricultural and Food Chemistry*. 60(22):5667–5675. DOI: 10.1021/jf3016333.

Arias, S.L., Mary, V.S., Otaiza, S.N., Wunderlin, D.A., Rubinstein, H.R. & Theumer, M.G. 2016. Toxin distribution and sphingoid base imbalances in *Fusarium verticillioides*-infected and fumonisin B1-watered maize seedlings. *Phytochemistry*. 125:54–64. DOI: 10.1016/j.phytochem.2016.02.006.

Ashwin, N.M.R., Barnabas, L., Ramesh Sundar, A., Malathi, P., Viswanathan, R., Masi, A., Agrawal, G.K. & Rakwal, R. 2017. Advances in proteomic technologies and their scope of application in understanding plant–pathogen interactions. *Journal of Plant Biochemistry and Biotechnology*. 26(4):371–386. DOI: 10.1007/s13562-017-0402-1.

Asselbergh, B., Curvers, K., França, S.C., Audenaert, K., Vuylsteke, M., Van Breusegem, F. & Höfte, M. 2007. Resistance to *Botrytis cinerea* in *sitiens*, an Abscisic Acid-Deficient Tomato Mutant, Involves Timely Production of Hydrogen Peroxide and Cell Wall Modifications in the Epidermis. *Plant Physiology*. 144(4):1863–1877. DOI: 10.1104/pp.107.099226.

Attjioui, M., Gillet, D., El Gueddari, N.E. & Moerschbacher, B.M. 2021. Synergistic Antimicrobial Effect of Chitosan Polymers and Oligomers. *Molecular Plant-Microbe Interactions*. 34(7):770–778. DOI: 10.1094/MPMI-07-20-0185-R.

Audenaert, K., De Meyer, G.B. & Höfte, M.M. 2002. Abscisic Acid Determines Basal Susceptibility of Tomato to *Botrytis cinerea* and Suppresses Salicylic Acid-Dependent Signaling Mechanisms. *Plant Physiology*. 128(2):491–501. DOI: 10.1104/pp.010605.

Awadalla, O.A. & Mahamoud, G. 2005. New Chitosan Derivatives Induced Resistance to *Fusarium* Wilt Disease through Phytoalexin (Gossypol) Production. *Sains Malaysian*. 34(2):141–146.

Aziz, A., Trotel-Aziz, P., Dhuicq, L., Jeandet, P., Couderchet, M. & Vernet, G. 2006. Chitosan Oligomers and Copper Sulfate Induce Grapevine Defense Reactions and Resistance to Gray Mold and Downy Mildew. *Phytopathology*. 96(11):1188–1194. DOI: 10.1094/PHYTO-96-1188.

Bacon, C.W., Yates, I.E., Hinton, D.M. & Meredith, F. 2001. Biological control of *Fusarium* moniliforme in maize. *Environmental health perspectives*. 109:325–32. DOI: 10.2307/3435026.

Badawy, M.E.I. & Rabea, E.I. 2009. Potential of the biopolymer chitosan with different molecular weights to control postharvest gray mold of tomato fruit. *Postharvest Biology and Technology*. 51(1):110–117. DOI: 10.1016/j.postharvbio.2008.05.018.

Badawy, M.E.I. & Rabea, E.I. 2011. A Biopolymer Chitosan and Its Derivatives as Promising Antimicrobial Agents against Plant Pathogens and Their Applications in Crop Protection. *International Journal of Carbohydrate Chemistry*. 2011:1–29. DOI: 10.1155/2011/460381.

Baiphethi, M.N. & Jacobs, P.T. 2009. The contribution of subsistence farming to food security in South Africa. *Agrekon*. 48(4):459–482. DOI: 10.1080/03031853.2009.9523836.

Baker, N.R. 2008. Chlorophyll Fluorescence: A Probe of Photosynthesis *in vivo*. *Annual Review of Plant Biology*. 59(1):89–113. DOI: 10.1146/annurev.arplant.59.032607.092759.

Baldwin, T.T., Zitomer, N.C., Mitchell, T.R., Zimeri, A.-M., Bacon, C.W., Riley, R.T. & Glenn, A.E. 2014. Maize Seedling Blight Induced by *Fusarium verticillioides* : Accumulation of Fumonisin B1 in Leaves without Colonization of the Leaves. *Journal of Agricultural and Food Chemistry*. 62(9):2118–2125. DOI: 10.1021/jf5001106.

Bautista-Baños, S., Necha, L.L.B., Hernández-López, M. & Rodríguez-González, F. 2016. Morphological and Ultrastructural Modifications of Chitosan-Treated Fungal Phytopathogens. In *Chitosan in the Preservation of Agricultural Commodities*. Elsevier. 251–275. DOI: 10.1016/B978-0-12-802735-6.00009-4.

Bavaresco, L., Zamboni, M., Squeri, C., Xu, S., Abramowicz, A. & Lucini, L. 2017. Chitosan and grape secondary metabolites: A proteomics and metabolomics approach. *BIO Web of Conferences*. 9:01004. DOI: 10.1051/bioconf/20170901004.

Bayçu, G., Moustaka, J., Gevrek, N. & Moustakas, M. 2018. Chlorophyll Fluorescence Imaging Analysis for Elucidating the Mechanism of Photosystem II Acclimation to Cadmium Exposure in the Hyperaccumulating Plant *Noccaea caerulescens*. *Materials*. 11(12):2580. DOI: 10.3390/ma11122580.

Bebber, D.P., Holmes, T. & Gurr, S.J. 2014. The global spread of crop pests and pathogens. *Global Ecology and Biogeography*. 23(12):1398–1407. DOI: 10.1111/geb.12214.

Beccaccioli, M., Salustri, M., Scala, V., Ludovici, M., Cacciotti, A., D'Angeli, S., Brown, D.W. & Reverberi, M. 2021. The Effect of *Fusarium verticillioides* Fumonisins on Fatty Acids, Sphingolipids, and Oxylipins in Maize Germlings. *International Journal of Molecular Sciences*. 22(5):2435. DOI: 10.3390/ijms22052435.

Bellich, B., D'Agostino, I., Semeraro, S., Gamini, A. & Cesàro, A. 2016. "The Good, the Bad and the Ugly" of Chitosans. *Marine Drugs*. 14(5):99. DOI: 10.3390/md14050099.

Bellincampi, D., Cervone, F. & Lionetti, V. 2014. Plant cell wall dynamics and wall-related susceptibility in plant-pathogen interactions. *Frontiers in Plant Science*. 5:1–8. DOI: 10.3389/fpls.2014.00228.

Benhamou, N. & Thériault, G. 1992. Treatment with chitosan enhances resistance of tomato plants to the crown and root rot pathogen *Fusarium oxysporum* f. sp. *radicis-lycopersici*. *Physiological and Molecular Plant Pathology*. 41(1):33–52. DOI: 10.1016/0885-5765(92)90047-Y.

Benito, E.P., Ten Have, A., Van 'T Klooster, J.W. & Van Kan, J.A.L. 1998. Fungal and plant gene expression during synchronized infection of tomato leaves by *Botrytis cinerea*. *European Journal of Plant Pathology*. 104(2):207–220. DOI: 10.1023/A:1008698116106.

Berger, S., Papadopoulos, M., Schreiber, U., Kaiser, W. & Roitsch, T. 2004. Complex regulation of gene expression, photosynthesis and sugar levels by pathogen infection in tomato. *Physiologia Plantarum*. 122(4):419–428. DOI: 10.1111/j.1399-3054.2004.00433.x.

Berger, S., Benediktyová, Z., Matouš, K., Bonfig, K., Mueller, M.J., Nedbal, L. & Roitsch, T. 2007. Visualization of dynamics of plant–pathogen interaction by novel combination of chlorophyll fluorescence imaging and statistical analysis: differential effects of virulent and avirulent strains of *P. syringae* and of oxylipins on *A. thaliana*. *Journal of Experimental Botany*. 58(4):797–806. DOI: 10.1093/jxb/erl208.

Besford, R.T., Richardson, C.M., Campos, J.L. & Tiburcio, A.F. 1993. Effect of polyamines on stabilization of molecular complexes in thylakoid membranes of osmotically stressed oat leaves. *Planta*. 189(2):201–206. DOI: 10.1007/BF00195077.

Betsuyaku, S., Katou, S., Takebayashi, Y., Sakakibara, H., Nomura, N. & Fukuda, H. 2018. Salicylic Acid and Jasmonic Acid Pathways are Activated in Spatially Different Domains around the Infection Site during Effector-Triggered Immunity in *Arabidopsis thaliana*. *Plant and Cell Physiology*. 59(1):8–16. DOI: 10.1093/pcp/pcx181.

Beukes, I., Rose, L.J., Shephard, G.S., Flett, B.C. & Viljoen, A. 2017. Mycotoxigenic *Fusarium* species associated with grain crops in South Africa-A review. *South African Journal of Science*. 113(3–4):1–12. DOI: 10.17159/sajs.2017/20160121.

Bhaskara Reddy, M. V., Angers, P., Castaigne, F. & Arul, J. 2000. Chitosan effects on blackmold rot and pathogenic factors produced by *Alternaria alternata* in postharvest tomatoes. *Journal of the American Society for Horticultural Science*. 125(6):742–747. DOI: 10.21273/jashs.125.6.742.

Bi, K., Liang, Y., Mengiste, T. & Sharon, A. 2022. Killing softly: a roadmap of *Botrytis cinerea* pathogenicity. *Trends in Plant Science*. 28(2):211–222. DOI: 10.1016/j.tplants.2022.08.024.

Bilgin, D.D., Zavala, J.A., Zhu, J., Clough, S.J., Ort, D.R. & Delucia, E.H. 2010. Biotic stress globally downregulates photosynthesis genes. *Plant, Cell and Environment*. 33(10):1597–1613. DOI: 10.1111/j.1365-3040.2010.02167.x.

Block, A.K., Vaughan, M.M., Schmelz, E.A. & Christensen, S.A. 2018. Biosynthesis and function of terpenoid defense compounds in maize (*Zea mays*). *Planta*. 249(1):21–30. DOI: 10.1007/s00425-018-2999-2.

Bonfig, K.B., Schreiber, U., Gabler, A., Roitsch, T. & Berger, S. 2006. Infection with virulent and avirulent P. syringae strains differentially affects photosynthesis and sink metabolism in *Arabidopsis* leaves. *Planta*. 225(1):1–12. DOI: 10.1007/s00425- 006-0303-3.

Boumaaza, B., Benkhelifa, M. & Belkhoudja, M. 2015. Effects of two salts compounds on mycelial growth, sporulation, and spore germination of six isolates of *Botrytis cinerea* in the western north of algeria. *International Journal of Microbiology*. 2015:1-8 DOI: 10.1155/2015/572626.

Brasselet, C., Pierre, G., Dubessay, P., Dols-Lafargue, M., Coulon, J., Maupeu, J., Vallet-Courbin, A., de Baynast, H., et al. 2019. Modification of Chitosan for the Generation of Functional Derivatives. *Applied Sciences*. 9(7):1321. DOI: 10.3390/app9071321.

Burger, H.M., Lombard, M.J., Shephard, G.S., Rheeder, J.R., van der Westhuizen, L. & Gelderblom, W.C.A. 2010. Dietary fumonisin exposure in a rural population of South Africa. *Food and Chemical Toxicology*. 48(8–9):2103–2108. DOI: 10.1016/j.fct.2010.05.011.

Caarls, L., Pieterse, C.M.J. & Van Wees, S.C.M. 2015. How salicylic acid takes transcriptional control over jasmonic acid signaling. *Frontiers in Plant Science*. 6:1–11. DOI: 10.3389/fpls.2015.00170.

Chan, K.X., Phua, S.Y., Crisp, P., McQuinn, R. & Pogson, B.J. 2016. Learning the Languages of the Chloroplast: Retrograde Signaling and Beyond. *Annual Review of Plant Biology*. 67(1):25–53. DOI: 10.1146/annurev-arplant-043015-111854.

Cheng, Y., Ma, W., Li, X., Miao, W., Zheng, L. & Cheng, B. 2012. Polyamines stimulate hyphal branching and infection in the early stage of *Glomus etunicatum* colonization. *World Journal of Microbiology and Biotechnology*. 28(4):1615–1621. DOI: 10.1007/s11274-011-0967-0.

Chou, H.-M., Bundock, N., Rolfe, S.A. & Scholes, J.D. 2000. Infection of *Arabidopsis thaliana* leaves with *Albugo candida* (white blister rust) causes a reprogramming of host metabolism. *Molecular Plant Pathology*. 1(2):99–113. DOI: 10.1046/j.1364-3703.2000.00013.x.

Choudhary, D.K., Prakash, A. & Johri, B.N. 2007. Induced systemic resistance (ISR) in plants: Mechanism of action. *Indian Journal of Microbiology*. 47(4):289–297. DOI: 10.1007/s12088-007-0054-2.

Choudhary, R.C., Kumaraswamy, R. V., Kumari, S., Sharma, S.S., Pal, A., Raliya, R., Biswas, P. & Saharan, V. 2017. Cu-chitosan nanoparticle boost defense responses and plant growth in maize (*Zea mays* L.). *Scientific Reports*. 7(1):3–31. DOI: 10.1038/s41598-017-08571-0.

Chowdhury, S., Basu, A. & Kundu, S. 2015. Cloning, Characterization, and Bacterial Over-Expression of an Osmotin-like Protein Gene from *Solanum nigrum* L. with Antifungal Activity Against Three Necrotrophic Fungi. *Molecular Biotechnology*. 57(4):371–381. DOI: 10.1007/s12033-014-9831-4.

Christensen, S. a, Nemchenko, A., Park, Y.-S., Borrego, E., Huang, P.-C., Schmelz, E. a, Kunze, S., Feussner, I., et al. 2014. The novel monocot-specific 9-lipoxygenase *ZmLOX12* is required to mount an effective jasmonate-mediated defense against *Fusarium verticillioides* in maize. *Molecular plant-microbe interactions : MPMI*. 27(11):1263–76. DOI: 10.1094/MPMI-06-13-0184-R.

Christie, N., Myburg, A.A., Joubert, F., Murray, S.L., Carstens, M., Lin, Y.C., Meyer, J., Crampton, B.G., et al. 2017. Systems genetics reveals a transcriptional network associated with susceptibility in the maize–grey leaf spot pathosystem. *Plant Journal*. 89(4):746–763. DOI: 10.1111/tpj.13419.

Conrath, Uwe. (2009). Chapter 9 Priming of Induced Plant Defense Responses. Advances in Botanical Research. 51. 361-395. 10.1016/S0065-2296(09)51009-9.

Conrath, U., Beckers, G.J.M., Flors, V., García-Agustín, P., Jakab, G., Mauch, F., Newman, M.-A., Pieterse, C.M.J., et al. 2006. Priming: Getting Ready for Battle. *Molecular Plant-Microbe Interactions*. 19(10):1062–1071. DOI: 10.1094/MPMI-19-1062.

Conrath, U., Beckers, G.J.M., Langenbach, C.J.G. & Jaskiewicz, M.R. 2015. Priming for Enhanced Defense. *Annual Review of Phytopathology*. 53(1):97–119. DOI: 10.1146/annurev-phyto-080614-120132.

Cook, D.E., Mesarich, C.H. & Thomma, B.P.H.J. 2015. Understanding Plant Immunity as a Surveillance System to Detect Invasion. *Annual Review of Phytopathology*. 53(1):541–563. DOI: 10.1146/annurev-phyto-080614-120114.

Cord-Landwehr, S. & Moerschbacher, B.M. 2021. Deciphering the ChitoCode: fungal chitins and chitosans as functional biopolymers. *Fungal Biology and Biotechnology*. 8(1):19. DOI: 10.1186/s40694-021-00127-2.

Crini, G. 2019. Historical review on chitin and chitosan biopolymers. *Environmental Chemistry Letters*. 17(4):1623–1643. DOI: 10.1007/s10311-019-00901-0.

Croisier, F. & Jérôme, C. 2013. Chitosan-based biomaterials for tissue engineering. *European Polymer Journal*. 49(4):780–792. DOI: 10.1016/j.eurpolymj.2012.12.009.

Czékus, Z., Iqbal, N., Pollák, B., Martics, A., Ördög, A. & Poór, P. 2021. Role of ethylene and light in chitosan-induced local and systemic defence responses of tomato plants. *Journal of Plant Physiology*. 263:153461. DOI: 10.1016/j.jplph.2021.153461.

Daou, M. & Faulds, C.B. 2017. Glyoxal oxidases: their nature and properties. *World Journal of Microbiology and Biotechnology*. 33(5):87. DOI: 10.1007/s11274-017-2254-1.

Daraban, G.M., Hlihor, R.-M. & Suteu, D. 2023. Pesticides vs. Biopesticides: From Pest Management to Toxicity and Impacts on the Environment and Human Health. *Toxics*. 11(12):983. DOI: 10.3390/toxics11120983.

Das, K. & Roychoudhury, A. 2014. Reactive oxygen species (ROS) and response of antioxidants as ROS-scavengers during environmental stress in plants. *Frontiers in Environmental Science*. 2:1–13. DOI: 10.3389/fenvs.2014.00053.

De Bona, G.S., Vincenzi, S., De Marchi, F., Angelini, E. & Bertazzon, N. 2021. Chitosan induces delayed grapevine defense mechanisms and protects grapevine against *Botrytis cinerea*. *Journal of Plant Diseases and Protection*. 128(3):715–724. DOI: 10.1007/s41348-021-00432-3.

Deery, M.J., Stimson, E. & Chappell, C.G. 2001. Size exclusion chromatography/mass spectrometry applied to the analysis of polysaccharides. *Rapid Communications in Mass*

Spectrometry. 15(23):2273–2283. DOI: 10.1002/rcm.458.

Desjardins, A.E. & Plattner, R.D. 2000. Fumonisin B1-nonproducing strains of *Fusarium verticillioides* cause maize (*Zea mays*) ear infection and ear rot. *Journal of Agricultural and Food Chemistry*. 48(11):5773–5780. DOI: 10.1021/jf000619k.

de Vega, D., Newton, A.C. & Sadanandom, A. 2018. Post-translational modifications in priming the plant immune system: ripe for exploitation? *FEBS Letters*. 592(12):1929–1936. DOI: 10.1002/1873-3468.13076.

De Vega, D., Holden, N., Hedley, P.E., Morris, J., Luna, E. & Newton, A. 2021. Chitosan primes plant defence mechanisms against *Botrytis cinerea* , including expression of Avr9/Cf-9 rapidly elicited genes. *Plant, Cell & Environment*. 44(1):290–303. DOI: 10.1111/pce.13921.

De Waard, M. 1993. Chemical Control of Plant Diseases: Problems and Prospects. *Annual Review of Phytopathology*. 31(1):403–421. DOI: 10.1146/annurev.phyto.31.1.403.

De Zutter, N., Ameye, M., Debode, J., De Tender, C., Ommeslag, S., Verwaeren, J., Vermeir, P., Audenaert, K., et al. 2021. Shifts in the rhizobiome during consecutive in planta enrichment for phosphate-solubilizing bacteria differentially affect maize P status. *Microbial Biotechnology*. 14(4):1594–1612. DOI: 10.1111/1751-7915.13824.

Dhawan, R., Luo, H., Foerster, A.M., AbuQamar, S., Du, H.-N., Briggs, S.D., Scheid, O.M. & Mengiste, T. 2009. HISTONE MONOUBIQUITINATION1 Interacts with a Subunit of the Mediator Complex and Regulates Defense against Necrotrophic Fungal Pathogens in *Arabidopsis*. *The Plant Cell*. 21(3):1000–1019. DOI: 10.1105/tpc.108.062364.

Ding, B. & Wang, G.-L. 2015. Chromatin versus pathogens: the function of epigenetics in plant immunity. *Frontiers in Plant Science*. 6:1–8. DOI: 10.3389/fpls.2015.00675.

Ding, L., Xu, H., Yi, H., Yang, L., Kong, Z., Zhang, L., Xue, S., Jia, H., et al. 2011. Resistance to Hemi-Biotrophic *F. graminearum* Infection Is Associated with Coordinated and Ordered Expression of Diverse Defense Signaling Pathways. *PLoS ONE*. 6(4):e19008. DOI: 10.1371/journal.pone.0019008.

Diwan, D., Rashid, M.M. & Vaishnav, A. 2022. Current understanding of plant-microbe interaction through the lenses of multi-omics approaches and their benefits in sustainable agriculture. *Microbiological Research*. 265:127180. DOI: 10.1016/j.micres.2022.127180.

DoH, S.A.N.D. of H. (2016). R. 2016. Regulations governing tolerances for fungus-produced toxins in foodstuffs: Amendment. *Government Notices, Government Gazette*.

Dorokhov, Y.L., Sheshukova, E. V. & Komarova, T. V. 2018. Methanol in Plant Life. *Frontiers in Plant Science*. 9:1–6. DOI: 10.3389/fpls.2018.01623.

Doughari, J. 2015. An Overview of Plant Immunity. *Journal of Plant Pathology & Microbiology*. 6(11). DOI: 10.4172/2157-7471.1000322.

Durrant, W.E., Rowland, O., Piedras, P., Hammond-Kosack, K.E. & Jones, J.D.G. 2000. cDNA-AFLP Reveals a Striking Overlap in Race-Specific Resistance and Wound Response Gene Expression Profiles. *The Plant Cell*. 12(6):963–977. DOI: 10.1105/tpc.12.6.963.

El Amerany, F., Meddich, A., Wahbi, S., Porzel, A., Taourirte, M., Rhazi, M. & Hause, B. 2020.

Foliar application of chitosan increases tomato growth and influences mycorrhization and expression of endochitinase-encoding genes. *International Journal of Molecular Sciences*. 21(2):1–18. DOI: 10.3390/ijms21020535.

El-Ghaouth, A., Arul, J., Asselin, A. & Benhamou, N. 1992. Antifungal activity of chitosan on post-harvest pathogens: induction of morphological and cytological alterations in *Rhizopus stolonifer*. *Mycological Research*. 96(9):769–779. DOI: 10.1016/S0953-7562(09)80447-4.

El-Ghaouth, A., Smilanick, J.L. & Wilson, C.L. 2000. Enhancement of the performance of *Candida saitoana* by the addition of glycolchitosan for the control of postharvest decay of apple and citrus fruit. *Postharvest Biology and Technology*. 19(1):103–110. DOI: 10.1016/S0925-5214(00)00076-4.

El Hadrami, A., Adam, L.R., El Hadrami, I. & Daayf, F. 2010. Chitosan in Plant Protection. *Marine Drugs*. 8(4):968–987. DOI: 10.3390/md8040968.

Elmore, J.M. & Coaker, G. 2011. The Role of the Plasma Membrane H^+-ATPase in Plant–Microbe Interactions. *Molecular Plant*. 4(3):416–427. DOI: 10.1093/mp/ssq083.

ElSayed, A.I., Mohamed, A.H., Rafudeen, M.S., Omar, A.A., Awad, M.F. & Mansour, E. 2022. Polyamines mitigate the destructive impacts of salinity stress by enhancing photosynthetic capacity, antioxidant defense system and upregulation of calvin cycle-related genes in rapeseed (*Brassica napus* L.). *Saudi Journal of Biological Sciences*. 29(5):3675–3686. DOI: 10.1016/j.sjbs.2022.02.053.

Fagard, M., Launay, A., Clement, G., Courtial, J., Dellagi, A., Farjad, M., Krapp, A., Soulie, M.-C., et al. 2014. Nitrogen metabolism meets phytopathology. *Journal of Experimental Botany*. 65(19):5643–5656. DOI: 10.1093/jxb/eru323.

Faoro, F., Maffi, D., Cantu, D. & Iriti, M. 2008. Chemical-induced resistance against powdery mildew in barley: the effects of chitosan and benzothiadiazole. *BioControl*. 53(2):387–401. DOI: 10.1007/s10526-007-9091-3.

FAOSTAT. 2022. *FAO Agricultural production statistics 2000–2021*. Rome: FAO. DOI: 10.4060/cc3751en.

Fenner, K., Canonica, S., Wackett, L.P. & Elsner, M. 2013. Evaluating Pesticide Degradation in the Environment: Blind Spots and Emerging Opportunities. *Science*. 341(6147):752–758. DOI: 10.1126/science.1236281.

Ferri, M., Tassoni, A., Franceschetti, M., Righetti, L., Naldrett, M.J. & Bagni, N. 2009. Chitosan treatment induces changes of protein expression profile and stilbene distribution in *Vitis vinifera* cell suspensions. *Proteomics*. 9(3):610–624. DOI: 10.1002/pmic.200800386.

Ferrochio, L. V., Cendoya, E., Zachetti, V.G.L., Farnochi, M.C., Massad, W. & Ramirez, M.L. 2014. Combined effect of chitosan and water activity on growth and fumonisin production by *Fusarium verticillioides* and *Fusarium proliferatum* on maize-based media. *International Journal of Food Microbiology*. 185:51–56. DOI: 10.1016/j.ijfoodmicro.2014.05.011.

Feussner, I. & Polle, A. 2015. What the transcriptome does not tell — proteomics and metabolomics are closer to the plants' patho-phenotype. *Current Opinion in Plant Biology*. 26:26–31. DOI: 10.1016/j.pbi.2015.05.023.

Fillinger, S. & Elad, Y. 2016. *Botrytis – the Fungus, the Pathogen and its Management in Agricultural Systems*. S. Fillinger & Y. Elad, Eds. New York, NY: Springer International Publishing. DOI: 10.1007/978-3-319-23371-0.

Flood, J. 2010. The importance of plant health to food security. *Food Security*. 2(3):215–231. DOI: 10.1007/s12571-010-0072-5.

Fu, Z.Q. & Dong, X. 2013. Systemic Acquired Resistance: Turning Local Infection into Global Defense. *Annual Review of Plant Biology*. 64(1):839–863. DOI: 10.1146/annurev-arplant-042811-105606.

Furniss, J.J. & Spoel, S.H. 2015. Cullin-RING ubiquitin ligases in salicylic acid-mediated plant immune signaling. *Frontiers in Plant Science*. 6:1–10. DOI: 10.3389/fpls.2015.00154.

Galed, G., Diaz, E., Goycoolea, F.M. & Heras, A. 2008. Influence of N -Deacetylation Conditions on Chitosan Production from α-Chitin. *Natural Product Communications*. 3(4):1934578X0800300. DOI: 10.1177/1934578X0800300414.

Galston, A.W. & Sawhney, R.K. 1990. Polyamines in plant physiology. *Plant Physiology*. 94(2):406–410. DOI: 10.1104/pp.94.2.406.

Gelderblom, W.C.A., Jaskiewicz, K., Marasas, W.F.O., Thiel, P.G., Horak, R.M., Vleggaar, R. & Kriek, N.P.J. 1988. Fumonisins - novel mycotoxins with cancer-promoting activity produced by *Fusarium moniliforme*. *Applied and Environmental Microbiology*. 54(7):1806–1811.

Gericke, M., Amaral, A.J.R., Budtova, T., De Wever, P., Groth, T., Heinze, T., Höfte, H., Huber, A., et al. 2024. The European Polysaccharide Network of Excellence (EPNOE) research roadmap 2040: Advanced strategies for exploiting the vast potential of polysaccharides as renewable bioresources. *Carbohydrate Polymers*. 326:121633. DOI: 10.1016/j.carbpol.2023.121633.

Gitelson, A.A., Chivkunova, O.B. & Merzlyak, M.N. 2009. Nondestructive estimation of anthocyanins and chlorophylls in anthocyanic leaves. *American Journal of Botany*. 96(10):1861–1868. DOI: 10.3732/ajb.0800395.

Glazebrook, J. 2005. Contrasting Mechanisms of Defense Against Biotrophic and Necrotrophic Pathogens. *Annual Review of Phytopathology*. 43(1):205–227. DOI: 10.1146/annurev.phyto.43.040204.135923.

Gonugunta, V.K., Srivastava, N. & Raghavendra, A.S. 2009. Cytosolic alkalinization is a common and early messenger preceding the production of ROS and NO during stomatal closure by variable signals, including abscisic acid, methyl jasmonate and chitosan. *Plant Signaling and Behavior*. 4(6):561–564. DOI: 10.4161/psb.4.6.8847.

Govrin, E.M. & Levine, A. 2000. The hypersensitive response facilitates plant infection by the necrotrophic pathogen *Botrytis cinerea*. *Current Biology*. 10(13):751–757. DOI: 10.1016/S0960-9822(00)00560-1.

Goy, R.C., Britto, D. de & Assis, O.B.G. 2009. A review of the antimicrobial activity of chitosan. *Polímeros*. 19(3):241–247. DOI: 10.1590/S0104-14282009000300013.

Grafi, G., Zemach, A. & Pitto, L. 2007. Methyl-CpG-binding domain (MBD) proteins in plants.

Biochimica et Biophysica Acta. 1769(5–6):287–294. DOI: 10.1016/j.bbaexp.2007.02.004.

Griffiths, G. 2015. Biosynthesis and analysis of plant oxylipins. *Free Radical Research*. 49(5):565–582. DOI: 10.3109/10715762.2014.1000318.

Grover, A. 2012. Plant Chitinases: Genetic Diversity and Physiological Roles. *Critical Reviews in Plant Sciences*. 31(1):57–73. DOI: 10.1080/07352689.2011.616043.

Gu, N., Zhang, X., Gu, X., Zhao, L., Godana, E.A., Xu, M. & Zhang, H. 2021. Transcriptomic and proteomic analysis of the mechanisms involved in enhanced disease resistance of strawberries induced by *Rhodotorula mucilaginosa* cultured with chitosan. *Postharvest Biology and Technology*. 172:111355. DOI: 10.1016/j.postharvbio.2020.111355.

Guan, Y.J., Hu, J., Wang, X.J. & Shao, C.X. 2009. Seed priming with chitosan improves maize germination and seedling growth in relation to physiological changes under low temperature stress. *Journal of Zhejiang University: Science B*. 10(6):427–433. DOI: 10.1631/jzus.B0820373.

Guo, Z., Chen, R., Xing, R., Liu, S., Yu, H., Wang, P., Li, C. & Li, P. 2006. Novel derivatives of chitosan and their antifungal activities *in vitro*. *Carbohydrate Research*. 341(3):351–354. DOI: 10.1016/j.carres.2005.11.002.

Gupta, K., Sengupta, A., Chakraborty, M. & Gupta, B. 2016. Hydrogen Peroxide and Polyamines Act as Double Edged Swords in Plant Abiotic Stress Responses. *Frontiers in Plant Science*. 7. DOI: 10.3389/fpls.2016.01343.

Gururani, M., Mohanta, T. & Bae, H. 2015. Current Understanding of the Interplay between Phytohormones and Photosynthesis under Environmental Stress. *International Journal of Molecular Sciences*. 16(8):19055–19085. DOI: 10.3390/ijms160819055.

Hadwiger, L.A. 2013. Multiple effects of chitosan on plant systems: Solid science or hype. *Plant Science*. 208:42–49. DOI: 10.1016/j.plantsci.2013.03.007.

Hadwiger, L.A. 2015. Anatomy of a nonhost disease resistance response of pea to *Fusarium solani*: PR gene elicitation via DNase, chitosan and chromatin alterations. *Frontiers in Plant Science*. 6:1–11. DOI: 10.3389/fpls.2015.00373.

Hadwiger, L. a & Beckman, J.M. 1980. Chitosan as a Component of Pea-*Fusarium solani* Interactions. *Plant physiology*. 66(2):205–211. DOI: 10.1104/pp.66.2.205.

Hadwiger, L.A. & Tanaka, K. 2017. Non-host Resistance: DNA Damage Is Associated with SA Signaling for Induction of PR Genes and Contributes to the Growth Suppression of a Pea Pathogen on Pea Endocarp Tissue. *Frontiers in Plant Science*. 08:1–12. DOI: 10.3389/fpls.2017.00446.

Hadwiger, L.A. & Tanaka, K. 2018. DNA Damage and Chromatin Conformation Changes Confer Nonhost Resistance: A Hypothesis Based on Effects of Anti-cancer Agents on Plant Defense Responses. *Frontiers in Plant Science*. 9:1–16. DOI: 10.3389/fpls.2018.01056.

Hadwiger, L.A., Beckman, J.M. & Adams, M.J. 1981. Localization of Fungal Components in the Pea-*Fusarium* Interaction Detected Immunochemically with Anti-chitosan and Anti-fungal Cell Wall Antisera . *Plant Physiology*. 67(1):170–175. DOI: 10.1104/pp.67.1.170.

Hakim, Ullah, A., Hussain, A., Shaban, M., Khan, A.H., Alariqi, M., Gul, S., Jun, Z., et al. 2018.

Osmotin: A plant defense tool against biotic and abiotic stresses. *Plant Physiology and Biochemistry*. 123:149–159. DOI: 10.1016/j.plaphy.2017.12.012.

Hamed, I., Özogul, F. & Regenstein, J.M. 2016. DOI: 10.1016/j.tifs.2015.11.007.

Han, Z., Tangni, E.K., Huybrechts, B., Munaut, F., Scauflaire, J., Wu, A. & Callebaut, A. 2014. Screening survey of co-production of fusaric acid, fusarin C, and fumonisins B1, B2 and B3 by *Fusarium* strains grown in maize grains. *Mycotoxin Research*. 30(4):231–240. DOI: 10.1007/s12550-014-0207-1.

Harish Prashanth, K. V. & Tharanathan, R.N. 2007. Chitin/chitosan: modifications and their unlimited application potential - an overview. *Trends in Food Science and Technology*. 18(3):117–131. DOI: 10.1016/j.tifs.2006.10.022.

Harper, A.M., Strange, R.N. & Langcake, P. 1981. Characterization of the nutrients required by *Botrytis cinerea* to infect broad bean leaves. *Physiological Plant Pathology*. 19(2):153–167. DOI: 10.1016/S0048-4059(81)80018-5.

Hassan, R.A., Sand, M.I. & El-Kadi, S.M. 2012. Effect of some organic acids on fungal growth and their toxins production. *Journal of Agricultural Chemistry and Biotechnology*. 3(9):391–397. DOI: 10.21608/jacb.2012.55011.

Hatier, J.-H.B. & Gould, K.S. 2008. Foliar anthocyanins as modulators of stress signals. *Journal of Theoretical Biology*. 253(3):625–627. DOI: 10.1016/j.jtbi.2008.04.018.

Hernández-Lauzardo, A.N., Bautista-Baños, S., Velázquez-del Valle, M.G., Méndez-Montealvo, M.G., Sánchez-Rivera, M.M. & Bello-Pérez, L.A. 2008. Antifungal effects of chitosan with different molecular weights on *in vitro* development of *Rhizopus stolonifer* (Ehrenb.:Fr.) Vuill. *Carbohydrate Polymers*. 73(4):541–547. DOI: 10.1016/j.carbpol.2007.12.020.

Hernández-Verdeja, T. & Strand, Å. 2018. Retrograde Signals Navigate the Path to Chloroplast Development. *Plant Physiology*. 176(2):967–976. DOI: 10.1104/pp.17.01299.

Hönig, M., Roeber, V.M., Schmülling, T. & Cortleven, A. 2023. Chemical priming of plant defense responses to pathogen attacks. *Frontiers in Plant Science*. 14(1):347–375. DOI: 10.3389/fpls.2023.1146577.

Hou, S., Liu, Z., Shen, H. & Wu, D. 2019. Damage-associated molecular pattern-triggered immunity in plants. *Frontiers in Plant Science*. 10. DOI: 10.3389/fpls.2019.00646.

Howe, G.A. & Schilmiller, A.L. 2002. Oxylipin metabolism in response to stress. *Current Opinion in Plant Biology*. 5(3):230–236. DOI: 10.1016/S1369-5266(02)00250-9.

Hu, L., Meng, X., Xing, R., Liu, S., Chen, X., Qin, Y., Yu, H. & Li, P. 2016. Design, synthesis and antimicrobial activity of 6-N-substituted chitosan derivatives. *Bioorganic & Medicinal Chemistry Letters*. 26(18):4548–4551. DOI: 10.1016/j.bmcl.2015.08.047.

Huffaker, A., Kaplan, F., Vaughan, M.M., Dafoe, N.J., Ni, X., Rocca, J.R., Alborn, H.T., Teal, P.E.A., et al. 2011. Novel Acidic Sesquiterpenoids Constitute a Dominant Class of Pathogen-Induced Phytoalexins in Maize. *Plant Physiology*. 156(4):2082–2097. DOI: 10.1104/pp.111.179457.

Huot, B., Yao, J., Montgomery, B.L. & He, S.Y. 2014. Growth–Defense Tradeoffs in Plants: A

Balancing Act to Optimize Fitness. *Molecular Plant*. 7(8):1267–1287. DOI: 10.1093/mp/ssu049.

In, Y.-W., Kim, J.-J., Kim, H.-J. & Oh, S.-W. 2013. Antimicrobial Activities of Acetic Acid, Citric Acid and Lactic Acid against *Shigella* Species. *Journal of Food Safety*. 33(1):79–85. DOI: 10.1111/jfs.12025.

Inzé, D. & Montagu, M. Van. 1995. Oxidative stress in plants. *Current Opinion in Biotechnology*. 6(2):153–158. DOI: 10.1016/0958-1669(95)80024-7.

Iriti, M. & Faoro, F. 2008. Abscisic acid is involved in chitosan-induced resistance to tobacco necrosis virus (TNV). *Plant Physiology and Biochemistry*. 46(12):1106–1111. DOI: 10.1016/j.plaphy.2008.08.002.

Iriti, M., Picchi, V., Rossoni, M., Gomarasca, S., Ludwig, N., Gargano, M. & Faoro, F. 2009. Chitosan antitranspirant activity is due to abscisic acid-dependent stomatal closure. *Environmental and Experimental Botany*. 66(3):493–500. DOI: 10.1016/j.envexpbot.2009.01.004.

Isaac, J., Hartney, S.L., Druffel, K. & Hadwiger, L.A. 2009. The non-host disease resistance response in peas; alterations in phosphorylation and ubiquitination of HMG A and histones H2A/H2B. *Plant Science*. 177(5):439–449. DOI: 10.1016/j.plantsci.2009.07.007.

Iula, G., Miras-Moreno, B., Rouphael, Y., Lucini, L. & Trevisan, M. 2022. The Complex Metabolomics Crosstalk Triggered by Four Molecular Elicitors in Tomato. *Plants*. 11(5):678. DOI: 10.3390/plants11050678.

Jabeen, N. & Ahmad, R. 2013. The activity of antioxidant enzymes in response to salt stress in safflower (*Carthamus tinctorius* L.) and sunflower (*Helianthus annuus* L.) seedlings raised from seed treated with chitosan. *Journal of the Science of Food and Agriculture*. 93(7):1699–1705. DOI: 10.1002/jsfa.5953.

Jackson, L.S., DeVries, J.W. & Bullerman, L.B. Eds. 1996. *Fumonisins in Food*. V. 392. *Advances in Experimental medicine and Biology.* Boston, MA: Springer US. DOI: 10.1007/978-1-4899-1379-1.

Jain, D. & Khurana, J.P. 2018. Role of Pathogenesis-Related (PR) Proteins in Plant Defense Mechanism. In *Molecular Aspects of Plant-Pathogen Interaction*. Springer Singapore. 265–281. DOI: 10.1007/978-981-10-7371-7_12.

Janse van Rensburg, H.C., Limami, A.M. & Van den Ende, W. 2021. Spermine and Spermidine Priming against *Botrytis cinerea* Modulates ROS Dynamics and Metabolism in *Arabidopsis*. *Biomolecules*. 11(2):223. DOI: 10.3390/biom11020223.

Jeandet, P., Bessis, R., Sbaghi, M. & Meunier, P. 1995. Production of the Phytoalexin Resveratrol by Grapes as a Response to Botrytis Attack Under Natural Conditions. *Journal of Phytopathology*. 143(3):135–139. DOI: 10.1111/j.1439-0434.1995.tb00246.x.

Ji, H., Wang, J., Chen, F., Fan, N., Wang, X., Xiao, Z. & Wang, Z. 2022. Meta-analysis of chitosan-mediated effects on plant defense against oxidative stress. *Science of The Total Environment*. 851:158212. DOI: 10.1016/j.scitotenv.2022.158212.

Jia, X., Meng, Q., Zeng, H., Wang, W. & Yin, H. 2016. Chitosan oligosaccharide induces resistance to Tobacco mosaic virus in *Arabidopsis* via the salicylic acid-mediated signalling pathway. *Scientific Reports*. 6:1–12. DOI: 10.1038/srep26144.

Jia, X., Zeng, H., Wang, W., Zhang, F. & Yin, H. 2018. Chitosan Oligosaccharide Induces Resistance to *Pseudomonas syringae* pv. tomato DC3000 in *Arabidopsis thaliana* by Activating Both Salicylic Acid– and Jasmonic Acid–Mediated Pathways. *Molecular Plant-Microbe Interactions*. 31(12):1271–1279. DOI: 10.1094/MPMI-03-18-0071-R.

Jia, X., Qin, H., Bose, S.K., Liu, T., He, J., Xie, S., Ye, M. & Yin, H. 2020. Proteomics analysis reveals the defense priming effect of chitosan oligosaccharides in *Arabidopsis*-Pst DC3000 interaction. *Plant Physiology and Biochemistry*. 149:301–312. DOI: 10.1016/j.plaphy.2020.01.037.

Jogaiah, S., Satapute, P., De Britto, S., Konappa, N. & Udayashankar, A.C. 2020. Exogenous priming of chitosan induces upregulation of phytohormones and resistance against cucumber powdery mildew disease is correlated with localized biosynthesis of defense enzymes. *International Journal of Biological Macromolecules*. 162:1825–1838. DOI: 10.1016/j.ijbiomac.2020.08.124.

Jones, J.D.G. & Dangl, J.L. 2006. The plant immune system. *Nature*. 444(7117):323–329. DOI: 10.1038/nature05286.

Kammers, K., Cole, R.N., Tiengwe, C. & Ruczinski, I. 2015. Detecting significant changes in protein abundance. *EuPA Open Proteomics*. 7:11–19. DOI: 10.1016/j.euprot.2015.02.002.

Kang, H.-C., Park, Y.-H. & Go, S.-J. 2003. Growth inhibition of a phytopathogenic fungus, *Colletotrichum* species by acetic acid. *Microbiological Research*. 158(4):321–326. DOI: 10.1078/0944-5013-00211.

Kang, H., Fan, T., Wu, J., Zhu, Y. & Shen, W.-H. 2022. Histone modification and chromatin remodeling in plant response to pathogens. *Frontiers in Plant Science*. 13:1–14. DOI: 10.3389/fpls.2022.986940.

Kangasjarvi, S., Neukermans, J., Li, S., Aro, E.-M. & Noctor, G. 2012. Photosynthesis, photorespiration, and light signalling in defence responses. *Journal of Experimental Botany*. 63(4):1619–1636. DOI: 10.1093/jxb/err402.

Kanwar, P. & Jha, G. 2019. Alterations in plant sugar metabolism: signatory of pathogen attack. *Planta*. 249(2):305–318. DOI: 10.1007/s00425-018-3018-3.

Kashige, N., Yamaguchi, T., Ohtakara, A., Mitsutomi, M., Brimacombe, J.S., Miake, F. & Watanabe, K. 1994. Structure-activity relationships in the induction of single-strand breakage in plasmid pBR322 DNA by amino sugars and derivatives. *Carbohydrate Research*. 257(2):285–291. DOI: 10.1016/0008-6215(94)80041-3.

Kaur, S., Dhillon, S.G., Verma, M., Brar, S.K., Chauhan, V.B. & Chand, R. 2012. Biopolymer based biocontrol strategies against phytopathogens: New dimensions to agriculture. In *Biocontrol: Management, Processes and Challenges*. S.K. Brar, Ed. New York, NY: Nova Science Publishers. 232.

Keinath, N.F., Kierszniowska, S., Lorek, J., Bourdais, G., Kessler, S.A., Shimosato-Asano, H.,

Grossniklaus, U., Schulze, W.X., et al. 2010. PAMP (Pathogen-associated Molecular Pattern)-induced Changes in Plasma Membrane Compartmentalization Reveal Novel Components of Plant Immunity. *Journal of Biological Chemistry*. 285(50):39140–39149. DOI: 10.1074/jbc.M110.160531.

Khan, A., Kamran, M., Imran, M., Al-Harrasi, A., Al-Rawahi, A., Al-Amri, I., Lee, I.-J. & Khan, A.L. 2019. Silicon and salicylic acid confer high-pH stress tolerance in tomato seedlings. *Scientific Reports*. 9(1):19788. DOI: 10.1038/s41598-019-55651-4.

Khanam, N.N., Ueno, M., Kihara, J., Honda, Y. & Arase, S. 2005. Suppression of red light-induced resistance in broad beans to *Botrytis cinerea* by salicylic acid. *Physiological and Molecular Plant Pathology*. 66(1–2):20–29. DOI: 10.1016/j.pmpp.2005.03.006.

Khokon, M.A.R., Uraji, M., Munemasa, S., Okuma, E., Nakamura, Y., Mori, I.C. & Murata, Y. 2010. Chitosan-induced stomatal closure accompanied by peroxidase-mediated reactive oxygen species production in *Arabidopsis*. *Bioscience, Biotechnology and Biochemistry*. 74(11):2313–2315. DOI: 10.1271/bbb.100340.

Kocięcka, J. & Liberacki, D. 2021. The potential of using chitosan on cereal crops in the face of climate change. *Plants*. 10(6). DOI: 10.3390/plants10061160.

Köhle, H., Young, D.H. & Kauss, H. 1984. Physiological changes in suspension-cultured soybean cells elicited by treatment with chitosan. *Plant Science Letters*. 33(2):221–230. DOI: 10.1016/0304-4211(84)90012-9.

Kong, M., Chen, X.G., Xing, K. & Park, H.J. 2010. Antimicrobial properties of chitosan and mode of action: A state of the art review. *International Journal of Food Microbiology*. 144(1):51–63. DOI: 10.1016/j.ijfoodmicro.2010.09.012.

Korbecka-Glinka, G., Piekarska, K. & Wiśniewska-Wrona, M. 2022. The Use of Carbohydrate Biopolymers in Plant Protection against Pathogenic Fungi. *Polymers*. 14(14):2854. DOI: 10.3390/polym14142854.

Korsman, J., Meisel, B., Kloppers, F.J., Crampton, B.G. & Berger, D.K. 2012. Quantitative phenotyping of grey leaf spot disease in maize using real-time PCR. *European Journal of Plant Pathology*. 133(2):461–471. DOI: 10.1007/s10658-011-9920-1.

Kuchitsu, K., Kikuyama, M. & Shibuya, N. 1993. N-Acetylchitooligosaccharides, biotic elicitor for phytoalexin production, induce transient membrane depolarization in suspension-cultured rice cells. *Protoplasma*. 174(1–2):79–81. DOI: 10.1007/BF01404046.

Kumar, S. & Singh, A. 2015. Biopesticides: Present Status and the Future Prospects. *Journal of Biofertilizers & Biopesticides*. 06(02):1–3. DOI: 10.4172/jbfbp.1000e129.

Kumar, A., Kumar, R., Shukla, P. & Pandey, M.K. 2021. Omics Technologies for Sustainable Agriculture and Global Food Security Volume 1. V. 1. Springer Singapore. DOI: 10.1007/978-981-16-0831-5.

Kumar, J., Ramlal, A., Mallick, D. & Mishra, V. 2021. An overview of some biopesticides and their importance in plant protection for commercial acceptance. *Plants*. 10(6):1–15. DOI: 10.3390/plants10061185.

Kyndt, T., Nahar, K., Haeck, A., Verbeek, R., Demeestere, K. & Gheysen, G. 2017. Interplay between carotenoids, abscisic acid and jasmonate guides the compatible rice - *Meloidogyne graminicola* interaction. *Frontiers in Plant Science*. 8:1–11. DOI: 10.3389/fpls.2017.00951.

Landi, L., De Miccolis Angelini, R.M., Pollastro, S., Feliziani, E., Faretra, F. & Romanazzi, G. 2017. Global transcriptome analysis and identification of differentially expressed genes in strawberry after preharvest application of benzothiadiazole and chitosan. *Frontiers in Plant Science*. 8:1–22. DOI: 10.3389/fpls.2017.00235.

Landi, M., Tattini, M. & Gould, K.S. 2015. Multiple functional roles of anthocyanins in plant-environment interactions. *Environmental and Experimental Botany*. 119:4–17. DOI: 10.1016/j.envexpbot.2015.05.012.

Lee, C.G., Koo, J.C. & Park, J.K. 2016. Antifungal Effect of Chitosan as Ca^{2+} Channel Blocker. *The Plant Pathology Journal*. 32(3):242–250. DOI: 10.5423/PPJ.OA.08.2015.0162.

Legocka, J. & Zajchert, I. 1999. Role of spermidine in the stabilization of the apoprotein of the light-harvesting chlorophyll a/b-protein complex of photosystem II during leaf senescence process. *Acta Physiologiae Plantarum*. 21(2):127–132. DOI: 10.1007/s11738-999-0066-0.

Lemke, P., Jünemann, L. & Moerschbacher, B.M. 2022. Synergistic Antimicrobial Activities of Chitosan Mixtures and Chitosan–Copper Combinations. *International Journal of Molecular Sciences*. 23(6):3345. DOI: 10.3390/ijms23063345.

Li, K., Xing, R., Liu, S. & Li, P. 2020. Chitin and Chitosan Fragments Responsible for Plant Elicitor and Growth Stimulator. *Journal of Agricultural and Food Chemistry*. 68(44):12203–12211. DOI: 10.1021/acs.jafc.0c05316.

Liaqat, F. & Eltem, R. 2018. Chitooligosaccharides and their biological activities: A comprehensive review. *Carbohydrate Polymers*. 184:243–259. DOI: 10.1016/j.carbpol.2017.12.067.

Lin, W., Hu, X., Zhang, W., John Rogers, W. & Cai, W. 2005. Hydrogen peroxide mediates defence responses induced by chitosans of different molecular weights in rice. *Journal of Plant Physiology*. 162(8):937–944. DOI: 10.1016/j.jplph.2004.10.003.

Lionetti, V., Raiola, A., Camardella, L., Giovane, A., Obel, N., Pauly, M., Favaron, F., Cervone, F., et al. 2007. Overexpression of Pectin Methylesterase Inhibitors in *Arabidopsis* Restricts Fungal Infection by *Botrytis cinerea*. *Plant Physiology*. 143(4):1871–1880. DOI: 10.1104/pp.106.090803.

Liu, D., He, X., Li, W., Chen, C. & Ge, F. 2012. Molecular cloning of a thaumatin-like protein gene from Pyrus pyrifolia and overexpression of this gene in tobacco increased resistance to pathogenic fungi. *Plant Cell, Tissue and Organ Culture*. 111(1):29–39. DOI: 10.1007/s11240-012-0167-0.

Liu, J., Tian, S., Meng, X. & Xu, Y. 2007. Effects of chitosan on control of postharvest diseases and physiological responses of tomato fruit. *Postharvest Biology and Technology*. 44(3):300–306. DOI: 10.1016/j.postharvbio.2006.12.019.

Liu, N., Sun, Y., Pei, Y., Zhang, X., Wang, P., Li, X., Li, F. & Hou, Y. 2018. A pectin methylesterase inhibitor enhances resistance to verticillium wilt. *Plant Physiology*. 176(3):2202–2220. DOI:

10.1104/pp.17.01399.

Liu, X., Cao, A., Yan, D., Ouyang, C., Wang, Q. & Li, Y. 2021. Overview of mechanisms and uses of biopesticides. *International Journal of Pest Management*. 67(1):65–72. DOI: 10.1080/09670874.2019.1664789.

Lodhi, G., Kim, Y.-S., Hwang, J.-W., Kim, S.-K., Jeon, Y.-J., Je, J.-Y., Ahn, C.-B., Moon, S.-H., et al. 2014. Chitooligosaccharide and Its Derivatives: Preparation and Biological Applications. *BioMed Research International*. 2014:1–13. DOI: 10.1155/2014/654913.

Lopez-Moya, F., Escudero, N., Zavala-Gonzalez, E.A., Esteve-Bruna, D., Blázquez, M.A., Alabadí, D. & Lopez-Llorca, L. V. 2017. Induction of auxin biosynthesis and WOX5 repression mediate changes in root development in *Arabidopsis* exposed to chitosan. *Scientific Reports*. 7(1):1–14. DOI: 10.1038/s41598-017-16874-5.

López, M.H., Molina, E.B. & Baños, S.B. 2004. Growth Inhibition of Selected Fungi by Chitosan and Plant Extracts. *Revista Mexicana de Fitopatología*. 22(2):178–186.

Loschke, D.C., Hadwiger, L.A. & Wagoner, W. 1983. Comparison of mRNA populations coding for phenylalanine ammonia lyase and other peptides from pea tissue treated with biotic and abiotic phytoalexin inducers. *Physiological Plant Pathology*. 23(1):163–173. DOI: 10.1016/0048-4059(83)90043-7.

Luan, F., Li, Q., Tan, W., Wei, L., Zhang, J., Dong, F., Gu, G. & Guo, Z. 2018. The evaluation of antioxidant and antifungal properties of 6-amino-6-deoxychitosan *in vitro*. *International Journal of Biological Macromolecules*. 107:595–603. DOI: 10.1016/j.ijbiomac.2017.09.028.

Lucini, L., Baccolo, G., Rouphael, Y., Colla, G., Bavaresco, L. & Trevisan, M. 2018. Chitosan treatment elicited defence mechanisms, pentacyclic triterpenoids and stilbene accumulation in grape (*Vitis vinifera* L.) bunches. *Phytochemistry*. 156:1–8. DOI: 10.1016/j.phytochem.2018.08.011.

Ma, P.L., Lavertu, M., Winnik, F.M. & Buschmann, M.D. 2009. New Insights into Chitosan−DNA Interactions Using Isothermal Titration Microcalorimetry. *Biomacromolecules*. 10(6):1490–1499. DOI: 10.1021/bm900097s.

Malerba, M. & Cerana, R. 2016. Chitosan Effects on Plant Systems. *International Journal of Molecular Sciences*. 17(7):996. DOI: 10.3390/ijms17070996.

Malerba, M. & Cerana, R. Recent Applications of Chitin- and Chitosan-Based Polymers in Plants. 2019. *Polymers*. 11(5):839. DOI: 10.3390/polym11050839.

Mandal, S., Kar, I., Mukherjee, A.K. & Acharya, P. 2013. Elicitor-induced defense responses in solanum lycopersicum against *Ralstonia solanacearum*. *The Scientific World Journal*. 2013. DOI: 10.1155/2013/561056.

Manoli, A., Sturaro, A., Trevisan, S., Quaggiotti, S. & Nonis, A. 2012. Evaluation of candidate reference genes for qPCR in maize. *Journal of Plant Physiology*. 169(8):807–815. DOI: 10.1016/j.jplph.2012.01.019.

Marina, M., Maiale, S.J., Rossi, F.R., Romero, M.F., Rivas, E.I., Gárriz, A., Ruiz, O.A. & Pieckenstain, F.L. 2008. Apoplastic Polyamine Oxidation Plays Different Roles in Local

Responses of Tobacco to Infection by the Necrotrophic Fungus *Sclerotinia sclerotiorum* and the Biotrophic Bacterium *Pseudomonas viridiflava*. *Plant Physiology*. 147(4):2164–2178. DOI: 10.1104/pp.108.122614.

Martinez-Medina, A., Flors, V., Heil, M., Mauch-Mani, B., Pieterse, C.M.., Pozo, M.J., Ton, J., van Dam, N.M., et al. 2016. Recognizing Plant Defense Priming. *Trends in Plant Science*. 21(10):818–822. DOI: 10.1016/j.tplants.2016.07.009.

Marzin, S., Hanemann, A., Sharma, S., Hensel, G., Kumlehn, J., Schweizer, G. & Röder, M.S. 2016. Are PECTIN ESTERASE INHIBITOR Genes Involved in Mediating Resistance to Rhynchosporium commune in Barley? *PLOS ONE*. 11(3):e0150485. DOI: 10.1371/journal.pone.0150485.

Matumba, L., Van Poucke, C., Njumbe Ediage, E. & De Saeger, S. 2017. Keeping mycotoxins away from the food: Does the existence of regulations have any impact in Africa? *Critical Reviews in Food Science and Nutrition*. 57(8):1584–1592. DOI: 10.1080/10408398.2014.993021.

Mauch-Mani, B., Baccelli, I., Luna, E. & Flors, V. 2017. Defense Priming: An Adaptive Part of Induced Resistance. *Annual Review of Plant Biology*. 68:485–512. DOI: 10.1146/annurev-arplant-042916-041132.

Mayer, A.M. 2006. Polyphenol oxidases in plants and fungi: Going places? A review. *Phytochemistry*. 67(21):2318–2331. DOI: 10.1016/j.phytochem.2006.08.006.

Mejía-Teniente, L., Durán-Flores, F. de D., Chapa-Oliver, A., Torres-Pacheco, I., Cruz-Hernández, A., González-Chavira, M., Ocampo-Velázquez, R. & Guevara-González, R. 2013. Oxidative and Molecular Responses in *Capsicum annuum* L. after Hydrogen Peroxide, Salicylic Acid and Chitosan Foliar Applications. *International Journal of Molecular Sciences*. 14(5):10178–10196. DOI: 10.3390/ijms140510178.

Meng, L., Höfte, M. & Van Labeke, M.-C. 2019. Leaf age and light quality influence the basal resistance against *Botrytis cinerea* in strawberry leaves. *Environmental and Experimental Botany*. 157:35–45. DOI: 10.1016/j.envexpbot.2018.09.025.

Meng, L., Mestdagh, H., Ameye, M., Audenaert, K., Höfte, M. & Van Labeke, M.-C. 2020. Phenotypic Variation of *Botrytis cinerea* Isolates Is Influenced by Spectral Light Quality. *Frontiers in Plant Science*. 11:1–15. DOI: 10.3389/fpls.2020.01233.

Merlot, S., Leonhardt, N., Fenzi, F., Valon, C., Costa, M., Piette, L., Vavasseur, A., Genty, B., et al. 2007. Constitutive activation of a plasma membrane H^+-ATPase prevents abscisic acid-mediated stomatal closure. *The EMBO Journal*. 26(13):3216–3226. DOI: 10.1038/sj.emboj.7601750.

Meyer, J., Murray, S.L. & Berger, D.K. 2016. Signals that stop the rot: Regulation of secondary metabolite defences in cereals. *Physiological and Molecular Plant Pathology*. 94:156–166. DOI: 10.1016/j.pmpp.2015.05.011.

Meyer, J., Berger, D.K., Christensen, S.A. & Murray, S.L. 2017. RNA-Seq analysis of resistant and susceptible sub-tropical maize lines reveals a role for kauralexins in resistance to grey leaf spot disease, caused by *Cercospora zeina*. *BMC Plant Biology*. 17(1):197. DOI: 10.1186/s12870-017-1137-9.

Minic, Z. & Jouanin, L. 2006. Plant glycoside hydrolases involved in cell wall polysaccharide degradation. *Plant Physiology and Biochemistry*. 44(7–9):435–449. DOI: 10.1016/j.plaphy.2006.08.001.

Misihairabgwi, J.M., Ezekiel, C.N., Sulyok, M., Shephard, G.S. & Krska, R. 2019. Mycotoxin contamination of foods in Southern Africa: A 10-year review (2007–2016). *Critical Reviews in Food Science and Nutrition*. 59(1):43–58. DOI: 10.1080/10408398.2017.1357003.

Mochizuki, N., Tanaka, R., Grimm, B., Masuda, T., Moulin, M., Smith, A.G., Tanaka, A. & Terry, M.J. 2010. The cell biology of tetrapyrroles: A life and death struggle. *Trends in Plant Science*. 15(9):488–498. DOI: 10.1016/j.tplants.2010.05.012.

Montilla-Bascón, G., Rubiales, D., Altabella, T. & Prats, E. 2016. Free polyamine and polyamine regulation during pre-penetration and penetration resistance events in oat against crown rust (*Puccinia coronata* f. sp. *avenae*). *Plant Pathology*. 65(3):392–401. DOI: 10.1111/ppa.12423.

Moran, H.B.T., Turley, J.L., Andersson, M. & Lavelle, E.C. 2018. Immunomodulatory properties of chitosan polymers. *Biomaterials*. 184:1–9. DOI: 10.1016/j.biomaterials.2018.08.054.

Mosblech, A., Feussner, I. & Heilmann, I. 2009. Oxylipins: Structurally diverse metabolites from fatty acid oxidation. *Plant Physiology and Biochemistry*. 47(6):511–517. DOI: 10.1016/j.plaphy.2008.12.011.

Mourya, V.K. & Inamdar, N. 2011. Chitosan and Anionic Polymers – Complex Formation and Applications. Polysaccharides: Development, Properties and Applications. 333–377.

Mukarram, M., Ali, J., Dadkhah-Aghdash, H., Kurjak, D., Kačík, F. & Ďurkovič, J. 2023. Chitosan-induced biotic stress tolerance and crosstalk with phytohormones, antioxidants, and other signalling molecules. *Frontiers in Plant Science*. 14:1–14. DOI: 10.3389/fpls.2023.1217822.

Muniz, C.R., Freire, F.C.O., Viana, F.M.P., Cardoso, J.E., Sousa, C.A.F., Guedes, M.I.F., van der Schoor, R. & Jalink, H. 2014. Monitoring cashew seedlings during interactions with the fungus Lasiodiplodia theobromae using chlorophyll fluorescence imaging. *Photosynthetica*. 52(4):529–537. DOI: 10.1007/s11099-014-0061-6.

Munkvold, G.P. & Desjardins, A.E. 1997. Fumonisins in Maize. *Plant Disease*. 81(6):556–565. DOI: 10.1094/PDIS.1997.81.6.556.

Munkvold, G.P., McGee, D.C. & Carlton, W.M. 1997. Importance of Different Pathways for Maize Kernel Infection by *Fusarium* moniliforme. *Phytopathology*. 87(2):209–217. DOI: 10.1094/PHYTO.1997.87.2.209.

Murchie, E.H. & Lawson, T. 2013. Chlorophyll fluorescence analysis: a guide to good practice and understanding some new applications. *Journal of Experimental Botany*. 64(13):3983–3998. DOI: 10.1093/jxb/ert208.

Nambeesan, S., AbuQamar, S., Laluk, K., Mattoo, A.K., Mickelbart, M. V., Ferruzzi, M.G., Mengiste, T. & Handa, A.K. 2012. Polyamines Attenuate Ethylene-Mediated Defense Responses to Abrogate Resistance to *Botrytis cinerea* in Tomato. *Plant Physiology*. 158(2):1034–1045. DOI: 10.1104/pp.111.188698.

Narendranath, N. V., Thomas, K.C. & Ingledew, W.M. 2001. Effects of acetic acid and lactic

acid on the growth of *Saccharomyces cerevisiae* in a minimal medium. *Journal of Industrial Microbiology and Biotechnology*. 26(3):171–177. DOI: 10.1038/sj.jim.7000090.

Ncube, E., Flett, B.C., Waalwijk, C. & Viljoen, A. 2011. *Fusarium* spp. and levels of fumonisins in maize produced by subsistence farmers in South Africa. *South African Journal of Science*. 107(1/2):1–7. DOI: 10.4102/sajs.v107i1/2.367.

Ndimba, B.K., Chivasa, S., Hamilton, J.M., Simon, W.J. & Slabas, A.R. 2003. Proteomic analysis of changes in the extracellular matrix of *Arabidopsis* cell suspension cultures induced by fungal elicitors. *Proteomics*. 3(6):1047–1059. DOI: 10.1002/pmic.200300413.

Nicolaisen, M., Suproniene, S., Nielsen, L.K., Lazzaro, I., Spliid, N.H. & Justesen, A.F. 2009. Real-time PCR for quantification of eleven individual *Fusarium* species in cereals. *Journal of Microbiological Methods*. 76(3):234–240. DOI: 10.1016/j.mimet.2008.10.016.

Nishad, R., Ahmed, T., Rahman, V.J. & Kareem, A. 2020. Modulation of Plant Defense System in Response to Microbial Interactions. *Frontiers in Microbiology*. 11(July):1–13. DOI: 10.3389/fmicb.2020.01298.

Nji, Q.N., Babalola, O.O., Nleya, N. & Mwanza, M. 2022. Underreported Human Exposure to Mycotoxins: The Case of South Africa. *Foods*. 11(17):1–19. DOI: 10.3390/foods11172714.

Oerke, E.C. 2006. Crop losses to pests. *The Journal of Agricultural Science*. 144(1):31–43. DOI: 10.1017/S0021859605005708.

Oliveira Junior, E.N. de, Melo, I.S. De & Franco, T.T. 2012. Changes in hyphal morphology due to chitosan treatment in some fungal species. *Brazilian Archives of Biology and Technology*. 55(5):637–646. DOI: 10.1590/S1516-89132012000500001.

Omotayo, O.P. & Babalola, O.O. 2023. *Fusarium verticillioides* of maize plant: Potentials of propitious phytomicrobiome as biocontrol agents. *Frontiers in Fungal Biology*. 4:1–12. DOI: 10.3389/ffunb.2023.1095765.

Omotayo, O.P., Omotayo, A.O., Mwanza, M. & Babalola, O.O. 2019. Prevalence of mycotoxins and their consequences on human health. *Toxicological Research*. 35(1):1–7. DOI: 10.5487/TR.2019.35.1.001.

Oren, L., Ezrati, S., Cohen, D. & Sharon, A. 2003. Early Events in the *Fusarium verticillioides*-Maize Interaction Characterized by Using a Green Fluorescent Protein-Expressing Transgenic Isolate. *Applied and Environmental Microbiology*. 69(3):1695–1701. DOI: 10.1128/AEM.69.3.1695-1701.2003.

Pabón-Baquero, D., Velázquez-del Valle, M.G., Evangelista-Lozano, S., León-Rodriguez, R. & Hernández-Lauzardo, A.N. 2015. Chitosan effects on phytopathogenic fungi and seed germination of *Jatropha curcas* L. *Revista Chapingo Serie Ciencias Forestales y del Ambiente*. XXI(3):241–253. DOI: 10.5154/r.rchscfa.2014.10.051.

Palma-Guerrero, J., Jansson, H.-B., Salinas, J. & Lopez-Llorca, L.V. 2007. Effect of chitosan on hyphal growth and spore germination of plant pathogenic and biocontrol fungi. *Journal of Applied Microbiology*. 104(2):541–553. DOI: 10.1111/j.1365-2672.2007.03567.x.

Palma-Guerrero, J., Huang, I.C., Jansson, H.B., Salinas, J., Lopez-Llorca, L. V. & Read, N.D. 2009.

Chitosan permeabilizes the plasma membrane and kills cells of *Neurospora crassa* in an energy dependent manner. *Fungal Genetics and Biology*. 46(8):585–594. DOI: 10.1016/j.fgb.2009.02.010.

Palma-Guerrero, J., Lopez-Jimenez, J.A., Pérez-Berná, A.J., Huang, I.-C., Jansson, H.-B., Salinas, J., Villalaín, J., Read, N.D., et al. 2010. Membrane fluidity determines sensitivity of filamentous fungi to chitosan. *Molecular Microbiology*. 75(4):1021–1032. DOI: 10.1111/j.1365-2958.2009.07039.x.

Papenbrock, J., Mock, H.-P., Tanaka, R., Kruse, E. & Grimm, B. 2000. Role of Magnesium Chelatase Activity in the Early Steps of the Tetrapyrrole Biosynthetic Pathway. *Plant Physiology*. 122(4):1161–1170. DOI: 10.1104/pp.122.4.1161.

Pastor, V., Luna, E., Ton, J., Cerezo, M., García-Agustín, P. & Flors, V. 2013. Fine tuning of reactive oxygen species homeostasis regulates primed immune responses in *Arabidopsis*. *Molecular Plant-Microbe Interactions*. 26(11):1334–1344. DOI: 10.1094/MPMI-04-13-0117-R.

Pavicic, M., Overmyer, K., Rehman, A.U., Jones, P., Jacobson, D. & Himanen, K. 2021. Image-Based Methods to Score Fungal Pathogen Symptom Progression and Severity in Excised *Arabidopsis* Leaves. *Plants*. 10(1):158. DOI: 10.3390/plants10010158.

Peian, Z., Haifeng, J., Peijie, G., Sadeghnezhad, E., Qianqian, P., Tianyu, D., Teng, L., Huanchun, J., et al. 2021. Chitosan induces jasmonic acid production leading to resistance of ripened fruit against *Botrytis cinerea* infection. *Food Chemistry*. 337:127772. DOI: 10.1016/j.foodchem.2020.127772.

Pengfei Leng. 2011. Applications and development trends in biopesticides. *African Journal of Biotechnology*. 10(86):19864–19873. DOI: 10.5897/AJBX11.009.

Pérez-Bueno, M.L., Pineda, M. & Barón, M. 2019. Phenotyping Plant Responses to Biotic Stress by Chlorophyll Fluorescence Imaging. *Frontiers in Plant Science*. 10(September):1–15. DOI: 10.3389/fpls.2019.01135.

Phoku, J.Z., Dutton, M.F., Njobeh, P.B., Mwanza, M., Egbuta, M.A. & Chilaka, C.A. 2012. *Fusarium* infection of maize and maize-based products and exposure of a rural population to fumonisin B1 in Limpopo Province, South Africa. *Food Additives and Contaminants*. 29(11):1743–1751. DOI: 10.1080/19440049.2012.708671.

Pienaar, L. & Traub, L.N. 2015. Understanding the smallholder farmer in South Africa: Towards a sustainable livelihoods classification. *International Association of Agricultural Economics*. 18. Available: https://ageconsearch.umn.edu/record/212633/.

Pieterse, C.M.J., Ton, J. & Loon, L.C. Van. 2001. Cross-talk between plant defence signalling pathways: boost or burden? *AgBiotechNet*. 3:1–8.

Pieterse, C.M.J., Van der Does, D., Zamioudis, C., Leon-Reyes, A. & Van Wees, S.C.M. 2012. Hormonal Modulation of Plant Immunity. *Annual Review of Cell and Developmental Biology*. 28(1):489–521. DOI: 10.1146/annurev-cellbio-092910-154055.

Pieterse, C.M.J., Zamioudis, C., Berendsen, R.L., Weller, D.M., Van Wees, S.C.M. & Bakker, P.A.H.M. 2014. Induced Systemic Resistance by Beneficial Microbes. *Annual Review of Phytopathology*. 52(1):347–375. DOI: 10.1146/annurev-phyto-082712-102340.

Pinstrup-Andersen, P. 2000. The future world food situation and the role of plant diseases. *Canadian Journal of Plant Pathology*. 22(4):321–331. DOI: 10.1080/07060660009500451.

Popp, J., Pető, K. & Nagy, J. 2013. Pesticide productivity and food security. A review. *Agronomy for Sustainable Development*. 33(1):243–255. DOI: 10.1007/s13593-012-0105-x.

Pourtau, N., Jennings, R., Pelzer, E., Pallas, J. & Wingler, A. 2006. Effect of sugar-induced senescence on gene expression and implications for the regulation of senescence in *Arabidopsis*. *Planta*. 224(3):556–568. DOI: 10.1007/s00425-006-0243-y.

Poveda, J., Barquero, M. & González-Andrés, F. 2020. Insight into the Microbiological Control Strategies against *Botrytis cinerea* Using Systemic Plant Resistance Activation. *Agronomy*. 10(11):1822. DOI: 10.3390/agronomy10111822.

Poznanski, P., Hameed, A. & Orczyk, W. 2023. Chitosan and Chitosan Nanoparticles: Parameters Enhancing Antifungal Activity. *Molecules*. 28(7):2996. DOI: 10.3390/molecules28072996.

Raafat, D., Von Bargen, K., Haas, A. & Sahl, H.G. 2008. Insights into the mode of action of chitosan as an antibacterial compound. *Applied and Environmental Microbiology*. 74(12):3764–3773. DOI: 10.1128/AEM.00453-08.

Rabea, E.I., Badawy, M.E.T., Stevens, C. V., Smagghe, G. & Steurbaut, W. 2003. Chitosan as Antimicrobial Agent: Applications and Mode of Action. *Biomacromolecules*. 4(6):1457–1465. DOI: 10.1021/bm034130m.

Raj, S.N., Lavanya, S.N., Sudisha, J. & Shetty, H.S. 2011. Applications of Biopolymers in Agriculture with Special Reference to Role of Plant Derived Biopolymers in Crop Protection. In *Biopolymers*. Wiley. 459–481. DOI: 10.1002/9781118164792.ch16.

Rajam, M. V., Weinstein, L.H. & Galston, A.W. 1985. Prevention of a plant disease by specific inhibition of fungal polyamine biosynthesis. *Proceedings of the National Academy of Sciences of the United States of America*. 82(20):6874–6878. DOI: 10.1073/pnas.82.20.6874.

Rakwal, R., Tamogami, S., Agrawal, G.K. & Iwahashi, H. 2002. Octadecanoid signaling component “burst” in rice (*Oryza sativa* L.) seedling leaves upon wounding by cut and treatment with fungal elicitor chitosan. *Biochemical and Biophysical Research Communications*. 295(5):1041–1045. DOI: 10.1016/S0006-291X(02)00779-9.

Ramirez-Prado, J.S., Piquerez, S.J.M., Bendahmane, A., Hirt, H., Raynaud, C. & Benhamed, M. 2018. Modify the histone to win the battle: Chromatin dynamics in plant–pathogen interactions. *Frontiers in Plant Science*. 9:1–18. DOI: 10.3389/fpls.2018.00355.

Ramírez, V., López, A., Mauch-Mani, B., Gil, M.J. & Vera, P. 2013. An Extracellular Subtilase Switch for Immune Priming in *Arabidopsis*. *PLOS Pathogens*. 9(6):e1003445. Available: https://doi.org/10.1371/journal.ppat.1003445.

Reimer-Michalski, E.M. & Conrath, U. 2016. Innate immune memory in plants. *Seminars in Immunology*. 28(4):319–327. DOI: 10.1016/j.smim.2016.05.006.

Rezzonico, F., Nicot, P.C. & Fahrentrapp, J. 2018. Expression of tomato reference genes using established primer sets: Stability across experimental set-ups. *Journal of Phytopathology*.

166(2):123–128. DOI: 10.1111/jph.12668.

Rheeder, J.P. 1992. *Fusarium* moniliforme and Fumonisins in Corn in Relation to Human Esophageal Cancer in Transkei. *Phytopathology*. 82(3):353. DOI: 10.1094/Phyto-82-353.

Rheeder, J.P., Van der Westhuizen, L., Imrie, G. & Shephard, G.S. 2016. *Fusarium* species and fumonisins in subsistence maize in the former Transkei region, South Africa: a multi-year study in rural villages. *Food Additives & Contaminants: Part B*. 9(3):176–184. DOI: 10.1080/19393210.2016.1154612.

Rinaudo, M. 2006. Chitin and chitosan: Properties and applications. *Progress in Polymer Science*. 31(7):603–632. DOI: 10.1016/j.progpolymsci.2006.06.001.

Robert-Seilaniantz, A., Grant, M. & Jones, J.D.G. 2011. Hormone crosstalk in plant disease and defense: more than just jasmonate-salicylate antagonism. *Annual Review of Phytopathology*. 49(1):317–343. DOI: 10.1146/annurev-phyto-073009-114447.

Roby, D., Gadelle, A. & Toppan, A. 1987. Chitin oligosaccharides as elicitors of chitinase activity in melon plants. *Biochemical and Biophysical Research Communications*. 143(3):885–892. DOI: 10.1016/0006-291X(87)90332-9.

Rojas, C.M., Senthil-Kumar, M., Tzin, V. & Mysore, K.S. 2014. Regulation of primary plant metabolism during plant-pathogen interactions and its contribution to plant defense. *Frontiers in Plant Science*. 5(FEB):1–12. DOI: 10.3389/fpls.2014.00017.

Rolfe, S.A. & Scholes, J.D. 2010. Chlorophyll fluorescence imaging of plant–pathogen interactions. *Protoplasma*. 247(3–4):163–175. DOI: 10.1007/s00709-010-0203-z.

Romanazzi, G., Feliziani, E., Baños, S.B. & Sivakumar, D. 2017. Shelf life extension of fresh fruit and vegetables by chitosan treatment. *Critical Reviews in Food Science and Nutrition*. 57(3):579–601. DOI: 10.1080/10408398.2014.900474.

Romanazzi, G., Feliziani, E. & Sivakumar, D. 2018. Chitosan, a Biopolymer With Triple Action on Postharvest Decay of Fruit and Vegetables: Eliciting, Antimicrobial and Film-Forming Properties. *Frontiers in Microbiology*. 9:1–9. DOI: 10.3389/fmicb.2018.02745.

Rossouw, S.C., Bendou, H., Blignaut, R.J., Bell, L., Rigby, J. & Christoffels, A. 2021. Evaluation of Protein Purification Techniques and Effects of Storage Duration on LC-MS/MS Analysis of Archived FFPE Human CRC Tissues. *Pathology and Oncology Research*. 27. DOI: 10.3389/pore.2021.622855.

Saharan, V., Mehrotra, A., Khatik, R., Rawal, P., Sharma, S.S. & Pal, A. 2013. Synthesis of chitosan based nanoparticles and their *in vitro* evaluation against phytopathogenic fungi. *International Journal of Biological Macromolecules*. 62:677–683. DOI: 10.1016/j.ijbiomac.2013.10.012.

Samarah, N.H., AL-Quraan, N.A., Massad, R.S. & Welbaum, G.E. 2020. Treatment of bell pepper (*Capsicum annuum* L.) seeds with chitosan increases chitinase and glucanase activities and enhances emergence in a standard cold test. *Scientia Horticulturae*. 269:109393. DOI: 10.1016/j.scienta.2020.109393.

Satoh, T., Kano, H., Nakatani, M., Sakairi, N., Shinkai, S. & Nagasaki, T. 2006. 6-Amino-6-deoxy-

chitosan. Sequential chemical modifications at the C-6 positions of N-phthaloyl-chitosan and evaluation as a gene carrier. *Carbohydrate Research*. 341(14):2406–2413. DOI: 10.1016/j.carres.2006.06.019.

Sayed, S. 2018. Synthesis of 6-Deoxy-6-Amino Chitosan and Applications thereof. University of Cape Town. Available: http://hdl.handle.net/11427/36909.

Sayed, S., Millard, T. & Jardine, A. 2018. Expedient synthesis and properties of 6-deoxy-6-amino chitosan. *Carbohydrate Polymers*. 196:187–198. DOI: 10.1016/j.carbpol.2018.05.030.

Schaller, A. & Oecking, C. 1999. Modulation of Plasma Membrane H^+-ATPase Activity Differentially Activates Wound and Pathogen Defense Responses in Tomato Plants. *The Plant Cell*. 11(2):263–272. DOI: 10.1105/tpc.11.2.263.

Scharte, J., Schon, H. & Weis, E. 2005. Photosynthesis and carbohydrate metabolism in tobacco leaves during an incompatible interaction with Phytophthora nicotianae. *Plant, Cell and Environment*. 28(11):1421–1435. DOI: 10.1111/j.1365-3040.2005.01380.x.

Schmelz, E.A., Kaplan, F., Huffaker, A., Dafoe, N.J., Vaughan, M.M., Ni, X., Rocca, J.R., Alborn, H.T., et al. 2011. Identity, regulation, and activity of inducible diterpenoid phytoalexins in maize. *Proceedings of the National Academy of Sciences of the United States of America*. 108(13):5455–60. DOI: 10.1073/pnas.1014714108.

Schmelz, E.A., Huffaker, A., Sims, J.W., Christensen, S.A., Lu, X., Okada, K. & Peters, R.J. 2014. Biosynthesis, elicitation and roles of monocot terpenoid phytoalexins. *Plant Journal*. 79(4):659–678. DOI: 10.1111/tpj.12436.

Schoeman, A., Flett, B.C., Janse van Rensburg, B., Ncube, E. & Viljoen, A. 2018. Pathogenicity and toxigenicity of *Fusarium verticillioides* isolates collected from maize roots, stems and ears in South Africa. *European Journal of Plant Pathology*. 1–13. DOI: 10.1007/s10658-018-1510-z.

Schwämmle, V., León, I.R. & Jensen, O.N. 2013. Assessment and improvement of statistical tools for comparative proteomics analysis of sparse data sets with few experimental replicates. *Journal of Proteome Research*. 12(9):3874–3883. DOI: 10.1021/pr400045u.

Seifi, H.S., Van Bockhaven, J., Angenon, G. & Höfte, M. 2013. Glutamate Metabolism in Plant Disease and Defense: Friend or Foe? *Molecular Plant-Microbe Interactions*. 26(5):475–485. DOI: 10.1094/MPMI-07-12-0176-CR.

Sergeant, K. & Renaut, J. 2010. Plant Biotic Stress and Proteomics. *Current Proteomics*. 7(4):275–297. DOI: 10.2174/157016410793611765.

Sewelam, N., Jaspert, N., Van Der Kelen, K., Tognetti, V.B., Schmitz, J., Frerigmann, H., Stahl, E., Zeier, J., et al. 2014. Spatial H_2O_2 Signaling Specificity: H_2O_2 from Chloroplasts and Peroxisomes Modulates the Plant Transcriptome Differentially. *Molecular Plant*. 7(7):1191–1210. DOI: 10.1093/mp/ssu070.

Sharma, A., Shukla, A., Attri, K., Kumar, M., Kumar, P., Suttee, A., Singh, G., Barnwal, R.P., et al. 2020. Global trends in pesticides: A looming threat and viable alternatives. *Ecotoxicology and Environmental Safety*. 201:110812. DOI: 10.1016/j.ecoenv.2020.110812.

Shephard, G.S., Leggott, N.L., Stockenström, S., Somdyala, N.I.M. & Marasas, W.F.O. 2002. Preparation of South African maize porridge: Effect on fumonisin mycotoxin levels. *South African Journal of Science*. 98(7–8):393–396.

Shephard, G.S., Marasas, W.F.O., Burger, H.M., Somdyala, N.I.M., Rheeder, J.P., Van der Westhuizen, L., Gatyeni, P. & Van Schalkwyk, D.J. 2007. Exposure assessment for fumonisins in the former Transkei region of South Africa. *Food Additives and Contaminants*. 24(6):621–629. DOI: 10.1080/02652030601101136.

Shephard, G.S., Burger, H.M., Rheeder, J.P., Alberts, J.F. & Gelderblom, W.C.A. 2019. The effectiveness of regulatory maximum levels for fumonisin mycotoxins in commercial and subsistence maize crops in South Africa. *Food Control*. 97:77–80. DOI: 10.1016/j.foodcont.2018.10.004.

Siddaiah, C.N., Prasanth, K.V.H., Satyanarayana, N.R., Mudili, V., Gupta, V.K., Kalagatur, N.K., Satyavati, T., Dai, X.-F., et al. 2018. Chitosan nanoparticles having higher degree of acetylation induce resistance against pearl millet downy mildew through nitric oxide generation. *Scientific Reports*. 8(1):2485. DOI: 10.1038/s41598-017-19016-z.

Singh, A., Gairola, K., Upadhyay, V. & Kumar, J. 2018. Chitosan: An elicitor and antimicrobial Bio-resource in plant protection. *Agricultural Reviews*. 39(00):163–168. DOI: 10.18805/ag.R-1723.

Smith, A.M., Moxon, S. & Morris, G.A. 2016. Biopolymers as wound healing materials. In *Wound Healing Biomaterials*. M.S.B.T.-W.H.B. Ågren, Ed. Elsevier. 261–287. DOI: 10.1016/B978-1-78242-456-7.00013-1.

Smith, J.E., Mengesha, B., Tang, H., Mengiste, T. & Bluhm, B.H. 2014. Resistance to *Botrytis cinerea* in *Solanum lycopersicoides* involves widespread transcriptional reprogramming. *BMC Genomics*. 15(1):334. DOI: 10.1186/1471-2164-15-334.

Stamelou, M.-L., Sperdouli, I., Pyrri, I., Adamakis, I.-D.S. & Moustakas, M. 2021. Hormetic Responses of Photosystem II in Tomato to *Botrytis cinerea*. *Plants*. 10(3):521. DOI: 10.3390/plants10030521.

Statistics South Africa. 2020. *Census of commercial agriculture, 2017 Financial and production statistics*. Available: www.statssa.gov.za.

Statistics South Africa. 2021. *Assessing food inadequacy and hunger in South Africa in 2021 using the General Household Survey (GHS)*.

Strand, S.P., Danielsen, S., Christensen, B.E. & Vårum, K.M. 2005. Influence of Chitosan Structure on the Formation and Stability of DNA−Chitosan Polyelectrolyte Complexes. *Biomacromolecules*. 6(6):3357–3366. DOI: 10.1021/bm0503726.

Suarez-Fernandez, M., Marhuenda-Egea, F.C., Lopez-Moya, F., Arnao, M.B., Cabrera-Escribano, F., Nueda, M.J., Gunsé, B. & Lopez-Llorca, L.V. 2020. Chitosan Induces Plant Hormones and Defenses in Tomato Root Exudates. *Frontiers in Plant Science*. 11:1–15. DOI: 10.3389/fpls.2020.572087.

Sun, T., Zhou, D., Xie, J. & Mao, F. 2007. Preparation of chitosan oligomers and their antioxidant activity. *European Food Research and Technology*. 225(3–4):451–456. DOI:

10.1007/s00217-006-0439-1.

Suwanchaikasem, P., Nie, S., Idnurm, A., Selby-Pham, J., Walker, R. & Boughton, B.A. 2023. Effects of chitin and chitosan on root growth, biochemical defense response and exudate proteome of Cannabis sativa. *Plant-Environment Interactions*. 4(3):115–133. DOI: 10.1002/pei3.10106.

Sydenham, E.W., Thiel, P.G., Marasas, W.F.O., Shephard, G.S., Van Schalkwyk, D.J. & Koch, K.R. 1990. Natural occurrence of some *Fusarium* mycotoxins in corn from low and high esophageal cancer prevalence areas of the Transkei, Southern Africa. *Journal of Agricultural and Food Chemistry*. 38(10):1900–1903. DOI: 10.1021/jf00100a004.

Tan, J. 2021. New insights in the ecology , physiology and genome editing of *Fusarium poae*, a weakly-pathogenic member of the *Fusarium* head blight disease complex in wheat. Gent University. Available: http://hdl.handle.net/1854/LU-8708299.

Tan, J., Ameye, M., Landschoot, S., De Zutter, N., De Saeger, S., De Boevre, M., Abdallah, M.F., Van der Lee, T., et al. 2020. At the scene of the crime: New insights into the role of weakly pathogenic members of the *Fusarium* head blight disease complex. *Molecular Plant Pathology*. 21(12):1559–1572. DOI: 10.1111/mpp.12996.

Tanaka, R., Kobayashi, K. & Masuda, T. 2011. Tetrapyrrole Metabolism in *Arabidopsis thaliana* . *The Arabidopsis Book*. 9(9):e0145. DOI: 10.1199/tab.0145.

Terkula Iber, B., Azman Kasan, N., Torsabo, D. & Wese Omuwa, J. 2022. A Review of Various Sources of Chitin and Chitosan in Nature. *Journal of Renewable Materials*. 10(4):1097–1123. DOI: 10.32604/jrm.2022.018142.

Thaler, J.S., Humphrey, P.T. & Whiteman, N.K. 2012. Evolution of jasmonate and salicylate signal crosstalk. *Trends in Plant Science*. 17(5):260–270. DOI: 10.1016/j.tplants.2012.02.010.

Tholl, D. 2006. Terpene synthases and the regulation, diversity and biological roles of terpene metabolism. *Current Opinion in Plant Biology*. 9(3):297–304. DOI: 10.1016/j.pbi.2006.03.014.

Thordal-Christensen, H., Zhang, Z., Wei, Y. & Collinge, D.B. 1997. Subcellular localization of H_2O_2 in plants. H_2O_2 accumulation in papillae and hypersensitive response during the barley-powdery mildew interaction. *The Plant Journal*. 11(6):1187–1194. DOI: 10.1046/j.1365-313X.1997.11061187.x.

Tikhonov, V.E., Stepnova, E.A., Babak, V.G., Yamskov, I.A., Palma-Guerrero, J., Jansson, H.B., Lopez-Llorca, L. V., Salinas, J., et al. 2006. Bactericidal and antifungal activities of a low molecular weight chitosan and its N-/2(3)-(dodec-2-enyl)succinoyl/-derivatives. *Carbohydrate Polymers*. 64(1):66–72. DOI: 10.1016/j.carbpol.2005.10.021.

Tornero, P., Gadea, J., Conejero, V. & Vera, P. 1997. Two PR-1 Genes from Tomato Are Differentially Regulated and Reveal a Novel Mode of Expression for a Pathogenesis-Related Gene During the Hypersensitive Response and Development. *Molecular Plant-Microbe Interactions*. 10(5):624–634. DOI: 10.1094/MPMI.1997.10.5.624.

Tran, B.Q. & Jung, S. 2020. Modulation of chloroplast components and defense responses during programmed cell death in tobacco infected with Pseudomonas syringae. *Biochemical and Biophysical Research Communications*. 528(4):753–759. DOI:

10.1016/j.bbrc.2020.05.086.

Tran, S.-L., Puhar, A., Ngo-Camus, M. & Ramarao, N. 2011. Trypan Blue Dye Enters Viable Cells Incubated with the Pore-Forming Toxin HlyII of *Bacillus cereus*. *PLoS ONE*. 6(9):e22876. DOI: 10.1371/journal.pone.0022876.

Tripathy, B.C. & Oelmüller, R. 2012. Reactive oxygen species generation and signaling in plants. *Plant Signaling & Behavior*. 7(12):1621–1633. DOI: 10.4161/psb.22455.

Tripathy, B.C., Mohapatra, A. & Gupta, I. 2007. Impairment of the photosynthetic apparatus by oxidative stress induced by photosensitization reaction of protoporphyrin IX. *Biochimica et Biophysica Acta (BBA) - Bioenergetics*. 1767(6):860–868. DOI: 10.1016/j.bbabio.2007.03.008.

Turk, H. 2019. Chitosan-induced enhanced expression and activation of alternative oxidase confer tolerance to salt stress in maize seedlings. *Plant Physiology and Biochemistry*. 141(June):415–422. DOI: 10.1016/j.plaphy.2019.06.025.

United Nations. 2022. *World Population Prospects 2022*. Available: www.un.org/development/ desa/pd/.

van Aubel, G., Cambier, P., Dieu, M. & Van Cutsem, P. 2016. Plant immunity induced by COS-OGA elicitor is a cumulative process that involves salicylic acid. *Plant Science*. 247:60–70. DOI: 10.1016/j.plantsci.2016.03.005.

van der Burgh, A.M. & Joosten, M.H.A.J. 2019. Plant Immunity: Thinking Outside and Inside the Box. *Trends in Plant Science*. 24(7):587–601. DOI: 10.1016/j.tplants.2019.04.009.

VanEtten, H.D., Mansfield, J.W., Bailey, J.A. & Farmer, E.E. 1994. Two Classes of Plant Antibiotics: Phytoalexins versus "Phytoanticipins". *The Plant Cell*. 6(9):1191. DOI: 10.2307/3869817.

van Hulten, M., Pelser, M., van Loon, L.C., Pieterse, C.M.J. & Ton, J. 2006. Costs and benefits of priming for defense in *Arabidopsis*. *Proceedings of the National Academy of Sciences*. 103(14):5602–5607. DOI: 10.1073/pnas.0510213103.

Van Meulebroek, L., Bussche, J. Vanden, Steppe, K. & Vanhaecke, L. 2012. Ultra-high performance liquid chromatography coupled to high resolution Orbitrap mass spectrometry for metabolomic profiling of the endogenous phytohormonal status of the tomato plant. *Journal of Chromatography A*. 1260:67–80. DOI: 10.1016/j.chroma.2012.08.047.

Vasyukova, N.I., Zinov'eva, S. V, Il'inskaya, L.I., Perekhod, E.A., Chalenko, G.I., Gerasimova, N.G., Il'ina, a V, Varlamov, V.P., et al. 2001. Modulation of Plant Resistance to Diseases by Water-Soluble Chitosan. *Applied Biochemistry and Microbiology*. 37(1):103–109. DOI: 10.1023/A:1002865029994.

Vaughan, M.M., Christensen, S., Schmelz, E.A., Huffaker, A., Mcauslane, H.J., Alborn, H.T., Romero, M., Allen, L.H., et al. 2015. Accumulation of terpenoid phytoalexins in maize roots is associated with drought tolerance. *Plant, Cell and Environment*. 38(11):2195–2207. DOI: 10.1111/pce.12482.

Verger, P.J.P. & Boobis, A.R. 2013. Reevaluate Pesticides for Food Security and Safety. *Science*. 341(6147):717–718. DOI: 10.1126/science.1241572.

Verlee, A., Mincke, S. & Stevens, C. V. 2017. Recent developments in antibacterial and antifungal chitosan and its derivatives. *Carbohydrate Polymers*. 164:268–283. DOI: 10.1016/j.carbpol.2017.02.001.

Vieira, H., Lestre, G.M., Solstad, R.G., Cabral, A.E., Botelho, A., Helbig, C., Coppola, D., de Pascale, D., et al. 2023. Current and Expected Trends for the Marine Chitin/Chitosan and Collagen Value Chains. *Marine Drugs*. 21(12). DOI: 10.3390/md21120605.

Viljoen, J.H. 2003. Mycotoxins in grain and grain products in South Africa and proposals for their regulation. 1–335. Available: http://hdl.handle.net/2263/27846.

Walters, D.R., McRoberts, N. & Fitt, B.D.L. 2007. Are green islands red herrings? Significance of green islands in plant interactions with pathogens and pests. *Biological Reviews*. 83(1):79–102. DOI: 10.1111/j.1469-185X.2007.00033.x.

Weissbach, H., Etienne, F., Hoshi, T., Heinemann, S.H., Lowther, W.T., Matthews, B., St. John, G., Nathan, C., et al. 2002. Peptide Methionine Sulfoxide Reductase: Structure, Mechanism of Action, and Biological Function. *Archives of Biochemistry and Biophysics*. 397(2):172–178. DOI: 10.1006/abbi.2001.2664.

Willekens, H. 1997. Catalase is a sink for H2O2 and is indispensable for stress defence in C3 plants. *The EMBO Journal*. 16(16):4806–4816. DOI: 10.1093/emboj/16.16.4806.

Williams, L.D., Glenn, A.E., Zimeri, A.M., Bacon, C.W., Smith, M.A. & Riley, R.T. 2007. Fumonisin Disruption of Ceramide Biosynthesis in Maize Roots and the Effects on Plant Development and *Fusarium verticillioides* -Induced Seedling Disease. *Journal of Agricultural and Food Chemistry*. 55(8):2937–2946. DOI: 10.1021/jf0635614.

Williamson, B., Tudzynski, B., Tudzynski, P. & Van Kan, J.A.L. 2007. *Botrytis cinerea*: the cause of grey mould disease. *Molecular Plant Pathology*. 8(5):561–580. DOI: 10.1111/j.1364-3703.2007.00417.x.

Wu, C.-T. & Bradford, K.J. 2003. Class I Chitinase and β-1,3-Glucanase Are Differentially Regulated by Wounding, Methyl Jasmonate, Ethylene, and Gibberellin in Tomato Seeds and Leaves. *Plant Physiology*. 133(1):263–273. DOI: 10.1104/pp.103.024687.

Wu, L., Wang, X.M., Xu, R.Q. & Li, H.J. 2011. Root Infection and Systematic Colonization of DsRed-Labeled *Fusarium verticillioides* in Maize. *Acta Agronomica Sinica*. 37(5):793–802. DOI: 10.1016/S1875-2780(11)60023-0.

Xing, K., Zhu, X., Peng, X. & Qin, S. 2015. Chitosan antimicrobial and eliciting properties for pest control in agriculture: a review. *Agronomy for Sustainable Development*. 35(2):569–588. DOI: 10.1007/s13593-014-0252-3.

Xu, J., Zhao, X., Han, X. & Du, Y. 2007. Antifungal activity of oligochitosan against Phytophthora capsici and other plant pathogenic fungi *in vitro*. *Pesticide Biochemistry and Physiology*. 87(3):220–228. DOI: 10.1016/j.pestbp.2006.07.013.

Yadav, M., Goswami, P., Paritosh, K., Kumar, M., Pareek, N. & Vivekanand, V. 2019. DOI: 10.1186/s40643-019-0243-y.

Yamada, A., Shibuya, N., Kodama, O. & Akatsuka, T. 1993. Induction of Phytoalexin Formation

in Suspension-cultured Rice Cells by N-Acetyl-chitooligosaccharides. *Bioscience, Biotechnology, and Biochemistry*. 57(3):405–409. DOI: 10.1271/bbb.57.405.

Yang, A., Yu, L., Chen, Z., Zhang, S., Shi, J., Zhao, X., Yang, Y., Hu, D., et al. 2017. Label-Free Quantitative Proteomic Analysis of Chitosan Oligosaccharide-Treated Rice Infected with Southern Rice Black-Streaked Dwarf Virus. *Viruses*. 9(5):115. DOI: 10.3390/v9050115.

Yang, J., Cai, J., Hu, Y., Li, D. & Du, Y. 2012. Preparation, characterization and antimicrobial activity of 6-amino-6-deoxychitosan. *Carbohydrate Polymers*. 87(1):202–209. DOI: 10.1016/j.carbpol.2011.07.039.

Yang, J., Xie, Q., Zhu, J., Zou, C., Chen, L., Du, Y. & Li, D. 2015. Preparation and *in vitro* antioxidant activities of 6-amino-6-deoxychitosan and its sulfonated derivatives. *Biopolymers*. 103(10):539–549. DOI: 10.1002/bip.22656.

Yang, X., Lu, Y., Zhao, X., Jiang, L., Xu, S., Peng, J., Zheng, H., Lin, L., et al. 2019. Downregulation of Nuclear Protein H2B Induces Salicylic Acid Mediated Defense Against PVX Infection in *Nicotiana benthamiana*. *Frontiers in Microbiology*. 10:1–10. DOI: 10.3389/fmicb.2019.01000.

Yang, Y., Saand, M.A., Huang, L., Abdelaal, W.B., Zhang, J., Wu, Y., Li, J., Sirohi, M.H., et al. 2021. Applications of Multi-Omics Technologies for Crop Improvement. *Frontiers in Plant Science*. 12:1–22. DOI: 10.3389/fpls.2021.563953.

Yin, H., Li, S., Zhao, X., Du, Y. & Ma, X. 2006. cDNA microarray analysis of gene expression in *Brassica napus* treated with oligochitosan elicitor. *Plant Physiology and Biochemistry*. 44(11–12):910–916. DOI: 10.1016/j.plaphy.2006.10.002.

Yoda, H., Yamaguchi, Y. & Sano, H. 2003. Induction of Hypersensitive Cell Death by Hydrogen Peroxide Produced through Polyamine Degradation in Tobacco Plants. *Plant Physiology*. 132(4):1973–1981. DOI: 10.1104/pp.103.024737.

Younes, I., Sellimi, S., Rinaudo, M., Jellouli, K. & Nasri, M. 2014. Influence of acetylation degree and molecular weight of homogeneous chitosans on antibacterial and antifungal activities. *International Journal of Food Microbiology*. 185:57–63. DOI: 10.1016/j.ijfoodmicro.2014.04.029.

Young, D.H., Köhle, H. & Kauss, H. 1982. Effect of Chitosan on Membrane Permeability of Suspension-Cultured Glycine max and *Phaseolus vulgaris* Cells. *Plant Physiology*. 70(5):1449–1454. DOI: 10.1104/pp.70.5.1449.

Yu, L., Zhang, X., Zhang, F., Tang, Y., Gong, D., Oyom, W., Li, Y., Prusky, D., et al. 2023. Chitosan and chitooligosaccharide regulated reactive oxygen species homeostasis at wounds of pear fruit during healing. *International Journal of Biological Macromolecules*. 240:124395. DOI: 10.1016/j.ijbiomac.2023.124395.

Zachetti, V., Cendoya, E., Nichea, M., Chulze, S. & Ramirez, M. 2019. Preliminary Study on the Use of Chitosan as an Eco-Friendly Alternative to Control *Fusarium* Growth and Mycotoxin Production on Maize and Wheat. *Pathogens*. 8(1):29. DOI: 10.3390/pathogens8010029.

Zahran, H.H. 1997. Diversity, adaptation and activity of the bacterial flora in saline environments. *Biology and Fertility of Soils*. 25(3):211–223. DOI: 10.1007/s003740050306.

Zeng, H.-Y., Li, C.-Y. & Yao, N. 2020. Fumonisin B1: A Tool for Exploring the Multiple Functions of Sphingolipids in Plants. *Frontiers in Plant Science*. 11:1–16. DOI: 10.3389/fpls.2020.600458.

Zhang, X., Wu, Q., Cui, S., Ren, J., Qian, W., Yang, Y., He, S., Chu, J., et al. 2015. Hijacking of the jasmonate pathway by the mycotoxin fumonisin B1 (FB1) to initiate programmed cell death in *Arabidopsis* is modulated by *RGLG3* and *RGLG4*. *Journal of Experimental Botany*. 66(9):2709–2721. DOI: 10.1093/jxb/erv068.

Zhang, Y., Yan, H., Wei, X., Zhang, J., Wang, H. & Liu, D. 2017. Expression analysis and functional characterization of a pathogen-induced thaumatin-like gene in wheat conferring enhanced resistance to *Puccinia triticina*. *Journal of Plant Interactions*. 12(1):332–339. DOI: 10.1080/17429145.2017.1367042.

Ziani, K., Fernández-Pan, I., Royo, M. & Maté, J.I. 2009. Antifungal activity of films and solutions based on chitosan against typical seed fungi. *Food Hydrocolloids*. 23(8):2309–2314. DOI: 10.1016/j.foodhyd.2009.06.005.

Ziegler, J., Stenzel, I., Hause, B., Maucher, H., Hamberg, M., Grimm, R., Ganal, M. & Wasternack, C. 2000. Molecular Cloning of Allene Oxide Cyclase. *Journal of Biological Chemistry*. 275(25):19132–19138. DOI: 10.1074/jbc.M002133200.

Zitomer, N.C., Jones, S., Bacon, C., Glenn, A.E., Baldwin, T. & Riley, R.T. 2010. Translocation of Sphingoid Bases and Their 1-Phosphates, but Not Fumonisins, from Roots to Aerial Tissues of Maize Seedlings Watered with Fumonisins. *Journal of Agricultural and Food Chemistry*. 58(12):7476–7481. DOI: 10.1021/jf100142d.

Ziv, C., Zhao, Z., Gao, Y.G. & Xia, Y. 2018. Multifunctional Roles of Plant Cuticle During Plant-Pathogen Interactions. *Frontiers in Plant Science*. 9:1–8. DOI: 10.3389/fpls.2018.01088.

Zuluaga, A.P., Bidzinski, P., Chanclud, E., Ducasse, A., Cayrol, B., Gomez Selvaraj, M., Ishitani, M., Jauneau, A., et al. 2020. The Rice DNA-Binding Protein ZBED Controls Stress Regulators and Maintains Disease Resistance After a Mild Drought. *Frontiers in Plant Science*. 11:1–15. DOI: 10.3389/fpls.2020.01265.

Curriculum vitae

Education and Qualifications

2018 PhD candidate Molecular and Cell Biology, University of Cape Town, South Africa

2017 MSc Molecular and Cell Biology, University of Cape Town, South Africa (upgraded to PhD)

2016 BSc (Hons) Molecular and Cell Biology, University of Cape Town, South Africa

2015 BSc Biochemistry and Genetics, University of Cape Town

Courses

2019 Green Chemistry Postgraduate Summer School online 2020

2018 Multi-toxin Analysis by LC-MS traineeship, IFA, Tulln, Austria

2017 MSc collaboration with the University of Ghent (4-month international stay and research)

Publications

2023 **Moola, N**., Jardine, A., Audenaert, K. and Rafudeen, M.S., 2023. 6-deoxy-6-amino chitosan: a preventative treatment in the tomato/*Botrytis cinerea* pathosystem. Frontiers in Plant Science, 14.

2020 Lambarey, H., **Moola, N.,** Veenstra, A., Murray, S. and Suhail Rafudeen, M., 2020. Transcriptomic Analysis of a Susceptible African Maize Line to *Fusarium verticillioides* Infection. Plants, 9(9), p.1112.

2018 Veenstra, A., **Moola, N.,** Wighard, S., Korsman, J., Christensen, S.A., Rafudeen, M.S. and Murray, S.L., Kauralexins and zealexins accumulate in sub-tropical maize lines and play a role in seedling resistance to *Fusarium verticillioides*. *European Journal of Plant Pathology*, pp.1-15.

Presentations

2023 1st place UCT Science Postgraduate Research Symposium

2022 Motivational speaker for woman in STEM at Sans Souci Primary School

2019 2nd place TEDx Gent Research Rally, Belgium

2018 Keynote speaker at African Centre for Gene Technologies (ACGT) forum

2018 Runner-up at the UCT 3MT® Challenge in the Science Category

2018 1st place oral presenter at the UCT Science Postgraduate Symposium

2018 1st place oral presenter at the UCT Muslim Student Association Expo

Membership of Professional Associations

2018-2023 Student representative on the African Society of Mycotoxicology committee

2021 Member of Royal Society of South Africa

Academic

2018 Outstanding demonstrator award for 3rd year research projects in MCB at UCT

2018 Outstanding tutor award for an undergraduate course in MCB

Scholarships

2022 UCT Scholarship

2021 Extended funding from National Research Foundation Innovations Scholarship

2020 National Research Foundation Innovations Scholarship

2020 Harry Crossley Foundation

2019 National Research Foundation Innovations Scholarship

2019 Harry Crossley Foundation

2018 National Research Foundation Innovations Scholarship

2017 National Research Foundation Master's Innovations Scholarship

2017 UCT International Travel Scholarship from Max and Lillie Sonnenberg

2016 UCT Merit Award (BSc Honours)

Leadership

2024 Head of Transformation and Development at Western Cape Climbing

2022 Head Coach and coordinator of Dream Higher (NPO)

2021 Head Coach and coordinator of Dream Higher (NPO)

2018 General member of Molecular & Cell Biology Postgraduate Representative Committee

2018 Mentor for undergraduates in the department of Molecular & Cell Biology (UCT)

2018 Demonstrator for a 3rd year undergraduate research project

2018 Judge at the Eskom Science Expo for Young Scientists